AD-A138 093 MULTIVARIABLE DIGITAL FLIGHT CONTROL DESIGN FOR THE FPCC (FLIGHT PROPULSI..(U) AIR FORCE INST OF TECH WRIGHT-PATTERSON AFB OH SCHOOL OF ENGI.. J A SIMMERS 1/3

UNCLASSIFIED DEC 83 AFIT/GE/EE/83D-61 F/G 1/3 NL

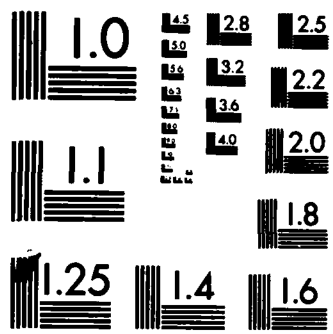
1.0
1.1
1.25
1.4
1.6
1.8
2.0
2.2
2.5
2.8
3.2
3.6
4.0

MULTIVARIABLE DIGITAL FLIGHT CONTROL

DESIGN FOR THE FPCC AIRCRAFT

THESIS

AFIT/GE/EE/83D-61 Jeffrey A Simmers
1Lt USAF

DEPARTMENT OF THE AIR FORCE

AIR UNIVERSITY

AIR FORCE INSTITUTE OF TECHNOLOGY

Wright-Patterson Air Force Base, Ohio

AFIT/GE/EE/83D-61

MULTIVARIABLE DIGITAL FLIGHT CONTROL DESIGN FOR THE FPCC AIRCRAFT

THESIS

AFIT/GE/EE/83D-61 Jeffrey A Simmers
1Lt USAF

AFIT/GE/EE/83D-61

MULTIVARIABLE DIGITAL FLIGHT CONTROL DESIGN FOR THE FPCC AIRCRAFT

THESIS

Presented to the Faculty of the School of Engineering

of the Air Force Institute of Technology

Air University

in Partial Fulfillment of the

Requirements for the Degree of

Master of Science

by

Jeffrey A Simmers

1Lt USAF

Graduate Engineering

December 1983

PREFACE

This thesis follows up work done by Joseph Smyth and Jon Bauschlicher in their thesis efforts at the Air Force Institute of Technology. It was supported by the Air Force Flight Dynamics Laboratory/Control Division at Wright-Patterson Air Force Base.

I thank my thesis advisor, Dr. John J. D'Azzo, without whose help this thesis would not have been possible. I also wish to thank my colleagues Captain William Locken, Lt Marc Hoffman, Lt Roger Feldmann, and Lt Brian Mayhew, all of whom contributed to this thesis.

I save my most heart-felt thanks for last, to my family for their patience and understanding. Thank you Susan and Steven.

1Lt Jeffrey A Simmers

CONTENTS

Title		Page
Preface		ii
List of Figures		v
List of Tables		ix
Abstract		x
I	Introduction	1
	Background	1
	Problem	3
	Current Knowledge	4
	Support	5
	Overview	5
II	Design of Linear Multivariable Tracking Systems Based Upon Singular Perturbation Methods	7
	Introduction	7
	Unknown Plant	10
	Known Plant	13
	Known/Regular Plant	16
	Known/Irregular Plant	19
	B* Design	22
	Summary	24
III	FPCC Aircraft/Simulation Program Description	25
	Introduction	25
	Aircraft Description	26
	FPCC Aircraft Simulation Program	29
IV	Controller Design	39
	Introduction	39
	Lateral Controller	42
	Maneuver Description	42
	Lateral Model	44
	Measurement Matrix Determination	47
	Controller Design	50
	Longitudinal Controller	62
	Maneuver Description	62
	Longitudinal Model	63
	Measurement Matrix Development	66
	Controller Design	68

Controller Response Analysis 92
Lateral Controller Response Analysis 92
Longitudinal Controller Response Analysis 93
Combined Lateral and Longitudinal Controller 94
Development 94
Conclusions 102

V Robustness Testing of Longitudinal Controller and
Compensation for Effects of Controller Delay 103

Introduction 103
Universal Controller 103
Testing 104
Results 105
Conclusions 114
Effects of Controller Delay 115
Results 115
Conclusions 146
Universal Controller Incorporating Delay 147
Results 147
Conclusions 154
Minimizing Controller Marices Elements 155
Lateral Controller 156
Longitudinal Controller 168
Conclusions 170

VI Results, Conclusions, and Recommendations 171

Introduction 171
Results 172
Conclusions 174
Recommendations 175
Design Method 175
Design Tool Multi 176

Bibliography 179

Appendix A: Justification for Elimination of Jet Flaps
From Lateral Model 181

Appendix B: Implementing a First Forward Difference
Approximation to the 1/S Routine Within
the PI Controller in Multi 185

Appendix C: Additions to Design Program MULTI 189

Appendix D: System Matrices, Controller Matrices, and
Design Parameters for 0.6 Mach, Sea Level,
and for 0.9 Mach, 30,000 Feet 197

Vita 200

LIST OF FIGURES

Figure	Title	Page
1	Proportional Plus Integral Controller	9
2	Known/Regular Plant	14
3	Known/Irregular Plant	20
4	FPCC Aircraft	27
5	1.5 G Horizontal Translation (0.15 Mach)	55
6	1.5 G Horizontal Translation (0.15 Mach)	56
7	1 G Flat Turn (0.15 Mach)	57
8	1 G Flat Turn (0.15 Mach)	58
9	3 Degree Yaw Pointing (0.15 Mach)	59
10	3 Degree Yaw Pointing (0.15 Mach)	60
11	3 Degree Yaw Pointing (0.15 Mach)	61
12	1.75 Degree Pitch Pointing (0.15 Mach)	69
13	1.75 Degree Pitch Pointing (0.15 Mach)	70
14	1.75 Degree Pitch Pointing (0.15 Mach)	71
15	0.5 G Direct Lift (0.15 Mach)	71
16	0.5 G Direct Lift (0.15 Mach)	72
17	0.5 G Direct Lift (0.15 Mach)	73
18	0.5 G Vertical Translation (0.15 Mach)	74
19	0.5 G Vertical Translation (0.15 Mach)	75
20	0.5 G Vertical Translation (0.15 Mach)	76
21	1.75 Degree Pitch Pointing (0.6 Mach)	76
22	1.75 Degree Pitch Pointing (0.6 Mach)	77
23	1.75 Degree Pitch Pointing (0.6 Mach)	78
24	1.8 G Direct Lift (0.6 Mach)	79
25	1.8 G Direct Lift (0.6 Mach)	80
26	1.8 G Direct Lift (0.6 Mach)	81
27	0.8 G Vertical Translation (0.6 Mach)	81
28	0.8 G Vertical Translation (0.6 Mach)	82
29	0.8 G Vertical Translation (0.6 Mach)	83
30	3 Degree Pitch Pointing (0.9 Mach)	84
31	3 Degree Pitch Pointing (0.9 Mach)	85
32	3 Degree Pitch Pointing (0.9 Mach)	86
33	2.4 G Direct Lift (0.9 Mach)	86
34	2.4 G Direct Lift (0.9 Mach)	87
35	2.4 G Direct Lift (0.9 Mach)	88
36	2.4 G Direct Lift (0.9 Mach)	89
37	1 G Vertical Translation (0.9 Mach)	89
38	1 G Vertical Translation (0.9 Mach)	90
39	1 G Vertical Translation (0.9 Mach)	91
40	Jink Maneuver (0.15 Mach)	97
41	Jink Maneuver (0.15 Mach)	98
42	Jink Maneuver (0.15 Mach)	99
43	Jink Maneuver (0.15 Mach)	101
44	1.75 Degree Pitch Pointing with Universal Controller (0.6 Mach)	106
45	1.75 Degree Pitch Pointing with Universal Controller (0.6 Mach)	107
46	1.75 Degree Pitch Pointing with Universal Controller (0.6 Mach)	108
47	1.8 G Direct Lift with Universal Controller (0.6 Mach)	108

Figure	Title	Page
48	1.8 G Direct Lift with Universal Controller (0.6 Mach)	109
49	1.8 G Direct Lift with Universal Controller (0.6 Mach)	110
50	0.8 G Vertical Translation with Universal Controller (0.6 Mach)	111
51	0.8 G Vertical Translation with Universal Controller (0.6 Mach)	112
52	0.8 G Vertical Translation with Universal Controller (0.6 Mach)	113
53	1.75 Degree Pitch Pointing with Delay (0.15 Mach)	116
54	1.75 Degree Pitch Pointing with Delay (0.15 Mach)	117
55	1.75 Degree Pitch Pointing with Delay (0.15 Mach)	118
56	0.5 G Direct Lift with Delay (0.15 Mach)	118
57	0.5 G Direct Lift with Delay (0.15 Mach)	119
58	0.5 G Direct Lift with Delay (0.15 Mach)	120
59	0.5 G Vertical Translation with Delay (0.15 Mach)	121
60	0.5 G Vertical Translation with Delay (0.15 Mach)	122
61	0.5 G Vertical Translation with Delay (0.15 Mach)	124
62	1.75 Degree Pitch Pointing with Delay, Control Ratio of Two (0.6 Mach)	125
63	1.75 Degree Pitch Pointing with Delay, Control Ratio of Two (0.6 Mach)	126
64	1.75 Degree Pitch Pointing with Delay, Control Ratio of Three (0.6 Mach)	127
65	1.75 Degree Pitch Pointing with Delay, Control Ratio of Three (0.6 Mach)	128
66	1.8 G Direct Lift with Delay, Control Ratio of Two (0.6 Mach)	129
67	1.8 G Direct Lift with Delay, Control Ratio of Two (0.6 Mach)	130
68	1.8 G Direct Lift with Delay, Control Ratio of Three (0.6 Mach)	131
69	1.8 G Direct Lift with Delay, Control Ratio of Three (0.6 Mach)	132
70	0.8 G Vertical Translation with Delay, Control Ratio of Two (0.6 Mach)	133
71	0.8 G Vertical Translation with Delay, Control Ratio of Two (0.6 Mach)	134
72	0.8 G Vertical Translation with Delay, Control Ratio of Three (0.6 Mach)	135
73	0.8 G Vertical Translation with Delay, Control Ratio of Three (0.6 Mach)	136
74	3 Degree Pitch Pointing with Delay, Control Ratio of Four (0.9 Mach)	137
75	3 Degree Pitch Pointing with Delay, Control Ratio of Four (0.9 Mach)	138

Figure	Title	Page
76	2.4 G Direct Lift with Delay, Control Ratio of Four (0.9 Mach)	139
77	2.4 G Direct Lift with Delay, Control Ratio of Four (0.9 Mach)	140
78	1 G Vertical Translation with Delay, Control Ratio of Four (0.9 Mach)	141
79	1 G Vertical Translation with Delay, Control Ratio of Four (0.9 Mach)	142
80	1.75 Degree Pitch Pointing with Delay, Universal Controller (0.6 Mach)	148
81	1.75 Degree Pitch Pointing with Delay, Universal Controller (0.6 Mach)	149
82	1.8 G Direct Lift with Delay, Universal Controller (0.6 Mach)	150
83	1.8 G Direct Lift with Delay, Universal Controller (0.6 Mach)	151
84	0.8 G Vertical Translation with Delay, Universal Controller (0.6 Mach)	152
85	0.8 G Vertical Translation with Delay, Universal Controller (0.6 Mach)	153
86	1.5 G Horizontal Translation with Reduced Controller Matrices (0.15 Mach)	157
87	1.5 G Horizontal Translation with Reduced Controller Matrices (0.15 Mach)	158
88	1 G Flat Turn with Reduced Controller Matrices (0.15 Mach)	158
89	1 G Flat Turn with Reduced Controller Matrices (0.15 Mach)	159
90	3 Degree Yaw Pointing with Reduced Controller Matrices (0.15 Mach)	160
91	3 Degree Yaw Pointing with Reduced Controller Matrices (0.15 Mach)	161
92	1.75 Degree Pitch Pointing with Reduced Controller Matrices (0.15 Mach)	161
93	1.75 Degree Pitch Pointing with Reduced Controller Matrices (0.15 Mach)	162
94	1.75 Degree Pitch Pointing with Reduced Controller Matrices (0.15 Mach)	163
95	0.5 G Direct Lift with Reduced Controller Matrices (0.15 Mach)	163
96	0.5 G Direct Lift with Reduced Controller Matrices (0.15 Mach)	164
97	0.5 G Direct Lift with Reduced Controller Matrices (0.15 Mach)	165
98	0.5 G Vertical Translation with Reduced Controller Matrices (0.15 Mach)	165
99	0.5 G Vertical Translation with Reduced Controller Matrices (0.15 Mach)	166
100	0.5 G Vertical Translation with Reduced Controller Matrices (0.15 Mach)	167
B-1	Forward Velocity Response to 0.5 G Direct Lift Command (0.15 Mach)	187

Figure	Title	Page
B-2	Forward Velocity Response to 0.5 G Vertical Translation Command (0.15 Mach) ..	188
B-3	Total Thrust Response to 0.5 G Vertical Translation Command (0.15 Mach)	188

LIST OF TABLES

Table	Title	Page
I	Summary Listing of Intitial FPCC Reference Aircraft Point Design Guidelines and Constraints	28
II	Control Surface Limits and Dynamics	30
III	Input Vector, $\underline{u}$	34
IV	State Vector, $\underline{x}$	35
V	Output Vector, $\underline{y}$	35
VI	FPCC Aircraft Response at Sea Level	37
VII	Summary of Output Responses For Lateral Controller	61
VIII	Summary of Output Responses For Longitudinal Controller	100
IX	Summary of Output Responses For Universal Controller	113
X	Summary of Output Responses For Longitudinal Controllers With Delay	123
XI	Summary of Output Responses For Universal Controller With Delay	124

ABSTRACT

This thesis details the application of the Porter Method to the design of a digital tracker controller for the FPCC aircraft. The aircraft is simulated with software models supplied by Lockheed, and incorporates horizontal and vertical canards, along with maneuver flaps, ailerons, rudder, and jet flaps for vectored thrust.

Separate lateral and longitudinal designs are accomplished at 0.15 mach, sea level. Longitudinal designs for 0.6 mach, sea level, and 0.9 mach at 30,000 ft. are also completed. For the one lateral design the following maneuvers are performed:

Yaw pointing

Flat turn

Horizontal translation

For the three longitudinal designs the following maneuvers are performed:

Pitch pointing

Direct lift

Vertical translation

One coupled maneuver, a jink maneuver incorporating both vertical and horizontal translation demonstrates the combined lateral and longitudinal controller at 0.15 mach. A "universal" controller is found for the 0.6 and 0.9 mach flight conditions and is tested with the same longitudinal maneuvers. All of the controllers are again tested with the addition of a one sampling period delay

included between the controller and the control input to the actuators. This represents the time delay that may be introduced in the controller by the microprocessor implementation. Finally, the controllers are minimized in regards to numbers of gains required in the control law matrices by finding common elements that can be set to zero.

CHAPTER I

INTRODUCTION

Background

Digital computers and electical wiring are rapidly replacing analog controllers and mechanical linkages in the design of aircraft flight control systems. This is true for both military and civilian aviation.

The digital flight control system must handle multiple inputs from the pilot and also command multiple outputs simultaneously, ensuring optimal aircraft performance for varied flight conditions. The digital flight control system (DFCS) can control more flight control surfaces than a pilot, and can also control them simultaneously. Sensing elements such as the gyros and the accelerometers allow the DFCS to use detailed information about the aircraft's attitude to command flight control surface deflections more efficiently than a pilot.

Using a DFCS allows the pilot to command a particular maneuver, instead of the pilot having to control the flight control surfaces directly. Thus, the pilot's workload is reduced, increasing pilot efficiency and allowing the pilot more time to concentrate on other vital tasks. In the combat arena, with the corresponding pressures that are applied to the pilot, the possibility of error should be reduced and the chances for survival should increase.

The DFCS generates the signals necessary to deflect the control surfaces in response to a commanded maneuver from the pilot. Consequently, classical single input single output (SISO) design techniques are not well suited to this multiple input multiple output (MIMO) problem. Other techniques, such as LQG, that require all states to be either accessable or estimated lead to complicated calculations due to the lack of full state information on the typical aircraft. An alternative design method has been developed by Professor Brain Porter and associates at the University of Salford, U.K.

The Porter method proposes a straight forward approach to the MIMO control system design that does not require complicated mathematics nor does it require considering each output-input pair separately (Ref 1). Previous AFIT master's theses have demonstrated the use of the method (Ref 2 and 3).

A hypothetical aircraft called the FPCC, for flight propulsion control coupling, has been proposed by Pratt-Whitney, Lockheed, and Honeywell. The aircraft's main feature is the use of thrust vectoring using jet flaps, hence the FPCC label. The aircraft also incorporates horizontal and vertical canards, along with maneuver flaps. The FPCC is longitudinally statically unstable, adding to the aircraft's maneuverability (Ref 4). Resulting from these features is the aircraft's ability to perform decoupled six degree of freedom (6DOF) maneuvers.

Design of a DFCS for this aircraft is aided by two computer programs, a flight simulation program for the FPCC provided by the contractors (Ref 5), and an interactive design program incorporating the Porter design method called MULTI (Ref 6).

Problem

This thesis extends previous design work done on a DFCS for the FPCC aircraft (Ref 2), by developing 3 multi-variable tracker control laws for each of 3 flight conditions, using the Porter method. Each controller performs coupled or decoupled, lateral or longitudinal maneuvers. Attempting to demonstrate robustness, a universal controller for two of the flight conditions is designed, and its performance evaluated compared to the individual controllers.

In an attempt to partially validate the short takeoff and landing (STOL) capability of the FPCC, the first flight condition is at 0.15 mach, with a low angle of attack, at sea level. The other two flight conditions are identical to those from Bauschlicher's thesis, 0.6 mach at sea level, and 0.9 mach at 30,000 feet. This thesis repeats designs at these flight conditions because the longitudinal aircraft model has been changed. Therefore, the designs for these flight conditions are in the longitudinal mode only.

The responses for each design are then reaccomplished incorporating a time delay of one sampling period between the output of the controller and the input of the aircraft plant model, demonstrating any destabilizing effects from this lag. The designs are redone, as necessary, to compensate for these effects. The simulations are also repeated with certain controller matrix elements set to zero, demonstrating possible simplifications that can be made to these matrices.

Additionally, this thesis includes two improvements to MULTI, the computer program used for controller design based on the Porter method. An additional option was added that calculates the figures of merit resulting from the time simulation used in the program. Specifically, the maximum, minimum, and final values are displayed, along with the times at which the maximum and minimum occur. The option then allows the user to use the default value of within 2% of the final value, or the user may specify the value, which is to be used to calculate the settling time.

The other modification to MULTI incorporates the option of command line file names when invoking the program. The files named contain system and design data to be used within the program.

Current Knowledge

Papers published by Professor Porter and associates detail the design technique that is used in this thesis (Ref 6). Also, previous theses have both used and explained in detail the Porter method. This thesis is the first to investigate the STOL capabilities of the FPCC aircraft, and extends upon the work done by Jon Bauschlicher completed in December, 1982. Bauschlicher's thesis designed multi-variable controllers for flight conditions reflecting high subsonic, transonic, and supersonic speeds. The MULTI modification in this thesis extends the work started by Douglas Porter as published in his thesis of December, 1981 (Ref 3). Bauschlicher's thesis and the reports by Lockheed constitute the background information on the FPCC aircraft and the simulation program (Ref 4,5).

Support

Computers used include the CDC mainframes (ASD) at Wright-Patterson Air Force Base, and the author's microcomputer. Computer support facilities used include the RJE (Remote Job Entry) sites at both AFIT and the Air Force Flight Dynamics Laboratory (AFFDL), along with the main site at the ASD Computer Center.

Overview

Chapter I is the general introduction, with Chapter II being an introduction to the Porter method of controller design. Chapter III is a description of the FPCC aircraft with a summary of the aircraft's behaviour within the STOL regime, presenting previously unpublished tabular analysis of the aircraft's response to flight control surfaces at slow speed and low altitude. Chapter IV describes the use of the FPCC simulation program, along with explanations of the input and output of the program.

Chapter IV details the design and testing of the controllers for each flight condition. Responses of the controllers to commanded inputs for six decoupled and one coupled maneuver are given.

Chapter V describes the design of a universal controller that can be used for the two non-STOL flight conditions. The effects of a one sampling period time delay in the output of the PI controller is studied for all the flight conditions and the universal controller. Finally, certain elements of the controller matrices for the STOL flight condition are set to zero to study the possibility of reducing the number of gains in these matrices.

Chapter VI summarizes the results and conclusions of this thesis, including insights gained from the use of the Porter method along with suggestions for its future use. Chapter VI also details the assumptions and problems associated with using the FPCC simulation program, and gives some suggestions for its continued use. Also in Chapter VI are ideas for possible future additions to MULTI.

CHAPTER II

DESIGN OF LINEAR MULTIVARIABLE TRACKING SYSTEMS BASED UPON SINGULAR PERTURBATION METHODS

Introduction

The methods used in this thesis for the design of the controllers were developed by Professor Brain Porter, University of Salford, England, and his associates (Ref 1,8,9). The references comprise a fairly complete documentation of the development of the design methodology commonly called the Porter method, but two of the references are more useful as summaries of the method. The first, (Ref 1), details the approach for both regular and irregular known plants using a proportional plus integral (PI) cascade compensator which is either analog or digital. The second (Ref 8), briefly explains the approach for an unknown plant with an analog PI compensator. This chapter summarizes the material from these references. Note that for the known plants only the digital controller is considered, since that is the type of controller used in this thesis and in the program MULTI.

If additional decoupling and/or reduction in the initial undershooting of the outputs is required, then a technique based upon the $\underline{B}$* approach is used, which is also included in this chapter. If the $\underline{B}$* method fails, then there is another alternative, which is not explained in this thesis but is referenced (Ref 9).

Throughout this thesis the description of the continuous time plant is given by:

$$\dot{\underline{x}}(t)=\underline{A}\underline{x}(t)+\underline{B}\underline{u}(t) \tag{1}$$

$$\underline{y}(t)=\underline{C}\underline{x}(t)+\underline{D}\underline{u}(t) \tag{2}$$

where

$\underline{A}$ = continuous time plant matrix (nxn)

$\underline{B}$ = continuous time control matrix (nxm)

$\underline{C}$ = continuous time output matrix (lxn)

$\underline{D}$ = continuous time feed forward matrix (lxm)

and

n = number of plant states

l = number of outputs

m = number of inputs (sometimes called p)

The PI controller performs both the tracking and disturbance rejection tasks, and as stated, is the discrete time type for this thesis. The equations governing the controller are:

$$\underline{x}[(k+1)T] = \exp\{\underline{A}T\} * \underline{x}(kT) + \int_0^T \exp\{\underline{A}T\} * \underline{B}dt * \underline{u}(kT) \tag{3}$$

$$\underline{y}[kT] = \underline{C} * \underline{x}(kT) + \underline{D} * \underline{u}(kT) \tag{4}$$

where

$\exp\{\underline{A}T\}$ = sampled data plant matrix

$\int_0^T \exp\{\underline{A}T\} * \underline{B}dt$ = sampled data control matrix

$\underline{C}$ = sampled data output marix

$\underline{D}$ = sampled data feed forward matrix

T = sampling time

Note that the u(kT) is piecewise constant over the sample period, resulting in its removal from inside the integral. The separate names designating the sampled data matrices are not used in this thesis since these marices are not explicitly used.

Figure 1 shows the PI controller used in this thesis. Since the computer aided design program MULTI is used to assist in the

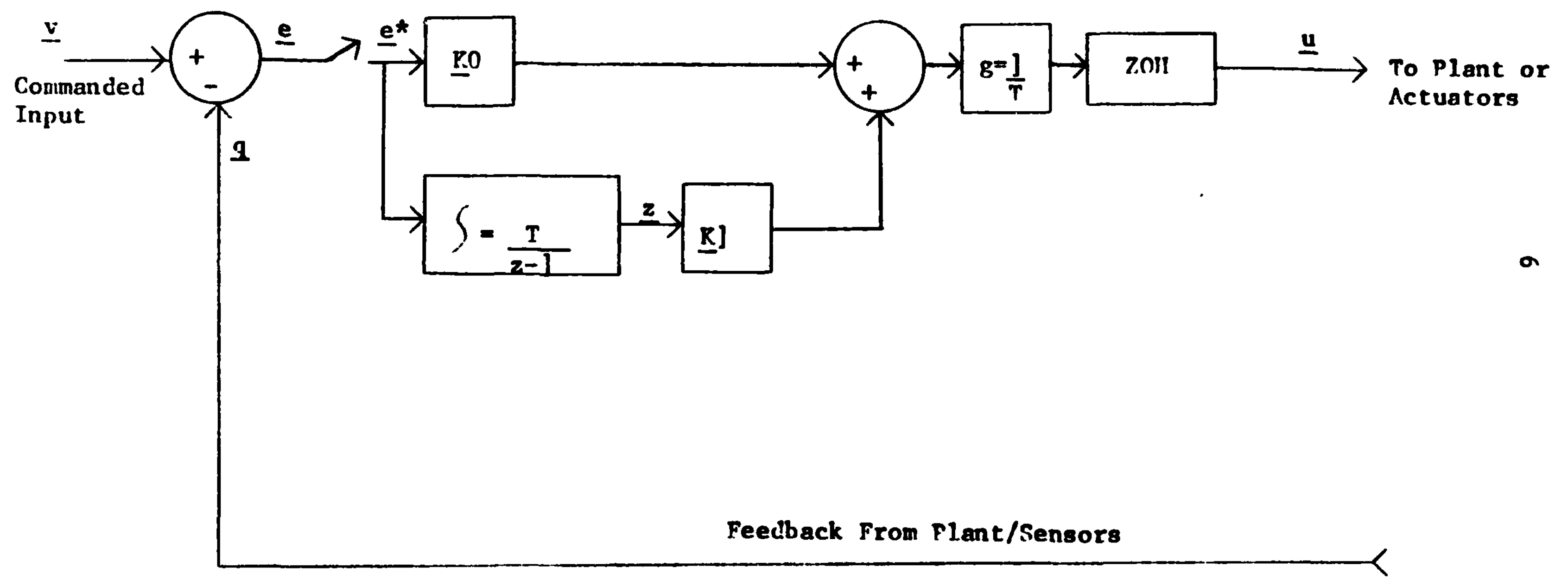

Figure 1. Proportional Plus Integral (PI) Controller

design of the controller, the placement of the sampler is dictated by MULTI's implementation of the controller. MULTI actually implements two samplers, one in the feedback loop from the plant, and the other in the commanded input. Mathematically, the one sampler shown in Figure 1 is equivalent to the other two. The zero order sample and hold device shown is indicative of the way MULTI passes the control input to the plant, with the duration of the hold controlled by an option within MULTI. The integral action shown in the figure is currently implemented in MULTI using an approximation to the 1/s function.

Since the choice of which design method to use, Unknown, Known/Regular, or Known/Irregular, is based upon the plant parameters, the rest of this chapter explains how the choice is made and summarizes the method used in each case. At the end of the chapter the $\underline{B}$* method is explained.

Unknown Plant (Ref 8)

This approach applies typically to an industrial process where little is known about the plant model, or in the situation where developing the state model is not desired. The problem is to develop the controller without knowledge of the $\underline{A}$, $\underline{B}$, $\underline{C}$, or $\underline{D}$ matrices.

The first step is to isolate the plant and determine its steady state transfer function $\underline{G}(0)$. This is possible as long as the plant is asymptotically stable. Since the transfer function

$$\underline{G}(\lambda)=\underline{C}(\lambda \underline{I}_n - \underline{A})^{-1}\ \underline{B}$$

then

$$\underline{G}(0)=-\underline{C}\underline{A}^{-1}\ \underline{B} \qquad (5)$$

implying that this approach could be used if the plant dynamics were known.

Since the addition of the PI controller must preserve stability, the rank of $\underline{G}(0)$ must be equal to 1, the number of outputs. This requirement means that the number of outputs must be less than or equal to the number of inputs, and that $\underline{G}(\lambda)$ must have no transmission zeros either at the origin or in the right half plane.

The control law for the PI controller is:

$$\underline{u}(t)=\alpha\epsilon\,\underline{K}\underline{e}(t)+\epsilon\underline{K}\underline{z}(t) \tag{6}$$

with

$$\underline{e}(t)=\underline{v}(t)-\underline{y}(t) \tag{7}$$

$$\underline{z}(t)=\int_0^T \underline{e}(t)dt \tag{8}$$

where

$\underline{u}(t)$ = control input to the plant

α = ratio of error to the integral of error

ϵ = scaler multiplier

$\underline{K}$ = the controller matrix

$\underline{e}(t)$ = error vector

$\underline{v}(t)$ = command input vector

$\underline{y}(t)$ = output vector

$\underline{z}(t)$ = integral of error vector

Since the system has a cascade vector integrator, a constant step command input vector yields zero steady state error and the output vector follows the input vector, hence tracking and disturbance rejection result.

Manipulation of the above equations, along with the fact the steady state error equals zero yields the following:

$$\underline{K}=\underline{G}(0)^T [\underline{G}(0)\underline{G}(0)^T]^{-1} \tag{9}$$

which, if the number of outputs equals the number of inputs means that $\underline{G}(0)$ is square and

$$\underline{K}=\underline{G}(0)^{-1} \tag{10}$$

The above development can be extended to the digital PI controller by writing the control law equations as:

$$\underline{u}(kT)=T[\underline{K}_0 \underline{e}(kT)+\underline{K}_1 \underline{z}(kT)] \tag{11}$$

$$\underline{e}(kT)=\underline{v}(kT)-\underline{y}(kT) \tag{12}$$

$$\underline{z}[(k+1)T]=\underline{z}(kT)+T\underline{e}(kT) \tag{13}$$

where

$$\underline{K}_0=\alpha\underline{K}_1 \tag{14}$$

$$\underline{K}_1=\epsilon\underline{K} \tag{15}$$

Note that Equation (13) is an approximation to Equation (8).

Following the same basic reasoning us^d above to derive Equation (9), the controller matrices $\underline{K}_0$ and $\underline{K}_1$ can be found from:

$$\underline{K} = \{\underline{G}(0)^T [\underline{G}(0)\underline{G}(0)^T]^{-1}\} \tag{16}$$

where $\underline{\Sigma}$ is a weighting matrix of scalar diagonal entries chosen by the designer.

The choice of the diagonal elements of $\underline{\Sigma}$ and of the sampling time T will affect the output response. This means that fine tuning of the output time responses can be accomplished by adjusting these values.

Unfortunately, this method is only valid for a plant with negative eigenvalues, since $\underline{G}(0)$ must be stable. This precludes its use with statically unstable aircraft such as the FPCC. Additionally, if an angle is used in the state vector then the derivative of that angle (a rate) cannot be used in the output vector since that would generate a transmission zero at the origin.

Reference 2 discusses the effects of varying the parameters in the above equations. Increasing an element in the $\underline{\Sigma}$ matrix speeds up the corresponding output response. Multiplying the $\underline{\Sigma}$ matrix by a scalar greater than one increases the PI controller inputs and outputs, while multiplying by a scalar less than one decreases the inputs and outputs. Decreasing the sampling time T increases the response of the controller outputs. Changing α varies the amount of over or undershoot in the outputs.

Known Plant (Ref 1)

Figure 2 shows the block diagram of the plant with known $\underline{A}$, $\underline{B}$, $\underline{C}$, and $\underline{D}$ matrices. Note that the $\underline{D}$ matrix is missing, which is due to a requirement that the system representation not contain a $\underline{D}$ matrix. If there is a $\underline{D}$ matrix, then either the outputs or state representation must be changed to eliminate the feed forward matrix. A $\underline{D}$ matrix occurs whenever there is an acceleration term in the output vector. The plant equations must be expressed in the following format to use the Porter method:

$$\begin{bmatrix} \dot{\underline{x}}_1(t) \\ \dot{\underline{x}}_2(t) \end{bmatrix} = \begin{bmatrix} \underline{A}_{11} & \underline{A}_{12} \\ \underline{A}_{21} & \underline{A}_{22} \end{bmatrix} \begin{bmatrix} \underline{x}_1(t) \\ \underline{x}_2(t) \end{bmatrix} + \begin{bmatrix} \underline{0} \\ \underline{B}_2 \end{bmatrix} \underline{u}(t) \tag{17}$$

with

$$\underline{y}(t) = \begin{bmatrix} \underline{C}_1 & \underline{C}_2 \end{bmatrix} \begin{bmatrix} \underline{x}_1(t) \\ \underline{x}_2(t) \end{bmatrix} \tag{18}$$

The $\underline{A}$ matrix of Equation (1) has been partitioned into the following sections:

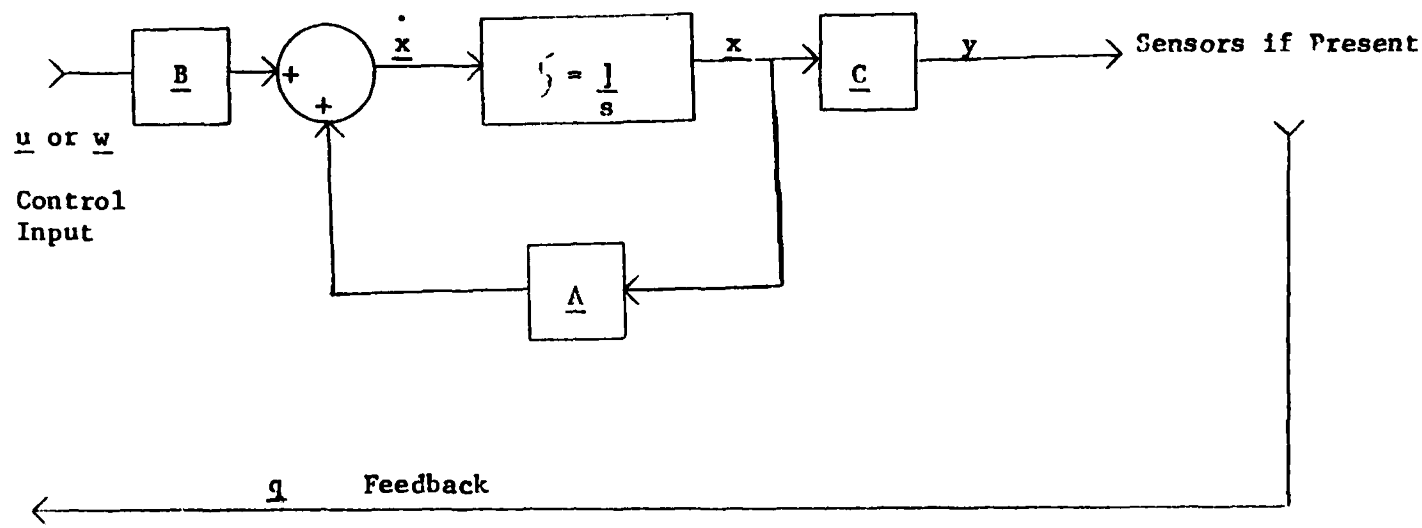

Figure 2. Known/Regular Plant

$\underline{A}_{11}$ $(n-1)x(n-1)$

$\underline{A}_{12}$ $(n-1)x1$

$\underline{A}_{21}$ $1x(n-1)$

$\underline{A}_{22}$ $1x1$

The $\underline{B}$ matrix has been also partitioned as:

$\underline{B}_2$ 1x1 (must have full rank)

with the $\underline{C}$ matrix partitioned as:

$\underline{C}_1$ $1x(n-1)$

$\underline{C}_2$ $1x1$

Note that in these equations, as in all that follow (and also in MULTI), the number of outputs equals the number of inputs, i.e. l=m. Therefore the representation of the matrix partitions uses l only.

Equations (1) and (2) may be put into the format of (17) and (18) with a similarity transformation. This transformation yields the transmission zeros directly, but does not actually have to be performed to apply the design method.

Implementation of the Porter method requires that the plant be controllable ($\underline{A}$,$\underline{B}$ be a controllable pair), and also observable ($\underline{A}$,$\underline{C}$ be an observable pair), along with the requirement that the matrix

$$\begin{bmatrix} \underline{A} & \underline{B} \\ -\underline{C} & \underline{0} \end{bmatrix}$$

have full rank of n+l to ensure controllability using the PI controller.

After these requirements have been satisfied, the next step is to calculate the rank of the first Markov parameter, which is the matrix product $\underline{C}\underline{B}$ ($=\underline{C}_2\ \underline{B}_2$). The choice of which design method to use, either regular or irregular, is based upon the rank of $\underline{C}\underline{B}$. If this rank is less than 1, then the irregular method must be used, while if this rank is equal to 1 then the regular method can be used.

Known/Regular Plant

If the product $\underline{C}\underline{B}$ (or $\underline{C}_2\underline{B}_2$) has full rank, then the plant is considered regular and C B can be inverted, which is a necessary condition to use this method. The control law for the digital controller is given by:

$$\underline{u}(kT)=(1/T)[\underline{K}_0\ \underline{e}(kT)+\underline{K}_1\ \underline{z}(kT)] \tag{19}$$

with

$$\underline{e}(kT)=\underline{v}(kT)-\underline{y}(kT) \tag{20}$$

and

$$\underline{z}[(k+1)T]=\underline{z}(kT)+T\underline{e}(kT) \tag{21}$$

The controller matrices are found:

$$\underline{K}_0=\alpha(\underline{C}_2\underline{B}_2)^{-1}\underline{\Sigma}\epsilon \tag{22}$$

$$\underline{K}_1=(\underline{C}_2\underline{B}_2)^{-1}\underline{\Sigma}\epsilon \tag{23}$$

where

$$\underline{\Sigma} = \text{diagonal matrix } \{\sigma_1, \sigma_2, \ldots, \sigma_\ell\}$$

constrained by

$$-1<(1-\sigma_i)<1$$

Note that in an actual design, the value of epsilon can be changed to obtain a required range of values for the elements in the controller matrices, and thus the magnitudes of the entries in the sigma matrix can be kept within the required range.

Once again the cascade vector integrator drives the steady state error vector to zero for a constant command input vector, which ensures tracking and disturbance rejection.

As the sampling time T approaches zero the transfer function matrix $\underline{G}(\lambda)$ approaches an asymptotic form:

$$\underline{\Gamma}(\lambda)=\underline{\tilde{\Gamma}}(\lambda)+\underline{\hat{\Gamma}}(\lambda) \tag{24}$$

where

$$\underline{\tilde{\Gamma}}(\lambda)=\underline{C}_0(\lambda\underline{I}_n-\underline{I}_n-T\underline{A}_0)^{-1}\ T\underline{B}_0 \tag{25}$$

$$\underline{\hat{\Gamma}}(\lambda)=(\lambda\underline{I}_\ell-\underline{I}_\ell+\underline{C}_2\underline{B}_2\underline{K}_0)^{-1}\ \underline{C}_2\underline{B}_2\underline{K}_0 \tag{26}$$

with

$$\underline{A}_0=\begin{bmatrix} -\underline{K}_0^{-1}\underline{K}_1 & \underline{0} \\ \underline{A}_{12}\underline{C}_2^{-1}\underline{K}_0^{-1}\underline{K}_1 & \underline{A}_{11}-\underline{A}_{12}\underline{C}_2^{-1}\underline{C}_1 \end{bmatrix} \tag{27}$$

$$\underline{B}_0=\begin{bmatrix} \underline{0} \\ \underline{A}_{12}\underline{C}_2^{-1} \end{bmatrix} \tag{28}$$

$$\underline{C}_0=\begin{bmatrix} \underline{K}_0^{-1}\underline{K}_1 & \underline{0} \end{bmatrix} \tag{29}$$

Equation (25) corresponds to what are called the slow modes and (26) corresponds to what are called the fast modes. Professor Porter shows that as T approaches zero the slow modes become both uncontrollable and unobservable while the fast modes remain both observable and controllable. Consequently, as T approaches zero, the slow modes vanish and the closed loop transfer function becomes:

$$\underline{\Gamma}(\lambda)=\underline{\hat{\Gamma}}(\lambda)=(\lambda\underline{I}_\ell-\underline{I}_\ell+\underline{C}_2\underline{B}_2\underline{K}_0)^{-1}\ \underline{C}_2\underline{B}_2\underline{K}_0 \tag{30}$$

This means that if $\underline{K}_0$ is chosen such that:

$$\underline{C}_2\underline{B}_2\underline{K}_0=\text{diagonal matrix }\{\sigma_1,\sigma_2,\ldots,\sigma_\ell\} \tag{31}$$

then

$$\underline{\Gamma}(\lambda)=\text{diagonal matrix }\{\sigma_1/\lambda-1+\sigma_1,\ \sigma_2/\lambda-1+\sigma_2,\ldots,\sigma_\ell/\lambda-1+\sigma_\ell\} \tag{32}$$

As stated earlier, the fast mode roots and the transmission zeros must lie within the unit circle to ensure stability. The transmission zeros are a subset of the slow modes and are given by:

$$\underline{Z}_t(\lambda)=\{\left|\lambda\underline{I} \quad -\underline{I} \quad -T\underline{A}_{11} +T\underline{A}_{12}\,\underline{C}_2^{-1}\,\underline{C}_1\right|=0\} \tag{33}$$

as long as the state equations are in the form of (17).

From Equation (32) the conclusion drawn is that as T goes to zero decoupling is achieved. However, the requirement that the transmission zeros lie within the unit circle in the z domain may dictate a change in the $\underline{C}$ matrix. This means a redefining of the output variables, which could entail a major change in the approach to the design, since changing $\underline{C}$ must not affect the controllability of the system.

Known/Irregular Plant (Ref 1)

When the product $\underline{C}\underline{B}$ does not have full rank, and thus is not invertible, the plant is called irregular. In this case extra plant output measurements are introduced and incorporated with inner loop compensators. This results in the feedback vector:

$$\underline{w}(t)=\begin{bmatrix}\underline{C}_1+\underline{M}\underline{A}_{11} & \underline{C}_2+\underline{M}\underline{A}_{12}\end{bmatrix}\begin{bmatrix}\underline{x}_1(t)\\ \underline{x}_2(t)\end{bmatrix} \tag{34}$$

$$=\begin{bmatrix}\underline{F}_1 & \underline{F}_2\end{bmatrix}\begin{bmatrix}\underline{x}_1(t)\\ \underline{x}_2(t)\end{bmatrix} \tag{35}$$

with

$\underline{M}$ 1x(n-1)

$\underline{F}_1$ 1x(n-1)

$\underline{F}_2$ 1x1

which is shown in Figure 3. The choice of the measurement matrix $\underline{M}$ is such that $\underline{F}\underline{B} = \underline{F}_2\underline{B}_2$ has full rank. Basically, the design method for the irregular plant is just like that for the regular plant, with $\underline{F}$ replacing $\underline{C}$. The control law equation for the PI controller is the same as for the regular plant, but the error vector becomes:

$$\underline{e}(kT)=\underline{v}(kT)-\underline{w}(kT) \tag{36}$$

Since

$$\lim_{t\to\infty}[\underline{A}_{11}\,\underline{x}_1(t)+\underline{A}_{12}\,\underline{x}_2(t)]=\underline{0}$$

then

$$\lim_{k\to\infty}\underline{e}(kT)=\lim_{\substack{k\to\infty\\ t\to\infty}}\{\underline{v}(kT)-\underline{y}(kT)-\underline{M}[\underline{A}_{11}\,\underline{x}_1(t)+\underline{A}_{12}\,\underline{x}_2(t)]\}$$

$$=\lim_{k\to\infty}\{\underline{v}(kT)-\underline{y}(kT)\}$$

$$=\underline{0} \tag{37}$$

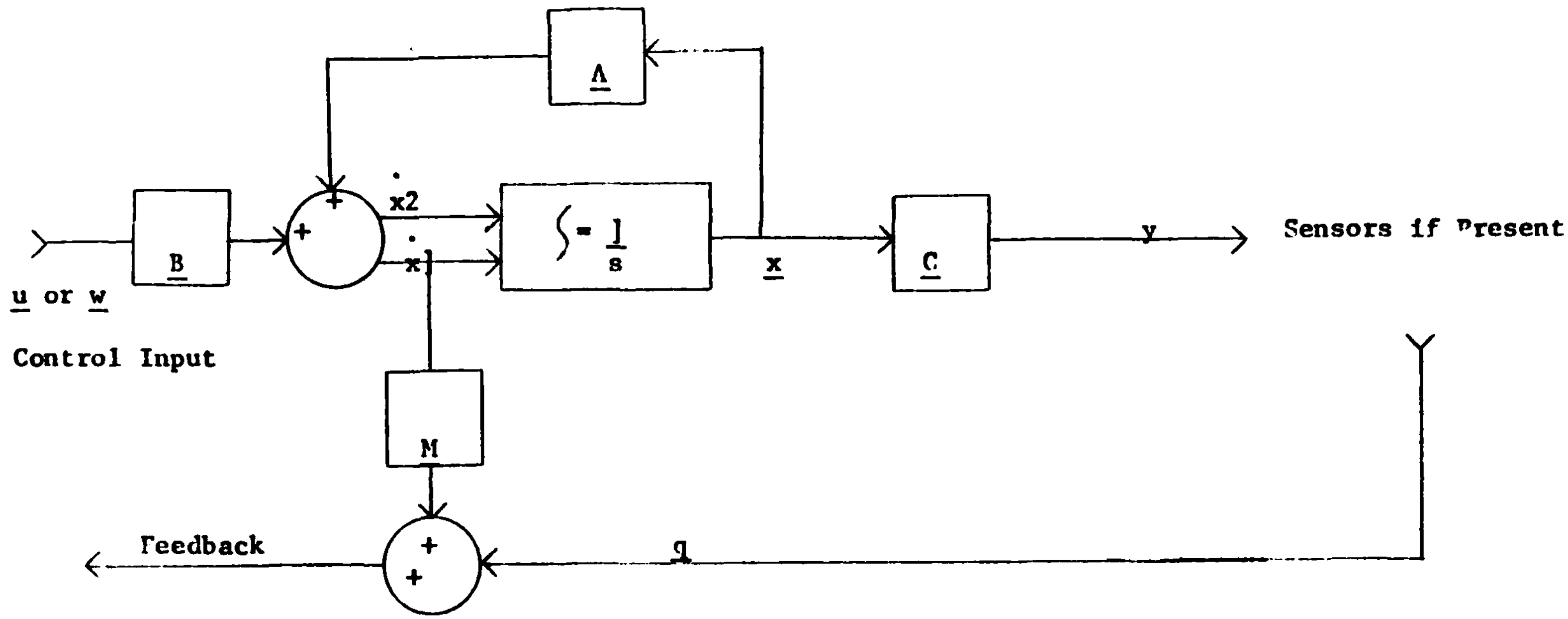

Figure 3. Known/Irregular Plant

Consequently the steady state error vector is zero for a constant command input vector. Once again tracking is achieved.

As in the case of the regular plant, the closed loop transfer function matrix approaches an asymptotic value as the gain 1/T goes to infinity, of:

$$\underline{\Gamma}(\lambda)=\underline{\tilde{\Gamma}}(\lambda)+\underline{\hat{\Gamma}}(\lambda) \tag{38}$$

where

$$\underline{\tilde{\Gamma}}(\lambda)=(\underline{C}_1-\underline{C}_2\underline{F}_2^{-1}\underline{F}_1)(\lambda\underline{I}_{n-\ell}-\underline{I}_{n-\ell}-T\underline{A}_{11}+T\underline{A}_{12}\underline{F}_2^{-1}\underline{F}_1)^{-1}(T\underline{A}_{12}\underline{F}_2^{-1}) \tag{39}$$

$$\underline{\hat{\Gamma}}(\lambda)=\underline{C}_2\underline{F}_2^{-1}(\lambda\underline{I}_\ell-\underline{I}_\ell+\underline{F}_2\underline{B}_2\underline{K}_o)^{-1}\underline{F}_2\underline{B}_2\underline{K}_o \tag{40}$$

Once again the $\underline{\tilde{\Gamma}}(\lambda)$ contains the slow modes and $\underline{\hat{\Gamma}}(\lambda)$ contains the fast modes. The transmission zeros are given by (see equation (33)):

$$\underline{Z}_t(\lambda)=\{\left|\lambda\underline{I}_{n-\ell}-\underline{I}_{n-\ell}-T\underline{A}_{11}+T\underline{A}_{12}\underline{F}_2^{-1}\underline{F}_1\right|=0\} \tag{41}$$

The transmission zeros must lie in the left half side of the s plane or within the unit circle in the z domain.

Unlike the regular plant case, $\underline{\tilde{\Gamma}}(\lambda)$ does not approach zero as the sampling time decreases, so that for the irregular plant both $\underline{\tilde{\Gamma}}(\lambda)$ and $\underline{\hat{\Gamma}}(\lambda)$ must be diagonal for decoupling. The choice of the measurement matrix $\underline{M}$ and the control law matrices $\underline{K}_o$ and $\underline{K}_1$ to achieve decoupling requires that the following conditions be satisfied:

1. $\underline{M}$ is chosen such that $\underline{F}_2$ and $\underline{F}_2\underline{B}_2$ have full rank = l
2. All closed loop poles must lie in the left half plane
3. $\underline{F}_2\underline{B}_2\underline{K}_o=(\underline{C}_2+\underline{M}\underline{A}_{12})\underline{B}_2\underline{K}_o$=diagonal matrix $\{\sigma_1,\sigma_2,\ldots,\sigma_\ell\}$
4. $-1<(1-\sigma_i)<1$ (roots must lie within unit circle)

The standard procedure for the selection of the measurement matrix is finding the sparsest $\underline{M}$ that yields an $\underline{F}_2$ of full rank, while also diagonalizing the product $\underline{C}_2\underline{F}_2^{-1}$. Although this technique is straightforward, it is not always possible to generate a diagonal transfer function matrix $\underline{\Gamma}(\lambda)$.

Another problem with this method is that the possible presence in the output of the modes corresponding to the transmission zeros prevents the output response from being improved beyond a certain point with the reduction of T.

Once the measurement matrix is chosen, then the controller matrices are chosen such that:

$$\underline{K}_0 = \alpha \underline{K}_1 = (\underline{F}_2 \underline{B}_2)^{-1} \operatorname{diag}\{\sigma_1, \sigma_2, \ldots, \sigma_\ell\} \tag{42}$$

$\underline{B}^*$ Design (Ref 1 and 9)

This design technique supplements the other methods when they do not achieve the desired decoupling and/or too much undershoot occurs in the output response. Additionally, under certain conditions the $\underline{B}^*$ matrix can be used to help pick the elements in the $\underline{M}$ matrix, which will be discussed at the end of this section.

The first step is to form the $\underline{B}^*$ matrix using the following formula:

$$\underline{B}^* = \begin{bmatrix} \underline{c}_1^T \underline{A}^{d_1} \underline{B} \\ \underline{c}_2^T \underline{A}^{d_2} \underline{B} \\ \vdots \\ \underline{c}_\ell^T \underline{A}^{d_\ell} \underline{B} \end{bmatrix} \tag{43}$$

where $\underline{c}_i$ is the ith row of $\underline{C}$, and d_i is the smallest integer such that the ith row of $\underline{B}^*$ contains at least one non-zero element. If, however, there is no value for d_i that yields a row not equal to all zeros, then $d_i = n-1$ and the ith row of $\underline{B}^*$ is set to all zeros. When this happens $\underline{B}^*$ is not of full rank and this method cannot be used. However, under certain constraints another approach can be used and is discussed in the last paragraph of this section.

When $\underline{B}^*$ has full rank the controller matrices can be determined from:

$$\underline{K}_0 = \underline{B}^{*-1} \underline{\Sigma}_1 \tag{44}$$

$$\underline{K}_1 = \underline{G}(0)^{-1} \underline{\Sigma}_2 \tag{45}$$

where $\underline{\Sigma}_1$ and $\underline{\Sigma}_2$ are diagonal lxl matrices chosen by the designer, based on the concepts that $\underline{\Sigma}_1$ controls the initial output response and $\underline{\Sigma}_2$ affects the steady-state response. As with the other methods the control law equations are:

$$\underline{u}(kT) = (1/T)\ [\underline{K}_0 \underline{e}(kT) + \underline{K}_1 \underline{z}(kT)] \tag{46}$$

and

$$\underline{e}(kT) = \underline{v}(kT) - \underline{y}(kT) \tag{47}$$

If $\underline{B}^*$ is singular, the above method cannot be used, but there is another possibility. If the row dimension of the $\underline{C}$ matrix (Equation (18)) is greater than the row dimension of $\underline{A}_{11}$ (Equation (17)), then $\underline{B}^*$ can be used to help pick the elements in the $\underline{M}$ matrix (using the irregular plant method). When using this approach, the $\underline{B}^*$ matrix must be formed by using

$$\underline{C} = \underline{C}_1$$

$$\underline{A} = \underline{A}_{11}$$

$$\underline{B} = \underline{A}_{12}$$

in Equation (43).

The technique is continued by forming:

$$\underline{F}_2 = \underline{C}_2 + \underline{M}\underline{A}_{12}$$

and assigning values to those entries in $\underline{F}_2$ that correspond to the non-zero elements of $\underline{B}^*$. The design is continued along the lines of the irregular plant method, with further refinement of $\underline{M}$ based upon the fact that $\underline{C}_2\underline{F}_2$ must be diagonal, $\underline{F}_2$ must have full rank and $\underline{M}$ should be as sparse as possible.

Summary

The design methods presented in this chapter form the basis for the Porter method, as developed by Professor Brian Porter and his associates. The computer program MULTI incorporates these concepts into an interactive tool used to design controllers such as those designed for this thesis. Although the presentation in this chapter specified digital PI controllers, since that is how MULTI is written, Professor Porter's publications include similar design techniques for analog controllers.

CHAPTER III

FPCC AIRCRAFT/SIMULATION PROGRAM DESCRIPTION

Introduction

This thesis designs controllers for the FPCC aircraft, an aircaft which exists in concept only. This "paper airplane" was conceived through the combined efforts of Lockheed, Pratt and Whitney, and Honeywell. FPCC designates Flight Propulsion Control Coupling, which summarizes the most striking feature of this plane, the ability to vector thrust with the jet flaps. This capability, taken with the other flight control surfaces, increases the control vector's dimensions, allowing for more commanded quantities in the input vector.

The contractors developed the model and simulation program between June 1976 and June 1977. At that time the techniques developed by Professor Porter had not yet been published, and the Air Force was not involved in designing aircraft flight control systems for aircraft capable of decoupled six degree of freedom maneuvers. But the FPCC aircraft was designed with the extra flight control surfaces needed for such maneuvers, so that as the Air Force developed an interest in decoupled maneuvers the FPCC became a logical plane to test the ideas on. In keeping with the concept of using the FPCC to test the Porter method of controller design, this thesis extends the work of Jon Bauschlicher (Ref 2), continuing to use the maneuvers similar to those currently being tested on the AFTI F-16 aircraft. Additional information on the FPCC aircraft can be found in References 4 and 10.

Aircraft Description

Figure 4 shows the FPCC aircraft. This aircraft is a single seat supersonic fighter with a primary mission of air superiority fighter, and a secondary mission of ground attack. The airframe has the following dimensions:

Aircraft Length = 60.0 ft

Wing Span (B) = 54.25 ft

Wing Mean Aerodynamic Chord = 14.00 ft

Wing Planform Area (S) = 654.00 ft

Aspect Ratio (B*B/S) = 4.50

Takeoff Mass = 1055.9 slugs

Maneuver Mass = 900.62 slugs

Maximum Angle of Attack = +23 degrees

Minimum Angle of Attack = -11.5 degrees

The FPCC has standard flight control surfaces in aileron and rudder, along with non-standard surfaces in its horizontal and vertical canards and maneuver and jet flaps. The vertical canards along with the rudder give the FPCC the opposing lateral moments which, when combined with the aileron, allow decoupled lateral maneuvers. Likewise, the jet flaps, maneuver flaps, and horizontal canards supply the opposing longitudinal moments necessary to perform decoupled longitudinal maneuvers. There are no elevators.

Table I shows a summary of the FPCC aircraft design guidelines and constraints, and Table II shows the control surface limits along with the actuator and sensor dynamics for the control surfaces. Note that although these are the same actuator

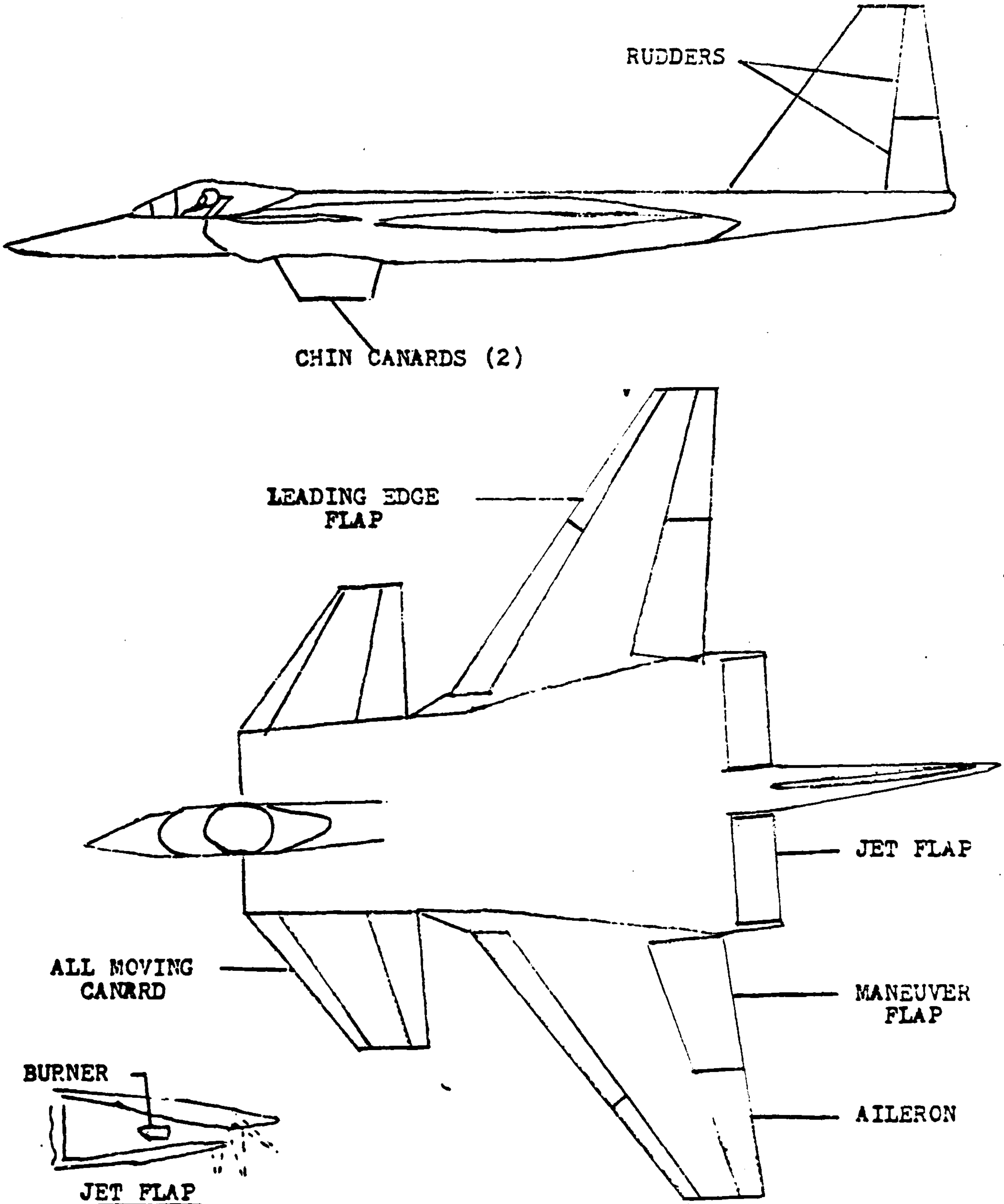

FIGURE 4. FPCC Aircraft

TABLE I

SUMMARY LISTING OF INITIAL FPCC REFERENCE AIRCRAFT POINT DESIGN GUIDELINES AND CONSTRAINTS (REF 2)

1. Primary aircraft design mission -- supersonic/transonic air superiority

   Secondary aircraft design mission -- transonic close air support

   Aircraft dash speed capability -- within the range of Mach 2.2 through 3.0

2. Advanced CTOL or STOL design emphasizing air combat maneuvering and air combat tracking requirements for high subsonic/transonic air-to-air and air-to-ground tasks

3. Mission range, payload, takeoff and landing distance requirements are to be considered of secondary importance

4. Aircraft and propulsion design not constrained to any specification except for those noted in the RFP Statement of Work

5. Flight control designs may include any advanced feature such as Relaxed Static Stability (RSS) and Direct Side Force Control (DSFC)

6. Aircraft design may include modulatory type Aerodynamic/Propulsive Interactive Force (APIF) systems

7. Digital control and fly-by-wire assumed

8. The supersonic engine air inlet shall be of the external or mixed compression type consistent with the selected aircraft dash speed Mach number. Inlet bypass air may be used for aircraft maneuvering augmentation

9. Aircraft design thrust to weight (T/W) ratio shall be higher than 1.0 with dry engine operation. However, engines shall incorporate afterburning. Engine control may include

   - variable fan guide vane angle
   - variable compressor stator angle
   - variable turbine area
   - variable exhaust nozzle area

   Engine bleed capabilities may be considered consistent with APIF system

10. The Lockheed reference aircraft point design will incorporate the current state of the art Pratt and Whitney aircraft F-100-PW-100 afterburning turbofan engine and controls

dynamics used in the program MULTI, these are not the same sensor dynamics. MULTI sensors refer to the sensors used to sense the aircraft states, not the flight control surfaces. The only possible overlap for this aircraft would be if the total thrust were used as both a flight control and a state.

The original design for the aircraft stipulated that the jet flaps would be limited to only positive deflection (trailing edge down) of 0 to 90 degrees, and also restricted the maneuver flaps to $\pm$ 15 degrees. Jon Bauschlicher had the simulation program changed to reflect the values listed for these control surfaces in Table II, and this author has let this modification stand.

More detailed information about the workings of the control surfaces is found in the next section on the simulation program.

FPCC Aircraft Simulation Program

In effect, the simulation program is the aircraft. All of the control surface limits depicted in Table II are set within the program, as are the actual implementations of these surfaces. The current version of the program deflects the ailerons and rudder in the standard manner (ailerons together in opposite directions), and deflects the maneuver flaps, the horizontal canards, the vertical canards, and the jet flaps symmetrically. The program allows asymmetric thrust, but this feature is not used in this thesis.

All of the matrices used in this thesis are generated by the simulation program, as are the initial state vectors. The simulation program is available from the Flight Dynamics Lab at Wright-Patterson Air Force Base, and was developed by Lockheed

TABLE II

CONTROL SURFACE LIMITS AND DYNAMICS

Control Surface	Deflection M<1.0	Limits M>1.0	Servo Dynamics	Sensor Dynamics
Maneuver Flap (δ_{MF})	$\pm 30°$	$\pm 15°$	$\frac{25}{s+25}$	$\frac{100}{s+100}$
Jet Flap (δ_j)	$\pm 90°$	$\pm 90°$	$\frac{25}{s+25}$	$\frac{100}{s+100}$
Horizontal Canard (δ_{HC})	$\pm 20°$	$\pm 10°$	$\frac{25}{s+25}$	$\frac{100}{s+100}$
Thrust (F_{TOT})	-	-	$\frac{0.574}{s+0.574}$	$\frac{100}{s+100}$
Aileron (δ_a)	$\pm 20°$ (per side)	$\pm 20°$ (per side)	$\frac{25}{s+25}$	$\frac{100}{s+100}$
Rudder (δ_r)	$\pm 30°$	$\pm 15°$	$\frac{25}{s+25}$	$\frac{100}{s+100}$
Vertical Canard (δ_{VC})	$\pm 35°$	$\pm 15°$	$\frac{25}{s+25}$	$\frac{100}{s+100}$

under contract to the Air Force. Running in batch mode, the program outputs the data used for this thesis in the form of Equations (48) and (49).

$$
\begin{bmatrix} \dot{p} \\ \dot{r} \\ \dot{v} \\ \dot{\phi} \\ \dot{\psi} \\ \dot{y} \\ \dot{q} \\ \dot{w} \\ \dot{u} \\ \dot{\theta} \\ \dot{h} \\ \dot{x} \end{bmatrix}
=
\begin{bmatrix}
-.696 & .364 & -.00818 & 0 & 0 & 0 & 0 & 0 & 0 & 0 & 0 & 0 \\
.0654 & -.212 & .00415 & 0 & 0 & 0 & 0 & 0 & 0 & 0 & 0 & 0 \\
31.5 & -164 & -.172 & 31.6 & 0 & 0 & 0 & 0 & 0 & 0 & 0 & 0 \\
1 & .19 & 0 & 0 & 0 & 0 & 0 & 0 & 0 & 0 & 0 & 0 \\
0 & 1 & 0 & 0 & 0 & 0 & 0 & 0 & 0 & 0 & 0 & 0 \\
0 & 0 & 1 & -31.3 & 167 & 0 & 0 & 0 & 0 & 0 & 0 & 0 \\
0 & 0 & 0 & 0 & 0 & 0 & -.103 & .0134 & -.000156 & 0 & .00000326 & .00000325 \\
0 & 0 & 0 & 0 & 0 & 0 & 166 & -.638 & -.215 & -6.01 & -.000410 & -.000415 \\
0 & 0 & 0 & 0 & 0 & 0 & -31.5 & .0867 & -.0214 & -31.6 & .0000443 & .00000935 \\
0 & 0 & 0 & 0 & 0 & 0 & 1 & 0 & 0 & 0 & 0 & 0 \\
0 & 0 & 0 & 0 & 0 & 0 & 0 & -.982 & .187 & 167 & 0 & 0 \\
0 & 0 & 0 & 0 & 0 & 0 & 0 & .187 & .982 & 0 & 0 & 0
\end{bmatrix}
\begin{bmatrix} p \\ r \\ v \\ \phi \\ \psi \\ y \\ q \\ w \\ u \\ \theta \\ h \\ x \end{bmatrix}
+
$$

$$
\begin{bmatrix}
0.0122 & 0 & 0 & .0118 & -.00212 & .00939 & .0000322 & -.0000322 & -.0605 & .0605 \\
0.00114 & 0 & 0 & -.0112 & .00220 & -.000238 & .0000288 & -.0000288 & -.644 & .644 \\
0 & 0 & 0 & .111 & .0363 & 0 & 0 & 0 & 0 & 0 \\
0 & 0 & 0 & 0 & 0 & 0 & 0 & 0 & 0 & 0 \\
0 & 0 & 0 & 0 & 0 & 0 & 0 & 0 & 0 & 0 \\
0 & 0 & 0 & 0 & 0 & 0 & 0 & 0 & 0 & 0 \\
0 & .0390 & 0 & 0 & 0 & -.00908 & -.0000298 & -.0000298 & -24.2 & -24.2 \\
0 & -.111 & 0 & 0 & 0 & -.118 & -.000367 & -.000367 & 0 & 0 \\
0 & -.0765 & 0 & 0 & 0 & -.0211 & .00105 & .00105 & 0 & 0 \\
0 & 0 & 0 & 0 & 0 & 0 & 0 & 0 & 0 & 0 \\
0 & 0 & 0 & 0 & 0 & 0 & 0 & 0 & 0 & 0 \\
0 & 0 & 0 & 0 & 0 & 0 & 0 & 0 & 0 & 0
\end{bmatrix}
\begin{bmatrix}
\delta_a \\ \delta_c \\ \delta_{mf} \\ \delta_r \\ \delta_{vc} \\ \delta_j \\ F_1 \\ F_2 \\ CDI_1 \\ CDI_2
\end{bmatrix}
\qquad (48)
$$

The output equation is

$$
\begin{bmatrix} \alpha \\ \beta \\ VEL \\ ACGX \\ ACGY \\ ACGZ \end{bmatrix}
=
\begin{bmatrix}
0 & 0 & 0 & 0 & 0 & 0 & 0 & .00585 & -.00112 & 0 & 0 & 0 \\
0 & 0 & .00598 & 0 & 0 & 0 & 0 & 0 & 0 & 0 & 0 & 0 \\
0 & 0 & 0 & 0 & 0 & 0 & 0 & .187 & .982 & 0 & 0 & 0 \\
0 & 0 & 0 & 0 & 0 & 0 & -.154 & .0867 & -.0214 & 0 & .0000443 & .00000935 \\
.125 & 1.02 & -.172 & 0 & 0 & 0 & 0 & 0 & 0 & 0 & 0 & 0 \\
0 & 0 & 0 & 0 & 0 & 0 & .937 & -.638 & -.215 & 0 & -.000410 & -.000415
\end{bmatrix}
\begin{bmatrix} p \\ r \\ v \\ \phi \\ \psi \\ y \\ q \\ w \\ u \\ \theta \\ h \\ x \end{bmatrix}
+
\begin{bmatrix}
0 & 0 & 0 & 0 & 0 & 0 & 0 & 0 & 0 & 0 \\
0 & 0 & 0 & 0 & 0 & 0 & 0 & 0 & 0 & 0 \\
0 & 0 & 0 & 0 & 0 & 0 & 0 & 0 & 0 & 0 \\
0 & -.0765 & 0 & 0 & 0 & -.0211 & .00105 & .00105 & -24.2 & -24.2 \\
0 & 0 & 0 & .111 & .0363 & 0 & 0 & 0 & 0 & 0 \\
0 & -.111 & 0 & 0 & 0 & -.118 & -.000367 & -.000367 & 0 & 0
\end{bmatrix}
\begin{bmatrix} \delta_a \\ \delta_c \\ \delta_{mf} \\ \delta_r \\ \delta_{vc} \\ \delta_j \\ F_1 \\ F_2 \\ CDI_1 \\ CDI_2 \end{bmatrix}
\qquad (49)
$$

Note that these equations contain the output for the trim condition of 0.15 mach at sea level, which is the first flight condition used. Tables III and IV show the input and state vectors, which are basically the same as those used in this thesis, while Table V list the output vector which is not the same as used in this thesis. While the simulation program generates data that is used for the controller design, the form of the matrix equations is changed slightly.

The simulation program actually trims the aircraft given a mach number, altitude, and settings for the maneuver flaps and jet flaps. The plane is then trimmed using the horizontal canards and the thrust. The ailerons, vertical canards, and the rudder are not deflected. Trimming is successful only if the limits on the flight control surfaces, thrust, and angle of at-

TABLE III

INPUT VECTOR, $\underline{u}$*

Variable	Units	Description
δa	deg	sum of both aileron deflections
δc	deg	horizontal canard deflection
δmf	deg	maneuver flap deflection
δr	deg	rudder deflection
δvc	deg	vertical canard deflection
δJ	deg	Jet flap deflection WRT fuselage ref line
F_1	lbs	Net thrust engine 1
F_2	lbs	Net thrust engine 2
CDI_1	-	Inlet drag coefficient engine 1
CDI_2	-	Inlet drag coefficient engine 2

TABLE IV

STATE VECTOR, $\underline{x}$*

Variable	Units	Description
p	rad/sec	Body axis roll rate
r	rad/sec	Body axis yaw rate
v	ft/sec	Body axis side velocity
ϕ	rad	Roll angle
ψ	rad	Yaw angle
y	ft	Cross-range position reference to initial body axis
q	rad/sec	Body axis pitch rate
w	ft/sec	Body axis vertical velocity
u	ft/sec	Body axis forward velocity
θ	rad	Pitch angle
h	ft	Altitude
x	ft	Down-range position referenced to initial body axis

TABLE V

OUTPUT VECTOR, $\underline{y}$*

Variable	Units	Description
α	rad	Angle-of-attack
β	rad	Sideslip angle
VEL	ft/sec	Total airspeed
ACGX	ft/sec^2	Accel. of c.g. along x-body axis
ACGY	ft/sec^2	Accel. of c.g. along y-body axis
ACGZ	ft/sec^2	Accel. of c.g. along z-body axis

tack are not exceeded. The flight conditions used in this thesis are:

1). 0.15 mach, 0 ft altitude

2). 0.60 mach, 0 ft altitude

3). 0.90 mach, 30,000 ft altitude

Since the first condition represents a landing configuration, the angle of attack is restricted for pilot visibility of the runway. The simulation program trimmed the aircraft to 11 degrees angle of attack with the maneuver flaps set for +25 degrees and the jet flaps set at +15 degrees, and the horizontal canard trimmed to +0.5 degrees.

The second flight condition represents a possible ground attack mode, high subsonic speed at low altitude. The third flight condition is a candidate for aerial combat, just below supersonic at high altitude.

Table VI shows the results of several different flight conditions run on the FPCC simulation program. These conditions were tested to observe the interaction between the trimmed angle of attack, horizontal canard setting, thrust, and the given settings of maneuver flaps and jet flaps at low speeds at sea level.

Table VI clearly shows the relationship between the angle of attack and the jet flap setting as slow speeds. However, to counter the moment caused by a large jet flap setting, the horizontal canards must be deflected possibly beyond their limits. To offset this drawback, the horizontal canards need more effectiveness, perhaps through increased area. This would allow for a smaller angle of attack at even slower airspeeds than used in this thesis, thus permitting a more STOL-like operation.

The values in Table VI often exceed the limits listed in Table II because the simulation program does not actually impose

TABLE VI

FPCC AIRCRAFT RESPONSE AT SEA LEVEL

Mach #	α	δ_c	δ_{mf}	δ_J	F_{TOT}
0.10*	65.62	-17.18	30	0	16,668
0.10*	57.81	- 1.79	30	10	15,564
0.10*	51.42	5.36	30	15	15,366
0.10*	44.22	12.34	30	20	15,296
0.10	33.04	27.16	0	30	16,586
0.10*	30.17	25.49	30	30	15,210
0.10*	10.39	74.00	30	60	16,504
0.15*	13.44	- 9.20	30	0	8,826
0.15	13.44	- 9.20	15	0	8,826
0.15*	11.48	- 2.52	30	10	7,730
0.15*	10.78	0.51	30	15	7,468
0.15*	10.78	0.51	25	15	7,468
0.20	5.92	- 2.31	15	0	6,846
0.20*	5.92	- 2.31	30	0	6,846
0.20*	4.84	2.07	30	10	6,702
0.20*	4.30	4.26	30	15	6,884

* Represents a flight condition with a column of all zeros in the B matrix corresponding to the maneuver flaps.

these limits on the aircraft during trimming. However, the program indicates whenever the limits have been exceeded, and then continues with the generation of the linear dynamics matrices.

Several of the flight conditions yield B matrices that have a column of zeros in the column corresponding to the manuever flaps. If the program is correct in generating these zeros, then the maneuver flaps have no effect (for small pertubations) at these flight conditions. This is the case for the flight condition at 0.15 mach used in this thesis, which is why the maneuver flaps are removed from the longitudinal model (Chapter IV). However, since the simulation program seems to be erroneous in certain other entries within the $\underline{B}$ matrix (Appendix A), then suspicion has to fall on all of the $\underline{B}$ matrix, including these columns of zeros. The position taken for this thesis is that these columns of zeros are correct, and the longitudinal model adjusted accordingly. This position resulted more from a lack of time to prove otherwise, than any other consideration.

An interesting aside is that STOL operation at very slow speeds is going to require large amounts of thrust, which may not be a desirable trait.

This thesis assumes that the maximum combined thrust is 30,000 pounds, based upon the specification of at least a 1.0 thrust to weight ratio and the weight of the aircraft.

CHAPTER IV

CONTROLLER DESIGN

Introduction

This chapter details the design of a complete controller for combined lateral and longitudinal maneuvers for the STOL like flight condition (0.15 mach, sea level), along with longitudinal controllers for two other flight conditions (0.6 mach, sea level and 0.9 mach, 30,000 ft.). The 0.15 mach flight condition has not previously been studied, but the other two have been (Ref 2). However, this thesis uses a different longitudinal model than any previous efforts (Ref 2 and 3), which led to the redesigning of the longitudinal controllers at the 0.6 and 0.9 mach flight conditions.

The change in the longitudinal model results from a forced change at the 0.15 mach flight condition which is then carried over to the other two flight conditions. This forced change results from a column of zeros in the $\underline{B}$ matrix at 0.15 mach corresponding to the maneuver flaps (Equation (48)). If this column of zeros is correct, then that means that the maneuver flaps have no effect upon the motion of the aircraft (for small pertubations) at this flight condition. Unfortunately, since the aircraft does not exist, there is no way to verify this. Considering that there are at least two other errors in this same $\underline{B}$ matrix (Appendix A), this column of zeros would have to be considered suspect. This thesis is based upon the idea of using just three of the longitudinal flight control surfaces to execute the maneuvers, and the decision to leave out the maneuver flaps was based upon this column of zeros. If this zero column were erroneous, the impact on these results would be minimal.

Since the maneuver flaps have no apparent effect at 0.15 mach, they can be eliminated from the longitudinal model for the purposes of performing the maneuvers. However, the maneuver flaps are needed to trim the aircraft, since without them the low angle of attack needed for landing would not be possible. Based on these considerations, it was decided to model the aircraft as using the maneuver flaps for trimming only and not using them for any of the maneuvers. Since this was contrary to previous efforts, the 0.6 mach and 0.9 mach flight conditions from Bauschlicher's thesis were reaccomplished using this new longitudinal model. This would allow comparisons between the different longitudinal models, along with drawing conclusions as to which model generates the best aircraft performance. Unfortunately, a design for the 2.3 mach flight condition was not found. Part of the reason for this was the limited time available to the author, but there had to be other reasons also, since the other designs were accomplished in a relatively short time compared to the time spent attempting to find a controller for 2.3 mach. One of the reasons might be the fact that the eigenvalues of the system $\underline{A}$ matrix for 2.3 mach are different than the other flight conditions. As stated later in this chapter, the short period roots for all of the flight conditions consist of two real roots, one in the left half s plane and one in the right half s plane. In fact, the short period roots for the 2.3 mach flight condition are very nearly identical to those for the 0.9 mach flight condition. The phugoid roots for 2.3 mach, however, have become real with both lying in the left half s plane. This is the only flight condition studied for which this occurs.

The design of a complete 12 state combined lateral and longitudinal controller would be beyond the capabilities of MULTI (currently limited to 10 states), and perhaps the author also. Consequently, the design is broken down into two parts, the longitudinal and lateral modes. After the lateral and longitudinal controllers are designed and tested independently, the lateral and longitudinal models are combined and a combined controller is then tested based on the combination of the separate controllers. The combined controller is tested using one coupled maneuver, to verify that lateral and longitudinal commands can be executed simultaneously. Although this phase is simplified by the decoupled nature of the original equations of motion (as represented by the matrices in equations (48) and (49)), the procedure should still be the same if the equations were not decoupled.

The computer program MULTI is used extensively in the design of the controllers for this thesis, and is the sole tool used to test the designs via simulation. MULTI was originally written by AFIT students in 1981 and was based upon a simulation program written by Professor Brain Porter (Ref 7). The program has undergone many alterations since then, including the addition of an option to calculate and display the figures of merit, and passing of the input data local filenames thru command line arguments into the program. Both were written by this author and detailed in Appendix C. Appendix D lists the addition of program code that would allow faster design times for the experienced MULTI user, and would also allow the true implementation of a $\underline{D}$ feedforward matrix. Although MULTI currently asks for a $\underline{D}$ matrix, the simulation does not include a $\underline{D}$ matrix in the calculations of the output used for feedback. A complete description of MULTI and its options can be obtained from the AFIT Electrical Engineering Department.

This chapter contains the design and testing of the separate lateral and longitudinal controllers for the 0.15 mach, sea level flight condition, along with the longitudinal controllers for the 0.6 mach, sea level and 0.9 mach, 30,000 ft. flight conditions. The approach used for each flight condition is that the controller designed will be used for all of the maneuvers, instead of trying to find a different, possibly more optimized controller for each maneuver. Finally, the lateral and longitudinal controllers for the 0.15 mach flight condition are combined and tested with one coupled lateral/longitudinal maneuver. Chapter V investigates using one controller for all of the flight conditions and the effect of delaying the control input to the actuators.

Lateral Controller

The lateral controller design is accomplished only for the first flight condition, 0.15 mach, sea level. The lateral controllers for the other flight conditions used in this thesis can be found in Bauschlicher's thesis (Ref 2).

Manuever Descriptions. Four maneuvers are used in

Bauschlicher's thesis to test the lateral controller, the flat turn, yaw pointing, horizontal translation, and the rollover. The same four maneuvers were attempted at 0.15 mach with the controller designed for this thesis, with the result that the rollover could not be performed at all. This is probably due to the very slow speed of the aircraft and subsequent lack of aerodynamic forces exerted on the flight control surfaces. Consequently, only the first three maneuvers, the flat turn, yaw pointing, and horizontal translation, are tested in this thesis.

The flat turn maneuver is commanded by deciding on what g forces are desired in the xy plane (body axes), and calculating the necessary yaw rate from:

$$Ay = w^2 * d/2 = U * r \tag{50}$$

where

Ay = acceleration in xy plane

w = r (body yaw rate)

$w*d/2$ = U (body velocity)

and with d/2 used instead of r for radius. The body axis side velocity v is commanded to zero, along with the euler roll angle ϕ. Henceforth, all coordinate systems are body axis, except for the euler angles, θ (pitch), Ψ (yaw), ϕ (roll).

Yaw pointing is accomplished by deciding upon the angle of pointing desired, then commanding the sideslip angle β to that value via the relationship

$$\beta = v/U \tag{51}$$

which is good for small values of sideslip. Roll angle is commanded to zero, and the command for r is based upon a curve whose integral (area under curve) will be equal to the sideslip angle. Note that an angle of less than 10 degrees insures an error of less than one percent in equation (51).

Horizontal translation consists of commanding the side velocity v depending upon desired g forces, while commanding both roll angle and yaw rate to zero.

Although the rollover maneuver is not tested in this thesis, it is performed by commanding both yaw rate and side velocity to zero while commanding the desired roll angle.

Lateral Model. These sections detailing the design of the lateral model and controller use the flight condition of 0.15 mach at sea level for the numerical examples to illustrate the procedure. The same techniques are used to develop the model and controllers for the other two flight conditions, with the actual matrices used listed in Appendix D.

The first step is to reduce the system model from its current form of equation (48). The six lateral states are p, r, v, y, ϕ, and Ψ. The lateral inputs are δa, δr, δvc, F_1, F_2, CDI_1, and CDI_2. To reduce the number of states without eliminating crucial information about the aircraft, the eigenvalues can be used. The complete set of eigenvalues for the lateral model of equation (48) are:

-0.1990 $\pm$j 0.9563 (dutch roll roots)

-0.6927 (roll subsidence)

0.01069 (spiral divergence)

$\pm$ 0.1471 E-06

The two roots near zero contain no essential aircraft information and so can be eliminated from the model. Based on previous experience, the choice is made to eliminate y and from the state model. Computing the eigenvalues of this new four state A matrix yields:

$-0.1990 \pm j\ 0.9563$

-0.6927

0.01069

and the important aircraft characteristics have been preserved.

Now that the state model has been reduced to four states, the inputs are going to have to be reduced to at most three (and still have the correct form for an irregular design). This is done by observing that the columns in the $\underline{B}$ matrix corresponding to F_1 and F_2 have equal and opposite values (in the lateral part of the $\underline{B}$ matrix). This means that as long as the two engines generate equal thrust these terms cancel out to zero, having no effect on the model. Likewise, since the terms corresponding to the two coefficients of drag for the inlets are also equal and opposite, they have no effect with equal thrust in the two engines. This reduces the inputs to three for the lateral model, δa, δr, and δvc. This model is satisfactory as long as the two engines produce the same thrust. Imposing this constraint would require extra circuitry in addition to the controller. Quite possibly, this constraint on the thrust would be valid even without any additional engine control.

The choice of the three outputs, v, ϕ, and r, is dictated by Bauschlicher's thesis, since one of the purposes of this thesis is to compare results with Bauschlicher. This choice of outputs satisfies the requirement for the number of inputs to equal the number of outputs. These outputs result in completely different output matrices than those in equation (49). Since there are no accelerations in the output, there is no feedforward matrix, and the $\underline{C}$ matrix is also different from equation (49).

These changes result in a new set of matrices describing the linear dynamics of the aircraft and are given by:

$$\begin{bmatrix} \dot{\phi} \\ \dot{v} \\ \dot{r} \\ \dot{p} \end{bmatrix} = \begin{bmatrix} 0 & 0 & .19 & 1 \\ 31.6 & -.172 & -164 & 31.5 \\ 0 & .00415 & -.212 & .0654 \\ 0 & -.00818 & .364 & -.696 \end{bmatrix} \begin{bmatrix} \phi \\ v \\ r \\ p \end{bmatrix} + \begin{bmatrix} 0 & 0 & 0 \\ 0 & .111 & .0363 \\ .00114 & -.0112 & .0022 \\ .0122 & .0118 & -.00212 \end{bmatrix} \begin{bmatrix} \delta_a \\ \delta_r \\ \delta_{vc} \end{bmatrix} \tag{52}$$

$$\begin{bmatrix} v \\ \phi \\ r \end{bmatrix} = \begin{bmatrix} 0 & 1 & 0 & 0 \\ 1 & 0 & 0 & 0 \\ 0 & 0 & 1 & 0 \end{bmatrix} \begin{bmatrix} \phi \\ v \\ r \\ p \end{bmatrix} \tag{53}$$

The above set of equations represents the lateral model for the FPCC aircraft at 0.15 mach at sea level. This system is checked for decoupling zeros, and since there aren't any it is both controllable and observable, two necessary requirements. Although Bauschlicher stated that the transmission zeros must also lie in the left half plane, this test is performed on the system with $\underline{F}$ $(=[\underline{C}_1 + \underline{M}\underline{A}_{11}][\underline{C}_2 + \underline{M}\underline{A}_{12}])$ substituted for $\underline{C}$. Making this substitution and then checking for transmission zeros yields none in the right half plane, another requirement. (Although it may be possible to design with transmission zeros at the origin).

Since the first Markov parameter (see Chapter II) $\underline{CB} = \underline{C}_{1}\underline{B}_{2}$ does not have full rank of 1, the design is irregular. Consequently, an $\underline{M}$ matrix must be found which meets the requirements specified in Chapter II. This measurement matrix supplies information to the feedback loop on the derivative of ϕ, which is not necessarily equal to the roll rate. The following section details the development of the $\underline{M}$ matrix.

<u>Measurement Matrix Determination</u>. The first step is partitioning the matrices of equations (52) and (53) so the methods of Chapter II can be used to find the $\underline{B}^*$ matrix. The partitioned matrices used in equation (43) are:

$$\underline{C} = \underline{C}_1 = \begin{bmatrix} 0 \\ 1 \\ 0 \end{bmatrix} \tag{54}$$

$$\underline{A} = \underline{A}_{11} = [0] \tag{55}$$

$$\underline{B} = \underline{A}_{12} = [0 \quad 0.19 \quad 1] \tag{56}$$

The resulting B* matrix is found to be:

$$\underline{B}^* = \begin{bmatrix} 0 & 0 & 0 \\ 0 & 0.19 & 1 \\ 0 & 0 & 0 \end{bmatrix} \tag{57}$$

with $\{d_1, d_2, d_3,\} = \{3,0,3\}$ as used in equation (43).

Next, the measurement matrix $\underline{M}$ must be found, so that $\underline{F}_2$ can be calculated. Since the dimensions of $\underline{M}$ are 1x(n-1), which for this system is 3x1, $\underline{M}$ can be generalized as:

$$\underline{M} = \begin{bmatrix} m_1 \\ m_2 \\ m_3 \end{bmatrix} \tag{58}$$

Using $\underline{F}_2 = \underline{C}_2 + \underline{M}\underline{A}_{12}$ and

$$\underline{C}_2 = \begin{bmatrix} 1 & 0 & 0 \\ 0 & 0 & 0 \\ 0 & 1 & 0 \end{bmatrix} \tag{59}$$

yields

$$\underline{F}_2 = \begin{bmatrix} 1 & 0.19m_1 & m_1 \\ 0 & 0.19m_2 & m_2 \\ 0 & 1+0.19m_3 & m_3 \end{bmatrix} \tag{60}$$

Since the rank of F must be equal to 1, or three, and the allowable non zero elements of $\underline{F}_2$ (due to $\underline{M}$) must have a corresponding non zero element in $\underline{B}^*$, the choice of $\underline{M}$ must be:

$$\underline{M} = \begin{bmatrix} 0 \\ m_2 \\ 0 \end{bmatrix} \tag{61}$$

which yields

$$\underline{F}_2 = \begin{bmatrix} 1 & 0 & 0 \\ 0 & 0.19m_2 & m_2 \\ 0 & 1 & 0 \end{bmatrix} \tag{62}$$

Using the above information the asymptotic transfer function from equation (38) can be derived:

$$\underline{F}_2^{-1} = \begin{bmatrix} 1 & 0 & 0 \\ 0 & 0 & 1 \\ 0 & 1/m & -0.19 \end{bmatrix}$$

$$\underline{C}_2\underline{F}_2^{-1} = \begin{bmatrix} 1 & 0 & 0 \\ 0 & 0 & 0 \\ 0 & 0 & 1 \end{bmatrix}$$

which is in the desired diagonal form.

$$\underline{F}_1 = \underline{C}_1 + \underline{M}\underline{A}_{11} = \underline{C}_1 = \begin{bmatrix} 0 \\ 1 \\ 0 \end{bmatrix}$$

Since $\underline{A}_{11} = [0]$

$$\underline{C}_1 - \underline{C}_2 \underline{F}_2^{-1} \underline{F}_1 = \begin{bmatrix} 0 \\ 1 \\ 0 \end{bmatrix}$$

$$[T\underline{A}_{12}\,\underline{F}_2^{-1}] = [T\,(0\;\; 1/m_2\;\; 0)]$$

$$[\lambda \underline{I}_{n-2} - \underline{I}_{n-2} - T\underline{A}_{11} + T\underline{A}_{12}\,\underline{F}_2^{-1}\,\underline{F}_1]^{-1} = [\lambda - 1 + T/m_2]^{-1}$$

$$= [1/(\lambda - 1 + T/m_2)] \qquad (63)$$

which yields:

$$\tilde{\underline{\Gamma}} = [\underline{C}_1 - \underline{C}_2 \underline{F}_2^{-1}\,\underline{F}_1][\lambda \underline{I}_{n-2} - \underline{I}_{n-2} - T\underline{A}_{11} + T\underline{A}_{12}\,\underline{F}_2^{-1}\,\underline{F}_1]^{-1}[T\underline{A}_{12}\,\underline{F}_2^{-1}]$$

$$= \begin{bmatrix} 0 & 0 & 0 \\ 0 & T/m_2 & 0 \\ 0 & 0 & 0 \end{bmatrix} \quad [1/(\lambda - 1 + T/m_2)]$$

This has the desired diagonal form.

$$\underline{F}_2 \underline{B}_2 \underline{K}_0 = \begin{bmatrix} \sigma_1 & 0 & 0 \\ 0 & \sigma_2 & 0 \\ 0 & 0 & \sigma_3 \end{bmatrix}$$

$$[\lambda \underline{I}_\ell - \underline{I}_\ell + \underline{F}_2 \underline{B}_2 \underline{K}_0]^{-1} = \begin{bmatrix} \lambda - 1 + \sigma_1 & 0 & 0 \\ 0 & \lambda - 1 + \sigma_2 & 0 \\ 0 & 0 & \lambda - 1 + \sigma_3 \end{bmatrix}^{-1}$$

$$= \begin{bmatrix} 1/(\lambda - 1 + \sigma_1) & 0 & 0 \\ 0 & 1/(\lambda - 1 + \sigma_2) & 0 \\ 0 & 0 & 1/(\lambda - 1 + \sigma_3) \end{bmatrix}$$

$$[\underline{C}_2 \underline{F}_2^{-1}]\;[\lambda \underline{I}_\ell - \underline{I}_\ell + \underline{F}_2 \underline{B}_2 \underline{K}_0]^{-1}\;[\underline{F}_2 \underline{B}_2 \underline{K}_0] = \begin{bmatrix} \sigma_1/(\lambda - 1 + \sigma_1) & 0 & 0 \\ 0 & 0 & 0 \\ 0 & 0 & \sigma_3/(\lambda - 1 + \sigma_3) \end{bmatrix}$$

$$= \hat{\Gamma}$$

which is also in the desired diagonal form.

Now, since $\Gamma = \tilde{\Gamma} + \hat{\Gamma}$

$$\Gamma = \begin{bmatrix} \sigma_1/(\lambda-1+\sigma_1) & 0 & 0 \\ 0 & (T/m_2)/(\lambda-1+T/m_2) & 0 \\ 0 & 0 & \sigma_3/(\lambda-1+\sigma_3) \end{bmatrix} \tag{64}$$

The asymptotic transfer function in equation (64) indicates that the desired design goal of output decoupling with infinite gain has been achieved. Note that a decrease in sampling time corresponds to an increase in gain, so that saying the sampling time goes to zero is equivalent to stating that the gain goes to infinity. From equation (64) the closed loop eigenvalues for this system are:

$$\lambda_1 = 1-\sigma_1$$

$$\lambda_2 = 1-T/m_2$$

$$\lambda_3 = 1-\sigma_3$$

These eigenvalues indicate that the time response of the outputs are greatly affected by the values of σ_1, m_2, and σ_3.

Going back to an intermediate step in the derivation of equation (64), the one (n-1) transmission zero for this system is (equation (63)):

$$Z_t = 1-T/m_2$$

<u>Controller Design</u>. Detailed below is the basic algorithm used for the controller design of all of the controllers designed for this thesis. This procedure is based mostly on the controllers within this thesis and as such should not be considered well tested. However, there is no reason not to expect this technique

to help the designer get started with a design. Implementing this process depends upon available design tools, and the one used for this thesis is the interactive program MULTI. Without MULTI this thesis would not have been possible. The design process follows these steps:

1. Set all of the design parameters equal to one: $\underline{M}$ elements; $\underline{\Sigma}$ elements; α; and ϵ.

2. Calculate $\underline{K}_0$ and $\underline{K}_1$. Reduce until the largest order of magnitude of elements in either controller matrix is 10E+03.

3. Run a simulation and use option #28 in MULTI (figures of merit) to check for a bounded (stable) response. Continue reducing ϵ ,but by relatively small increments, until the response is stable. Experience will best answer the question of what relatively small increments are, but a good starting guideline would be factors of two. (Based upon the designs in this thesis, step three will reduce the largest order of magnitude to 10E+02, but information obtained from other thesis efforts suggests the above guideline of 10E+03 in step two)

4. Further mold the controller matrices using the elements of $\underline{\Sigma}$. Increase or decrease the individual elements so as to increase or decrease the corresponding columns in the controller matrices by the same factor until the orders of magnitude lie within 10E-02 to 10E+02 (or as close as possible). Generally, numbers that are smaller than the suggested values are more desirable than numbers that are larger than suggested.

5. Run a simulation to observe which outputs need improved response. Generally, increasing an element in the $\underline{\Sigma}$ matrix will increase the speed of response of some of the outputs, but with

the resulting problem of increased overshoot. Experimentation will show which $\underline{\Sigma}$ element affects which output. Repeat this process until the best time responses are achieved.

6. Experiment with the value of α while observing output response. In this thesis increasing α sometimes reduced overshoot on the control surface deflections with little degredation in output response, but sometimes this parameter had little noticable effect.

7. Now vary the $\underline{M}$ elements to see if they will improve output response. Generally the $\underline{M}$ elements directly affect the corresponding output response depending upon which column they're in. For example, decreasing an entry in the second column might increase the speed of response of the state whose derivative is measured by that column. Most designs, including those from other theses, have values for $\underline{M}$ elements within the range of 0.25 to 1.0.

8. Repeat steps 5 thru 7 until the best responses are achieved, keeping in mind that tradeoffs will always be made between desirable and undesirable output responses and control surface deflections. Even though option #27 in MULTI does limit the control surface deflections based on physical limitations, a design that reduces the number of times a surface "hits the stops" is considered superior to one that doesn't.

Obviously different plants are going to respond in different ways to changes in the design parameters. This means that a satisfactory design is more the result of trial and error than any "cookbook" approach. One conclusion tentatively drawn from current and past theses is that fighter aircraft seem to respond to design parameter changes similarily, as do transport aircraft, although fighters differ from transports.

Since the asymptotic transfer function is valid only for values of gain approaching infinity, for values of gain much less than infinity there will be coupling between the outputs. This is probably one of the main causes of frustration that results when trying to shape one output response only to find that another is severely degraded. On real aircraft, the value for the sampling time will be dictated by the performance of the processor (computer) used. Unfortunately, it may be impossible to run the processor at the speed that yielded those good results when designing with MULTI.

For the lateral controller different controller matrices yielded the best results for the different commanded maneuvers at this one flight condition. Since the philosophy of this thesis is to try and follow Bauschlicher's approach so as to make comparisons, one set of controller matrices is chosen for each flight condition. This results in compromise among the individual responses to each commanded maneuver. The choice of which controller matrices to use is subjective, based on the author's evaluation of what constitutes the best "overall" response.

The final values selected for the lateral controller for the 0.15 mach at sea level flight condition are listed below.

$$\Sigma = \begin{bmatrix} 0.15 & 0 & 0 \\ 0 & 1 & 0 \\ 0 & 0 & 2.5 \end{bmatrix} \tag{65}$$

$$\alpha = 1, \quad T = 0.01 \tag{66}$$

$$\epsilon = 0.1 \tag{67}$$

$$\underline{M} = \begin{bmatrix} 0 \\ 0.25 \\ 0 \end{bmatrix} \tag{68}$$

$$\underline{K}_0 = \begin{bmatrix} -0.00382 & 29.9 & 15.5 \\ 0.0505 & 1.90 & -13.0 \\ 0.259 & -5.82 & 39.6 \end{bmatrix} \tag{69}$$

$$\underline{K}_1 = \underline{K}_0 \tag{70}$$

Figures 5 through 11 show the time responses for the outputs and the flight control surface deflections for the 0.15 mach, sea level flight condition. The figures of merit and commanded inputs for each maneuver are listed in Table VII.

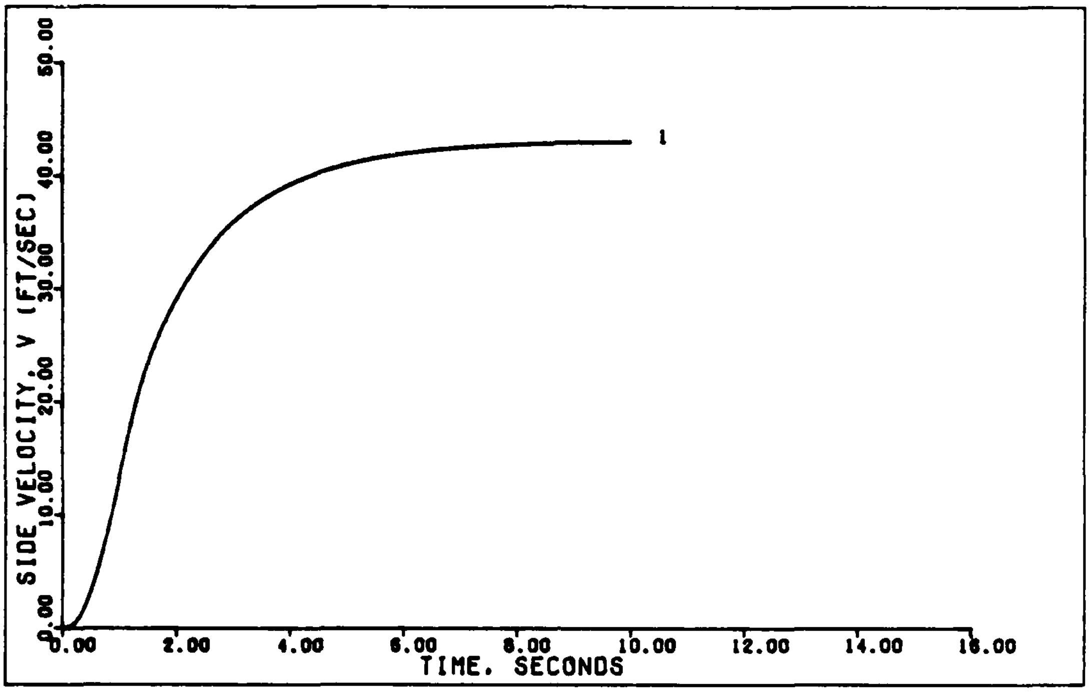

1.5 G HORIZONTAL TRANSLATION (D, 0.15 MACH, 0 FT)

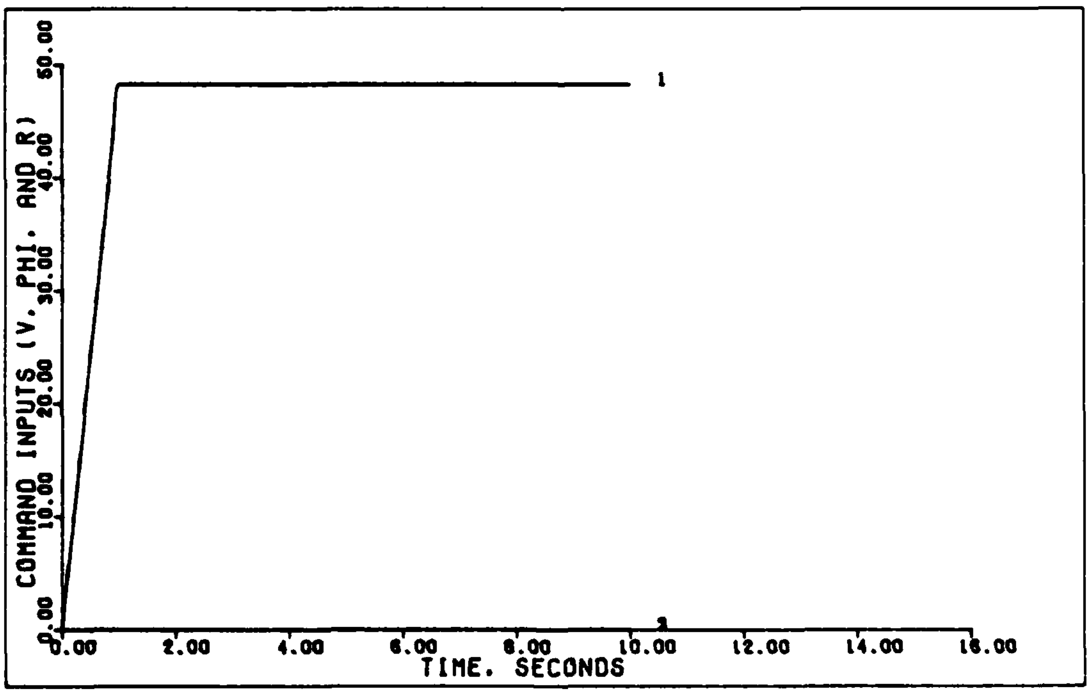

1.5 G HORIZONTAL TRANSLATION (0.15 MACH, 0 FT)

Figure 5. 1.5 g Horizontal Translation (0.15 Mach)

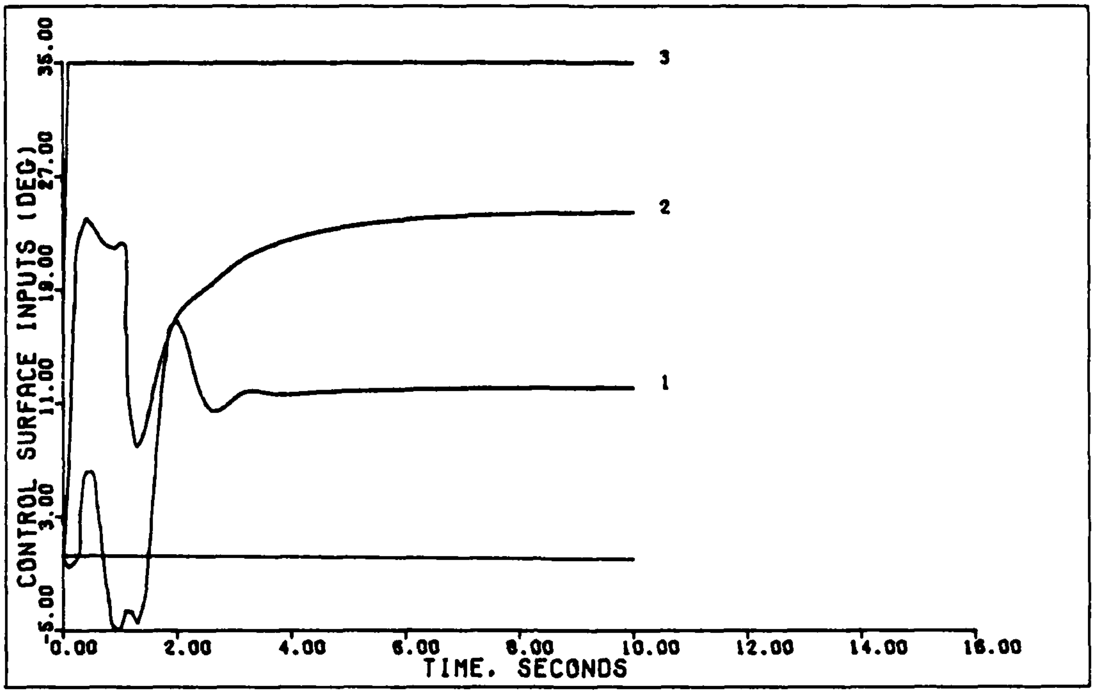

1.5 G HORIZONTAL TRANSLATION (D, 0.15 MACH, 0 FT)

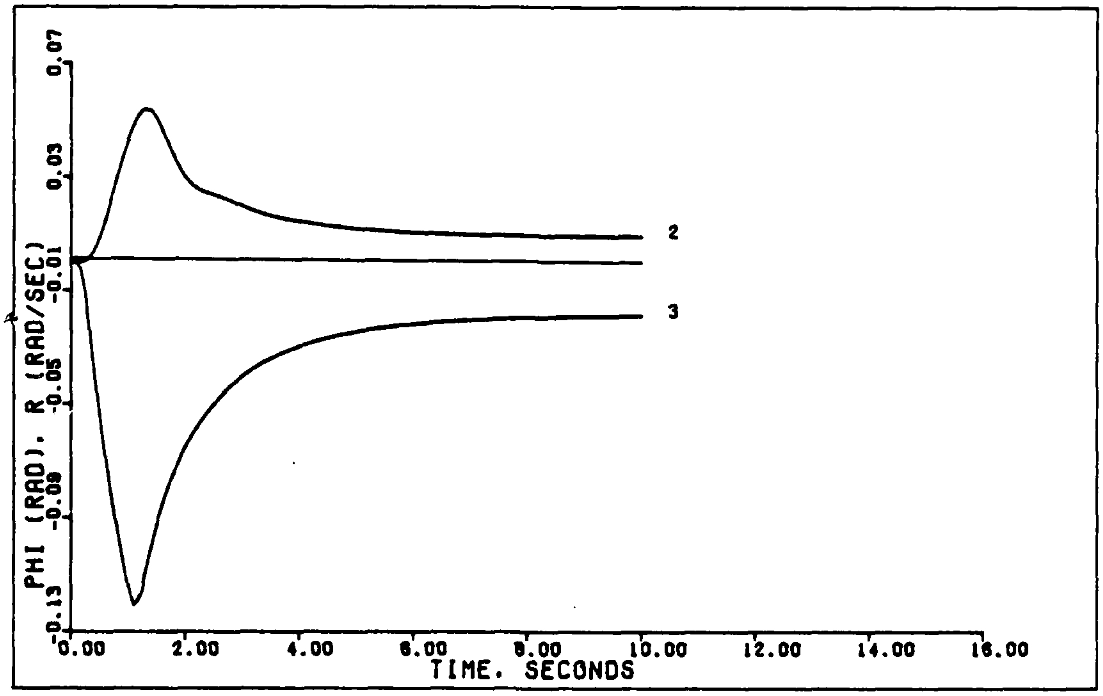

1.5 G HORIZONTAL TRANSLATION (D, 0.15 MACH, 0 FT)

Figure 6. 1.5 g Horizontal Translation (0.15 Mach)

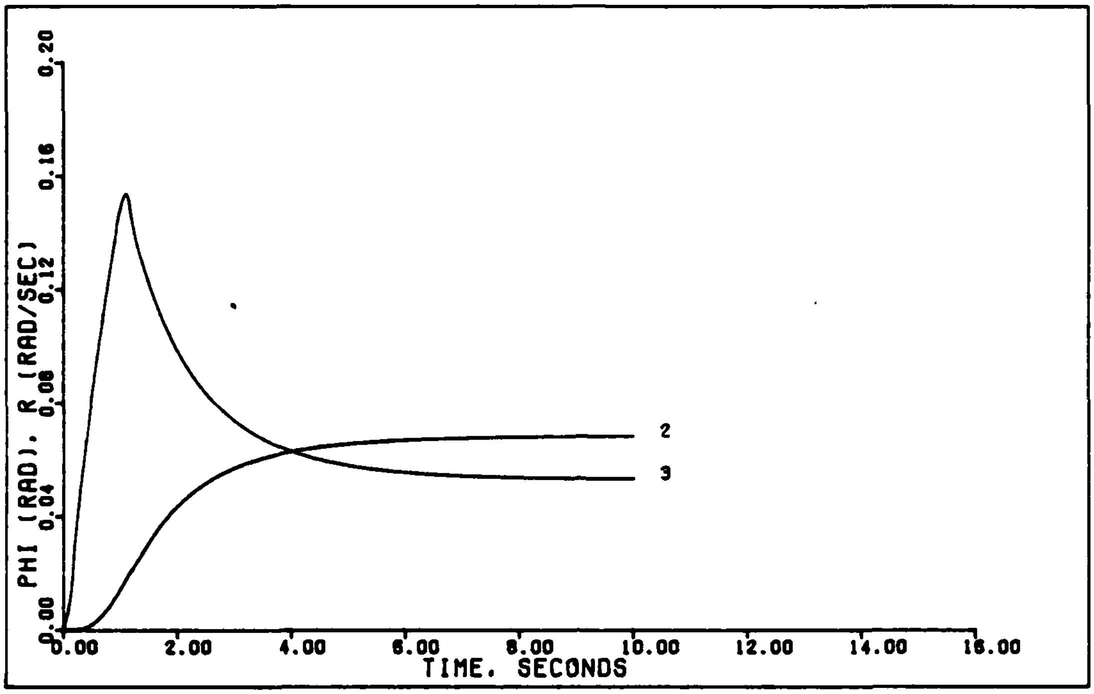

1 G FLAT TURN (0.15 MACH, 0 FT)

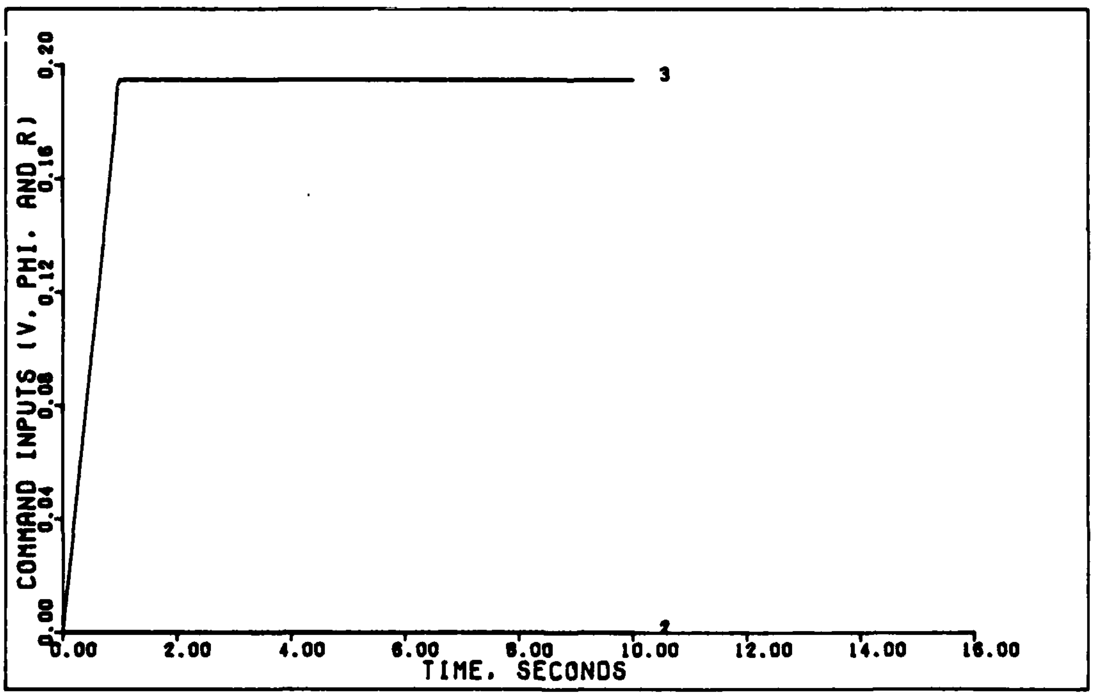

1 G FLAT TURN (D, 0.15 MACH, 0 FT)

Figure 7. 1 g Flat Turn (0.15 Mach)

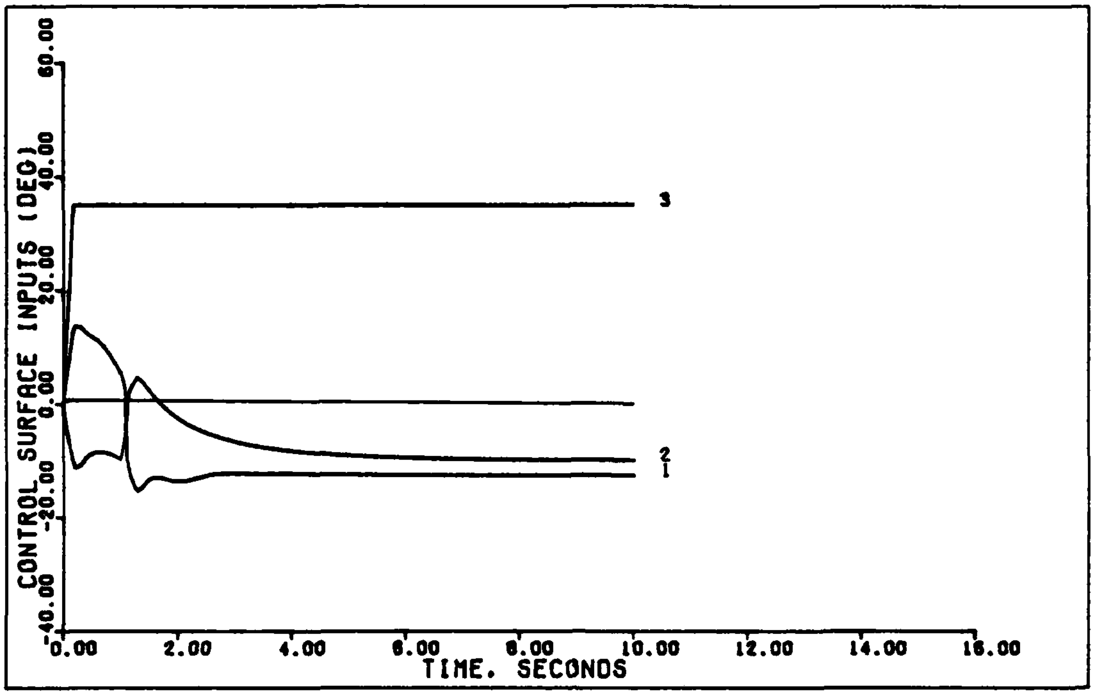

1 G FLAT TURN (D, 0.15 MACH, 0 FT)

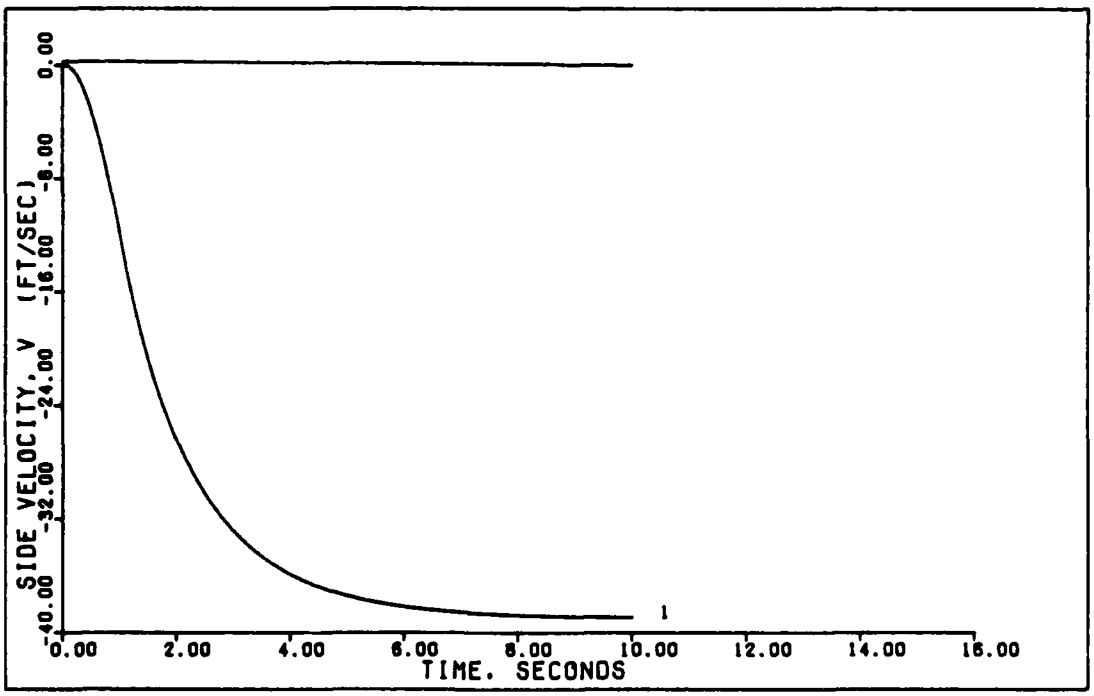

1 G FLAT TURN (0.15 MACH, 0 FT)

Figure 8. 1 g Flat Turn (0.15 Mach)

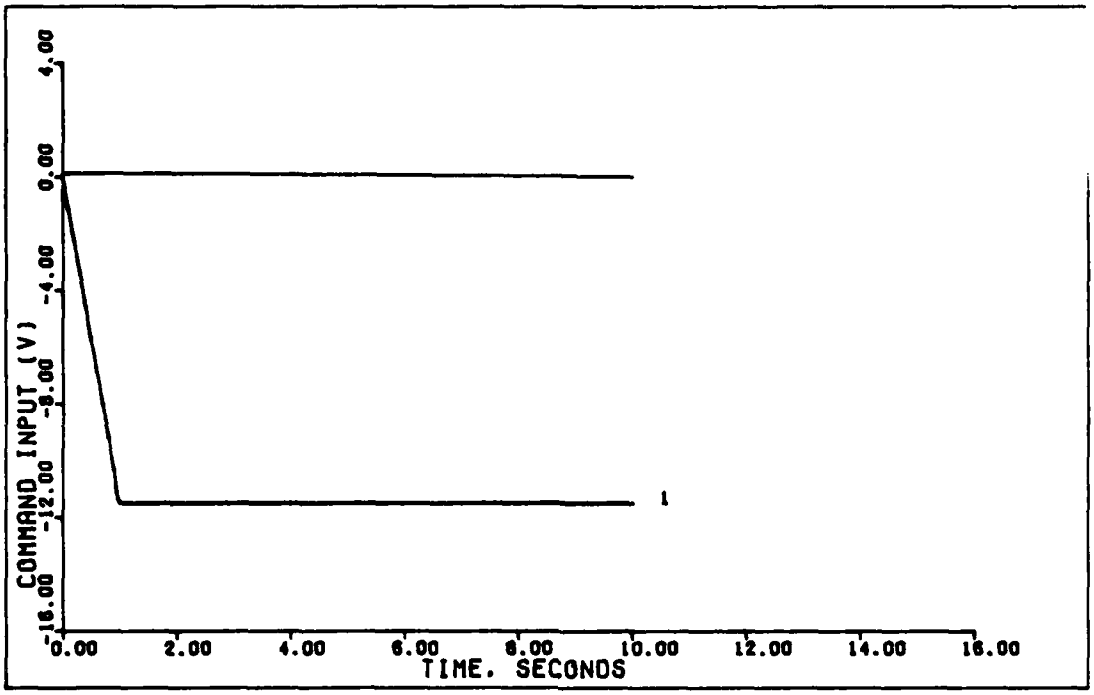

3 DEGREE YAW POINTING (0.15 MACH. 0 FT)

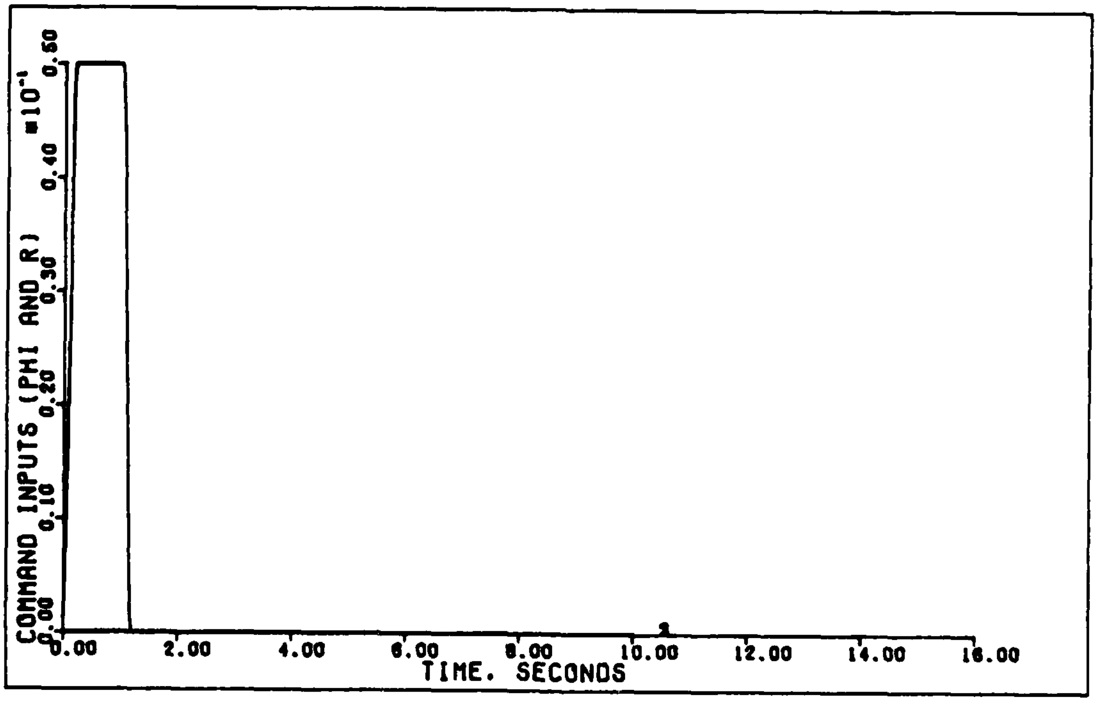

3 DEGREE YAW POINTING (0.15 MACH. 0 FT)

Figure 9. 3 Degree Yaw Pointing (0.15 Mach)

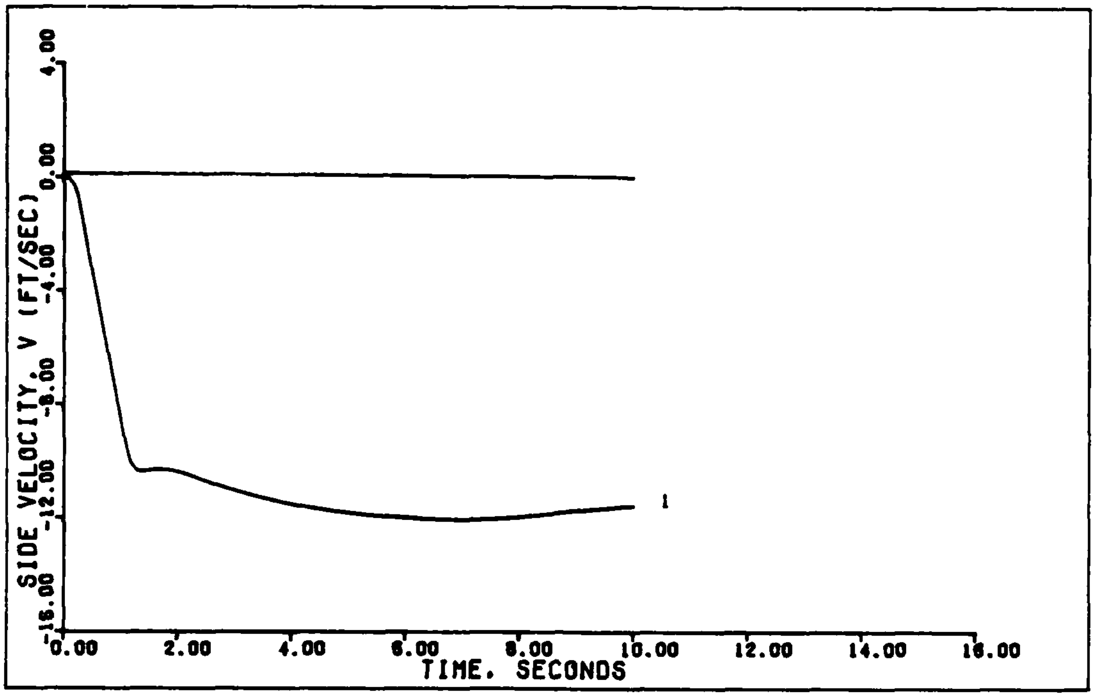

3 DEGREE YAW POINTING (D. 0.15 MACH, 0 FT)

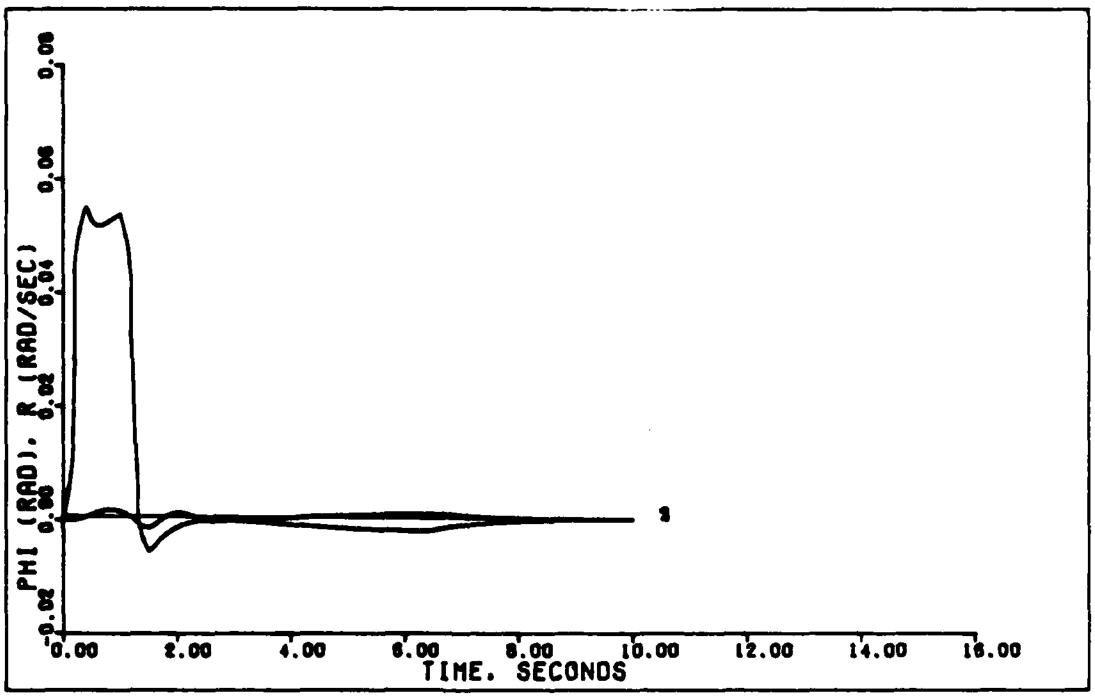

3 DEGREE YAW POINTING (D. 0.15 MACH, 0 FT)

Figure 10. 3 Degree Yaw Pointing (0.15 Mach)

TABLE VII

SUMMARY OF OUTPUT RESPONSES FOR LATERAL CONTROLLER

Flt. Cond.	Maneuver	Command, V	Overshoot	Rise Time
0.15 Mach	Yaw	1,-11.5,20,20	none	1 sec
0 ft.	Pointing	0,0,0,0	-0.001 rad	
		.2,.0524,1,1.2	8.2%	0.27 sec
	Flat	0,0,0,0	-38.9 ft/sec	
	Turn	0,0,0,0	.068 rad	
		1,.195,20,20	none	*
	Horiz.	1,48.3,20,20	none	10 sec
	Transl.	0,0,0,0	.052 rad	
		0,0,0,0	-.12 rad/sec	

Note: The command vector is $[\ v\ \phi\ r\ ]^T$.
Overshoot is the first peak for non zero commanded outputs or is the greatest deviation from zero for zero commanded outputs. Rise time is from initial value to 90% of commanded value.

* For this maneuver the output did not reach 90% of the command.

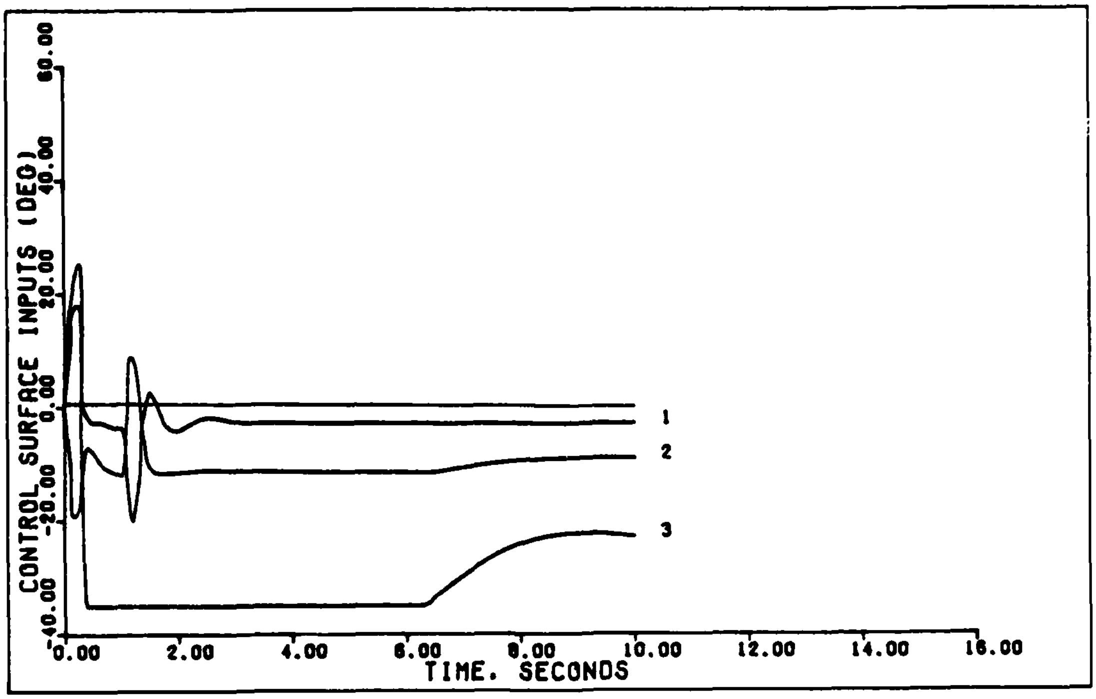

3 DEGREE YAW POINTING (D. 0.15 MACH, 0 FT)

Figure 11. 3 Degree Yaw Pointing (0.15 Mach)

Longitudinal Controller

Maneuver Description. Continuing with the concept of direct comparison with Bauschlicher's results, the same three longitudinal maneuvers that he used are chosen for this thesis. These maneuvers are the pitch pointing, vertical translation, and direct lift. These maneuvers are typically claimed to be very useful in the combat arena, both for air-to-air and air-to-ground combat.

Pitch pointing involves equal changes in the angle of attack and the pitch angle, resulting in the flight path angle $\gamma(\theta - \alpha)$ remaining constant. Therefore, the nose pitches while the aircraft remains on the current trajectory. Note that using the euler pitch angle implies that the aircraft has zero initial roll angle. To generalize this maneuver for any initial attitude, the integral of pitch rate could be used instead of θ. The change in velocity is commanded to zero.

Vertical translation results in the aircraft moving in the vertical direction (along z axis) with no change in the pitch angle. Consequently, the pitch angle change is commanded to zero, as is the change in velocity. The angle of attack is commanded so as to actually command a change in w, the velocity in the z direction. Since

$$\alpha = w/U \tag{71}$$

for small angles of attack, changes in α equate to changes in w (and thus commanded g forces in the z direction).

Previous thesis students have called the third maneuver a direct lift, even though direct lift has typically been used to describe a different maneuver while the constant g pull up has been used to describe this last maneuver. This thesis will follow previous theses in calling this maneuver the direct lift. To command this maneuver, equation (50) can be rewritten as

$$Az = q^*U \tag{72}$$

from which the pitch angle command necessary to generate the desired acceleration in the z direction (Az) can be found. Both the change in u and angle of attack are commanded to zero, so that the flight path angle follows the pitch angle.

Longitudinal Model. Just as with the lateral controller, modifications to the data generated by the FPCC simulation program are required. The modifications made to equations (48) and (49) in this chapter apply to the 0.15 mach flight condition, but the same changes are also made to the data for the other flight conditions (Appendix D).

The longitudinal states used in equation (48) are q, w, u, θ, h, and x. Just as with the lateral model, an analysis of the eigenvalues of the $\underline{A}$ matrix can be used to reduce the system state model. The eigenvalues of the original six state A matrix are:

$-0.02010 \pm j\ 0.2034$ (phugoid roots)

1.166 (unstable short period root)

-1.887 (stable short period root)

0.0001981

-0.001131

Since this aircraft is longitudinally unstable, one of the short period roots has migrated over into the right half s plane. The two roots near zero supply no essential information and so can be removed from the model. Once again from experience the decision is made to eliminate the two states h and x yielding the following eigenvalues:

$-0.02059 \pm j\ 0.2040$

1.166

-1.887

So the plant model has been reduced to four state, q, w, u, and θ with no loss of essential aircraft characteristics.

From equation (49) there are seven longitudinal control inputs, δc, δj, δmf, F_1, F_2, CDI_1, and CDI_2. However, for this particular flight condition there is a column of zeros in the $\underline{B}$ matrix corresponding to the maneuver flaps, implying they have no effect upon the aircraft in this configuration. Of the remaining six control inputs, the two engine thrusts can be combined into one input called F_{TOT}, by simply adding those two columns of the $\underline{B}$ matrix together. Once again the contributions of the terms in the equations due to CDI_1 and CDI_2 are minimal and can be dropped. This leaves just three control inputs, δc, δj, and F_{TOT}.

Since there are three inputs, there can be at most three outputs. The outputs chosen are the same as Bauschlicher used except for thrust. These outputs are θ, u, and α. Since angle of attack isn't one of the states, it is generated as an output by assuming that α is equal to w/U. This means that in each $\underline{C}$ matrix used for this thesis this entry is the reciprocal of the airspeed at trim.

The relationship between the input command to the thrust and the engine thrust is modeled as an actuator in this thesis. This is preferable to imbedding the engine thrust into the plant $\underline{A}$

matrix. Imbedding the thrust (or any other actuator) means that the model assumes instantaneous aircraft response to the change in thrust (or flight control surface), whereas keeping the actuator dynamics separate and using option #4 in MULTI means the model incorporates a (more realistic) one sampling period time delay between actuator movement and aircraft response.

With these new states, inputs, and outputs the longitudinal model used in this thesis is expressed by the following equations:

$$\begin{bmatrix} \dot{\theta} \\ \dot{u} \\ \dot{w} \\ \dot{q} \end{bmatrix} = \begin{bmatrix} 0 & 0 & 0 & 1 \\ -31.6 & -.0214 & .0867 & -31.5 \\ -6.01 & -.215 & -.638 & 166 \\ 0 & -.000156 & .0134 & -.103 \end{bmatrix} \begin{bmatrix} \theta \\ u \\ w \\ q \end{bmatrix} + \begin{bmatrix} 0 & 0 & 0 \\ -.0765 & -.0211 & .0021 \\ -.111 & -.118 & -.000734 \\ .039 & -.00908 & -.0000596 \end{bmatrix} \begin{bmatrix} \delta_c \\ \delta_J \\ F \end{bmatrix} \tag{73}$$

$$\begin{bmatrix} \theta \\ u \\ \alpha \end{bmatrix} = \begin{bmatrix} 1 & 0 & 0 & 0 \\ 0 & 1 & 0 & 0 \\ 0 & 0 & .00607 & 0 \end{bmatrix} \begin{bmatrix} \theta \\ u \\ w \\ q \end{bmatrix} \tag{74}$$

An interesting aside is that the system above yielded no transmission zeros and no decoupling zeros.

The above equations represent the longitudinal model for this aircraft at 0.15 mach, sea level. This system is checked (with $\underline{F}$ substituted for $\underline{C}$) for transmission zeros and none are found in the right half plane. No decoupling zeros are found, indicating that the system is controllable and observable.

Since the matrix $\underline{C}\ \underline{B}$ does not have full rank 1, the system is irregular and the measurement matrix must be found. The concept behind the irregular design is explained in Chapter II.

Measurement Matrix Development. Since n-1 is one, the $\underline{M}$ matrix is once again 3x1, this time measuring the derivative of the pitch angle. The first step is to find $\underline{B}^*$, which can be derived from:

$$\underline{C}_1 = \begin{bmatrix} 1 \\ 0 \\ 0 \end{bmatrix} \tag{75}$$

$$\underline{A}_{11} = [0] \tag{76}$$

$$\underline{A}_{12} = [0\ 0\ 1] \tag{77}$$

yielding

$$\underline{B}^* = \begin{bmatrix} 0 & 0 & 1 \\ 0 & 0 & 0 \\ 0 & 0 & 0 \end{bmatrix} \tag{78}$$

with

$$\{d_1, d_2, d_3\} = \{0, 3, 3\} \tag{79}$$

Using the general form for M:

$$\underline{M} = \begin{bmatrix} m_1 \\ m_2 \\ m_3 \end{bmatrix} \tag{80}$$

and

$$\underline{C}_2 = \begin{bmatrix} 0 & 0 & 0 \\ 1 & 0 & 0 \\ 0 & .00607 & 0 \end{bmatrix} \tag{81}$$

then

$$\underline{F}_2 = \begin{bmatrix} 0 & 0 & m_1 \\ 1 & 0 & m_2 \\ 0 & .00607 & m_3 \end{bmatrix} \tag{82}$$

For $\underline{F}_2$ to have full rank, yet be as sparse as possible, and using the guidelines of Chapter II in choosing the $\underline{M}$ elements based upon $\underline{B}^*$, the obvious choice for $\underline{M}$ is:

$$\underline{M} = \begin{bmatrix} m_1 \\ 0 \\ 0 \end{bmatrix} \tag{83}$$

which yields

$$\underline{F}_2 = \begin{bmatrix} 0 & 0 & m_1 \\ 1 & 0 & 0 \\ 0 & .00607 & 0 \end{bmatrix} \tag{84}$$

and

$$\underline{F}_2^{-1} = \begin{bmatrix} 0 & 1 & 0 \\ 0 & 0 & 1/.00607 \\ 1/m_1 & 0 & 0 \end{bmatrix} \tag{85}$$

The asymptotic transfer function matrix can be derived as in the lateral model earlier in this chapter and is found to be:

$$\underline{\Gamma} = \begin{bmatrix} (T/m_1)/(\lambda-1+T/m_1) & 0 & 0 \\ 0 & \sigma_2/(\lambda-1+\sigma_2) & 0 \\ 0 & 0 & \sigma_3/(\lambda-1+\sigma_3) \end{bmatrix} \tag{86}$$

From equation (86) the transmission zero is

$$Z_t = 1-T/m_1 \tag{87}$$

Equation (86) shows that the outputs become decoupled as the gain goes to infinity (or sampling time T goes to zero). Also, m_1, σ_2, and σ_3 have the greatest impact on the output time responses.

Controller Design. The same algorithm listed under lateral controller design is used for the longitudinal controller design. Actually, this algorithm is used for every controller design for this thesis. The choice of one set of controller matrices for all three maneuvers for each flight condition requires compromises in the performance of each maneuver. The design values used are listed below.

$$\underline{\Sigma} = \begin{bmatrix} 1 & 0 & 0 \\ 0 & 1 & 0 \\ 0 & 0 & 0.025 \end{bmatrix} \tag{88}$$

$$\alpha = 2 \tag{89}$$

$$\epsilon = 0.1, \quad T = 0.01 \tag{90}$$

$$\underline{M} = \begin{bmatrix} 0.25 \\ 0 \\ 0 \end{bmatrix} \tag{91}$$

with

$$\underline{K}_o = \begin{bmatrix} 16.856 & .00589 & -1.340 \\ -18.518 & -.564 & -5.0981 \\ 427.964 & 89.785 & -100.0318 \end{bmatrix} \tag{92}$$

$$\underline{K}_1 = \begin{bmatrix} 8.428 & .00295 & -.670 \\ -9.259 & -.282 & -2.549 \\ 213.982 & 44.893 & -50.0159 \end{bmatrix} \tag{93}$$

Appendix D lists all of the design parameters for the other flight conditions.

Figures 12 through 20 show the time responses for the outputs and control inputs for the three longitudinal maneuvers at 0.15 mach, sea level. Figures 21 through 39 show the same time responses for the same maneuvers at the other two flight

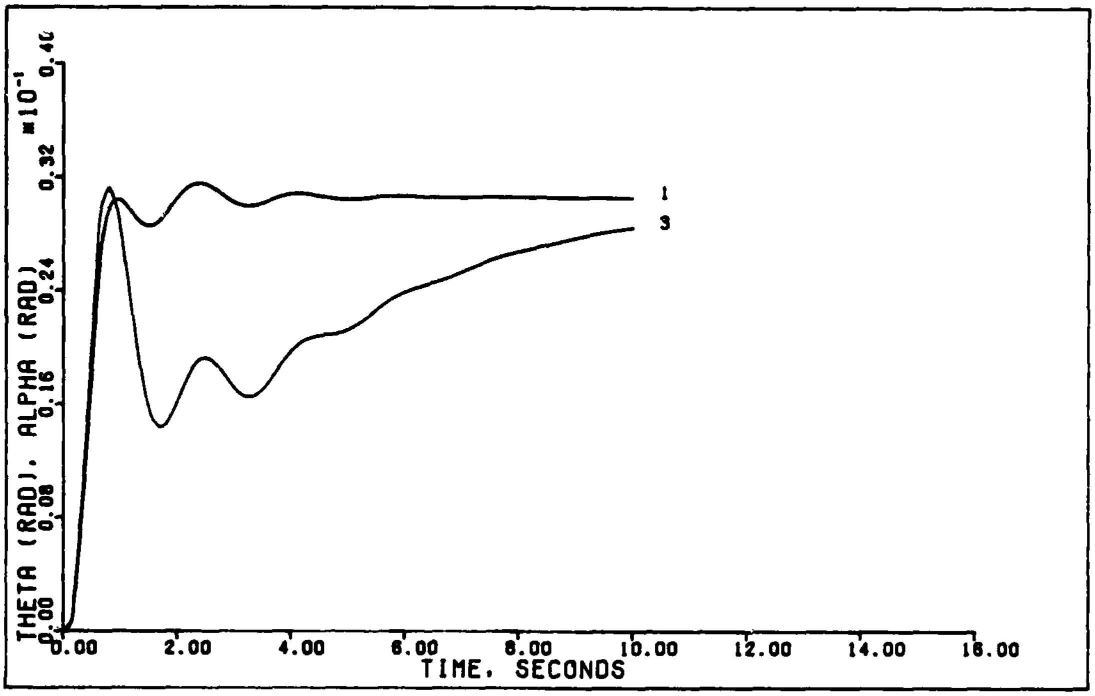

1.75 DEGREE PITCH POINTING (0.15 MACH, 0 FT)

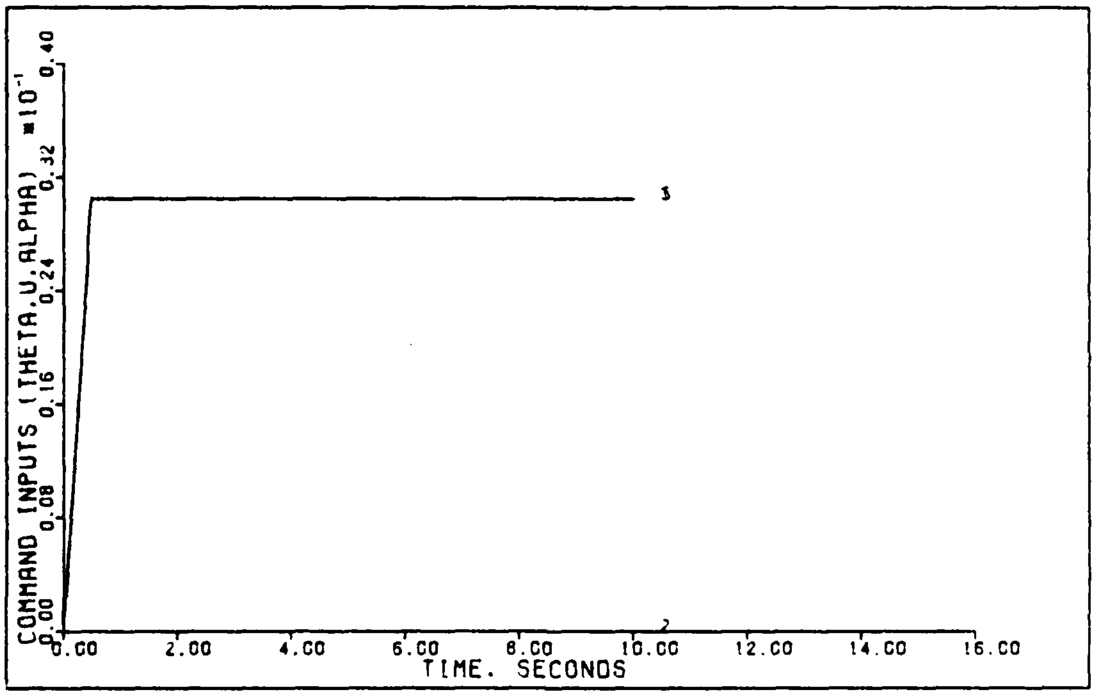

1.75 DEGREE PITCH POINTING (0.15 MACH, 0 FT)

Figure 12. 1.75 Degree Pitch Pointing (0.15 Mach)

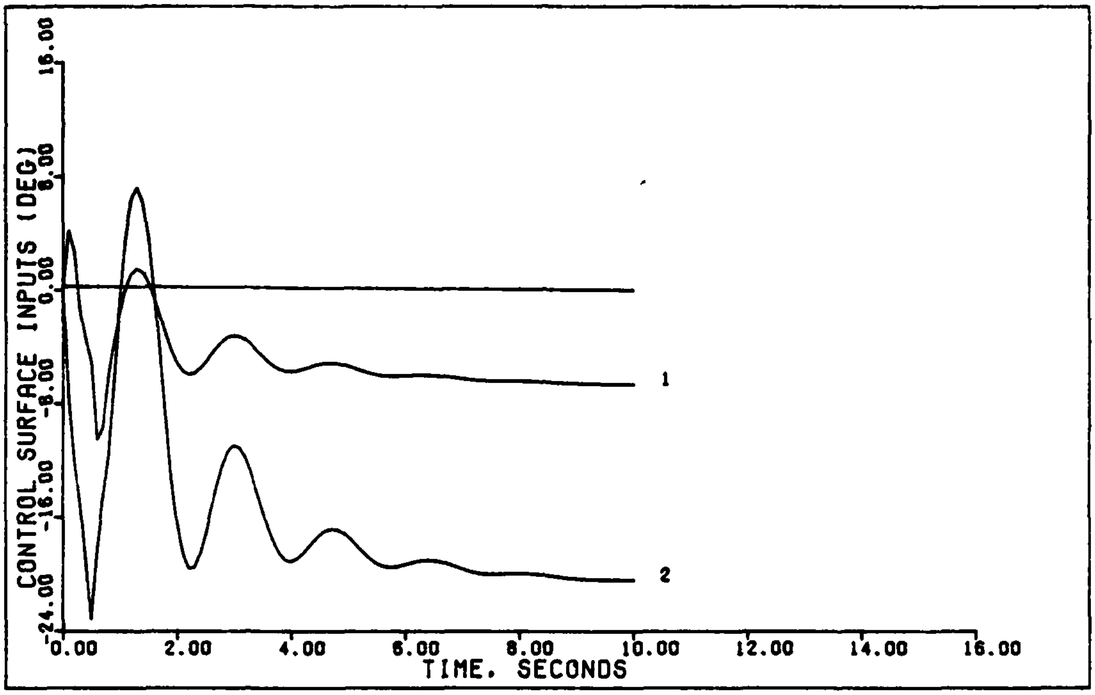

1.75 DEGREE PITCH POINTING

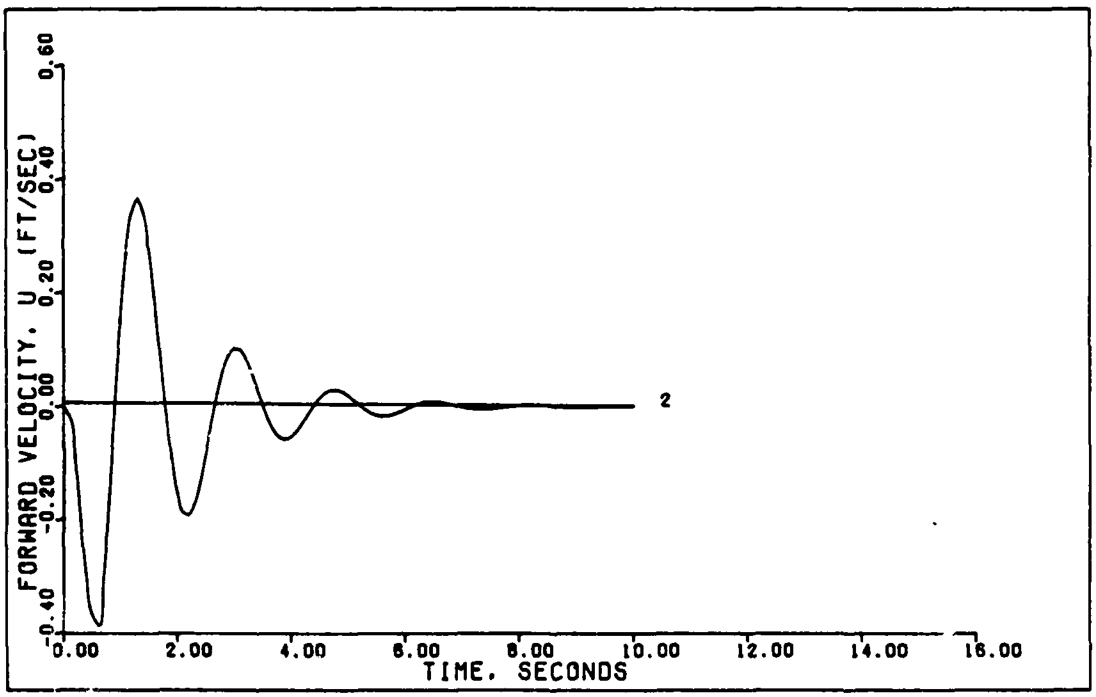

1.75 DEGREE PITCH POINTING (0.15 MACH, 0 FT)

Figure 13. 1.75 Degree Pitch Pointing (0.15 Mach)

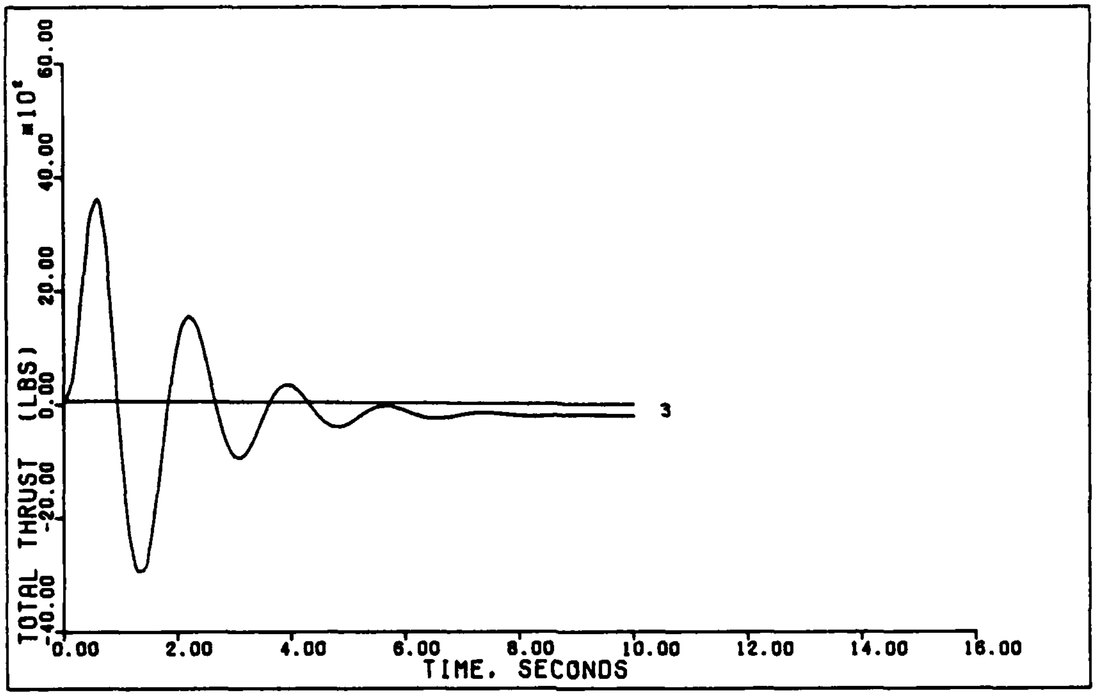

1.75 DEGREE PITCH POINTING (0.15 MACH, 0 FT)

Figure 14. 1.75 Degree Pitch Pointing (0.15 Mach)

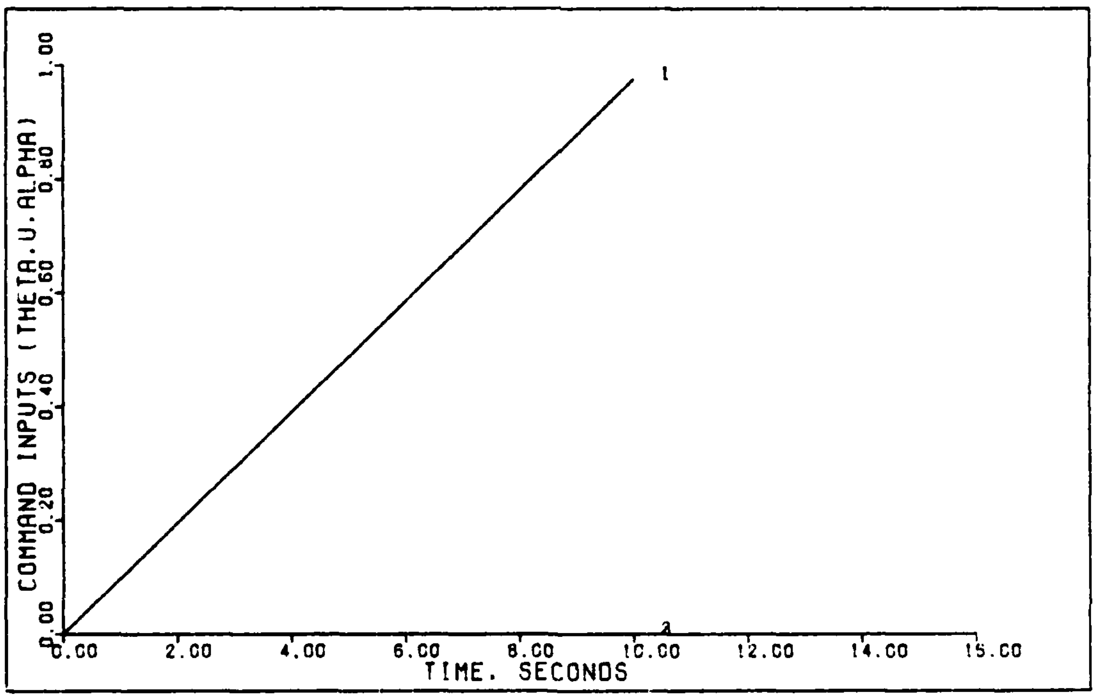

0.5 G DIRECT LIFT (0.15 MACH, 0 FT)

Figure 15. 0.5 g Direct Lift (0.15 Mach)

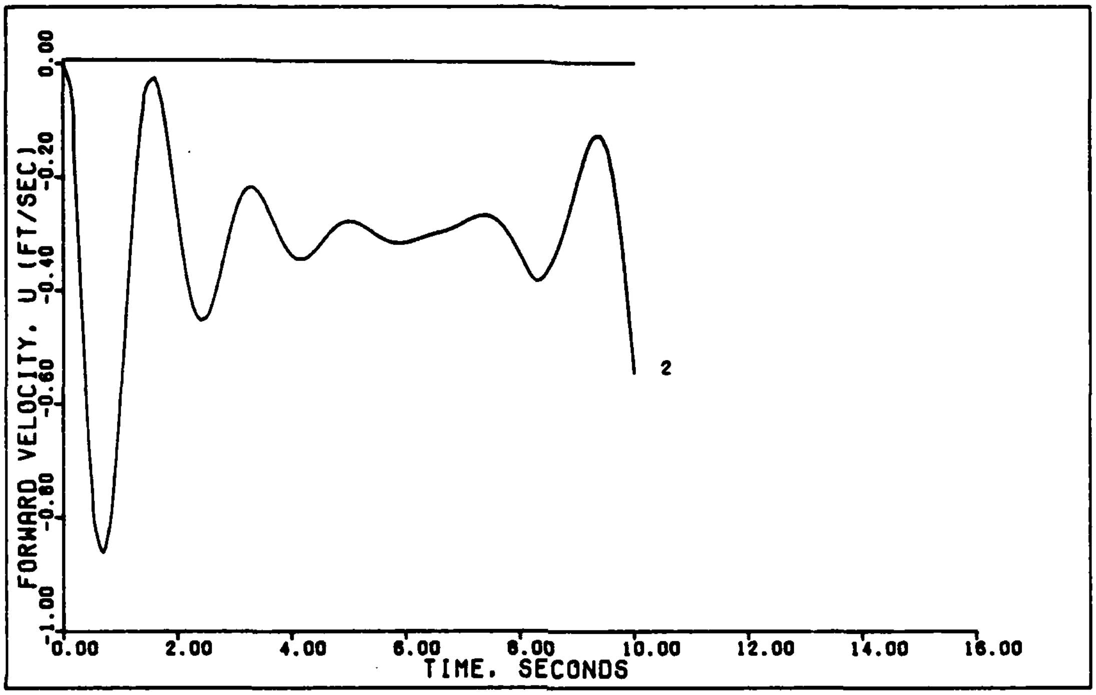

0.5 G DIRECT LIFT (0.15 MACH, 0 FT)

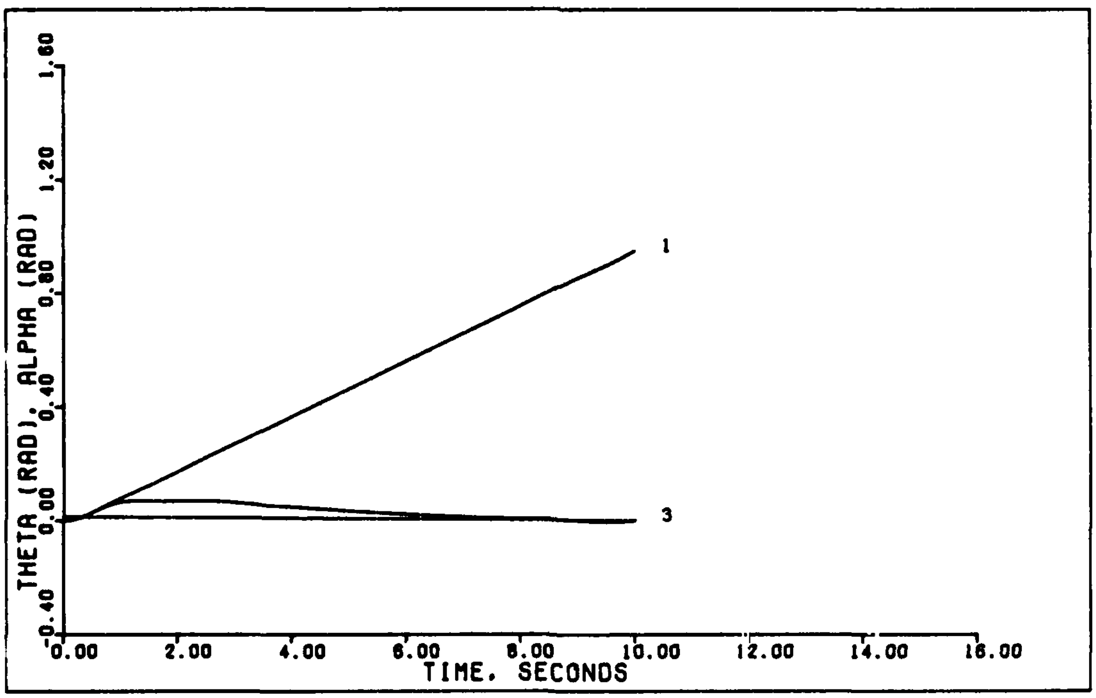

0.5 G DIRECT LIFT (0.15 MACH, 0 FT)

Figure 16. 0.5 g Direct Lift (0.15 Mach)

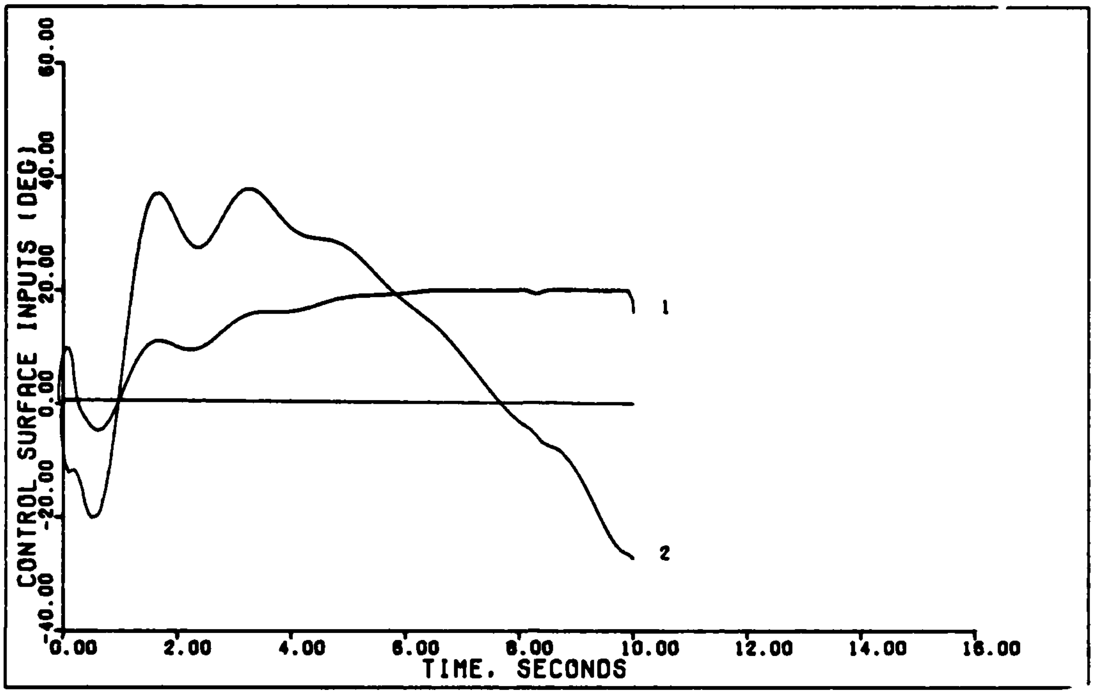

0.5 G DIRECT LIFT (0.15 MACH, 0 FT)

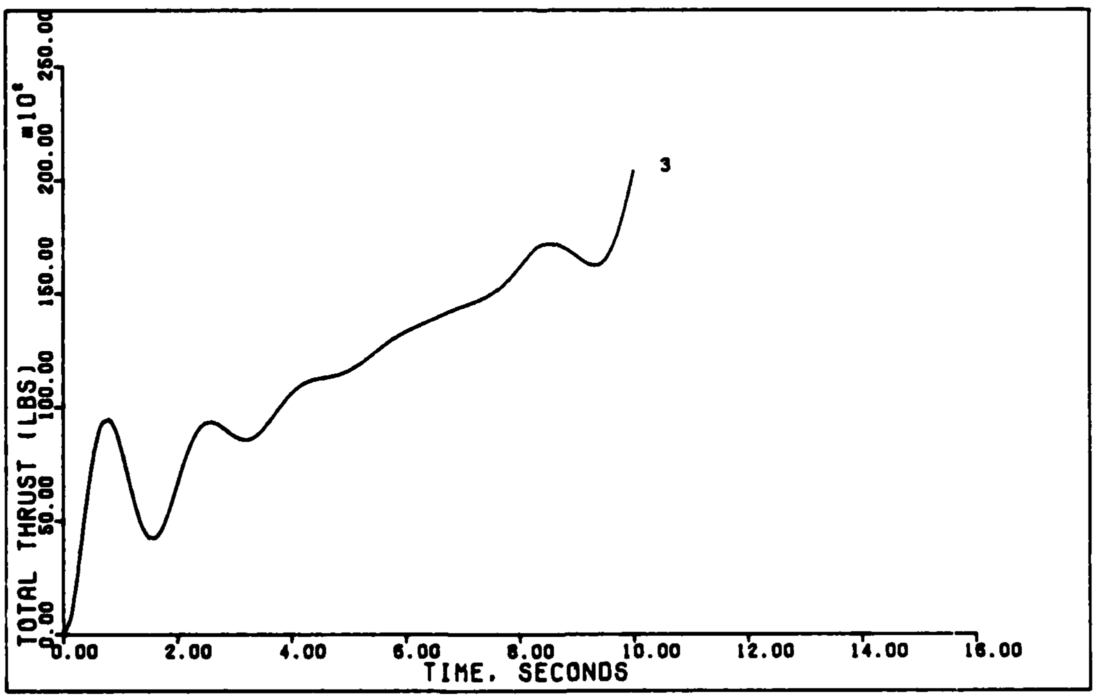

0.5 G DIRECT LIFT (0.15 MACH, 0 FT)

Figure 17. 0.5 g Direct Lift (0.15 Mach)

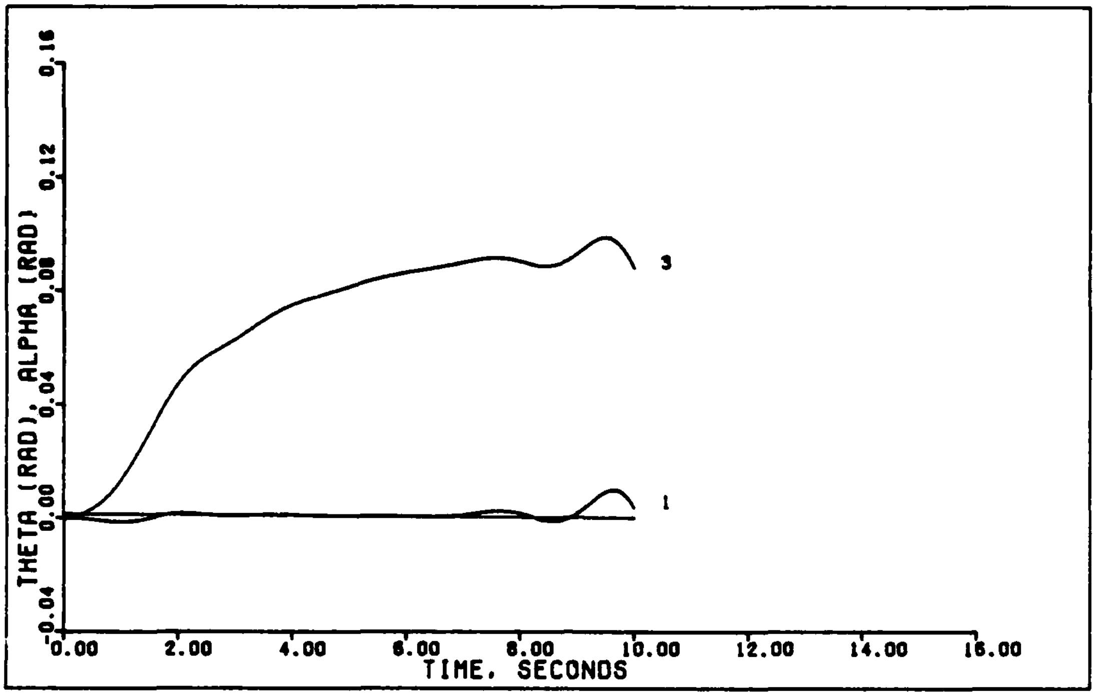

0.5 G VERTICAL TRANSLATION (0.15 MACH, 0 FT)

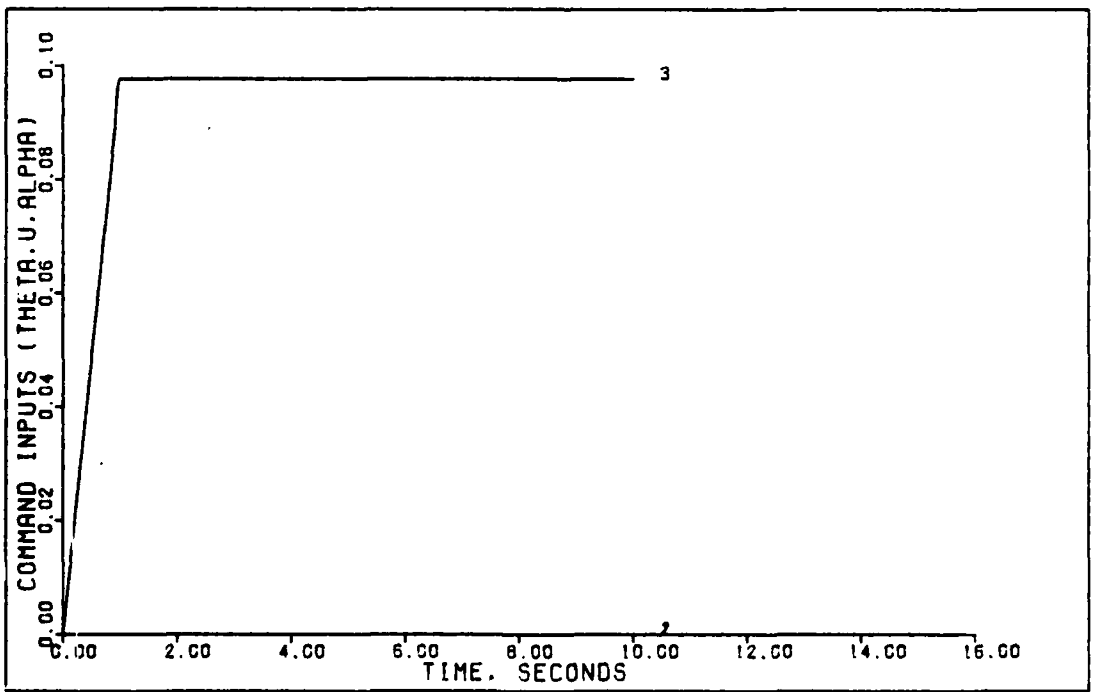

0.5 G VERTICAL TRANSLATION (0.15 MACH, 0 FT)

Figure 18. 0.5 g Vertical Translation (0.15 Mach)

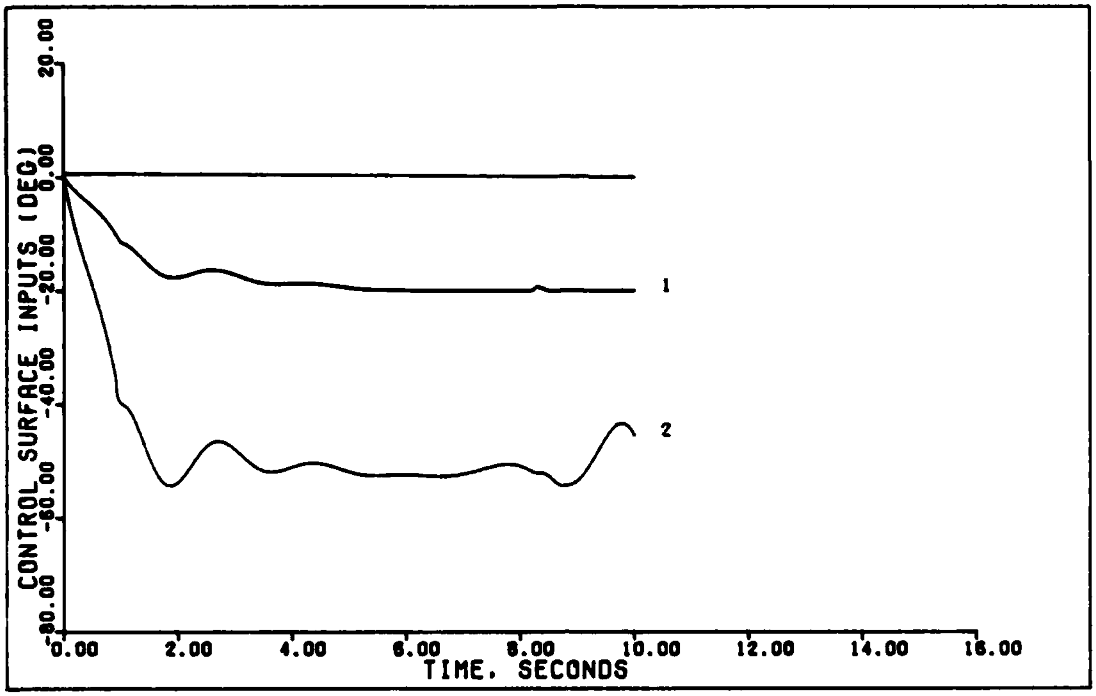

0.5 G VERTICAL TRANSLATION (0.15 MACH, 0 FT)

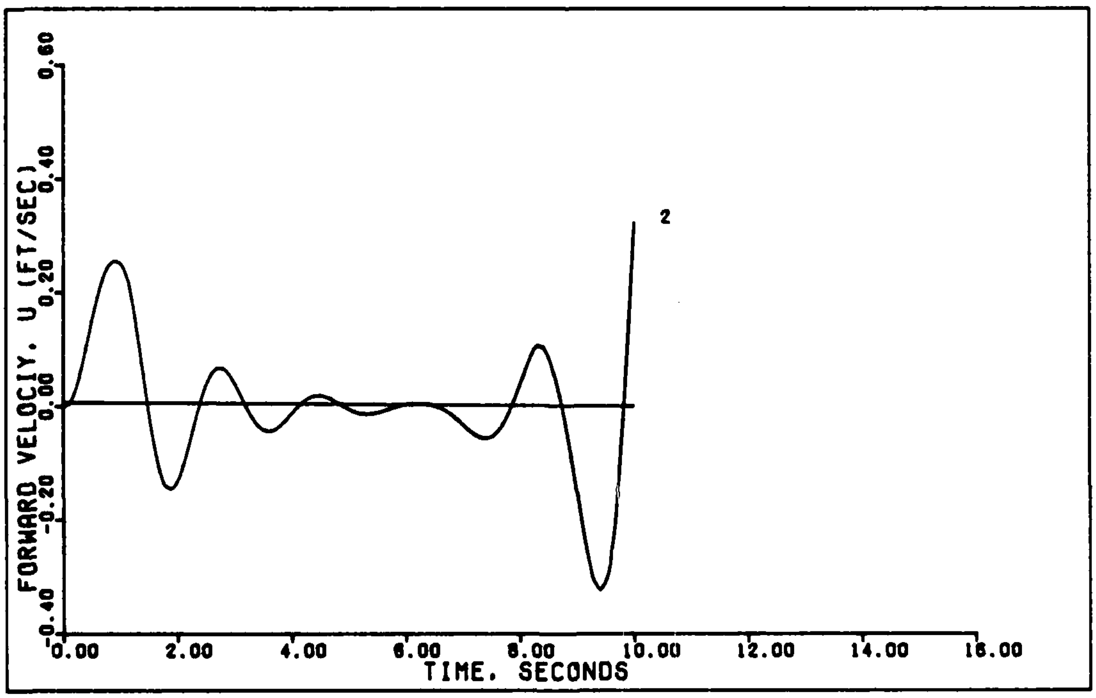

0.5 G VERTICAL TRANSLATION (0.15 MACH, 0 FT)

Figure 19. 0.5 g Vertical Translation (0.15 Mach)

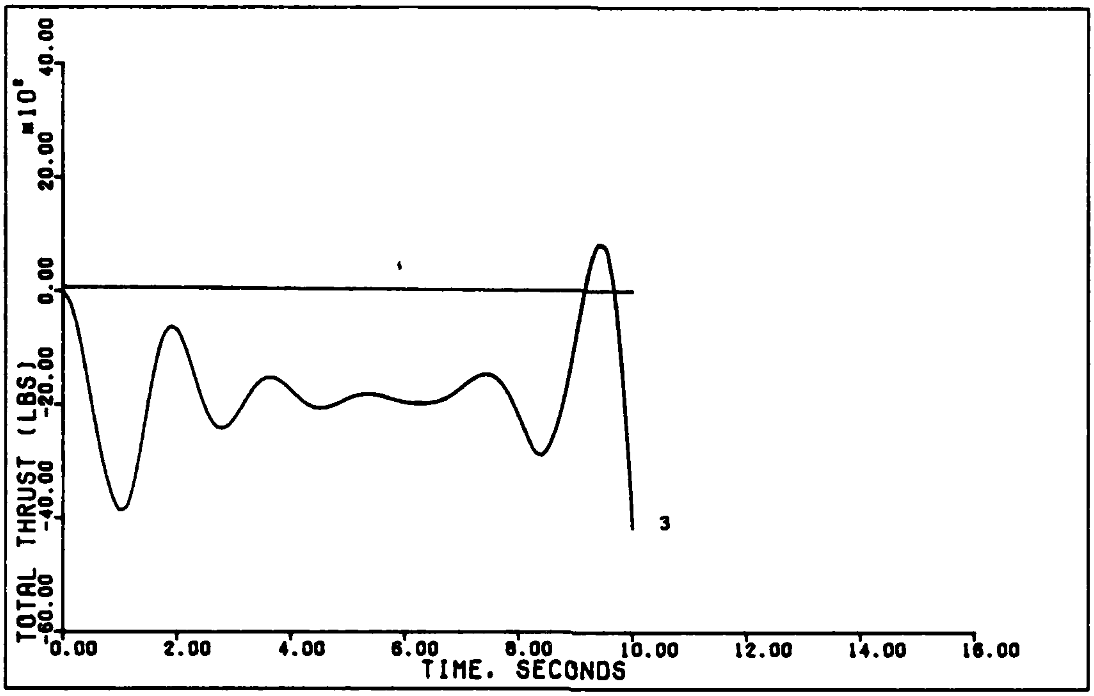

0.5 G VERTICAL TRANSLATION (0.15 MACH, 0 FT)

Figure 20. 0.5 g Vertical Translation (0.15 Mach)

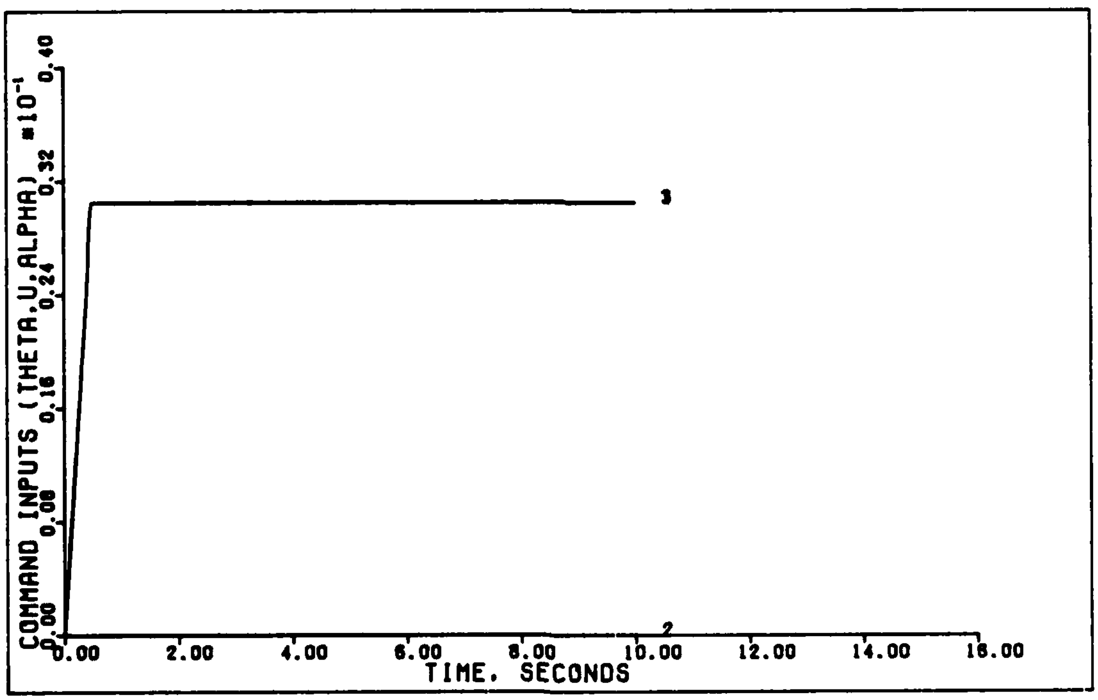

1.75 DEGREE PITCH POINTING (0.6 MACH, 0 FT)

Figure 21. 1.75 Degree Pitch Pointing (0.6 Mach)

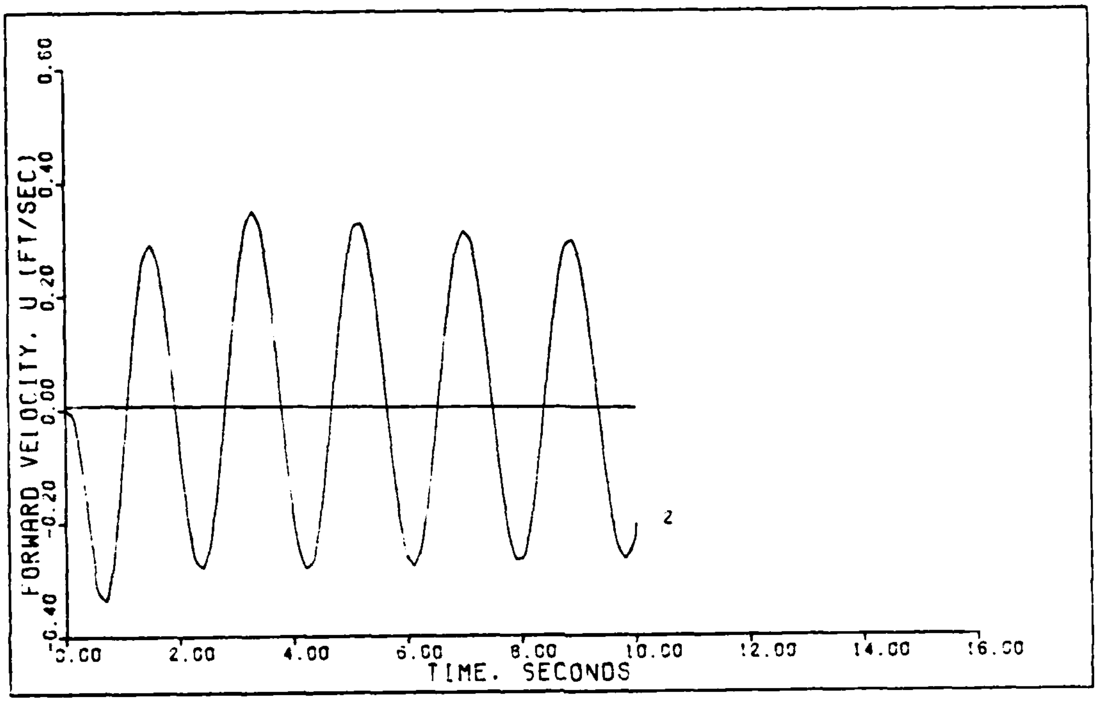

1.75 DEGREE PITCH POINTING (0.6 MACH. 0 FT)

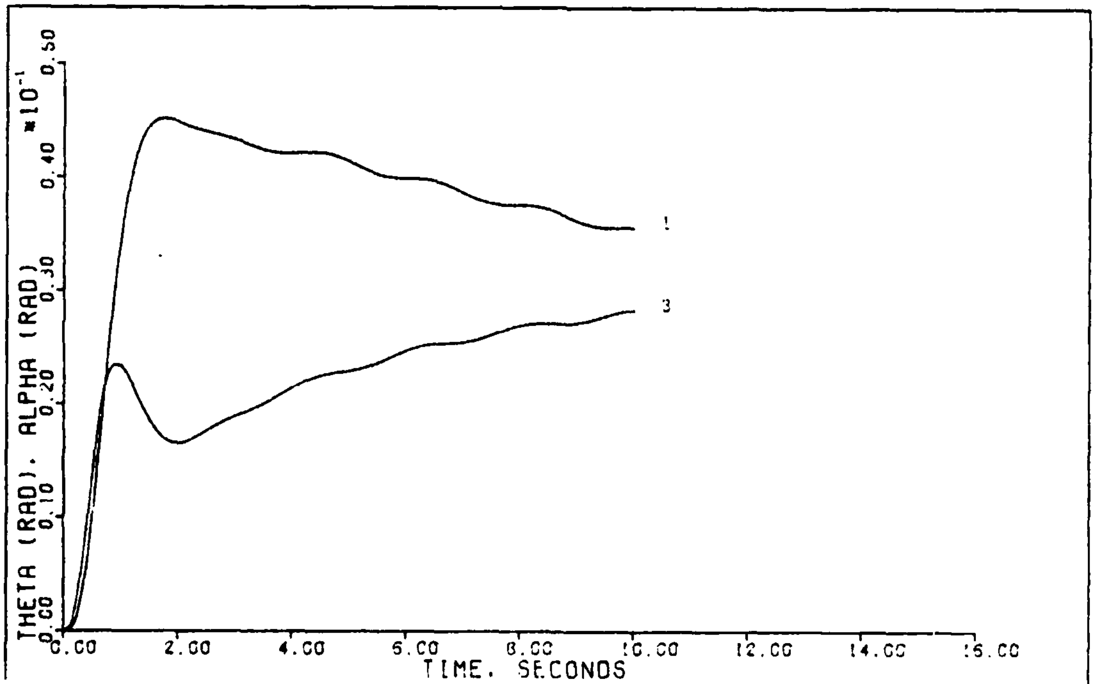

1.75 DEGREE PITCH POINTING (0.6 MACH. 0 FT)

Figure 22. 1.75 Degree Pitch Pointing (0.6 Mach)

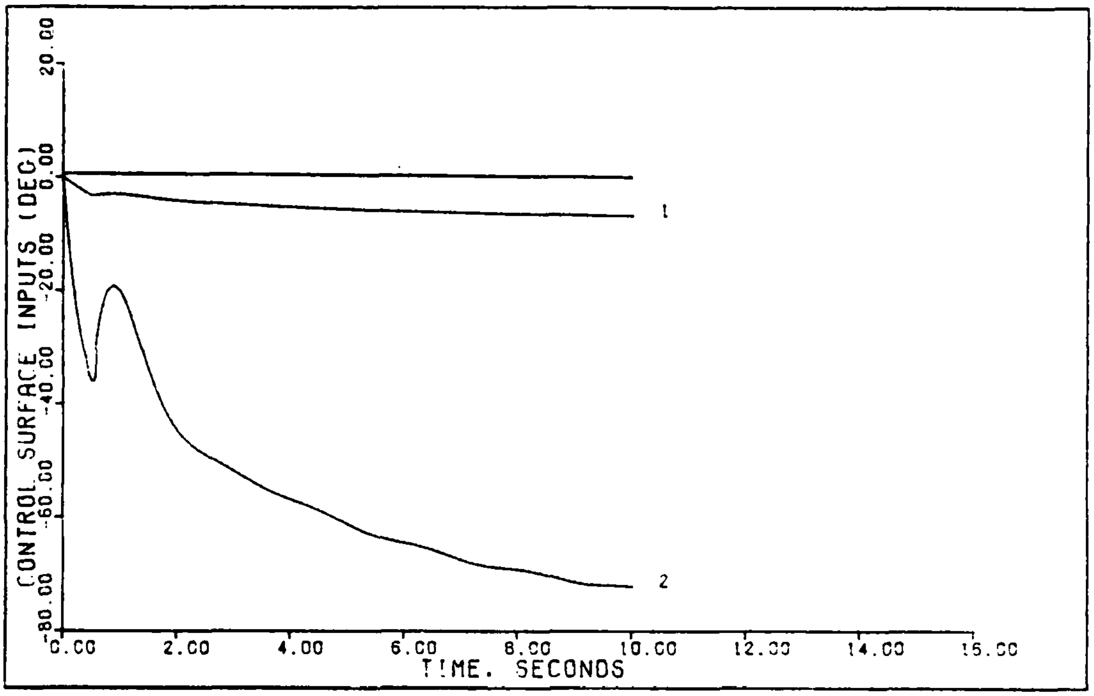

1.75 DEGREE PITCH POINTING (0.6 MACH. 0 FT)

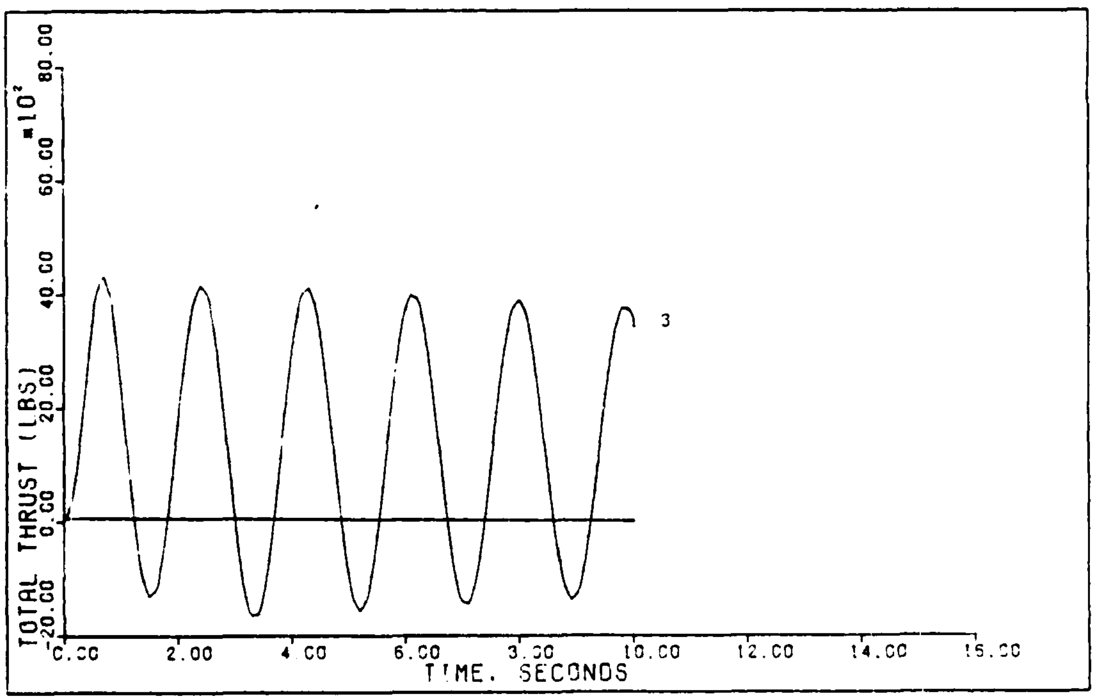

1.75 DEGREE PITCH POINTING (0.6 MACH. 0 FT)

Figure 23. 1.75 Degree Pitch Pointing (0.6 Mach)

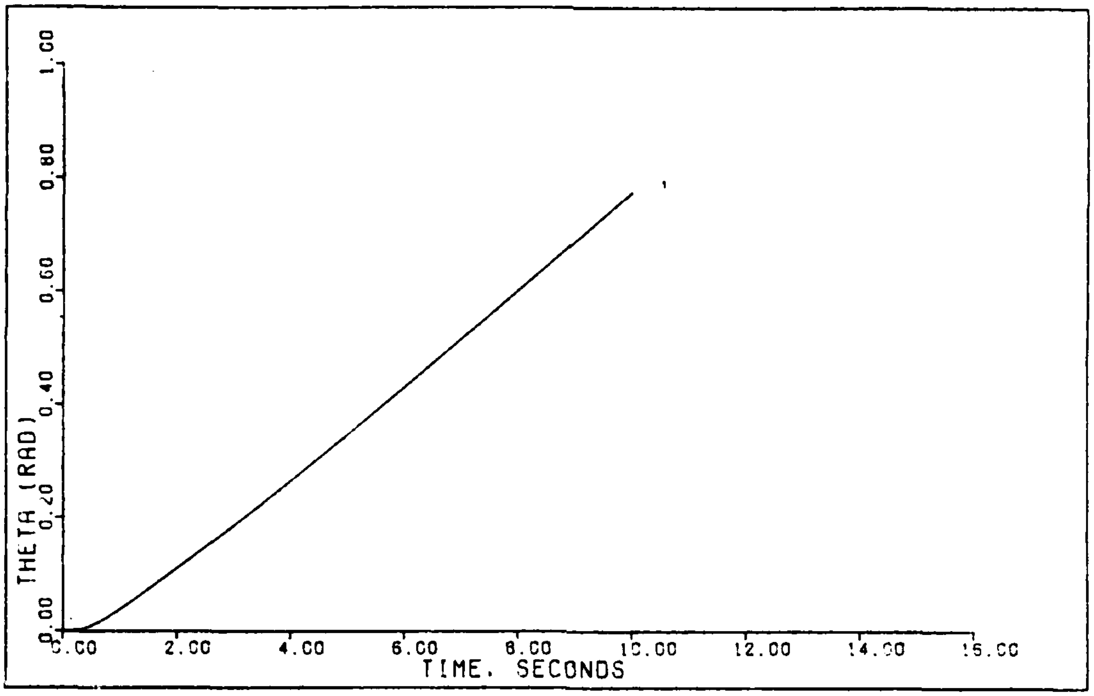

1.8 G DIRECT LIFT (0.6 MACH, 0 FT)

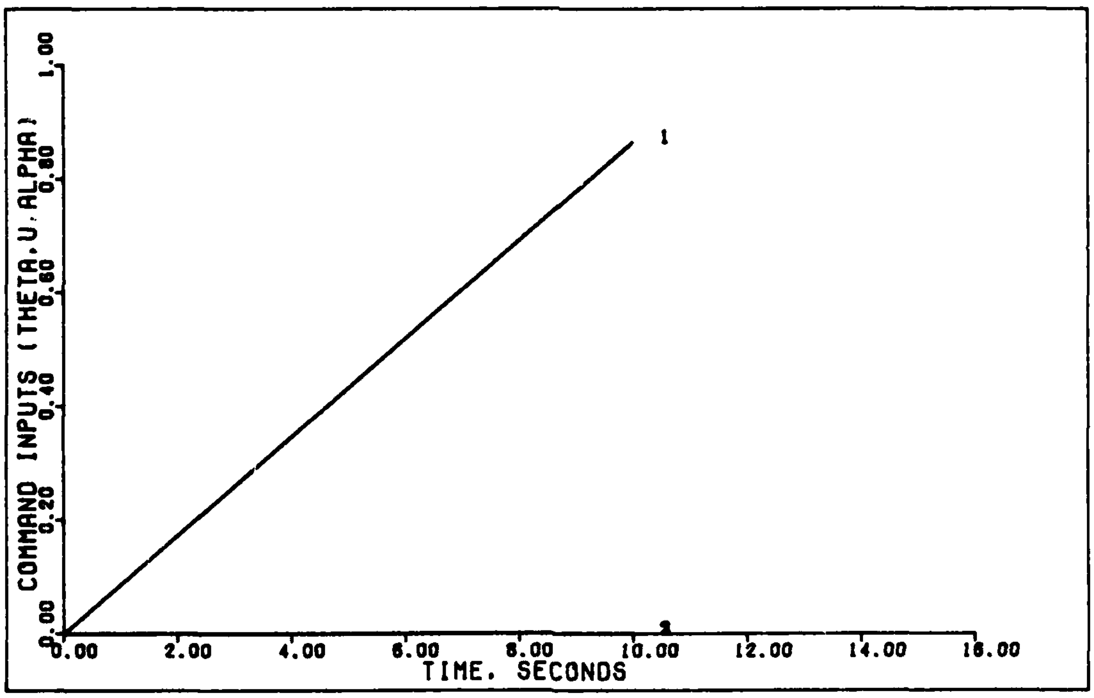

1.8 G DIRECT LIFT (0.6 MACH, 0 FT)

Figure 24. 1.8 g Direct Lift (0.6 Mach)

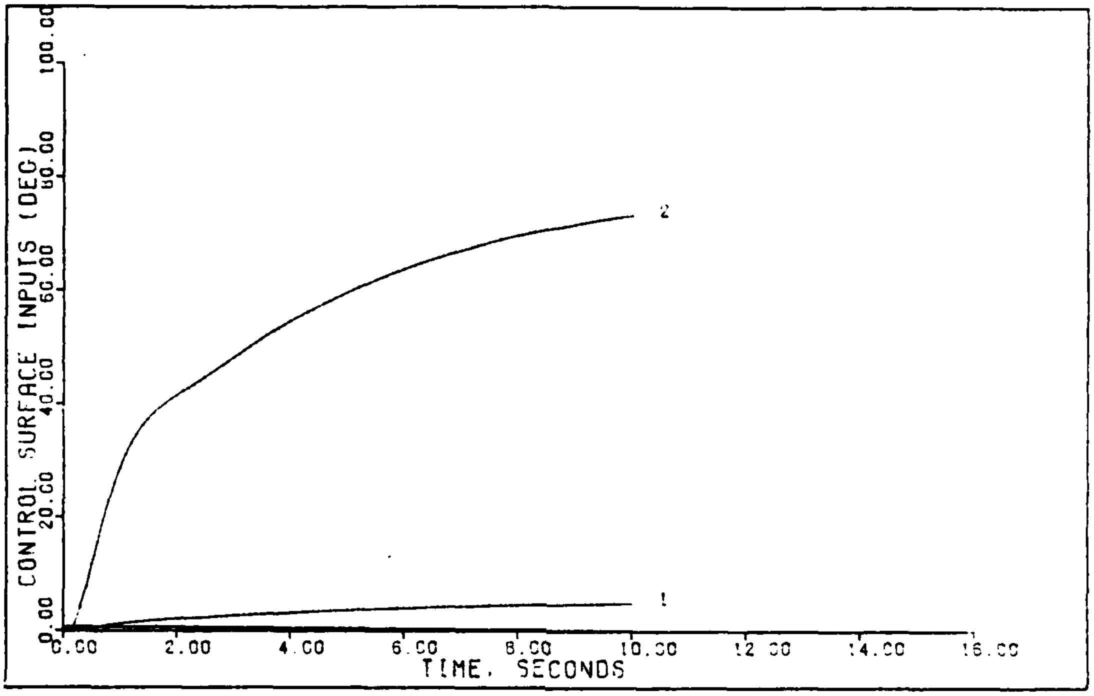

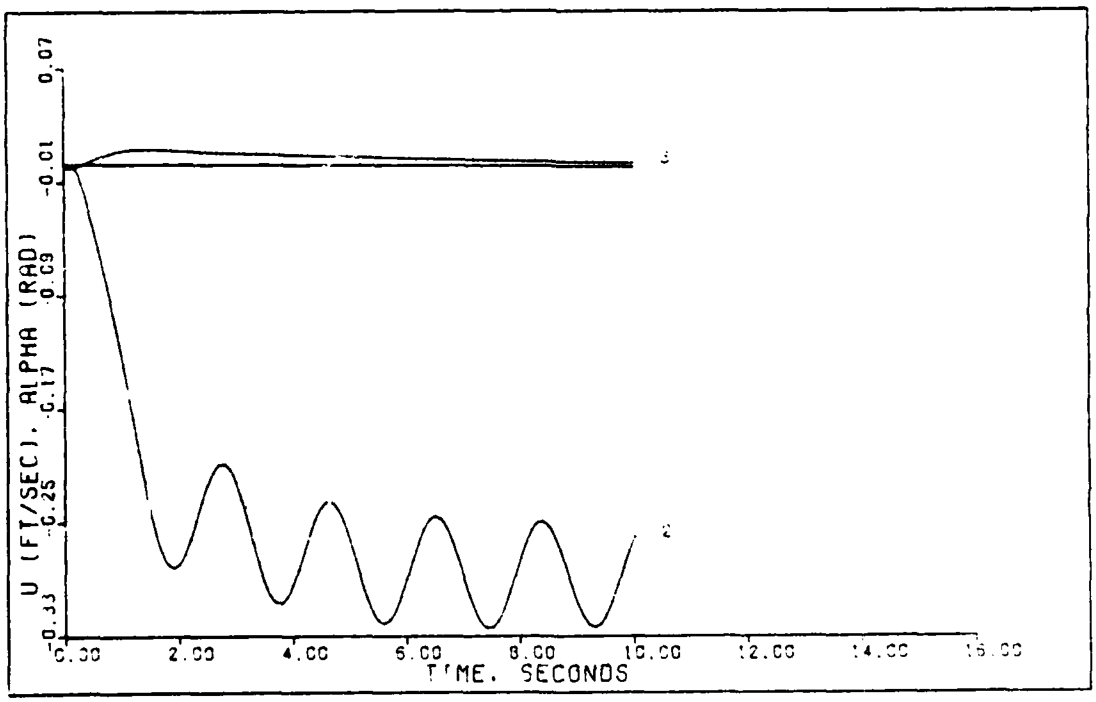

Figure 25. 1.8 g Direct Lift (0.6 Mach)

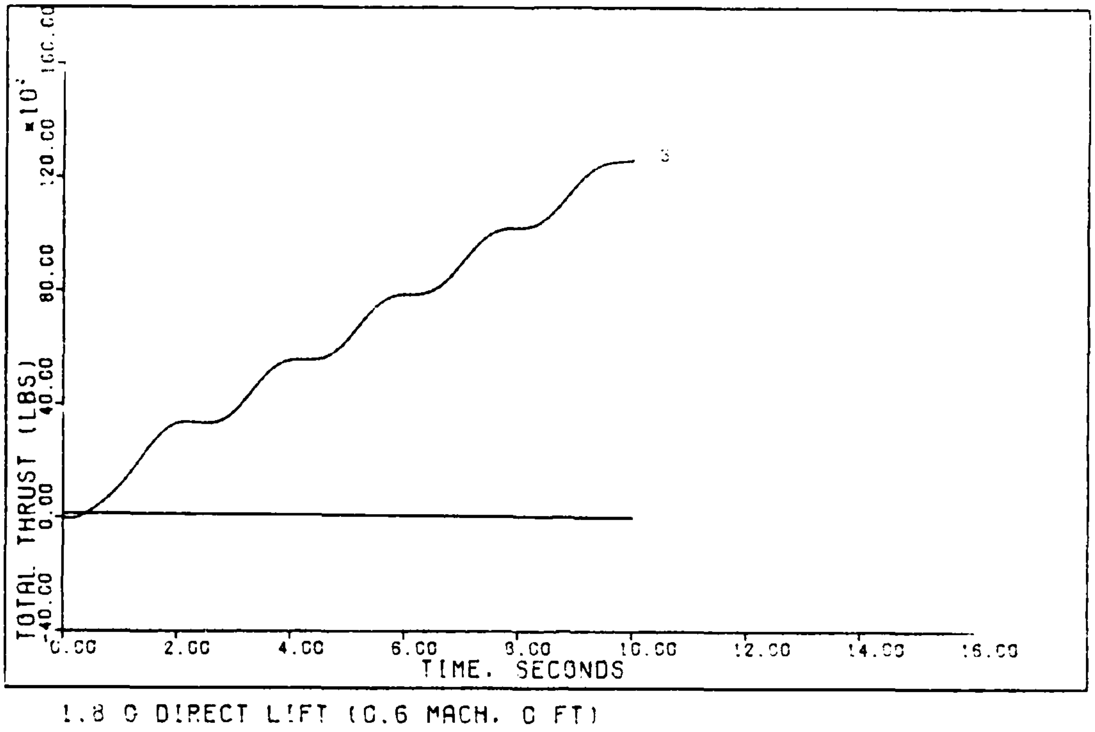

Figure 26. 1.8 g Direct Lift (0.6 Mach)

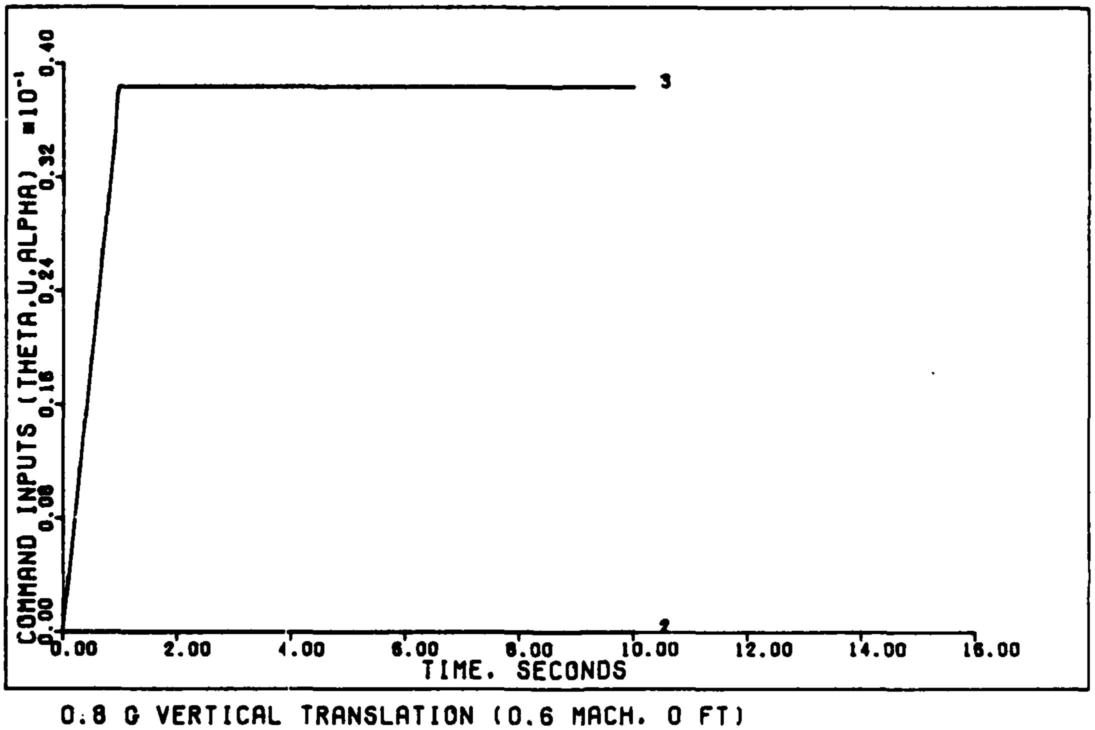

Figure 27. 0.8 g Vertical Translation (0.6 Mach)

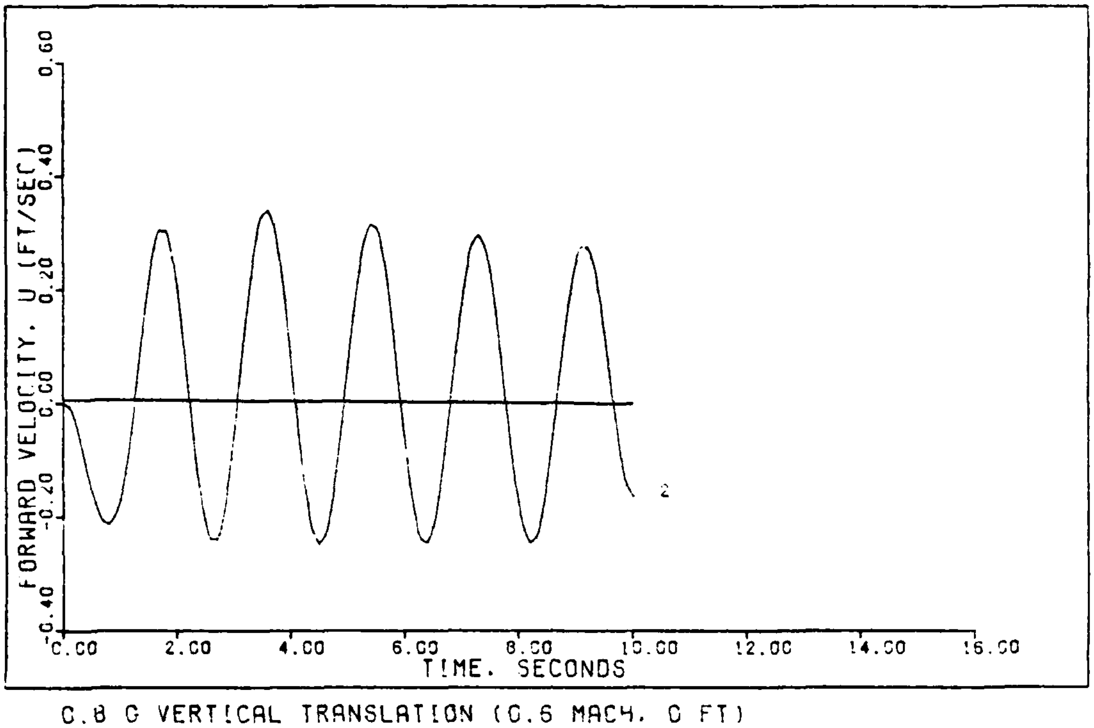

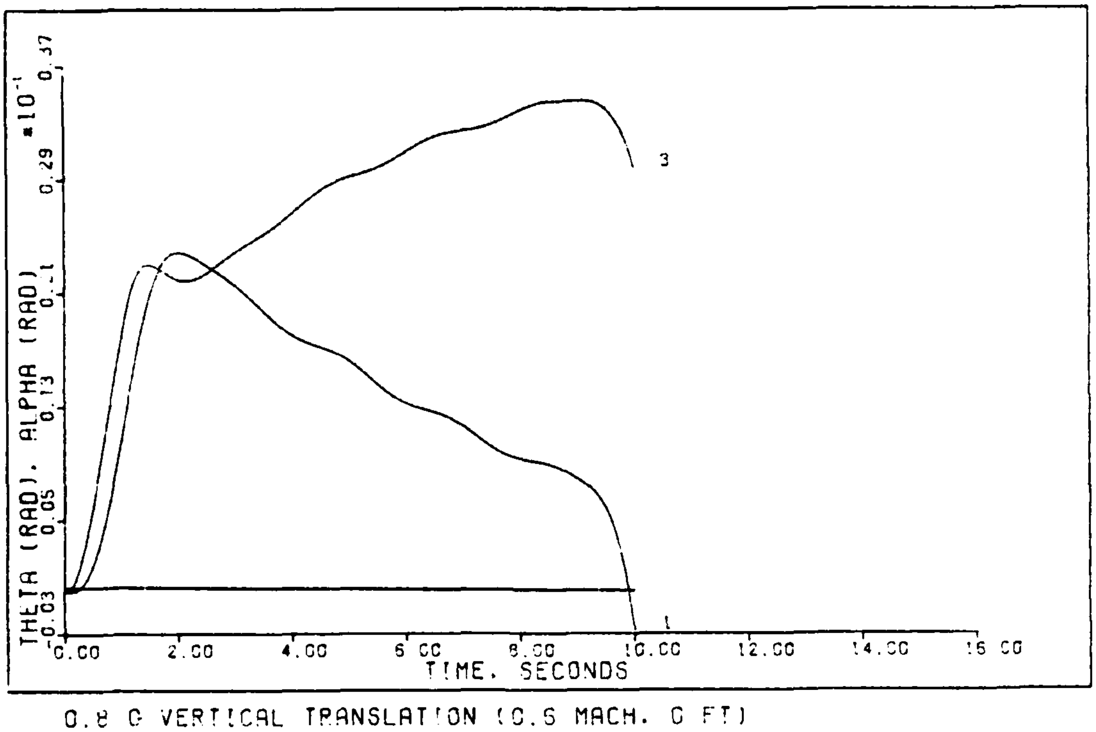

Figure 28. 0.8 g Vertical Translation (0.6 Mach)

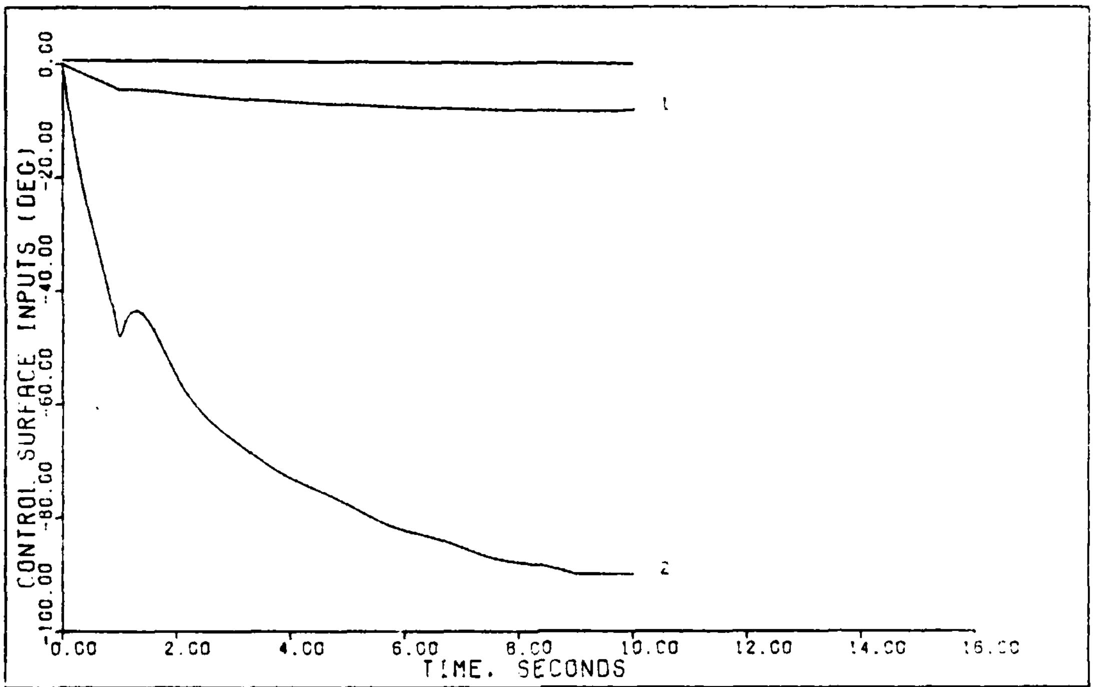

0.8 G VERTICAL TRANSLATION (0.6 MACH, 0 FT)

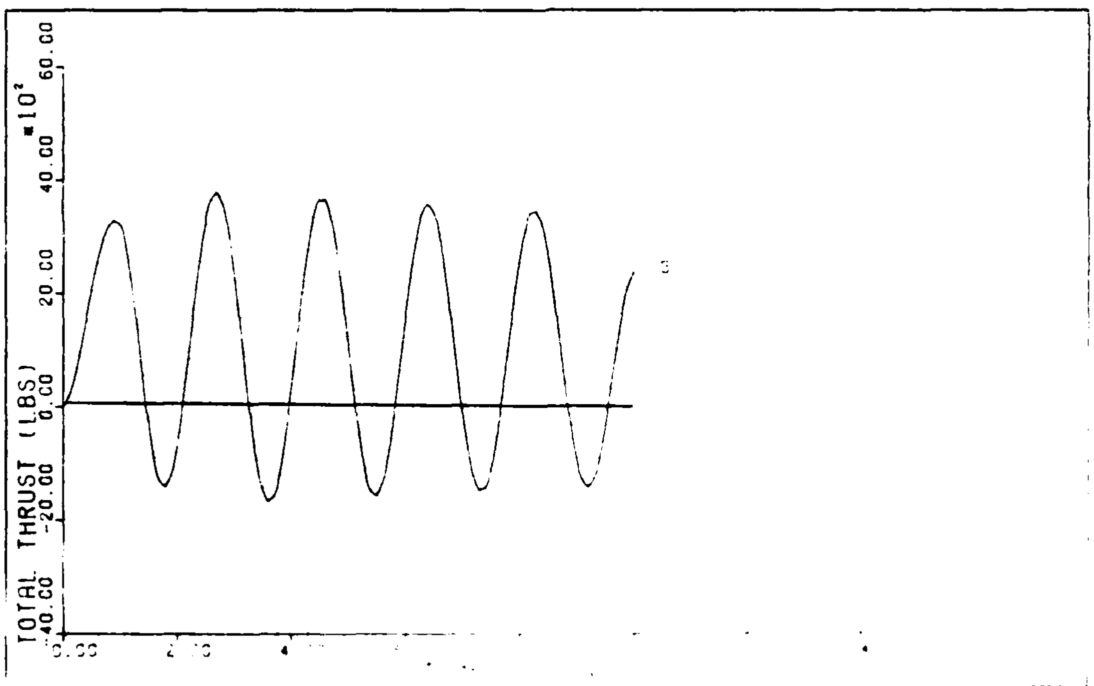

0.8 G VERT[illegible]

Figure 29. 0.8 g Vertical Translation ([illegible] Mach)

AD-A138 093 MULTIVARIABLE DIGITAL FLIGHT CONTROL DESIGN FOR THE FPCC (FLIGHT PROPULSI..(U) AIR FORCE INST OF TECH WRIGHT-PATTERSON AFB OH SCHOOL OF ENGI.. J A SIMMERS 2/3

UNCLASSIFIED DEC 83 AFIT/GE/EE/83D-61 F/G 1/3 NL

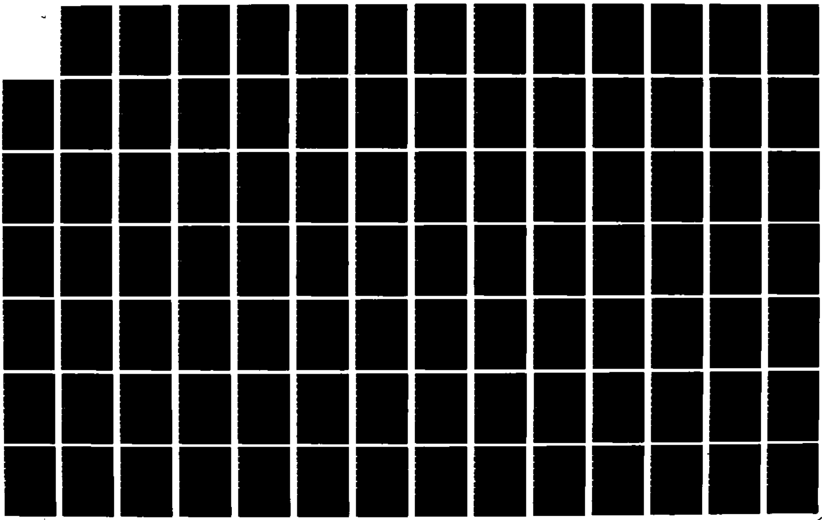

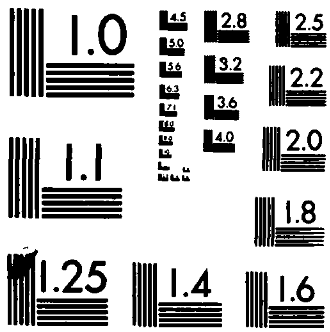

MICROCOPY RESOLUTION TEST CHART
NATIONAL BUREAU OF STANDARDS-1963-A

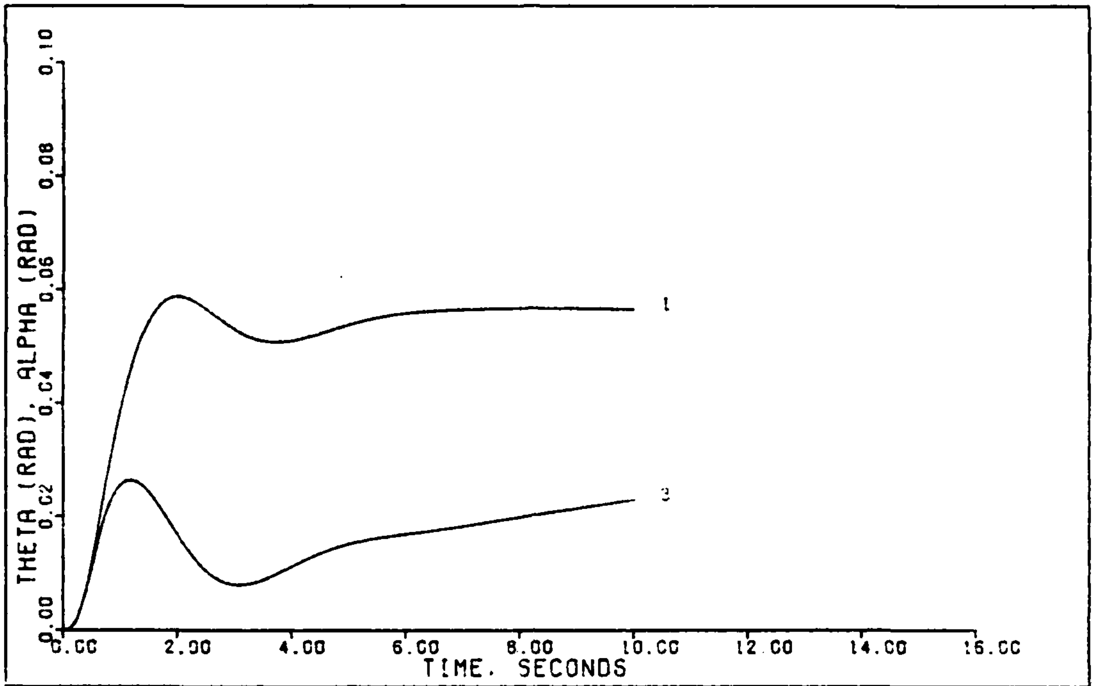

3 DEGREE PITCH POINTING (0.9 MACH, 0 FT)

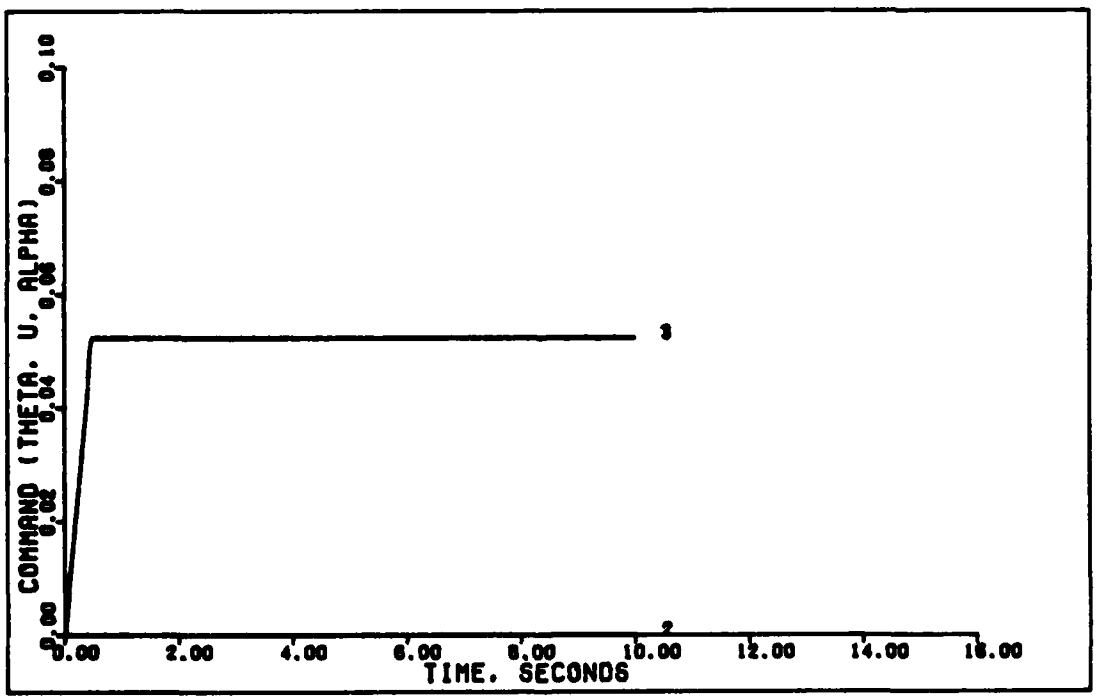

3 DEGREE PITCH POINTING (0.9 MACH)

Figure 30. 3 Degree Pitch Pointing (0.9 Mach)

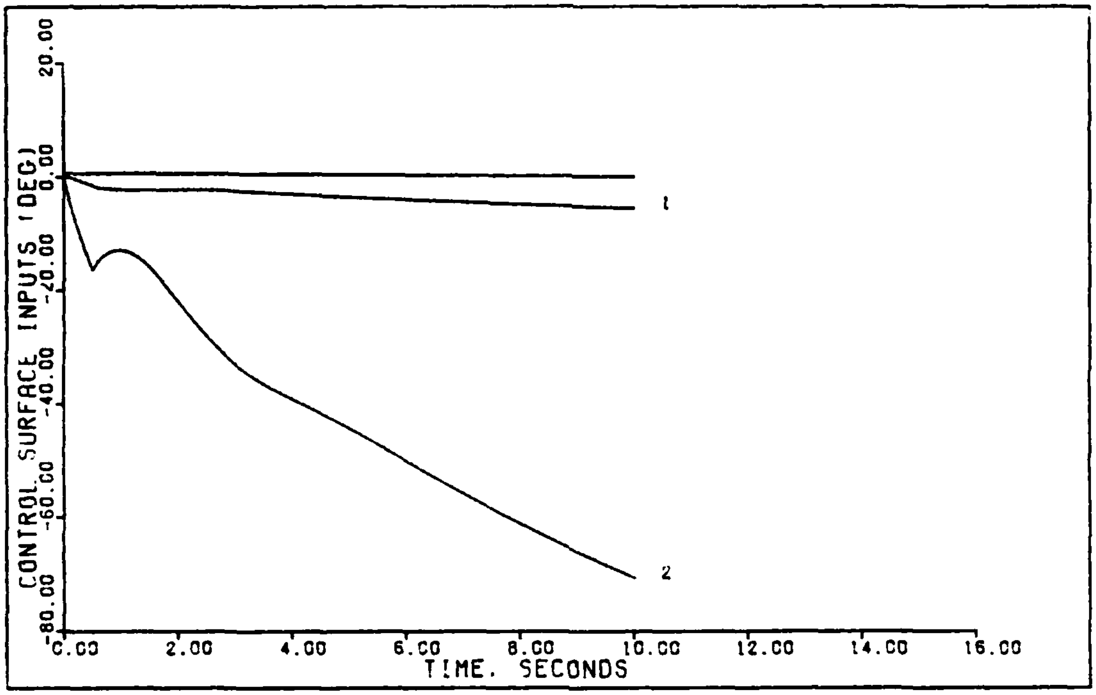

3 DEGREE PITCH POINTING (0.9 MACH, 0 FT)

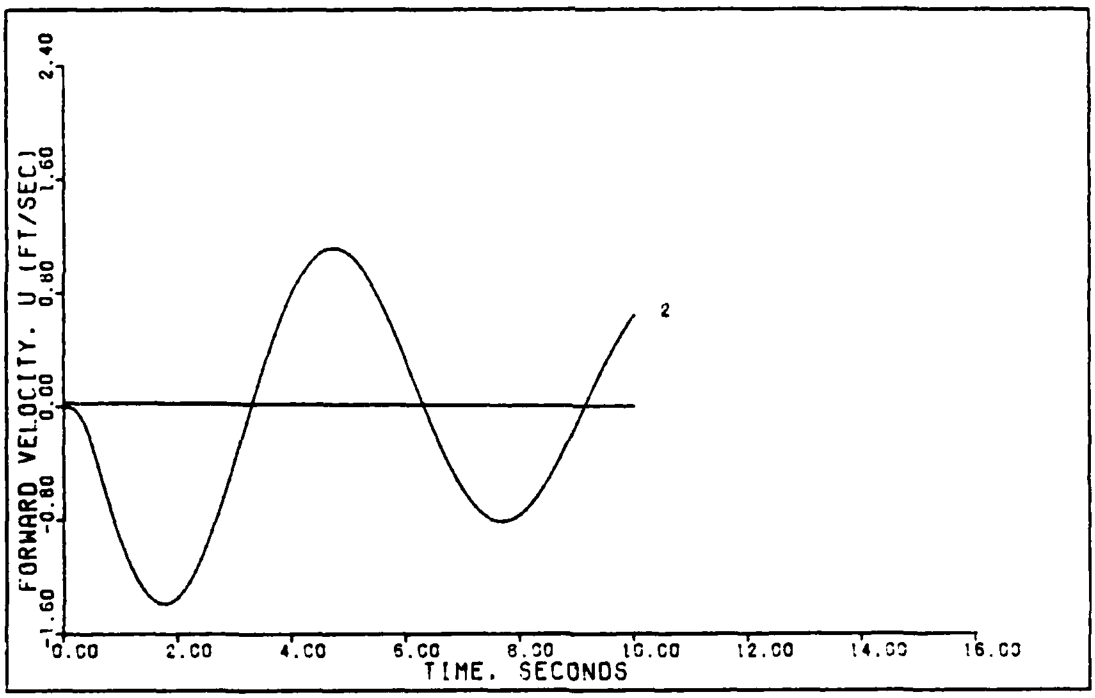

3 DEGREE PITCH POINTING (0.9 MACH, 0 FT)

Figure 31. 3 Degree Pitch Pointing (0.9 Mach)

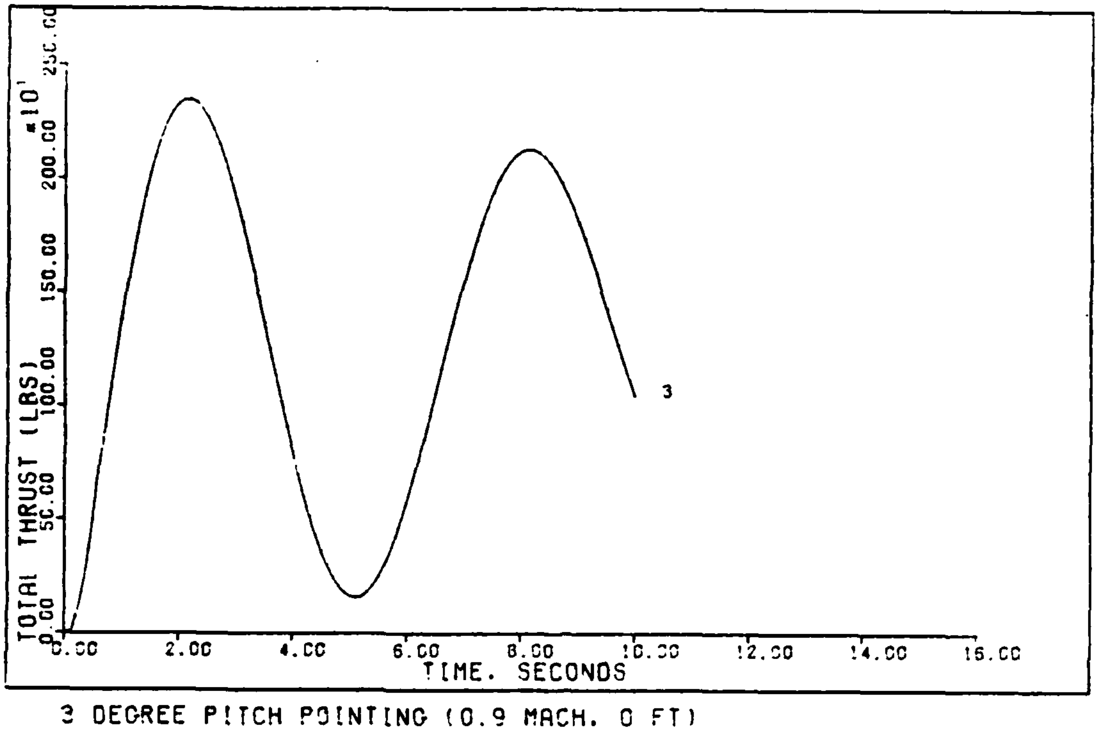

Figure 32. 3 Degree Pitch Pointing (0.9 Mach)

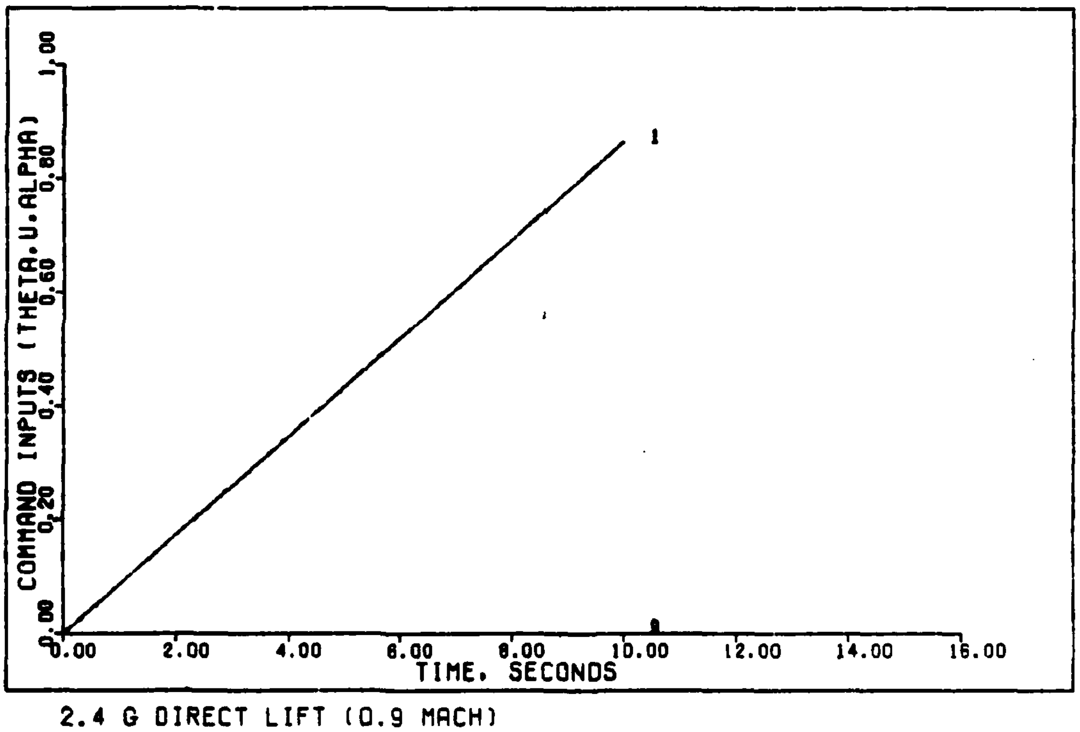

Figure 33. 2.4 g Direct Lift (0.9 Mach)

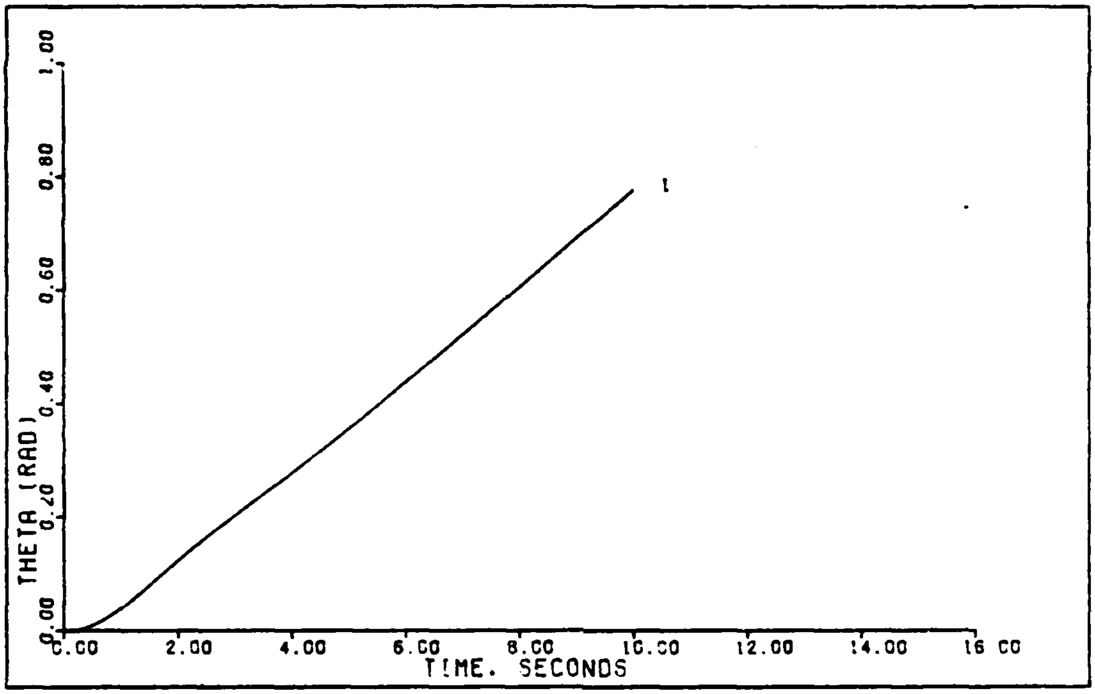

2.4 G DIRECT LIFT (0.9 MACH)

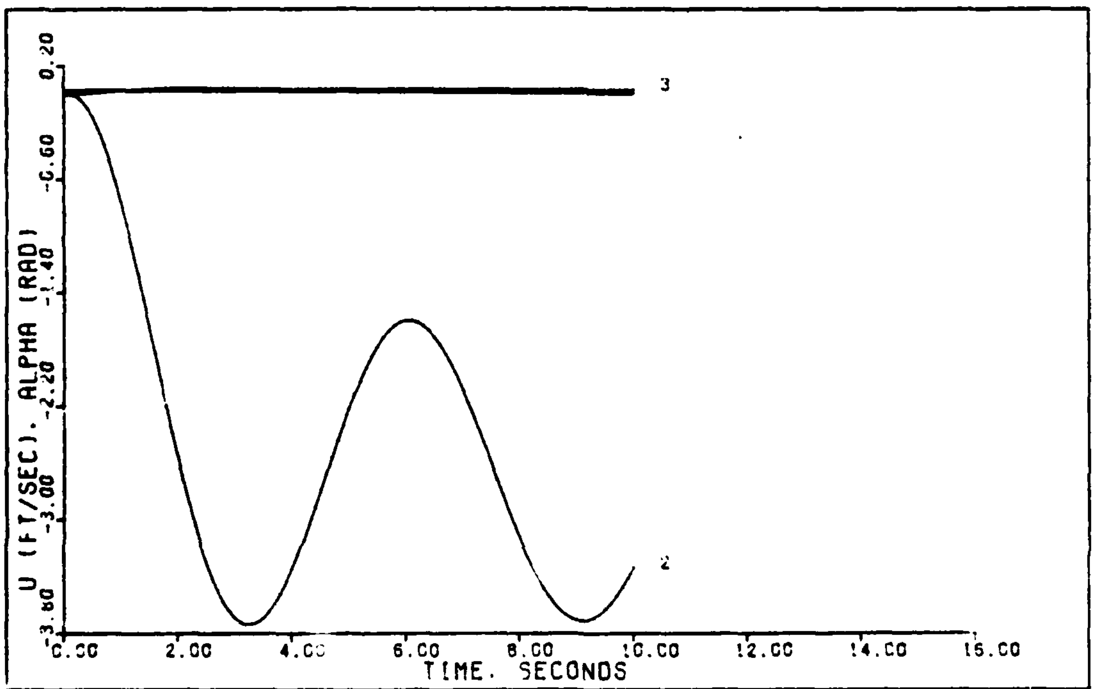

2.4 G DIRECT LIFT (0.9 MACH)

Figure 34. 2.4 g Direct Lift (0.9 Mach)

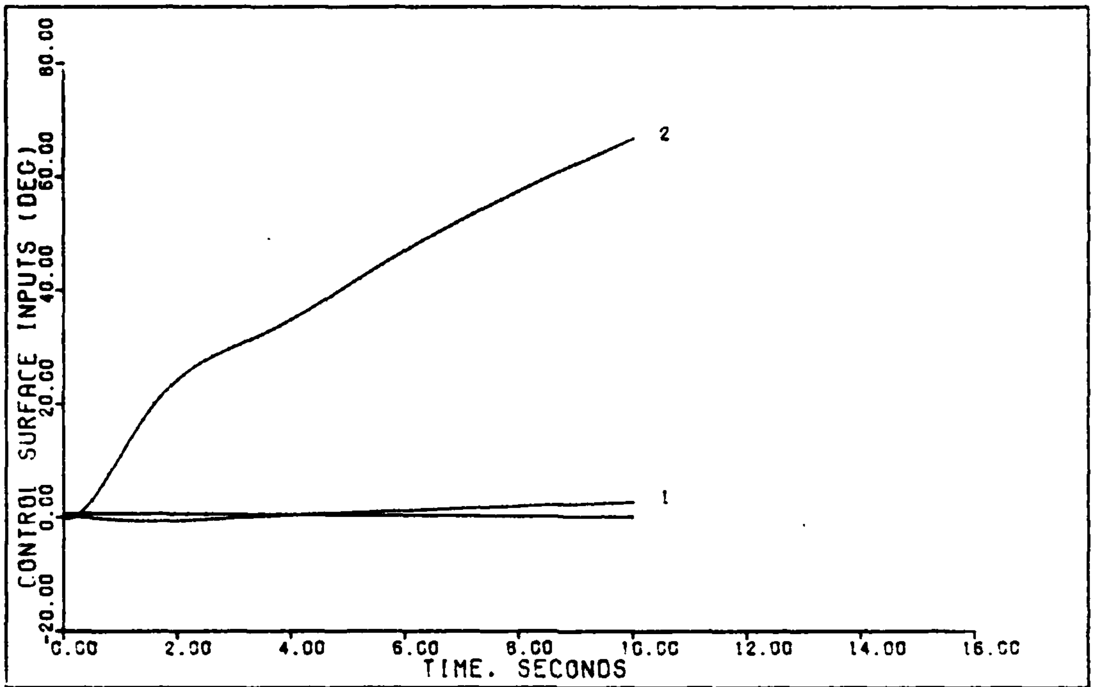

2.4 G DIRECT LIFT (0.9 MACH)

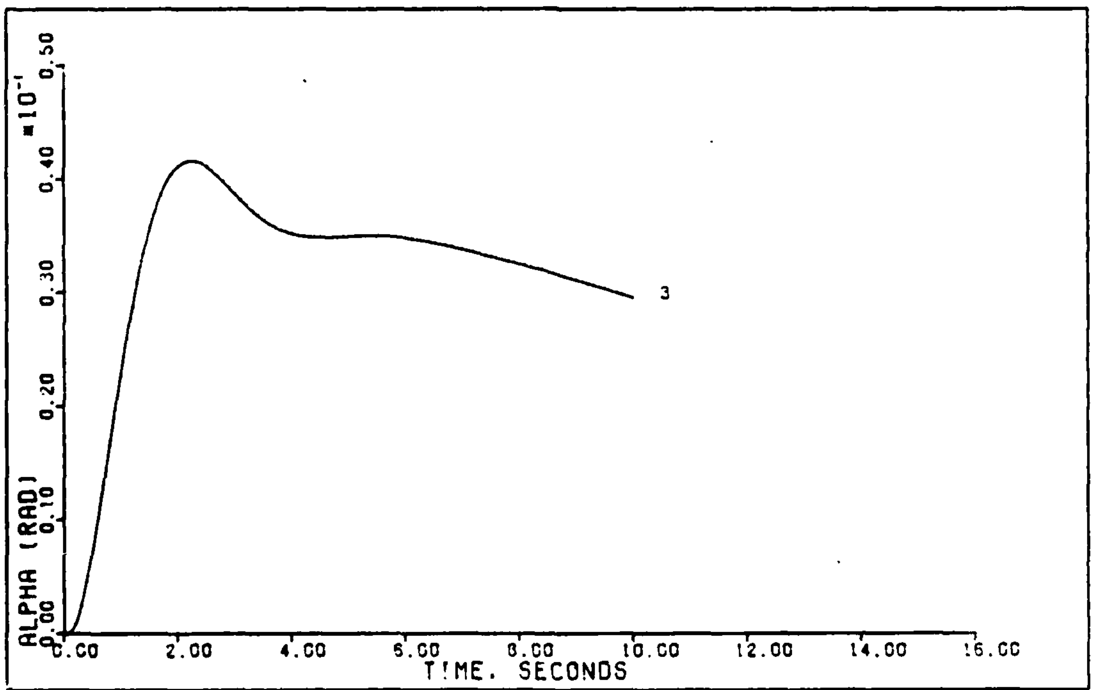

2.4 G DIRECT LIFT (0.9 MACH)

Figure 35. 2.4 g Direct Lift (0.9 Mach)

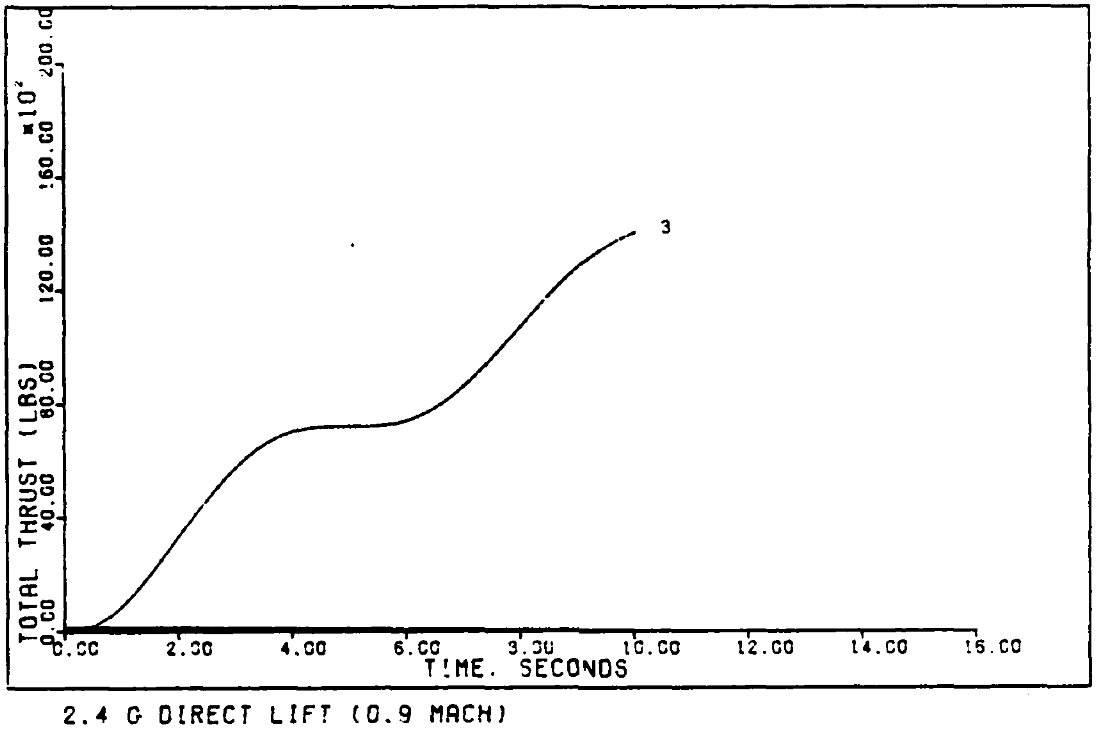

Figure 36. 2.4 g Direct Lift (0.9 Mach)

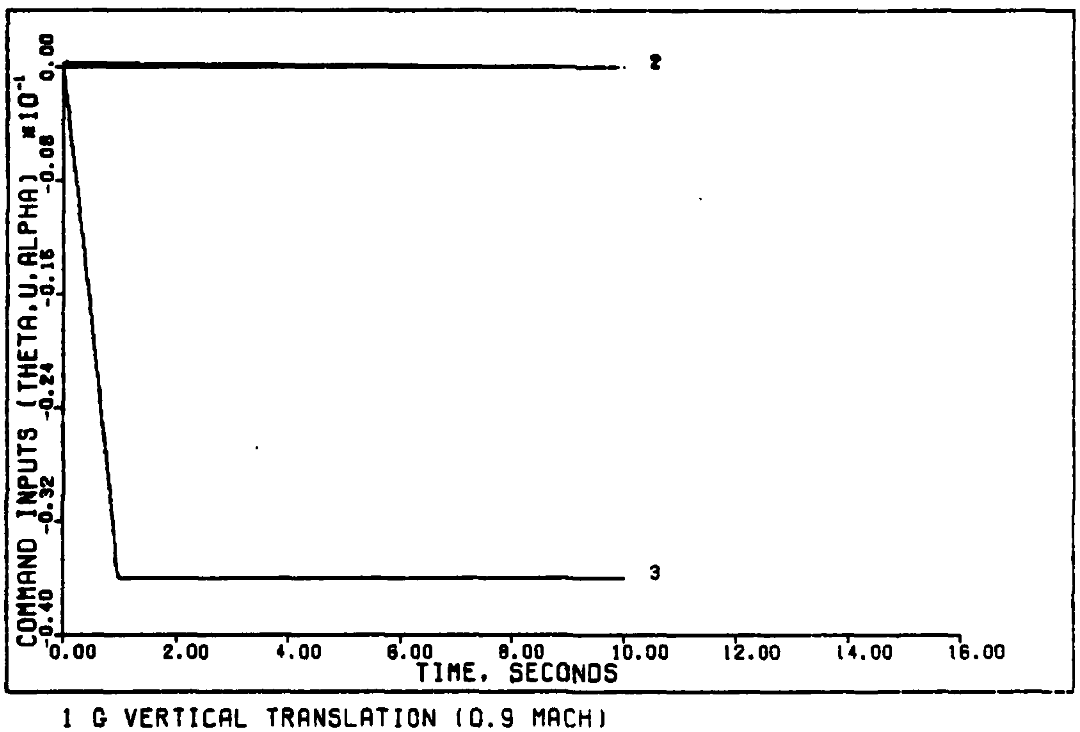

Figure 37. 1 g Vertical Translation (0.9 Mach)

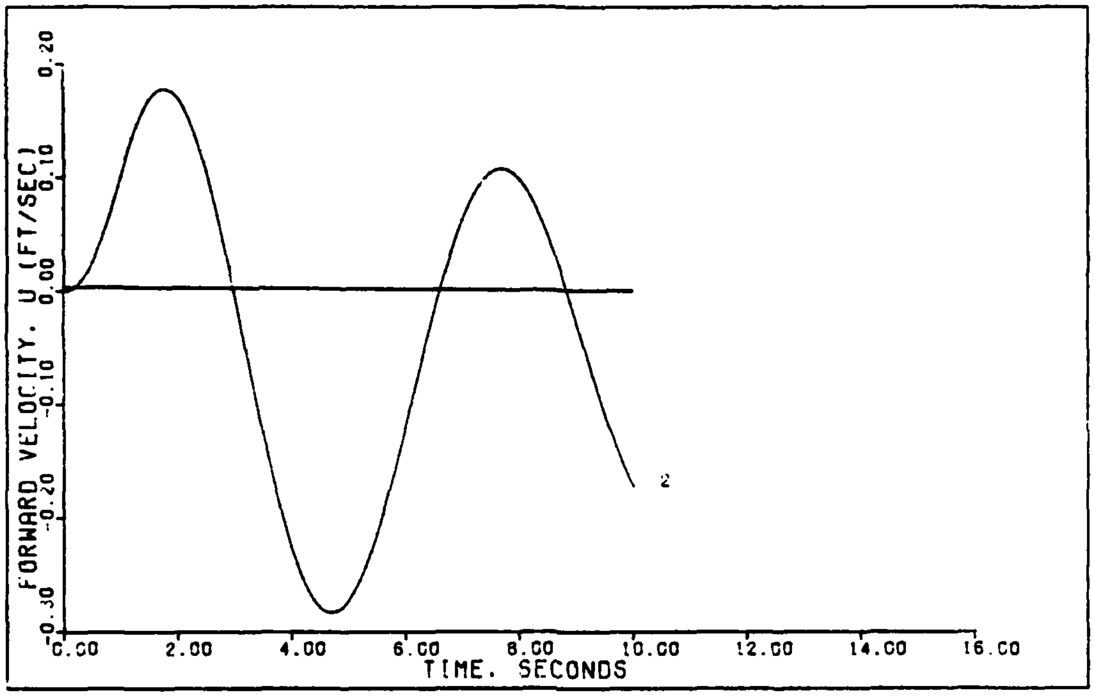

1 G VERTICAL TRANSLATION (0.9 MACH)

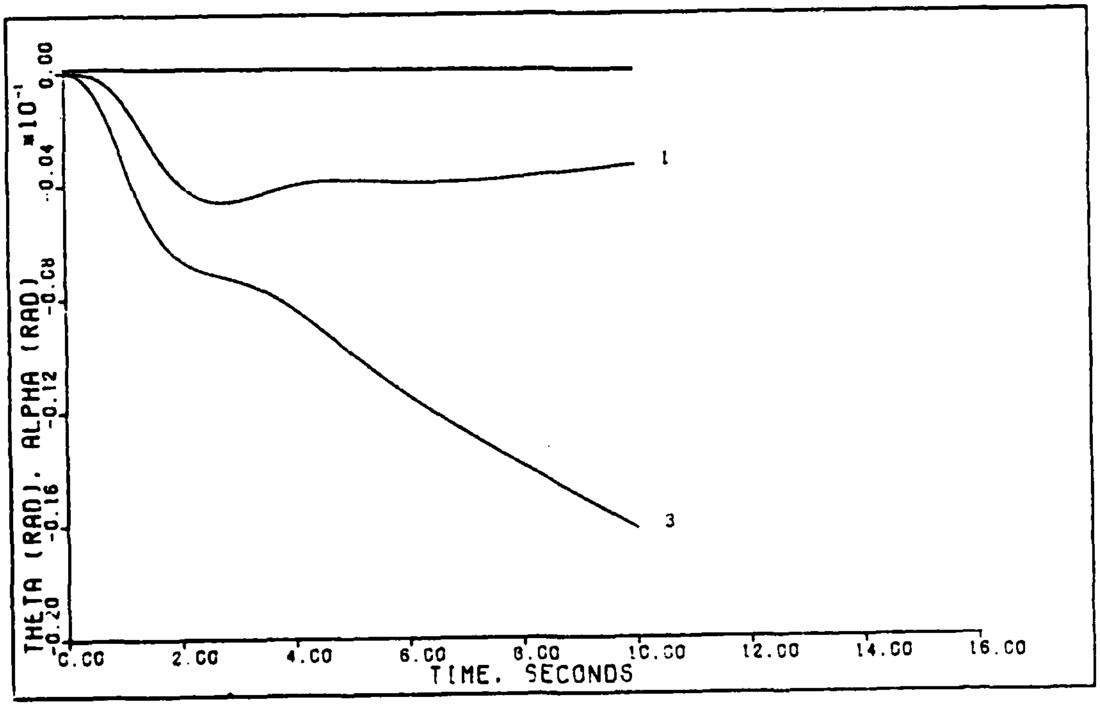

1 G VERTICAL TRANSLATION (0.9 MACH)

Figure 38. 1 g Vertical Translation (0.9 Mach)

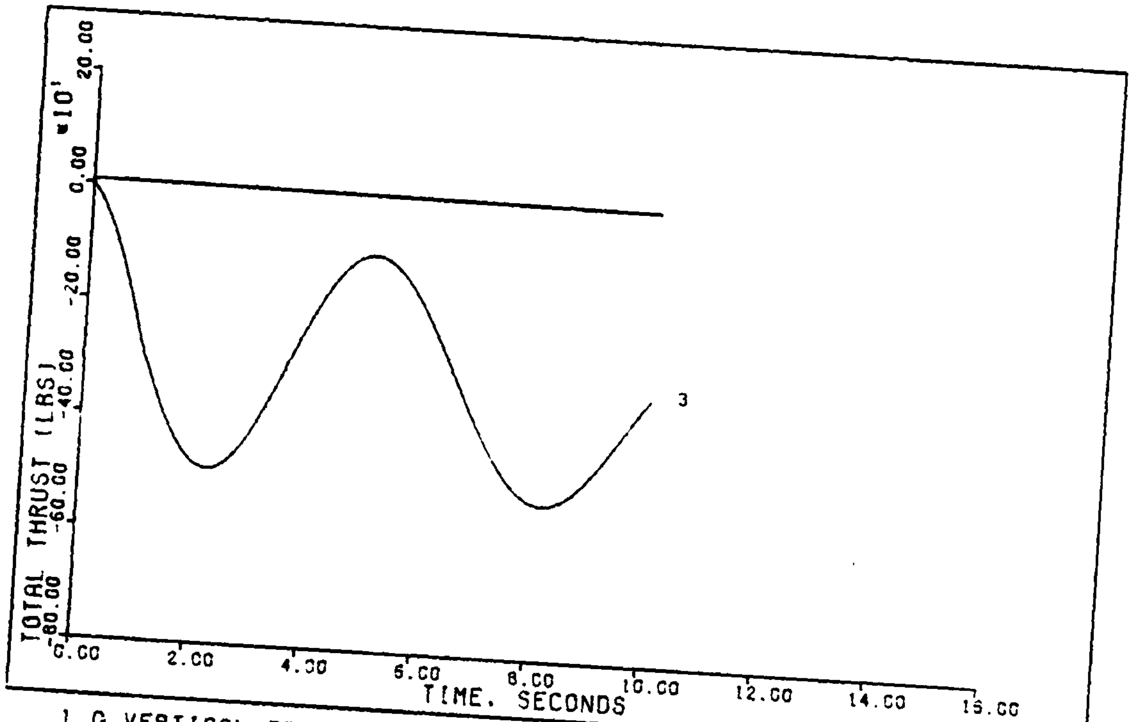

1 G VERTICAL TRANSLATION (0.9 MACH)

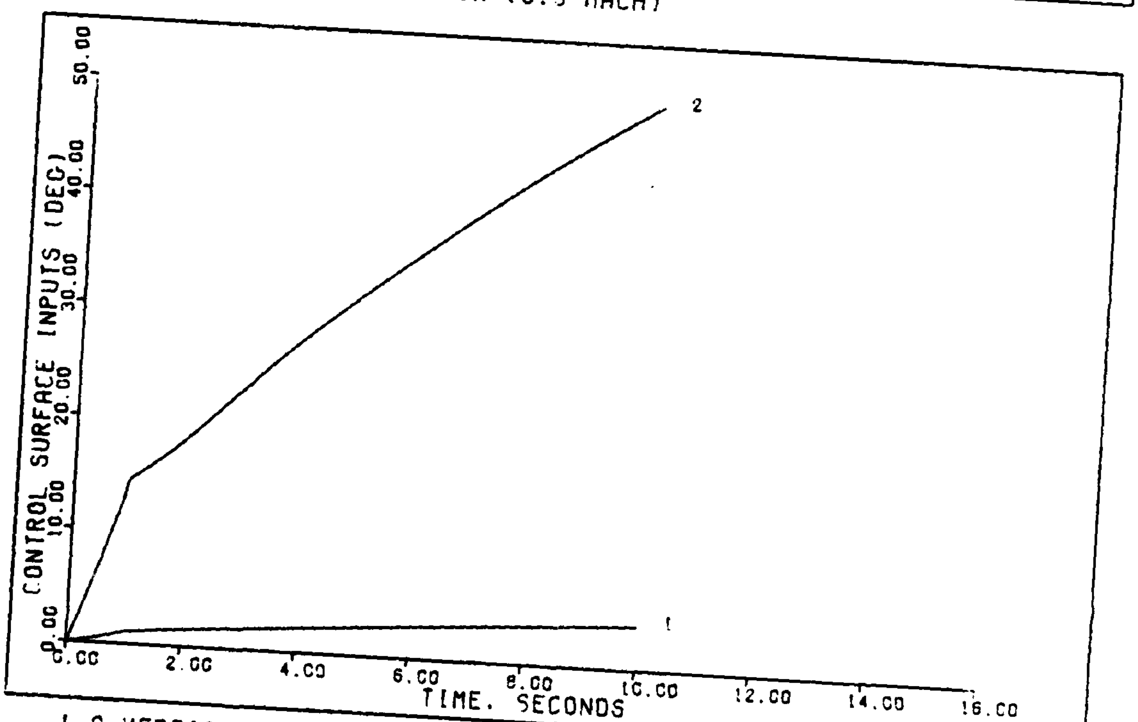

1 G VERTICAL TRANSLATION (0.9 MACH)

Figure 39. 1 g Vertical Translation (0.9 Mach)

conditions, 0.6 mach, sea level, and 0.9 mach, 30,000 ft. Table VIII shows the figures of merit from these time responses along with the commanded inputs for each maneuver.

Controller Response Analysis

Lateral Controller Response Analysis. Figure 5 shows the side velocity response for the horizontal translation maneuver, the only non-zero commanded input. Obviously the response does not follow the command, either in the transient stage or in the steady state (defined here as ten seconds after initial command input). Experimenting with other commanded g levels resulted in similar time responses of the side velocity. Optimizing the controller for just this one maneuver did not significantly improve the response. This may be due to the presence of a slow mode, due to a transmission zero, in the output.

Figure 7 shows the time response of the yaw rate for the flat turn, the only non-zero commanded input. For this flight condition, this is the worst responding maneuver of the three. Apparently the aircraft tracked the commanded yaw rate fairly well until one second, when the command was leveled off to a constant value. At this time the yaw rate falls off rapidly while the roll angle increases as does the side velocity, until in the steady state the aircraft is turning and sliding sideways through the airstream.

Figure 8 shows the control surface deflections, indicating that the control surfaces are being taxed due to the slow airspeed. The vertical canard runs immediately to full deflection, and the ailerons are run from full deflection in one direction to full deflection in the other in just one second.

Longitudinal Controller Response Analysis. For the 0.15 mach flight condition, Figure 12 shows the output responses for the 1.75 degree pitch pointing maneuver. Although the transient response is fairly acceptable, the steady state response is probably not, with alpha less than theta in magnitude. This results in a maximum flight path angle of about 0.9 degrees instead of the commanded zero degrees.

Figure 13 shows the oscillations in thrust and jet flap deflection, which have the same frequency as the oscillations in forward velocity. Here is the first indication that the jet flap is not going to work as well as the maneuver flap did for Bauschlicher in performing as an elevator. The problem is that deflecting the jet flap to induce a pitching moment also deflects the thrust and affects the forward velocity. The horizontal canard must deflect both to control any pitching moment from jet flap deflection and also to control changes in lift due to deflection of thrust (and consequent changes in velocity). The deflection rates of the horizontal canards and jet flaps present the least desirable (and possibly obtainable) aspects of this maneuver.

Figure 16 indicates that the aircraft response to the direct lift maneuver followed the commanded inputs quite well. However, the 0.5 g commanded was about the maximum possible using this controller. Even optimizing the controller for this maneuver did not add significantly to the aircraft performance. The apparent instability at the end of the simulation time probably results from either "wind up" or from an induced instability in the controller due to a lag in the integration routine. Appendix C contains more detail concerning this problem.

Another possible problem is the initial jet flap deflection needed to trim the aircraft at 0.15 mach, sea level. Obviously this adds complications not present with zero initial jet flap deflection, such as in Bauschlicher's thesis.

Figure 18 shows the output responses for the v tical translation maneuver at 0.15 mach, sea level. The out 's result in a lower g rating than commanded, but it is stil a vertical translation with almost no change in pitch angle. ..ce again an instability occurs at the end of the simulation. Appendix C contains more information on the causes and cures for this instability.

From the pitch pointing and vertical translation maneuvers, one conclusion is that the alpha response does not track commands as well as does the theta response.

Combined Lateral and Longitudinal Controller

Development. The last section of this chapter shows how the longitudinal and lateral models can be combined along with the lateral and longitudinal controllers. Since the system $\underline{A}$ matrix for the 0.15 mach, sea level flight condition is decoupled (equation (48)), as is the $\underline{B}$ matrix after dropping the columns corresponding to CDI_1 and CDI_2, combining the separate models together poses no problems. The original columns for each thrust input in the $\underline{B}$ matrix are added together, just as for the longitudinal model. Combining the lateral and longitudinal system equations into one set of system equations yields:

$$
\begin{bmatrix} \dot{\theta} \\ \dot{\phi} \\ \dot{u} \\ \dot{w} \\ \dot{q} \\ \dot{v} \\ \dot{r} \\ \dot{p} \end{bmatrix}
=
\begin{bmatrix}
0 & 0 & 0 & 0 & 1 & 0 & 0 & 0 \\
0 & 0 & 0 & 0 & 0 & 0 & .19 & 1 \\
-31.6 & 0 & -.0214 & .0867 & -31.5 & 0 & 0 & 0 \\
-6.01 & 0 & -.215 & -.638 & 166 & 0 & 0 & 0 \\
0 & 0 & -.000156 & .0134 & -.103 & 0 & 0 & 0 \\
0 & 31.6 & 0 & 0 & 0 & -.172 & -164 & 31.5 \\
0 & 0 & 0 & 0 & 0 & .00415 & -.212 & .0654 \\
0 & 0 & 0 & 0 & 0 & -.00818 & .364 & -.696
\end{bmatrix}
\begin{bmatrix} \theta \\ \phi \\ u \\ w \\ q \\ v \\ r \\ p \end{bmatrix}
+
\begin{bmatrix}
0 & 0 & 0 & 0 & 0 & 0 \\
0 & 0 & 0 & 0 & 0 & 0 \\
-.0765 & -.0211 & .0021 & 0 & 0 & 0 \\
-.111 & -.118 & -.000734 & 0 & 0 & 0 \\
.039 & -.00908 & -.0000596 & 0 & 0 & 0 \\
0 & 0 & 0 & 0 & .111 & .0363 \\
0 & 0 & 0 & .00114 & -.0112 & .0022 \\
0 & 0 & 0 & .0122 & .0118 & -.00212
\end{bmatrix}
\begin{bmatrix} \delta_c \\ \delta_J \\ F \\ \delta_a \\ \delta_r \\ \delta_{vc} \end{bmatrix}
$$

$$
\begin{bmatrix} \theta \\ u \\ \alpha \\ v \\ \phi \\ r \end{bmatrix}
=
\begin{bmatrix}
1 & 0 & 0 & 0 & 0 & 0 & 0 & 0 \\
0 & 0 & 1 & 0 & 0 & 0 & 0 & 0 \\
0 & 0 & 0 & .00607 & 0 & 0 & 0 & 0 \\
0 & 0 & 0 & 0 & 0 & 1 & 0 & 0 \\
0 & 1 & 0 & 0 & 0 & 0 & 0 & 0 \\
0 & 0 & 0 & 0 & 0 & 0 & 1 & 0
\end{bmatrix}
\begin{bmatrix} \theta \\ \phi \\ u \\ w \\ q \\ v \\ r \\ p \end{bmatrix}
\qquad (94)
$$

The combined system shown in equation (94) is both observable and controllable, and has no transmission zeros in the right half s plane. After substituting the $\underline{F}$ matrix for the $\underline{C}$ matrix the transmission zeros are found to be in the left half plane and are:

$$Z_t = \{1-T/m_1, 1-T/m_2\} \tag{95}$$

with

$$\underline{M} = \begin{bmatrix} .25 & 0 \\ 0 & 0 \\ 0 & 0 \\ 0 & 0 \\ 0 & .25 \\ 0 & 0 \end{bmatrix} \tag{96}$$

The $\underline{\Gamma}$, $\underline{\Sigma}$, $\underline{K}_o$, and $\underline{K}_1$ matrices are just the block diagonal combinations of the corresponding matrices for the individual designs with the off block diagonal terms equal to zero. However, the α scaler has now become a matrix and is given by:

$$\underline{\alpha} = \begin{bmatrix} 2 & 0 & 0 & 0 & 0 & 0 \\ 0 & 2 & 0 & 0 & 0 & 0 \\ 0 & 0 & 2 & 0 & 0 & 0 \\ 0 & 0 & 0 & 1 & 0 & 0 \\ 0 & 0 & 0 & 0 & 1 & 0 \\ 0 & 0 & 0 & 0 & 0 & 1 \end{bmatrix} \tag{97}$$

To demonstrate the decoupling of the combined system, the separate lateral inputs for the horizontal translation and the longitudinal inputs for the vertical translation are combined to command a jink maneuver. As can be seen in Figures 40 through 43, the responses to the combined jink maneuver are nothing more

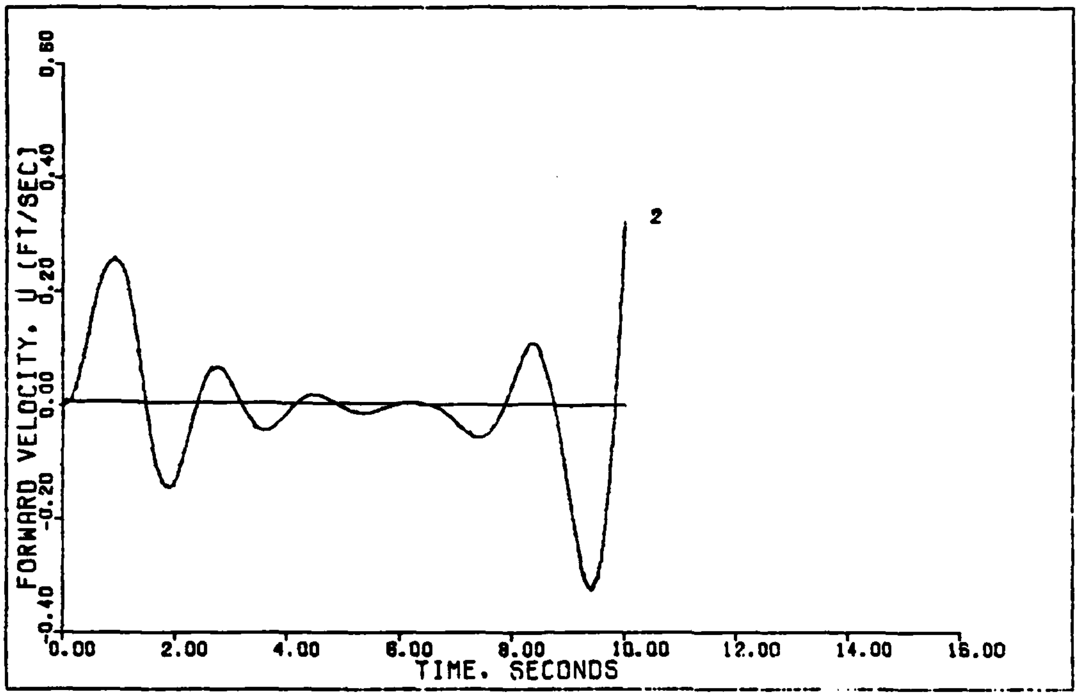

JINK MANEUVER (0.15 MACH, 0 FT)

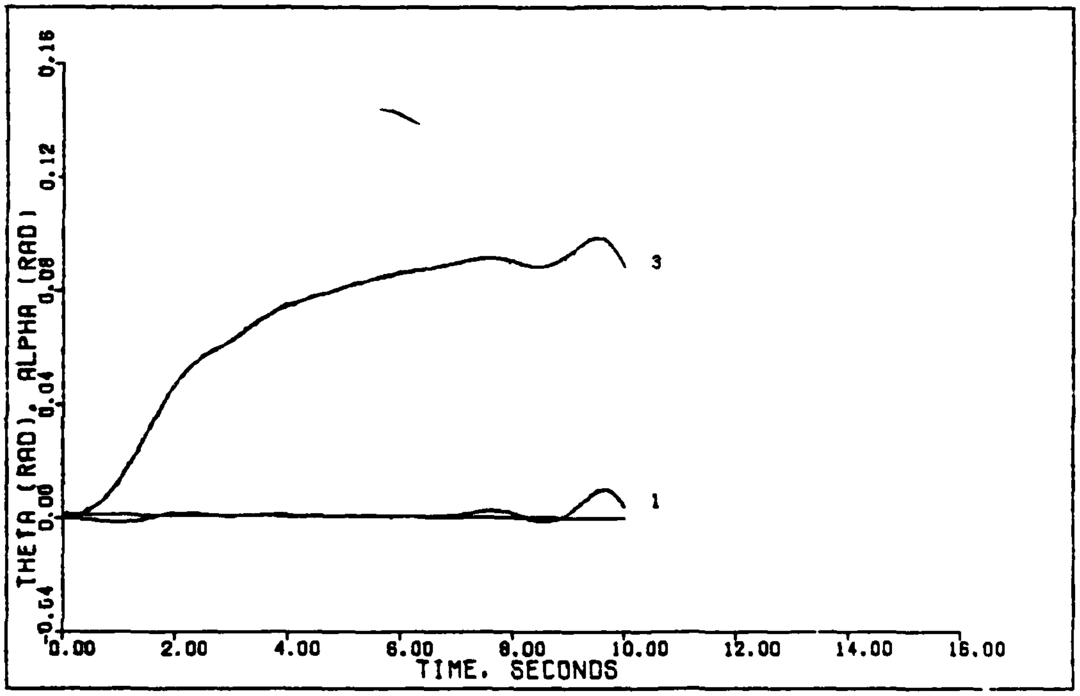

JINK MANEUVER (0.15 MACH, 0 FT)

Figure 40. Jink Maneuver (0.15 Mach)

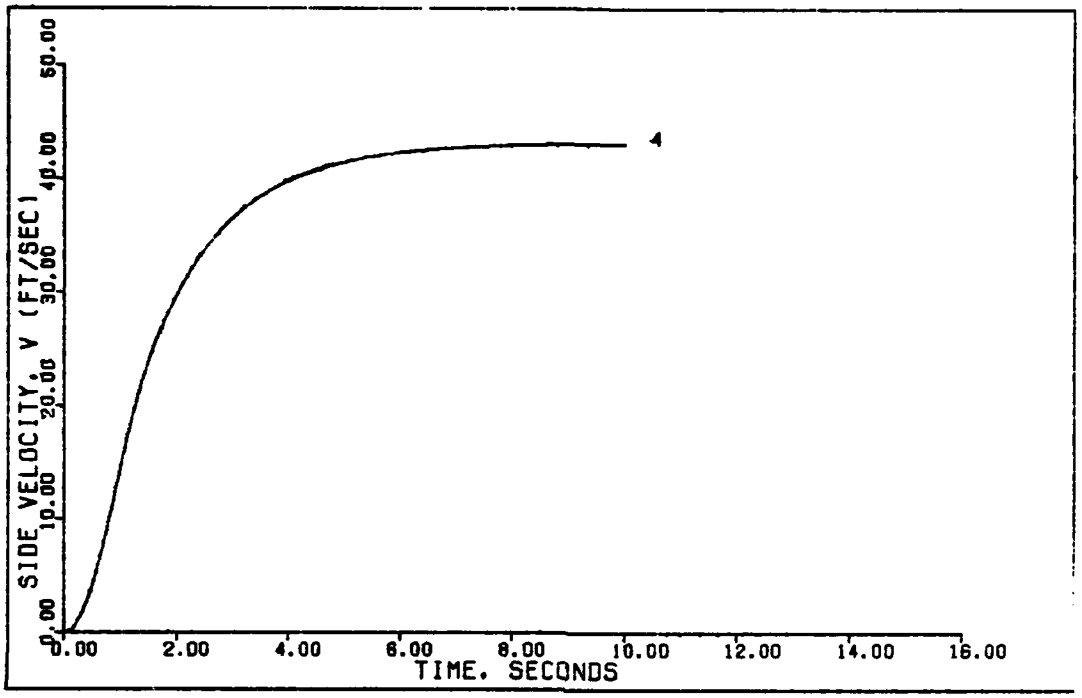

JINK MANEUVER (0.15 MACH, 0 FT)

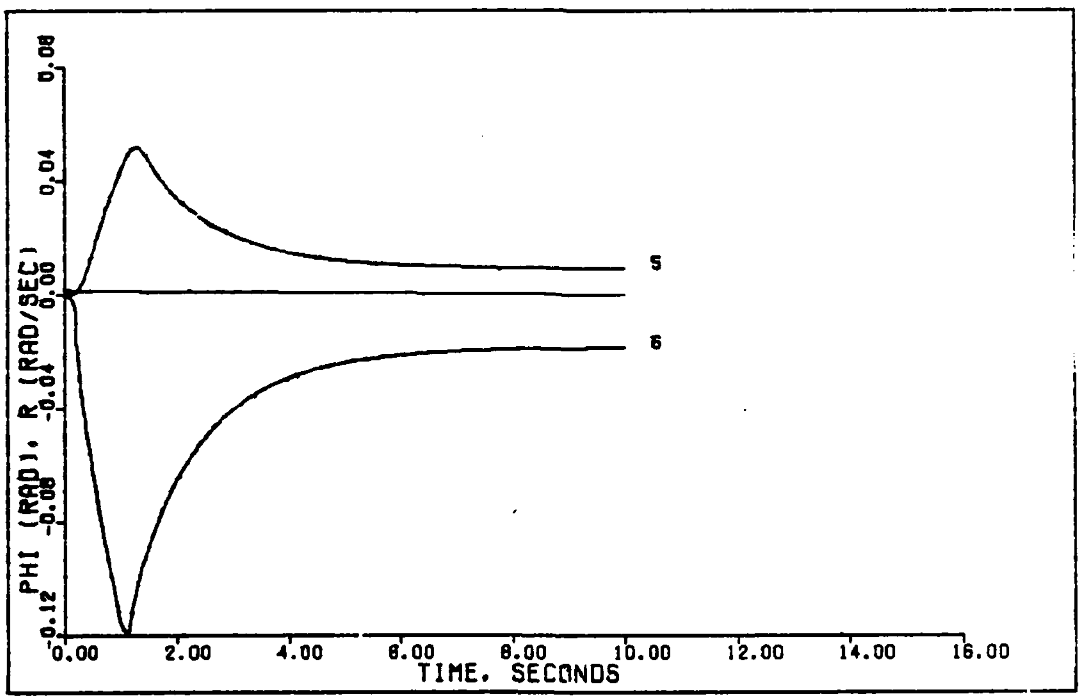

JINK MANEUVER (0.15 MACH, 0 FT)

Figure 41. Jink Maneuver (0.15 Mach)

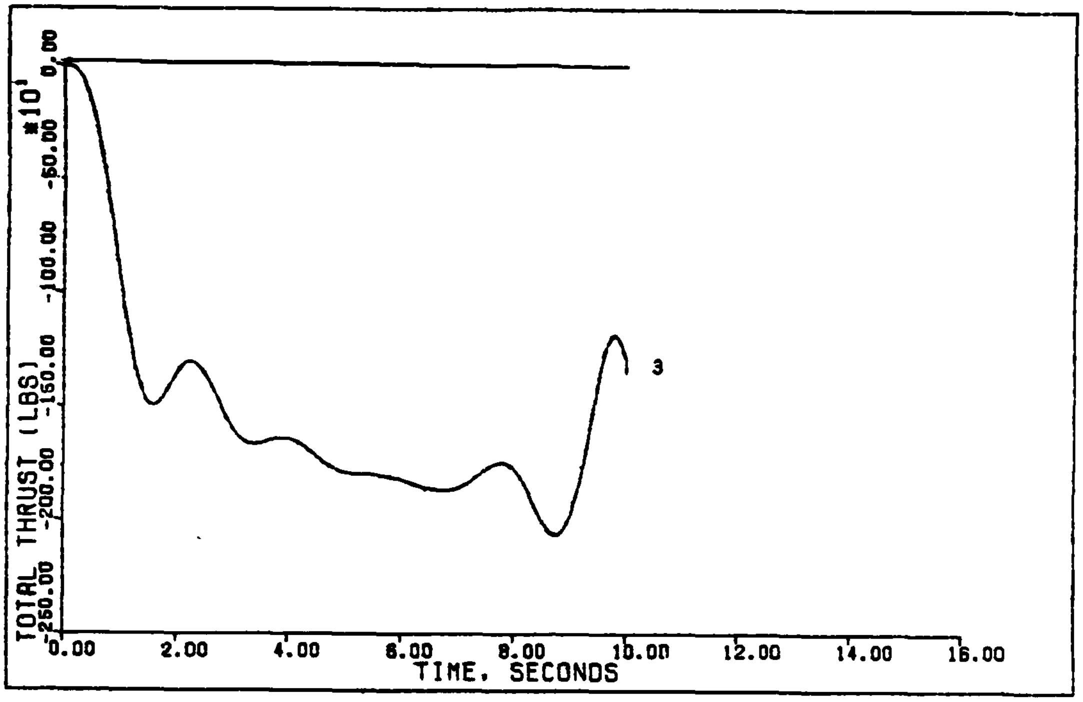

JINK MANEUVER (0.15 MACH, 0 FT)

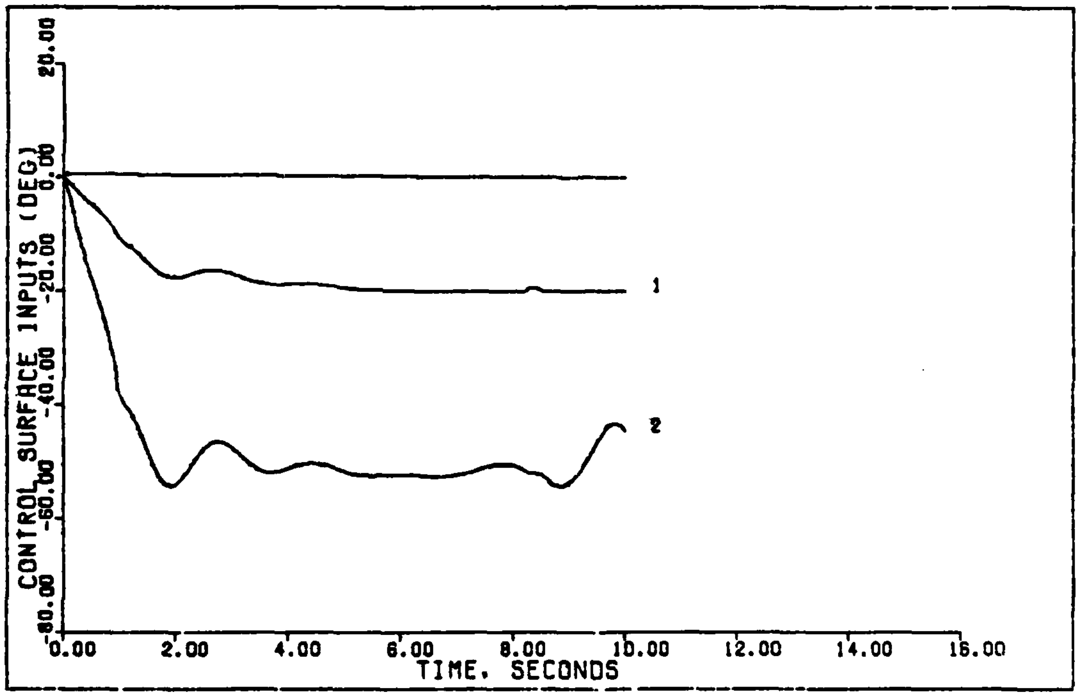

JINK MANEUVER (0.15 MACH, 0 FT)

Figure 42. Jink Maneuver (0.15 Mach)

TABLE VIII

SUMMARY OF OUTPUT RESPONSES FOR LONGITUDINAL CONTROLLERS

Flt. Cond.	Maneuver	Command, V	Overshoot	Rise Time
0.15 Mach	Pitch	.5,.0305,20,20	4%	.5 sec
0 ft.	Pointing	0,0,0,0	-.385 ft/sec	
		.5,.0305,20,20	3%	.75 sec
	Direct	10,.976,20,20	none	9.9 sec
	Lift	0,0,0,0	-.861 ft/sec	
		0,0,0,0	.07 rad	
	Vertical	0,0,0,0	.009 rad	
	Transl.	0,0,0,0	.323 ft/sec	
		1,.0977,20,20	*	9 sec
0.6 Mach	Pitch	.5,.0305,20,20	48%	.8 sec
0 ft.	Pointing	0,0,0,0	.348 ft/sec	
		.5,.0305,20,20	none	**
	Direct	10,.865,20,20	none	**
	Lift	0,0,0,0	-.324	
		0,0,0,0	.0132 rad	
	Vertical	0,0,0,0	.0239 rad	
	Transl.	0,0,0,0	.339 ft/sec	
		1,.0384,20,20	none	9.1 sec
0.9 Mach	Pitch	.5,.0524,20,20	12.2%	1.5 sec
30,000 ft.	Pointing	0,0,0,0	-1.39 ft/sec	
		.5,.0524,20,20	none	**
	Direct	10,.865,20,20	none	10 sec
	Lift	0,0,0,0	-3.74	
		0,0,0,0	.0416 rad	
	Vertical	0,0,0,0	-.00459 rad	
	Transl.	0,0,0,0	-.283 ft/sec	
		1,-.036,20,20	none	**

Note: Overshoot is the first peak for non zero commanded outputs and is the greatest deviation from zero for zero commanded outputs. Rise time is from initial value to 90% of the commanded value.
Command vector is $[\theta \;\; u \;\; \alpha]^T$.

* For this maneuver the shape of the curve did not yield an obvious value for overshoot.

** For this maneuver the output did not reach 90% of the commanded value.

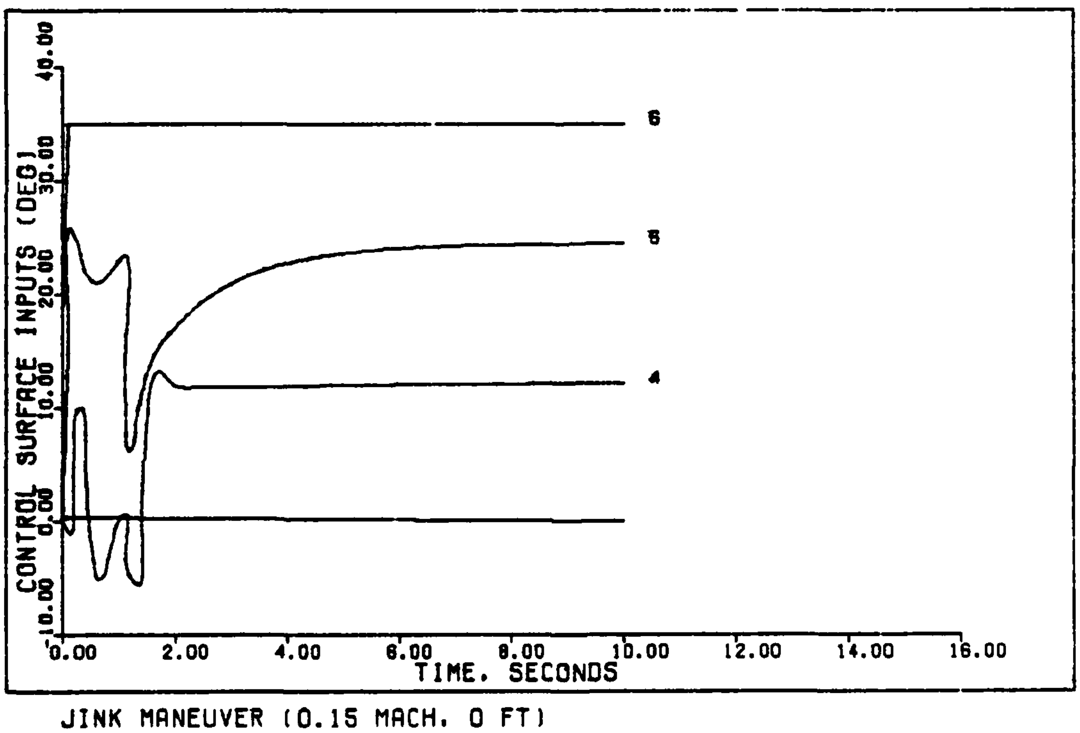

Figure 43. Jink Maneuver (0.15 Mach, 0 ft.)

than the responses to the vertical and horizontal translation commands (see Figures 5 through 11 and 12 through 20). However, if the aircraft were not decoupled, then this would not be true and the response to a coupled maneuver would be different than that obtained by commanding the lateral and longitudinal inputs separately. In this case the controller may have to be modified to compensate for coupling in the system matrices.

Conclusions

Not unexpectedly, the aircraft response to the commanded inputs is generally better for the lateral design than for the longitudinal designs. This may be due to the use of the jet flaps to induce a pitching moment (instead of maneuver flaps) which also vectors the thrust. Obviously, having one control surface affect two control inputs is not as efficient as separating the control inputs. Comparing these results to Bauschlicher's (using maneuver flaps), the conclusion is that using the maneuver flaps for longitudinal maneuvers yields significantly increased aircraft performance.

Designing one controller laterally and longitudinally for each flight condition that functioned nearly as well as separate controllers designed for each maneuver further demonstrates the power of the Porter method, and is an improvement over the current practice of gain scheduling by maneuver. Extending this concept further to one controller for multiple flight conditions is examined in the following chapter.

CHAPTER V

ROBUSTNESS TESTING OF LONGITUDINAL CONTROLLER

AND

COMPENSATION FOR EFFECTS OF CONTROLLER DELAY

Introduction

This chapter details the design and testing of a "universal controller" that can be used for multiple flight conditions. The obvious advantage to such a robust controller is that the controller matrices gains do not have to be changed as often as if this robustness was not possible, a practice called gain scheduling. Any valid claims for robustness using the Porter method would have to be substantiated with more complete robustness testing than is possible for this thesis. The attempt here is just to demonstrate that some robustness does exist and how to test robustness. This chapter also details the effects of a one sampling period time delay in the output of the PI controller. This time delay represents the time delay that would actually exist in the hardware realization of the design due to the sample and hold devices (A/D converters) and the processing delay. Another aspect of gain reduction is finding certain gains within the controller matrices that can be set to zero for multiple flight conditions. Unfortunately, this approach did not yield the hoped for results with this aircraft, but the limited results achieved are summarized in this chapter.

Universal Controller

The approach used for this thesis in searching for a universal controller was to test the controllers for each flight condition at the other flight conditions. Unfortunately, this did not result in any one controller that performed satisfactorily for all three flight conditions. (Since only multiple longitudinal controllers were designed, this chapter involves only longitudinal controllers) Further testing with redesigned controllers also did not result in any one controller showing acceptable results for all three flight conditions. Consequently, the requirement for a universal controller was downgraded to having good responses for two out of the three flight conditions. This resulted in a controller that yielded satisfactory results for the 0.6 mach, sea level, and 0.9 mach, 30,000 ft. flight conditions. This universal controller consists of the controller used for the 0.9 mach, 30,000 ft. flight condition. Interestingly, this corresponds to Bauschlicher's use of the longitudinal controller from the 0.9 mach flight condition as his universal longitudinal controller.

Not having a universal controller for all three flight conditions may not be a detriment in this case, because of the unique nature of the 0.15 mach, sea level flight condition. This flight condition is expected to be different from the other two due to the very slow airspeed and higher angle of attack. The controller found here would have to be tested with other more normal flight conditions to verify its use as a universal controller.

Testing. Testing the universal controller consisted of performing the longitudinal maneuvers for the 0.6 mach, sea level flight condition using the controller matrices and $\underline{M}$ matrix from the 0.9 mach, 30,000 ft. flight condition. The same maneuvers from Chapter IV are used and consist of:

Pitch Pointing

Direct Lift

Vertical Translation

Figures 44 through 52 show the results of these maneuvers, along with the commanded inputs and control surface deflections. Note that the title for each plot uses the abbreviation "U" to designate universal controller testing. Table IX summarizes the results of these plots.

Results. Generally, the results of the responses for the universal controller are fairly good. This section details the results for each maneuver.

Figures 44 through 46 show the responses for the 1.75 degree pitch pointing command. Comparing these plots with the ones for the responses of the aircraft with the controller designed for this flight condition (Figures 21 through 23), the worst feature of this maneuver is the decreased tracking of the angle of attack. However, there is less overshoot in the theta response but with greater error after about five seconds. The deviation of the flight path angle is greater with the universal controller than without. The velocity deviation from zero is greater with the universal controller, but the frequency of oscillation is much less, and the damping is greater. The control surface deflections aren't much different with the universal controller, and there is a significant decrease in both the required magnitude of thrust and its rate of oscillation.

Making the same comparisons of the universal controller

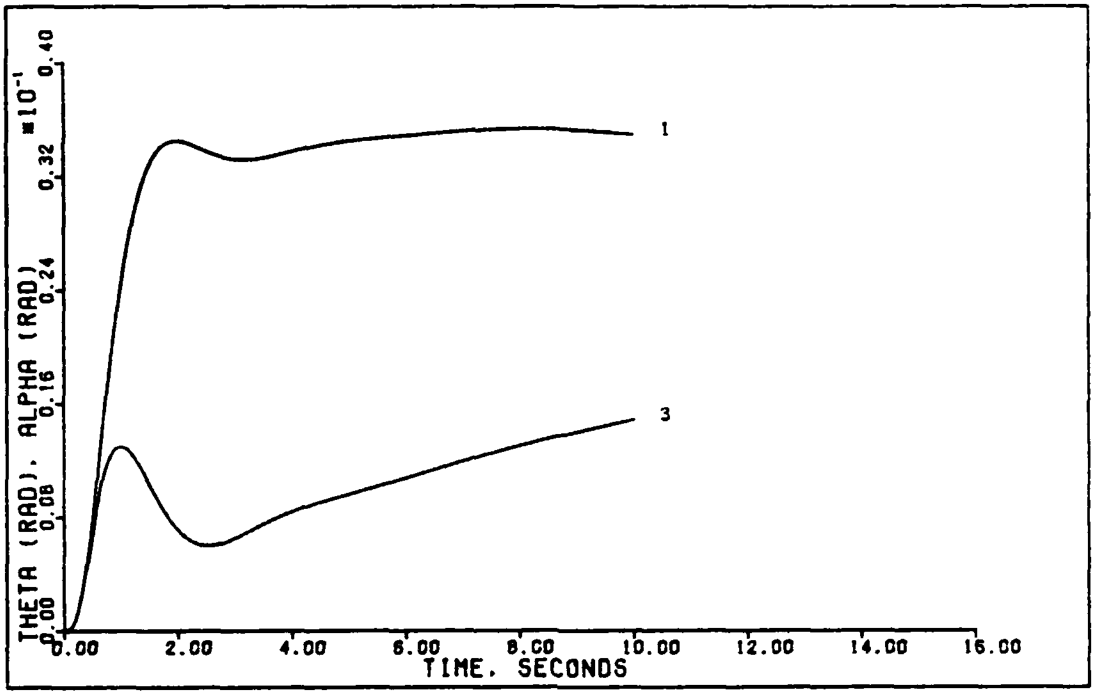

1.75 DEGREE PITCH POINTING (U, 0.6 MACH, 0 FT)

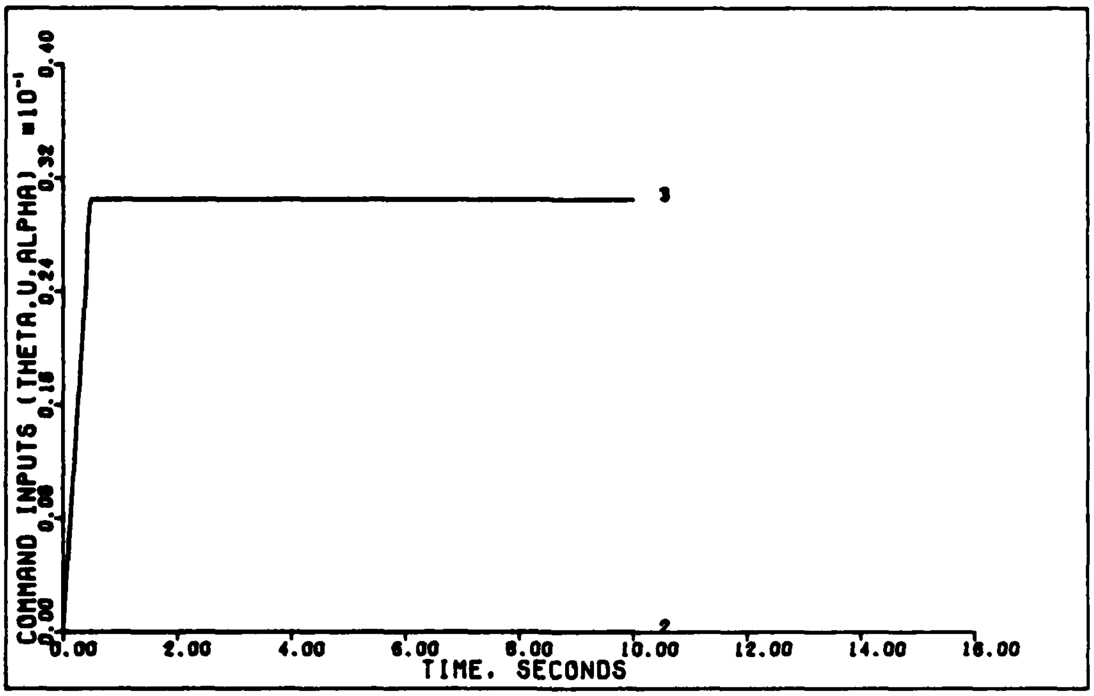

1.75 DEGREE PITCH POINTING (0.6 MACH, 0 FT)

Figure 44. 1.75 Degree Pitch Pointing With Universal Controller (0.6 Mach, 0 Ft.)

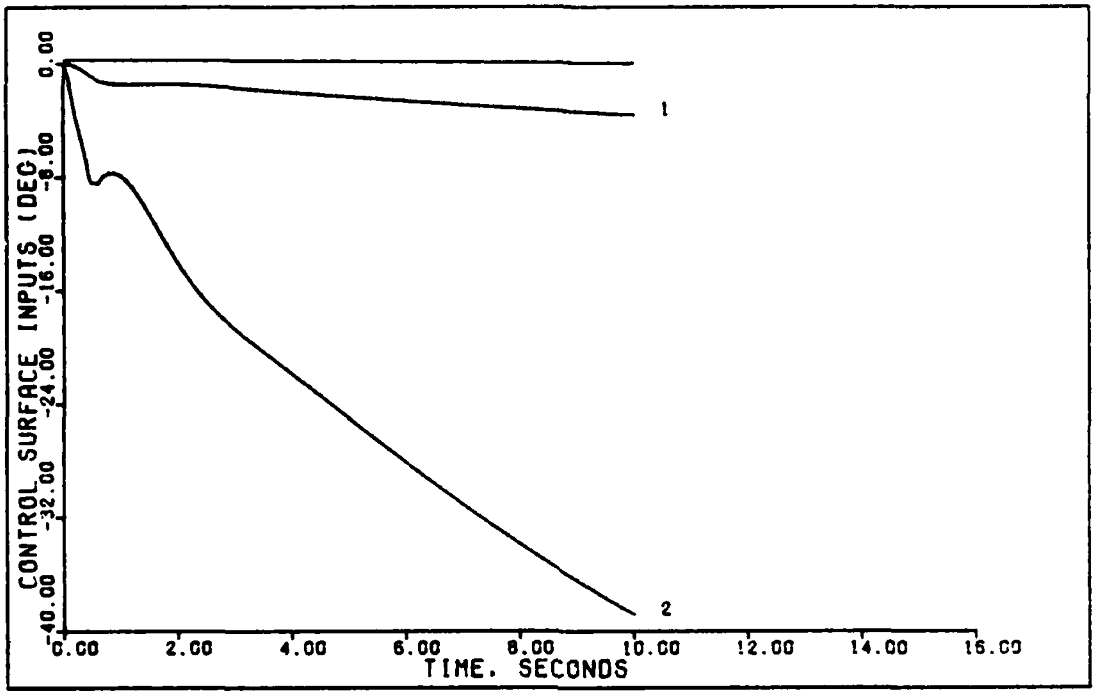

1.75 DEGREE PITCH POINTING (U, 0.6 MACH, 0 FT)

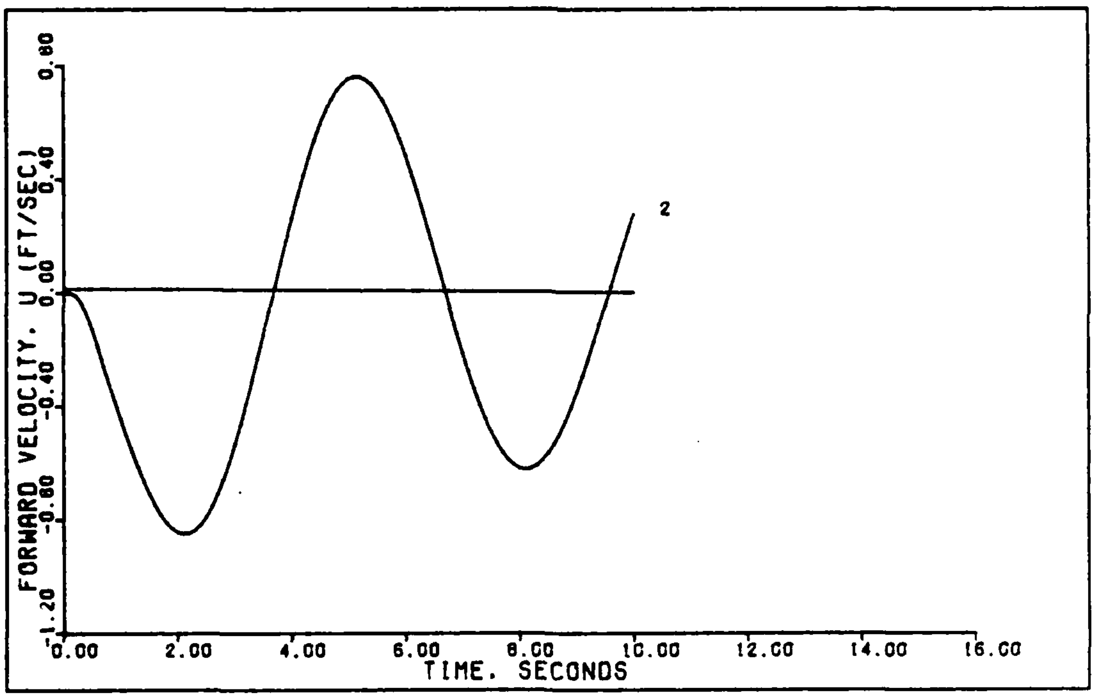

1.75 DEGREE PITCH POINTING (U, 0.6 MACH, 0 FT)

Figure 45. 1.75 Degree Pitch Pointing With Universal Controller (0.6 Mach, 0 Ft.)

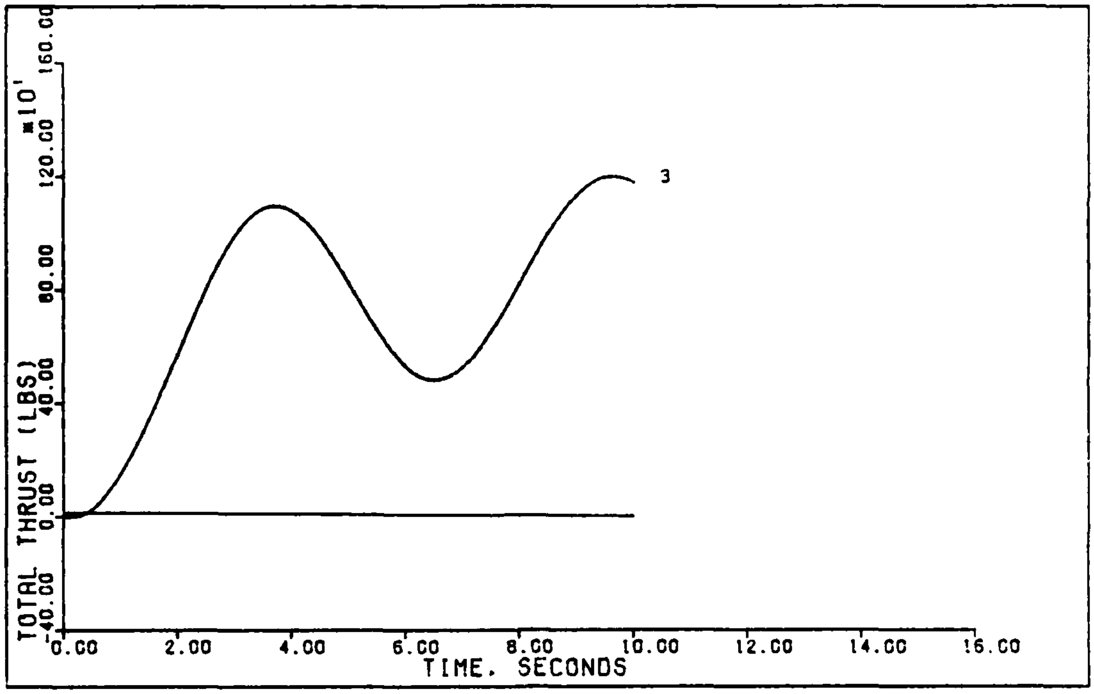

1.75 DEGREES PITCH POINTING (U, 0.6 MACH, 0 FT)

Figure 46. 1.75 Degree Pitch Pointing With Universal Controller (0.6 Mach, 0 Ft.)

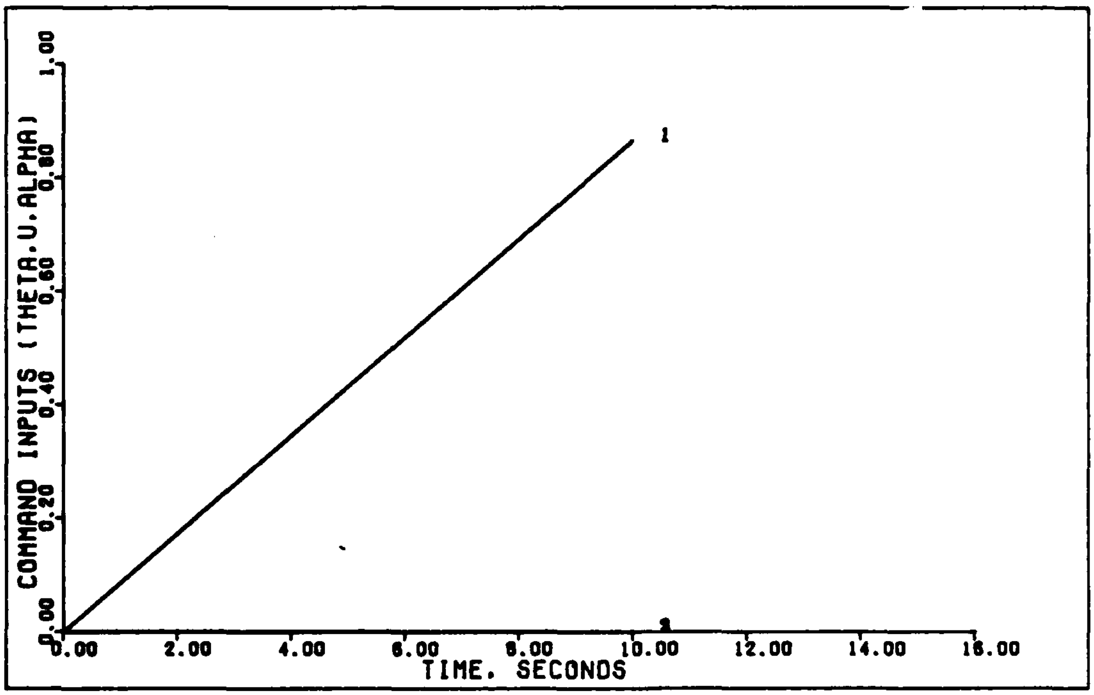

1.8 G DIRECT LIFT (0.6 MACH, 0 FT)

Figure 47. 1.8 G Direct Lift With Universal Controller (0.6 Mach, 0 Ft.)

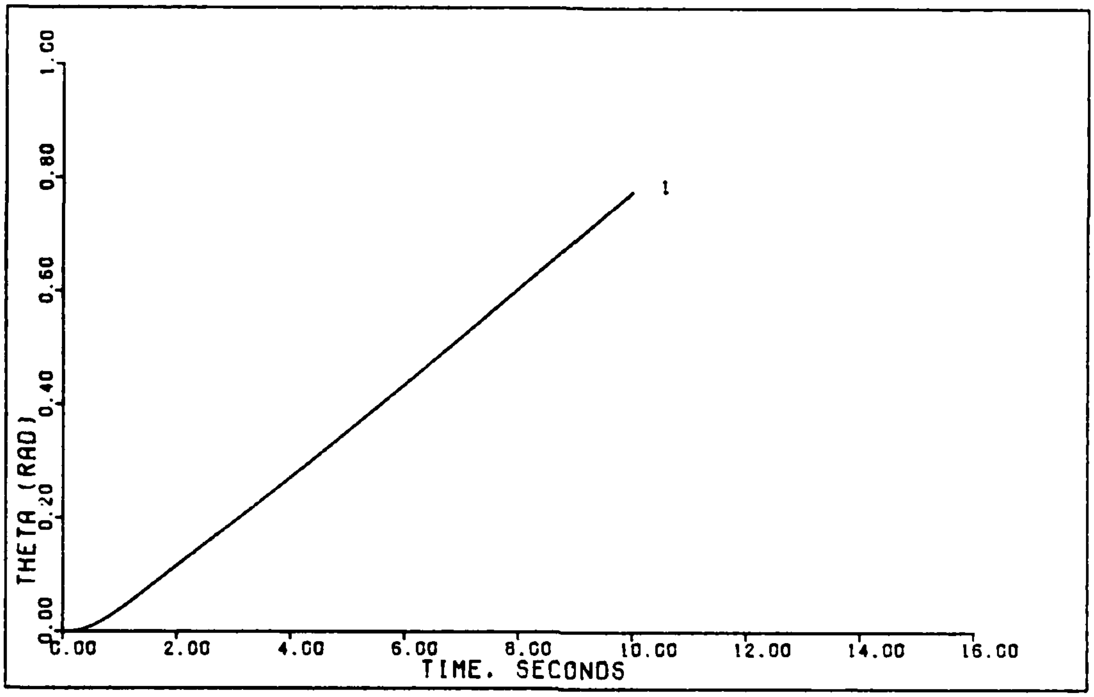

1.8 G DIRECT LIFT (U, 0.6 MACH, 0 FT)

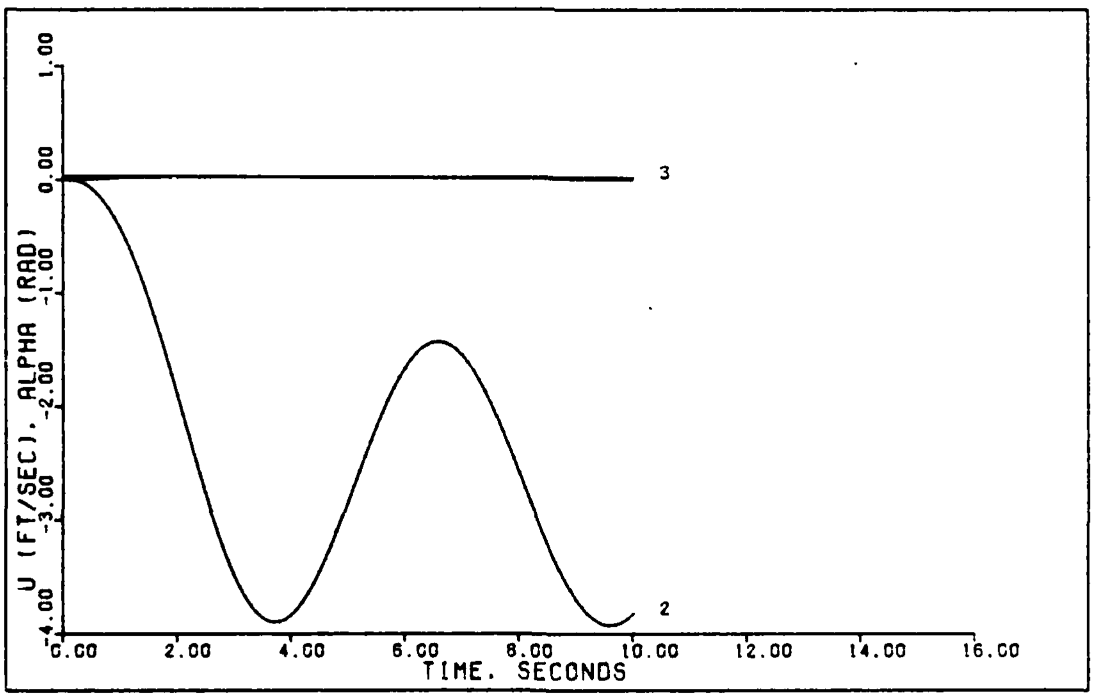

1.8 G DIRECT LIFT (U, 0.6 MACH, 0 FT)

Figure 48. 1.8 G Direct Lift With Universal Controller (0.6 Mach, 0 Ft.)

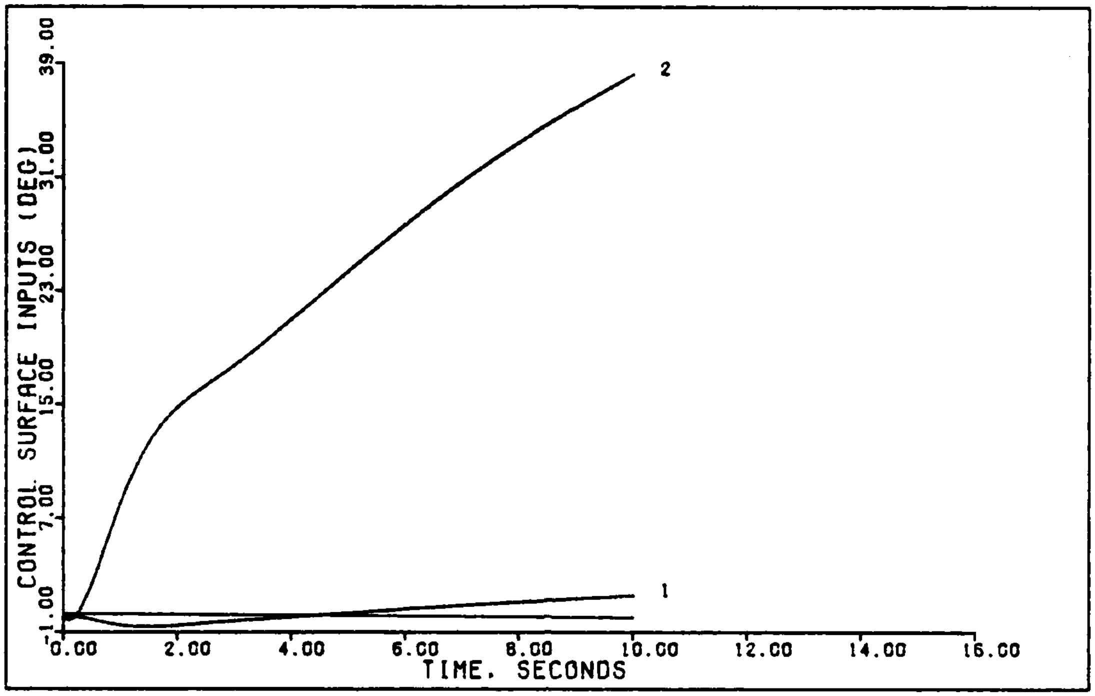

1.8 G DIRECT LIFT (U, 0.6 MACH, 0 FT)

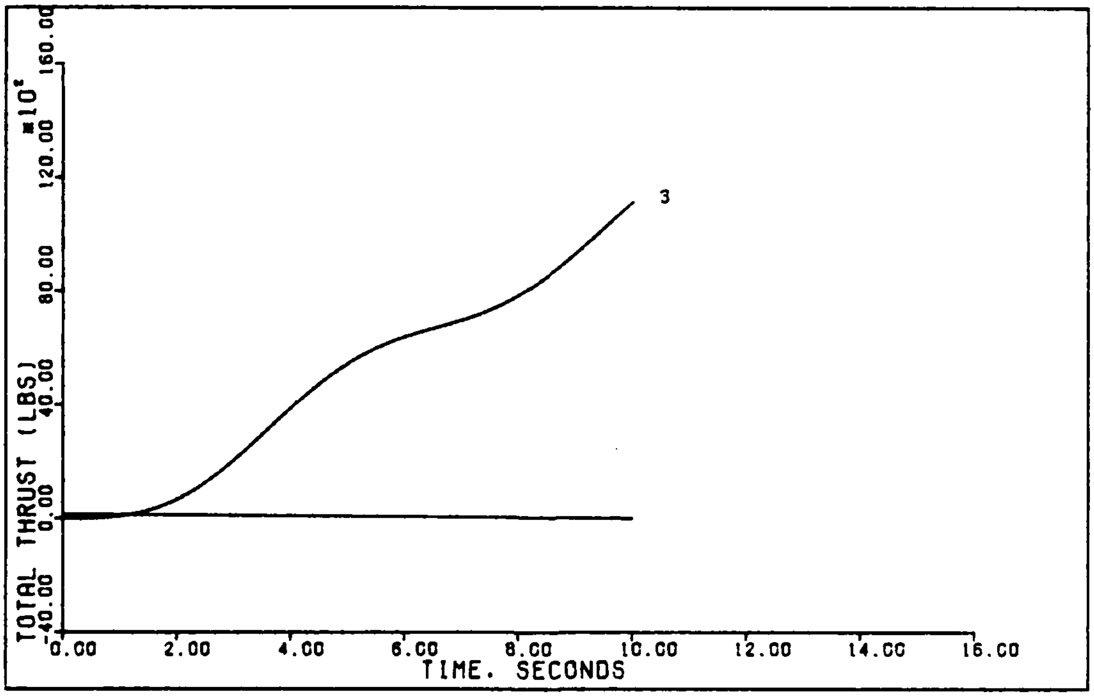

1.8 G DIRECT LIFT (U, 0.6 MACH, 0 FT)

Figure 49. 1.8 G Direct Lift With Universal Controller (0.6 Mach, 0 Ft.)

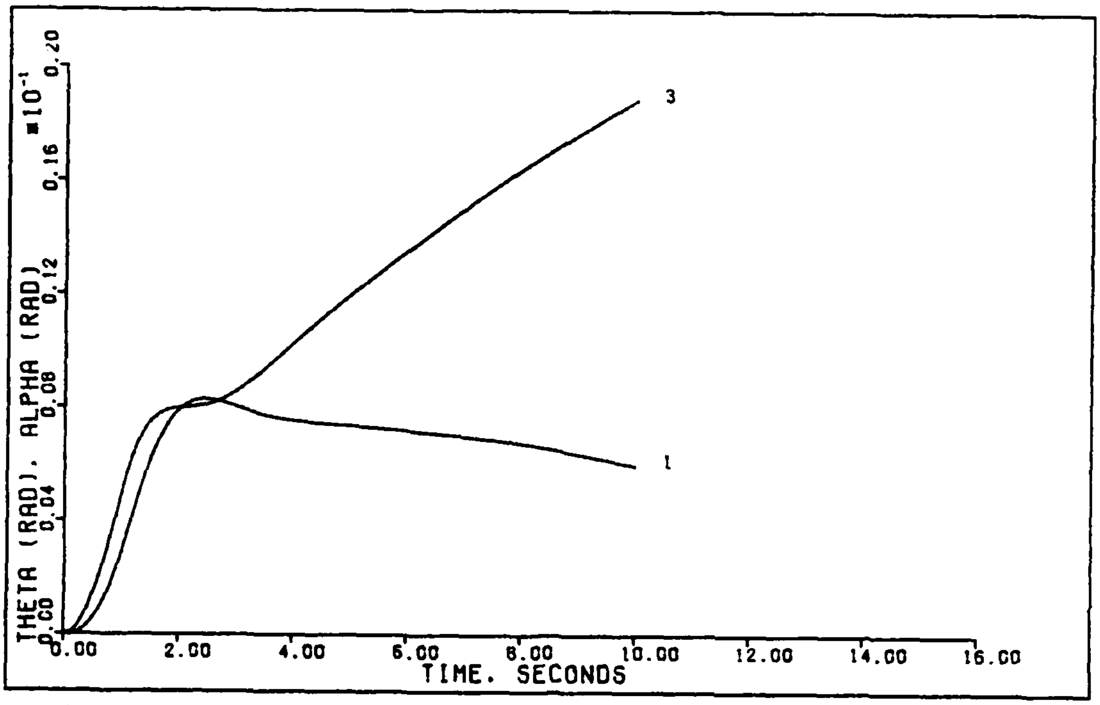

0.8 G VERTICAL TRANSLATION (U. 0.6 MACH. 0 FT)

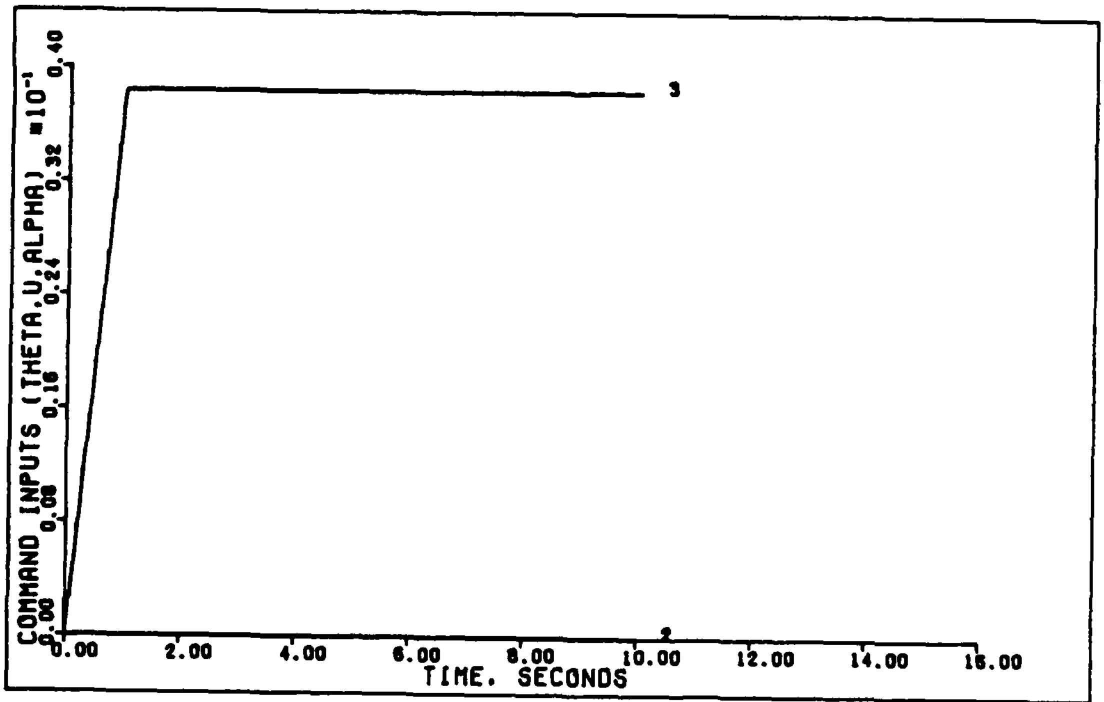

0.8 G VERTICAL TRANSLATION (0.6 MACH. 0 FT)

Figure 50. 0.8 G Vertical Translation With Universal Controller (0.6 Mach, 0 Ft.)

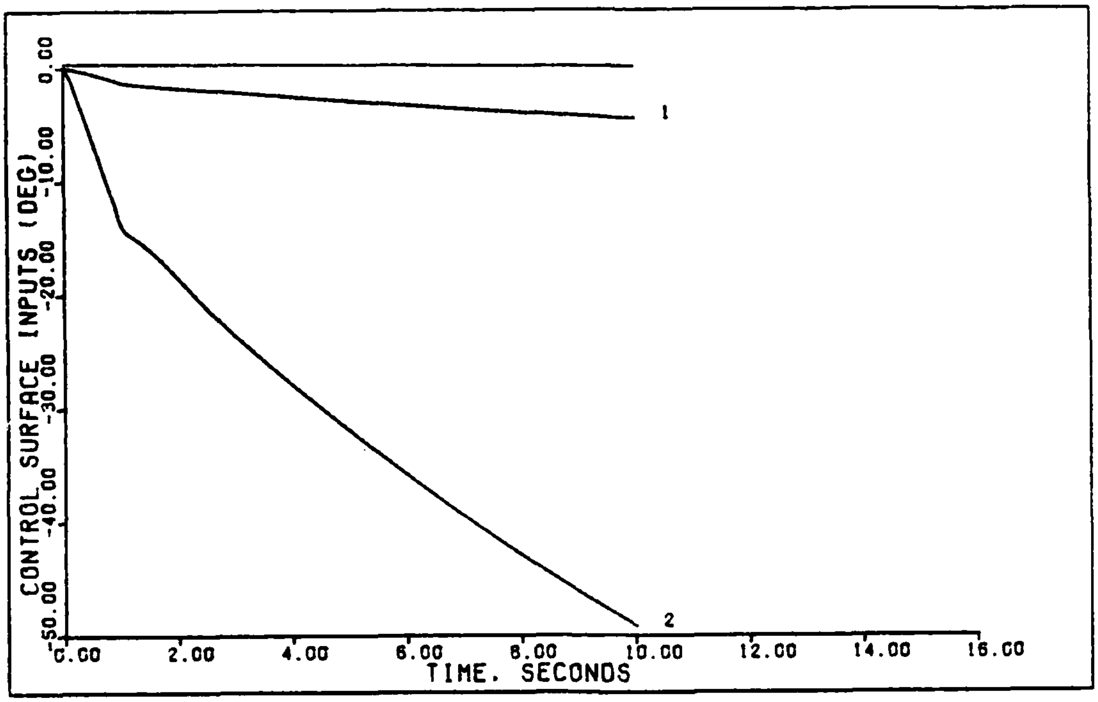

0.8 G VERTICAL TRANSLATION (U, 0.6 MACH, 0 FT)

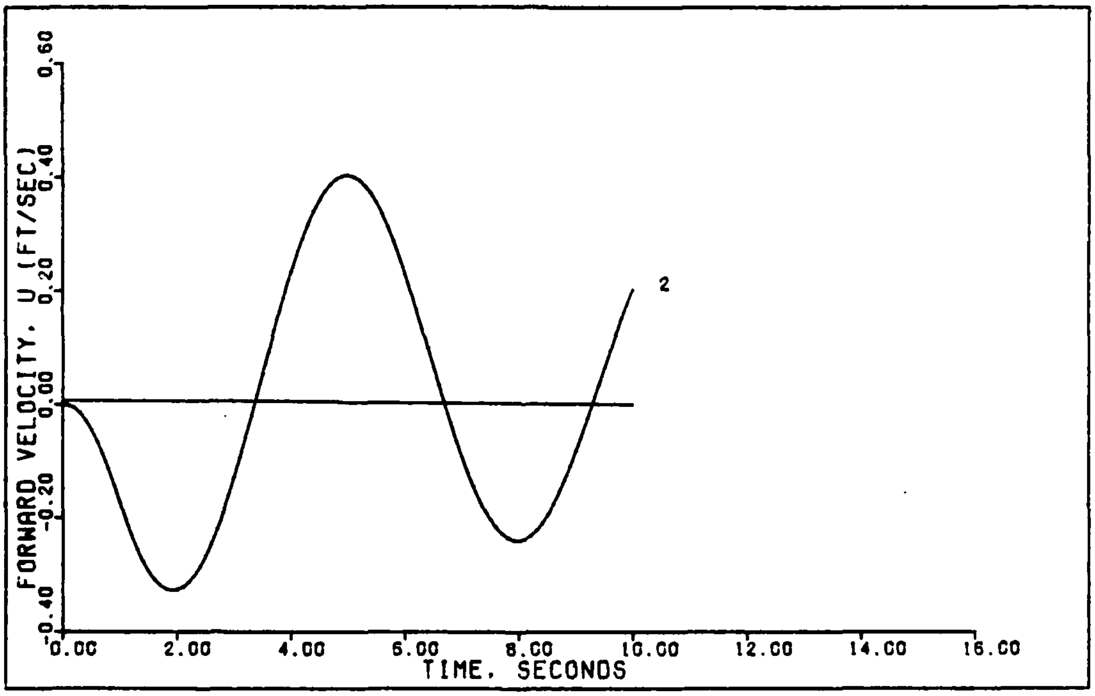

0.8 G VERTICAL TRANSLATION (U, 0.6 MACH, 0 FT)

Figure 51. 0.8 G Vertical Translation With Universal Controller (0.6 Mach, 0 Ft.)

TABLE IX

SUMMARY OF OUTPUT RESPONSES FOR UNIVERSAL CONTROLLER

Flt. Cond.	Maneuver	Command, V	Peak Value	Time To Peak	Final Value
0.60 Mach	Pitch	.5,.0305,20,20	.0354	8.1 sec	.0350
0 ft.	Pointing	0,0,0,0	-.849	2.1 sec	.277
		.5,.0305,20,20	.015	10 sec	.0149
	Direct	10,.865,20,20	.776	10 sec	.776
	Lift	0,0,0,0	-3.93	9.6 sec	-3.83
		0,0,0,0	.0237	1.9 sec	.0168
	Vertical	0,0,0,0	.00828	2.4 sec	.00597
	Transl.	0,0,0,0	.403	5 sec	.203
		1,.0384,20,20	.0189	10 sec	.0189

Note: The peak value is the greatest deviation from the initial value of zero. The command vector is composed of:

$$\underline{V} = \begin{bmatrix} \theta \text{ (rad)} \\ u \text{ (ft/sec)} \\ \alpha \text{ (rad)} \end{bmatrix}$$

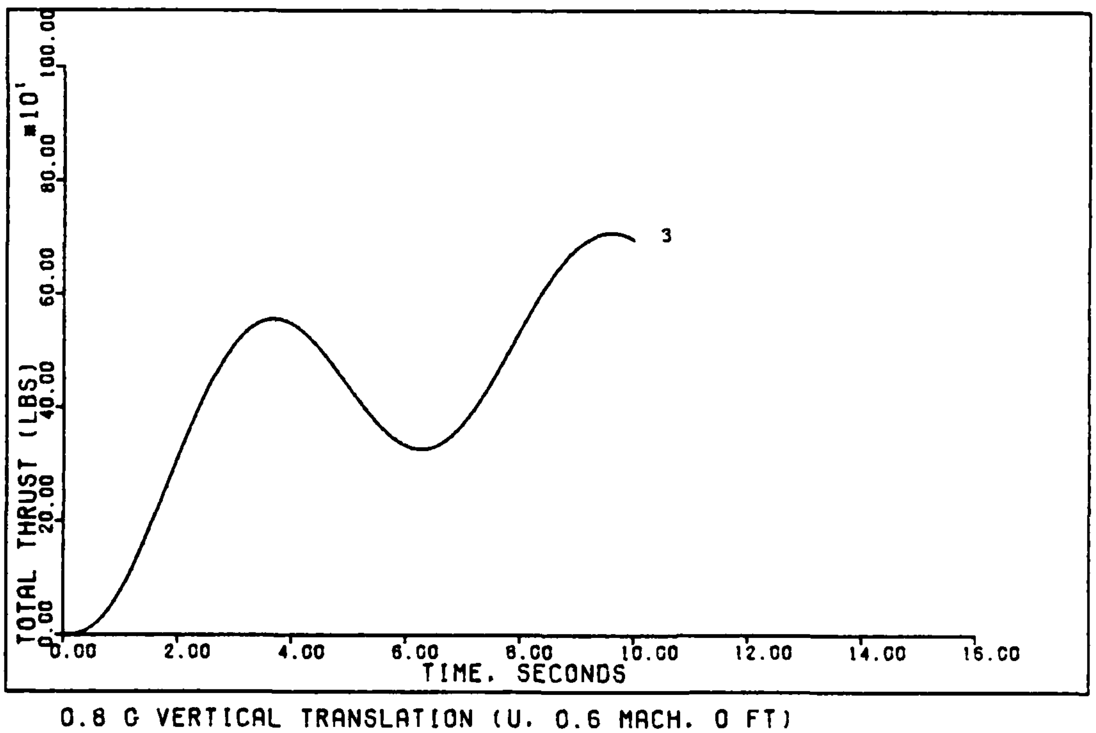

Figure 52. 0.8 G Vertical Translation With Universal Controller (0.6 Mach, 0 Ft.)

response (Figures 47 through 49) with the responses using the controller designed for this flight condition (Figures 24 through 26) for a 1.8 g direct lift maneuver, several conclusions can be drawn. The theta response with the universal controller is practically identical to the dedicated controller response, but once again the velocity response has greater magnitude of deviation but with less frequency of oscillation. The angle of attack response is also almost identical for both controllers. The control surface deflections along with the thrust required are not too dissimilar. Of the three maneuvers, this is the one with the best response using the unviversal controller.

Comparing the responses of the universal controller to a 0.8 g vertical translation (Figures 50 through 52) with those using the dedicated controller (Figures 27 through 29) yields the worst performance for the universal controller. Even though the theta response has improved, the angle of attack response has significantly degraded. Once again the forward velocity response with the universal controller exhibits greater deviation from the commanded zero level but has greater damping and lower frequency. And as with the other maneuvers the control surface deflections have not changed much, although the thrust, in addition to being smaller in magnitude, also has a marked change in the basic shape of the time response plot.

Conclusions. Even though the controller from the 0.9 mach flight condition proved to yield the best results of any of the controllers tested in the search for a universal controller, its performance is probably not adequate enough for a fighter aircraft, such as the FPCC. However, there is some degree of robustness to the universal controller, and perhaps this type of approach would yield an adequate universal controller for a transport type aircraft.

Effects of Controller Delay

This section details the testing of the effects of introducing a one sampling period time delay into the output of the PI controller. This delay represents a real world delay that would exist in the output of a digital controller using a sample and hold device (such as an analog to digital converter) to produce the input error signal. This is implemented in the simulation within the program MULTI by simply delaying the output of the controller one sampling period, i.e. the current control input to the actuators (or plant) is the previously calculated value, while the most recently calculated value is saved for the next sampling period (which is the "outer loop" within the MULTI simulation). MULTI also has the capability of allowing the analog plant (the aircraft in this thesis) to continue calculating new states and outputs by setting the calculation step size smaller than the sampling period. Using this feature would certainly make the simulation more true to life and should be considered for future thesis work.

Results. Figures 53 through 79 show the results of performing the longitudinal maneuvers for all of the flight conditions from Chapter IV with a one sampling period time delay in the output of the PI controller. Note that this delay is only valid for the case of a digital controller. Table X summarizes

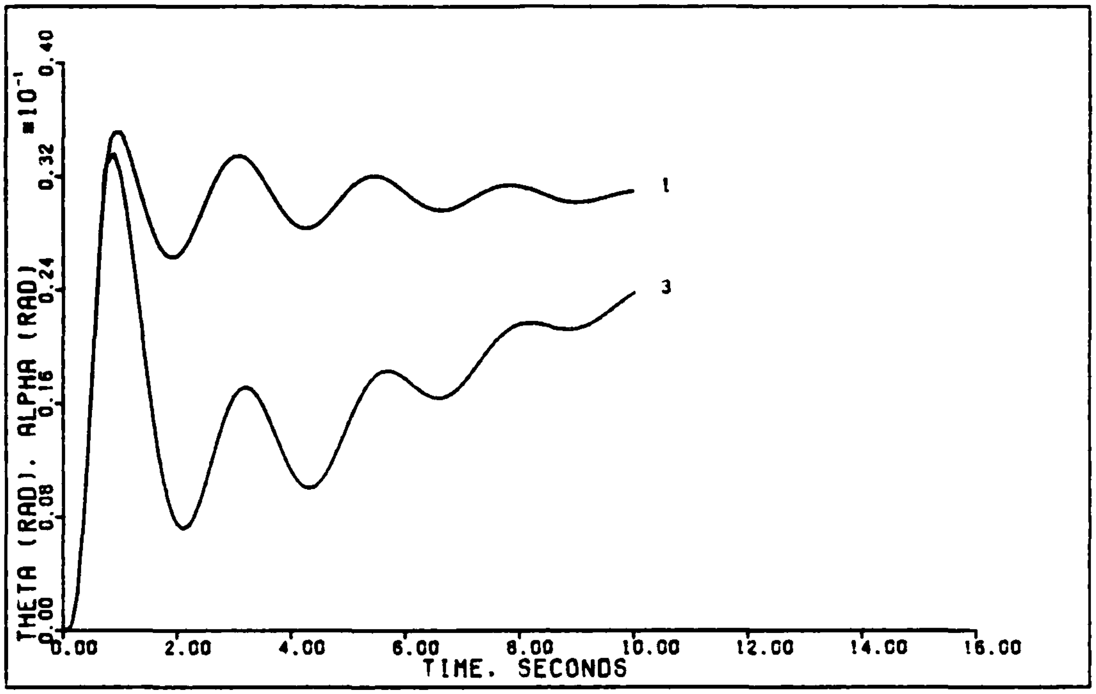

1.75 DEGREE PITCH POINTING (D. 0.15 MACH. 0 FT)

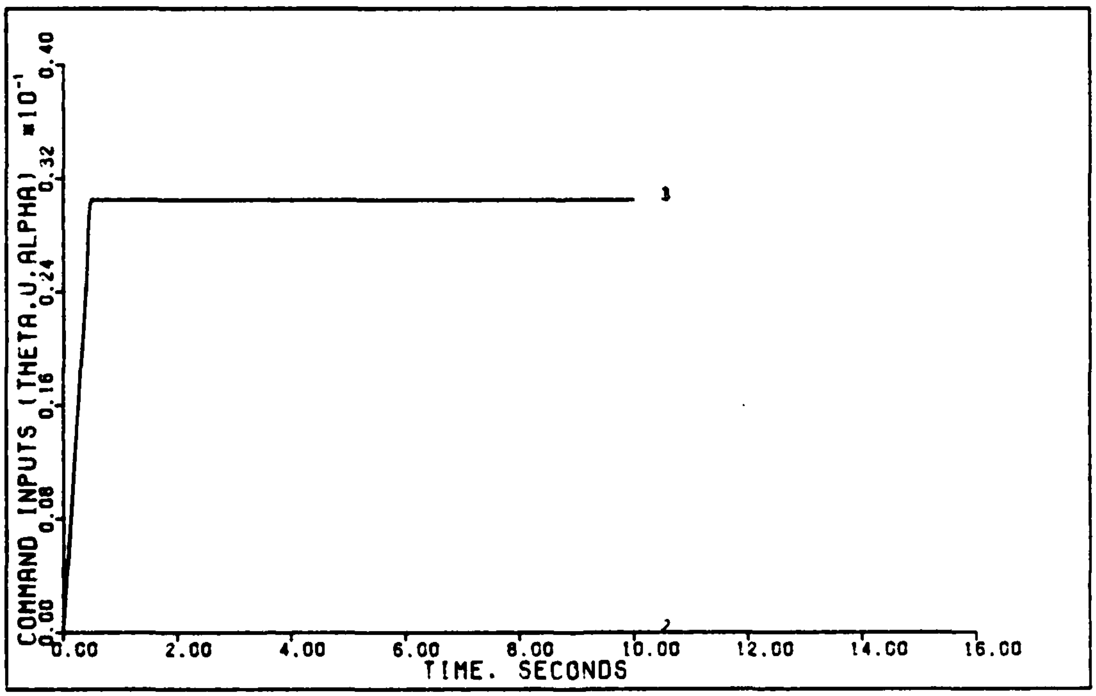

1.75 DEGREE PITCH POINTING (0.15 MACH. 0 FT)

Figure 53. 1.75 Degree Pitch Pointing With Delay (0.15 Mach, 0 Ft.)

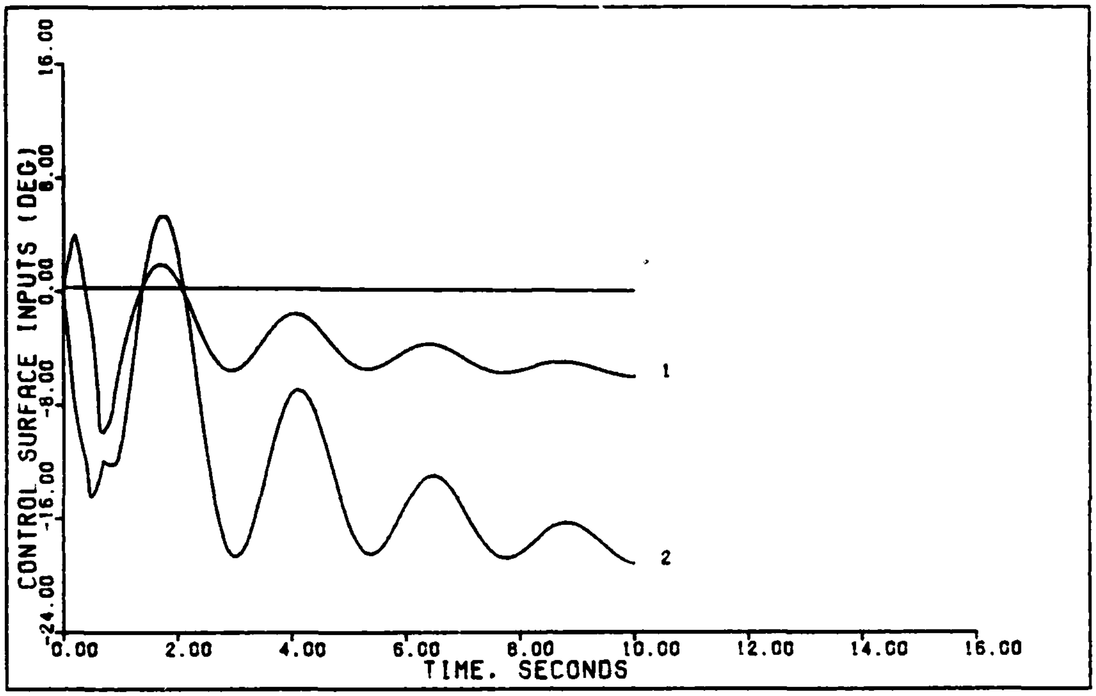

1.75 DEGREE PITCH POINTING (D, 0.15 MACH, 0 FT)

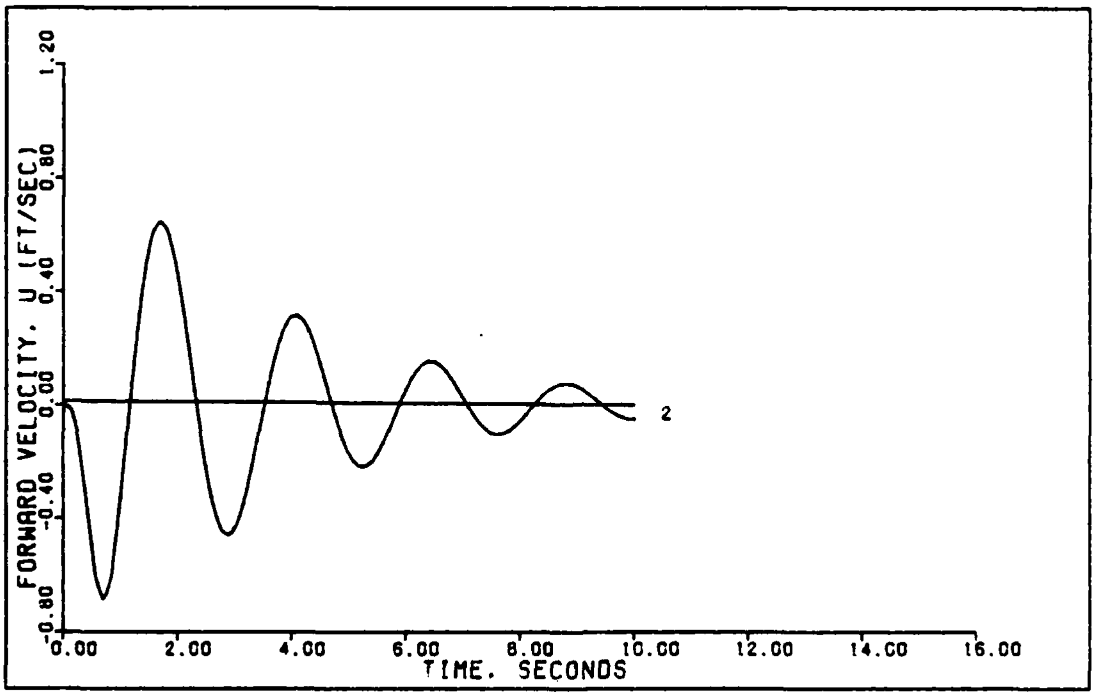

1.75 DEGREE PITCH POINTING (D, 0.15 MACH, 0 FT)

Figure 54. 1.75 Degree Pitch Pointing With Delay (0.15 Mach, 0 Ft.)

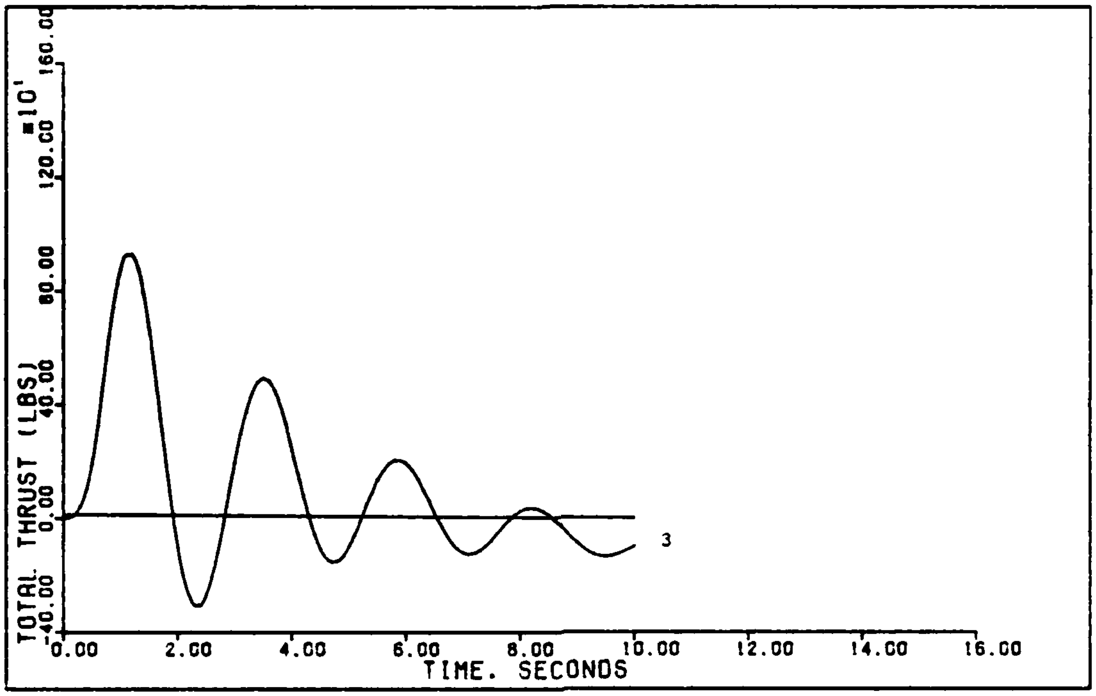

1.75 DEGREE PITCH POINTING (D, 0.15 MACH, 0 FT)

Figure 55. 1.75 Degree Pitch Pointing With Delay (0.15 Mach, 0 Ft.)

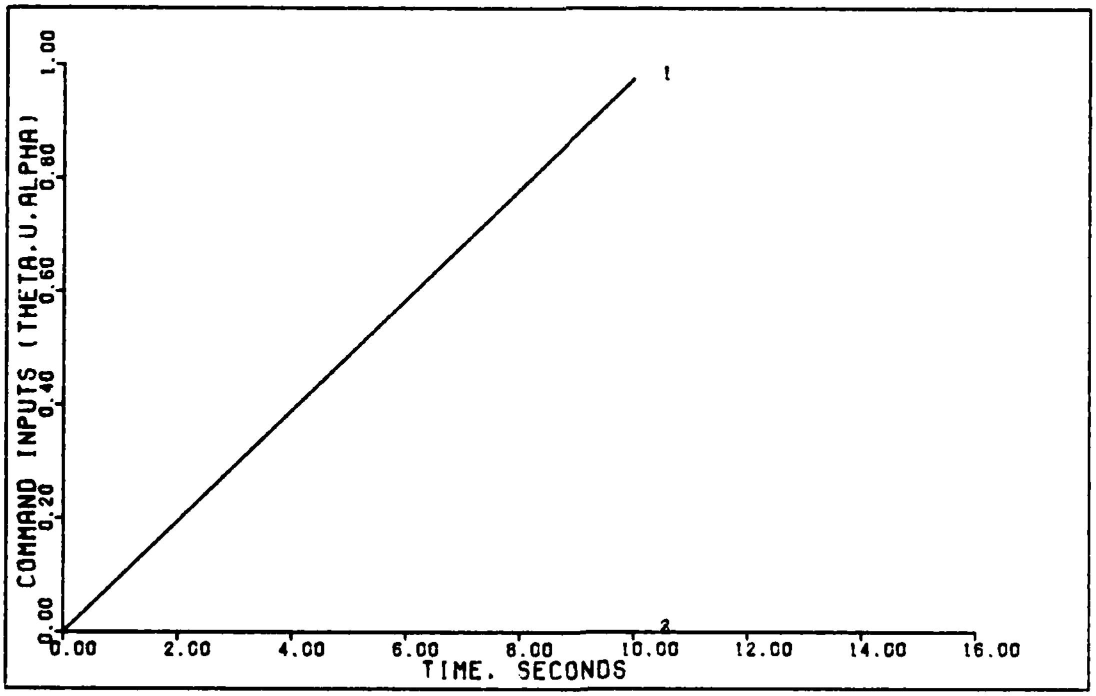

0.5 G DIRECT LIFT (0.15 MACH, 0 FT)

Figure 56. 0.5 G Direct Lift With Delay (0.15 Mach, 0 Ft.)

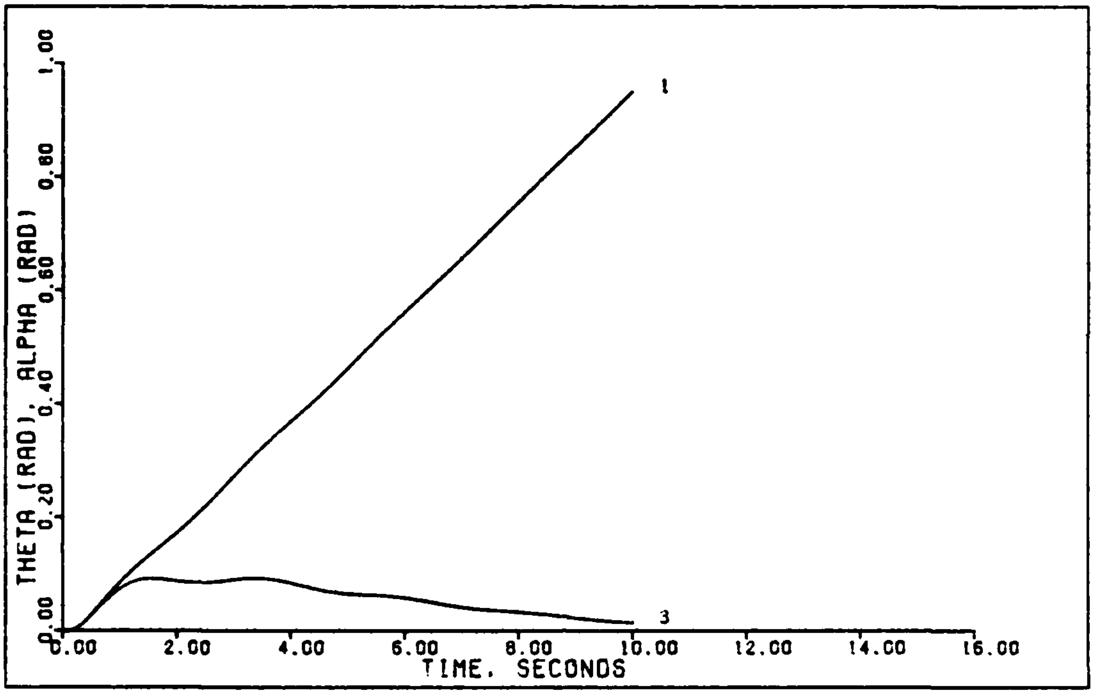

0.5 G DIRECT LIFT (D, 0.15 MACH, 0 FT)

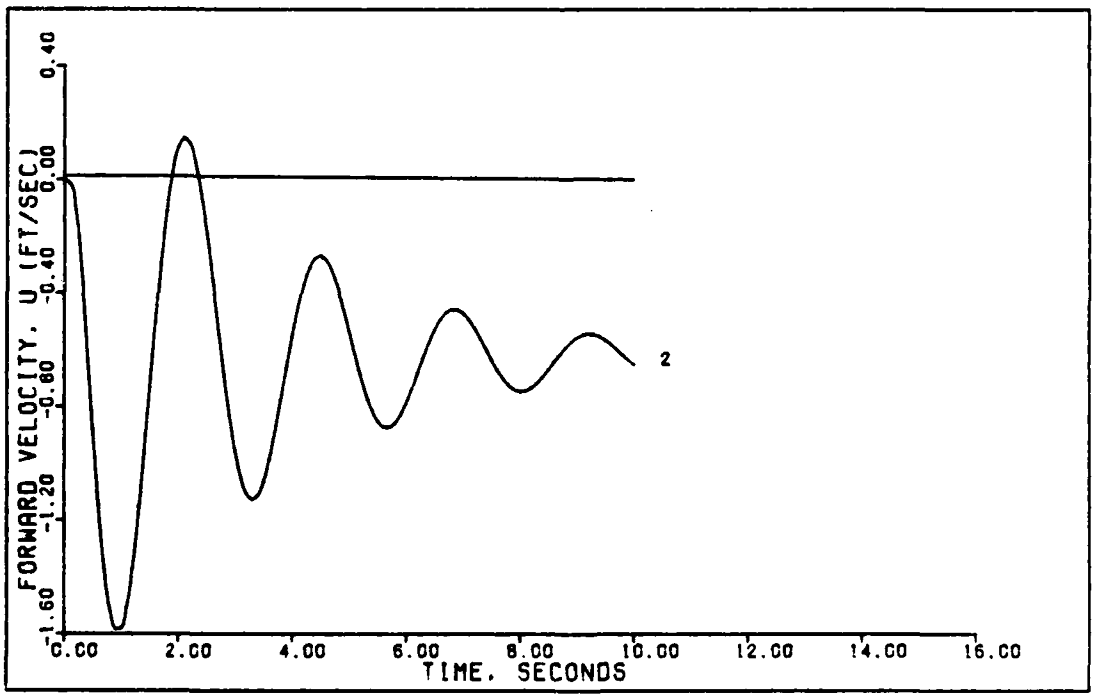

0.5 G DIRECT LIFT (D, 0.15 MACH, 0 FT)

Figure 57. 0.5 G Direct Lift With Delay (0.15 Mach, 0 Ft.)

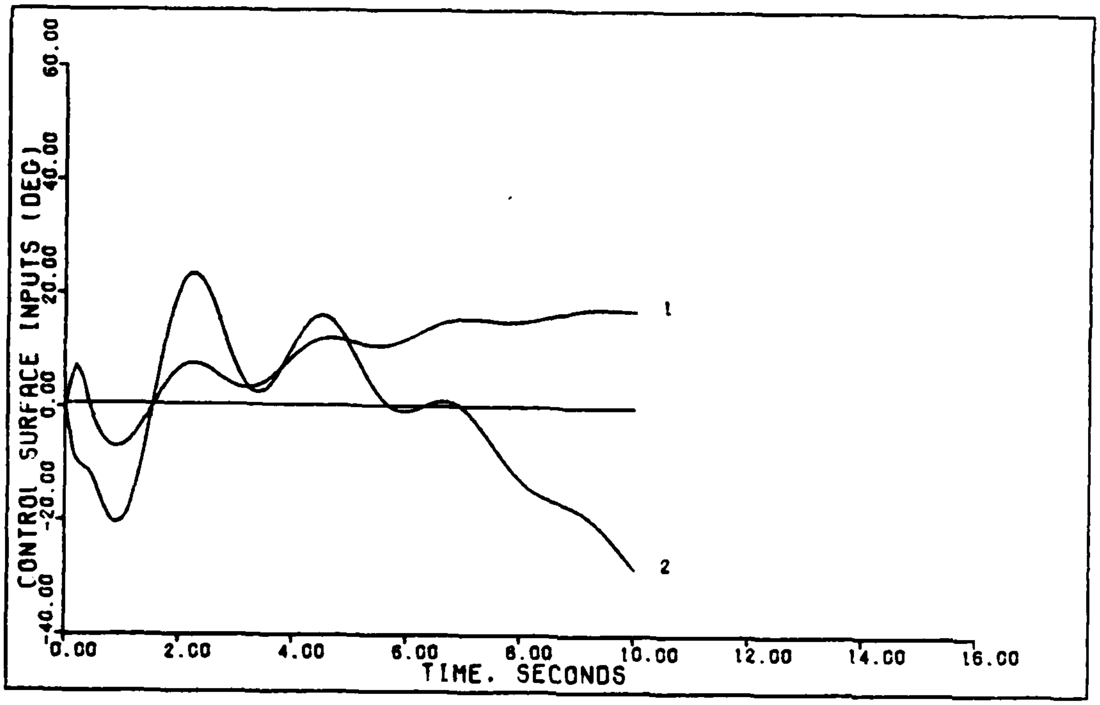

0.5 G DIRECT LIFT (D, 0.15 MACH, 0 FT)

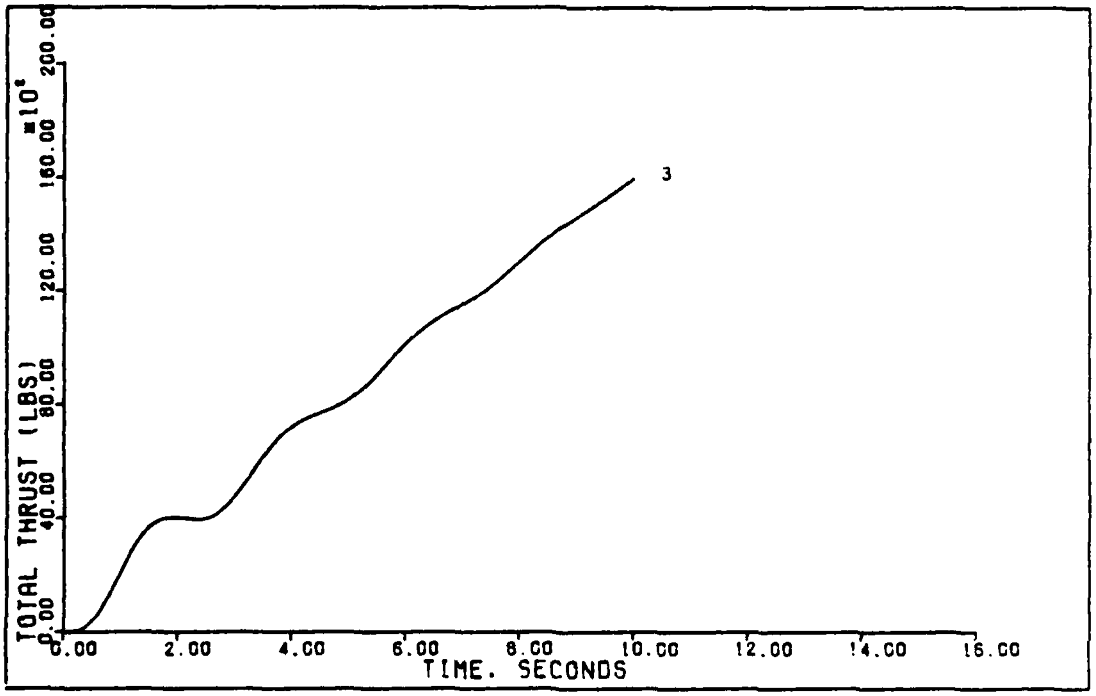

0.5 G DIRECT LIFT (D, 0.15 MACH, 0 FT)

Figure 58. 0.5 G Direct Lift With Delay (0.15 Mach, 0 Ft.)

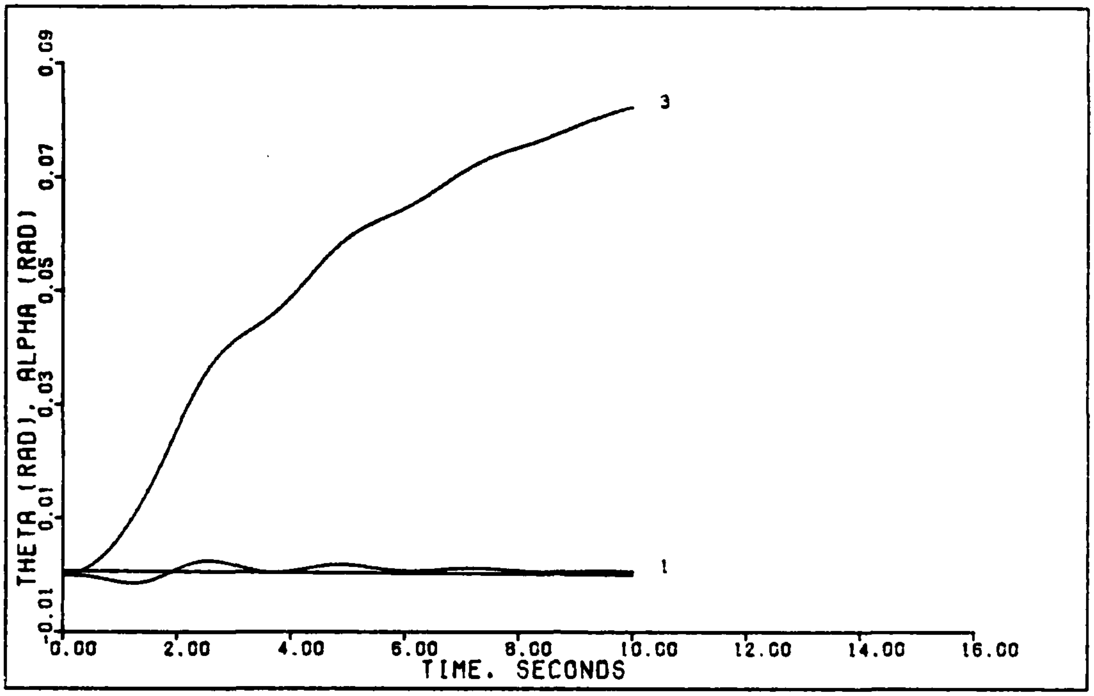

0.5 G VERTICAL TRANSLATION (D, 0.15 MACH, 0 FT)

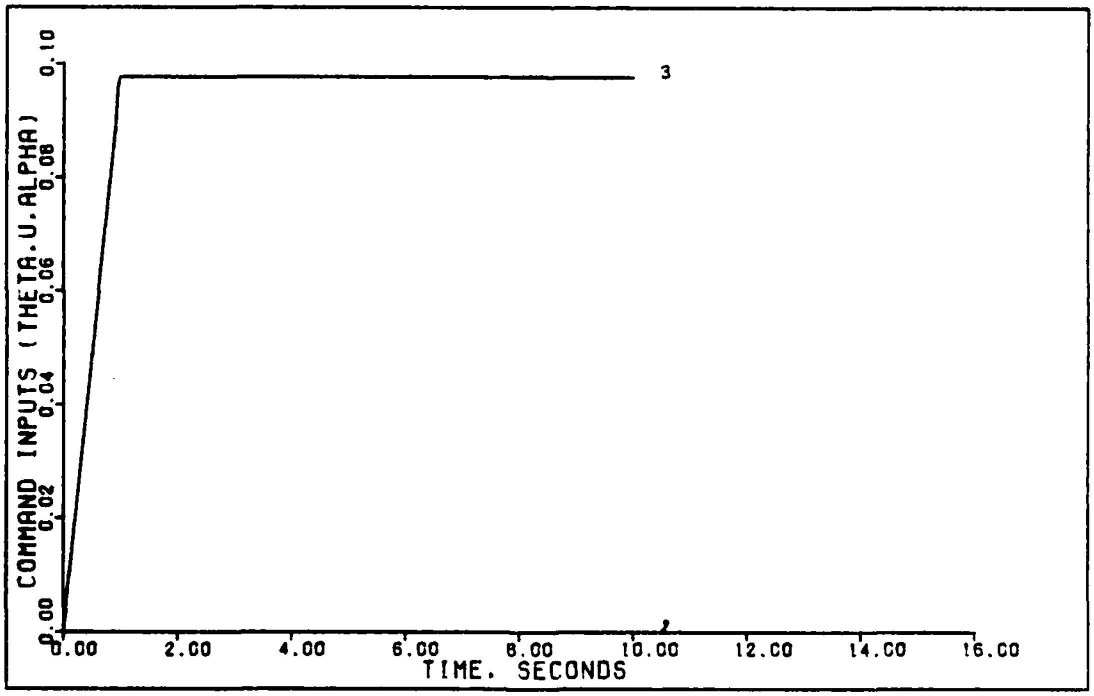

0.5 G VERTICAL TRANSLATION (0.15 MACH, 0 FT)

Figure 59. 0.5 G Vertical Translation With Delay (0.15 Mach, 0 Ft.)

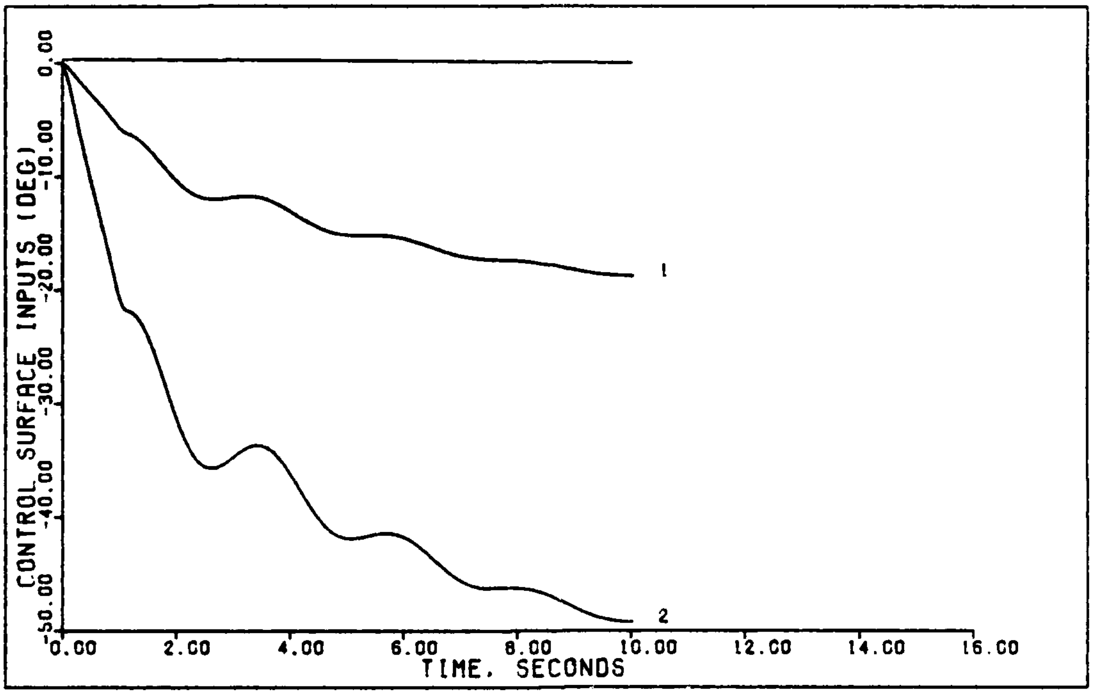

0.5 G VERTICAL TRANSLATION (D, 0.15 MACH, 0 FT)

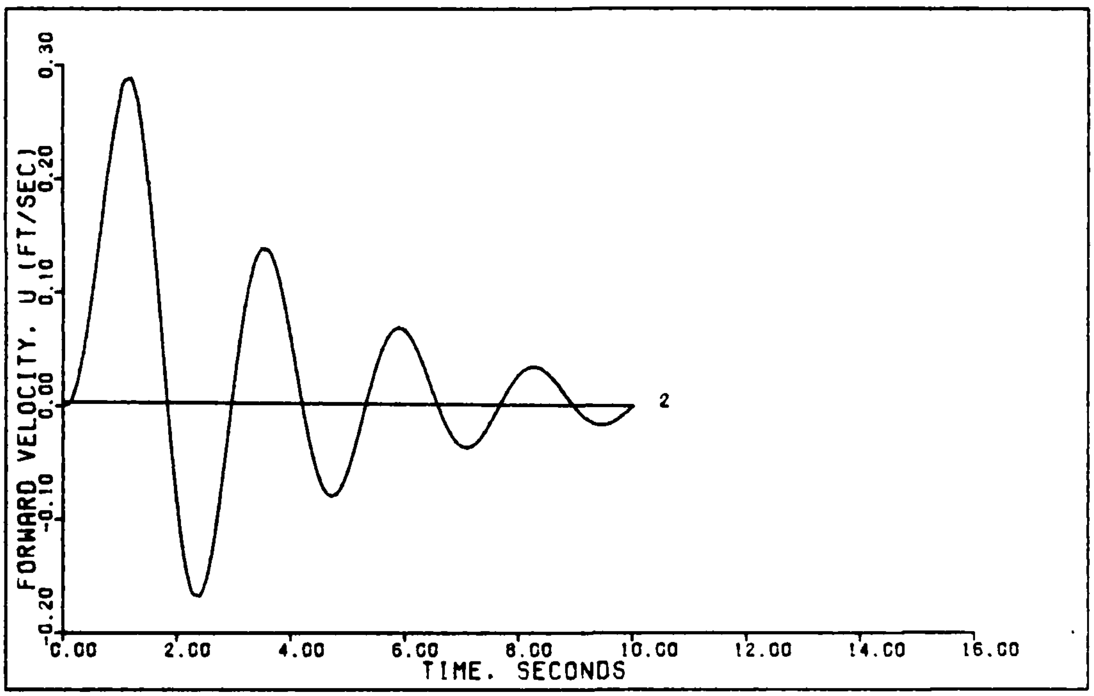

0.5 G VERTICAL TRANSLATION

Figure 60. 0.5 G Vertical Translation With Delay (0.15 Mach, 0 Ft.)

TABLE X

SUMMARY OF OUTPUT RESPONSES FOR LONGITUDINAL CONTROLLERS WITH DELAY

Flt. Cond.	Maneuver	Command, V	Peak Value	Time To Peak	Final Value
0.15 Mach	Pitch	.5,.0305,20,20	.0351	1 sec	.0310
0 ft.	Pointing	0,0,0,0	-.685	0.7 sec	-.0497
		.5,.0305,20,20	.0336	0.9 sec	.0238
	Direct	10,.976,20,20	.950	10 sec	.950
	Lift	0,0,0,0	-1.58	0.9 sec	-.651
		0,0,0,0	.0924	3.4 sec	.0141
	Vertical	0,0,0,0	.00244	2.6 sec	.000663
	Transl.	0,0,0,0	.289	1.2 sec	-.000325
		1,.0977,20,20	.0824	10 sec	.0824
(The following flight conditions reflect delay compensation)					
0.6 Mach	Pitch	.5,.0305,20,20	.0571	1.6 sec	.0416
0 ft.	Pointing	0,0,0,0	-.370	0.8 sec	.0893
		.5,.0305,20,20	.0248	1 sec	.0236
	Direct	10,.865,20,20	.774	10 sec	.774
	Lift	0,0,0,0	-.583	8.5 sec	-.540
		0,0,0,0	.0183	1.5 sec	.00723
	Vertical	0,0,0,0	.0329	2 sec	.0149
	Transl.	0,0,0,0	.242	4.1 sec	.0362
		1,.0384,20,20	.0299	10 sec	.0299
0.9 Mach	Pitch	.5,.0524,20,20	.0635	2.1 sec	.0569
30,000 ft.	Pointing	0,0,0,0	-1.516	1.9 sec	.110
		.5,.0524,20,20	.0267	1.2 sec	.0153
	Direct	10,.865,20,20	.784	10 sec	.784
	Lift	0,0,C,0	-5.50	9.9 sec	-5.49
		0,0,0,0	.0459	2.4 sec	.0361
	Vertical	0,0,0,0	-.005	2.9 sec	-.00407
	Transl.	0,0,0,0	-.187	4.9 sec	-.0852
		1,-.036,20,20	-.0107	10 sec	-.0107

Note: The delay compensation is described in text. The peak value is the greatest deviation from the initial value of zero. The command vector is composed of:

$$\underline{V} = \begin{bmatrix} \theta \text{ (rad)} \\ u \text{ (ft/sec)} \\ \alpha \text{ (rad)} \end{bmatrix}$$

TABLE XI

SUMMARY OF OUTPUT RESPONSES FOR UNIVERSAL CONTROLLER WITH DELAY

Flt. Cond.	Maneuver	Command, V	Peak Value	Time To Peak	Final Value
0.60 Mach	Pitch	.5,.0305,20,20	.0369	2.1 sec	.0358
0 ft.	Pointing	0,0,0,0	-.938	2.3 sec	-.0398
		.5,.0305,20,20	.0130	1 sec	.010
	Direct	10,.865,20,20	.781	10 sec	.781
	Lift	0,0,0,0	-5.60	10 sec	-5.60
		0,0,0,0	.0259	2.1 sec	.0212
	Vertical	0,0,0,0	.00906	2.6 sec	.00749
	Transl.	0,0,0,0	-.312	2 sec	.0586
		1,.0384,20,20	.0126	10 sec	.0126

Note: Figures shown represent compensated results, with compensation used explained in the text. The peak value is defined as greatest deviation from the initial zero value. The command vector is composed of:

$$\underline{V} = \begin{bmatrix} \theta \text{ (rad)} \\ u \text{ (ft/sec)} \\ \alpha \text{ (rad)} \end{bmatrix}$$

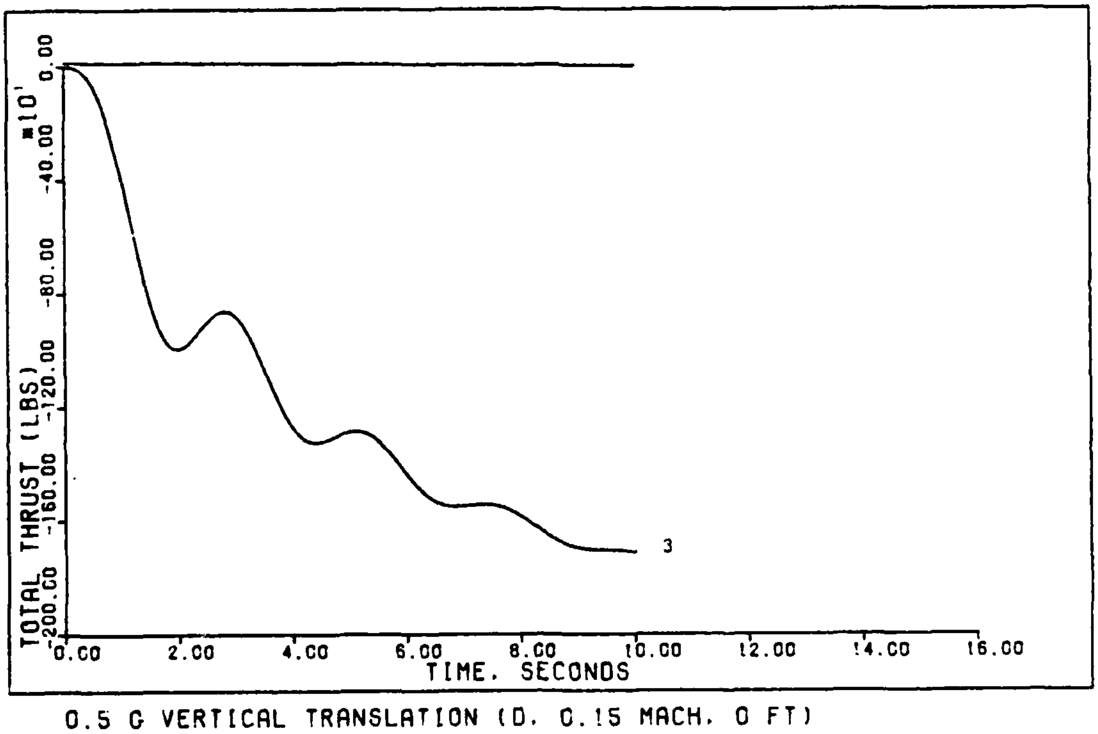

Figure 61. 0.5 G Vertical Translation With Delay (0.15 Mach, 0 Ft.)

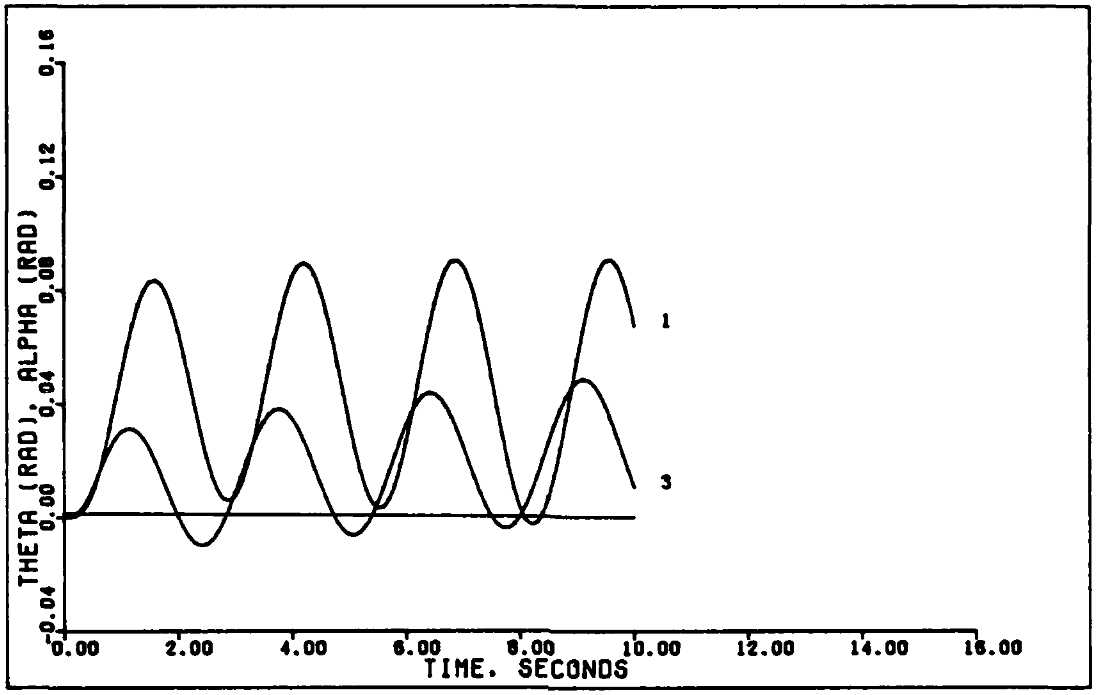

1.75 DEGREE PITCH POINTING (D. ALPHA=2, 0.6 MACH)

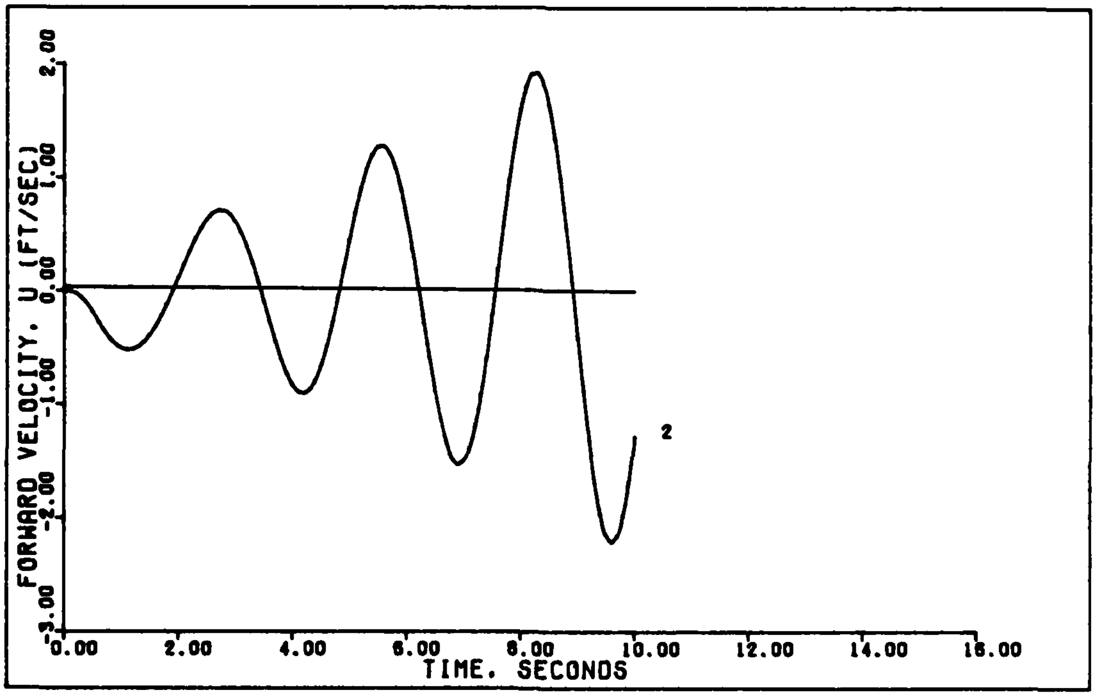

1.75 DEGREE PITCH POINTING (D. ALPHA=2, 0.6 MACH)

Figure 62. 1.75 Degree Pitch Pointing With Delay, Control Ratio Of Two (0.6 Mach, 0 Ft.)

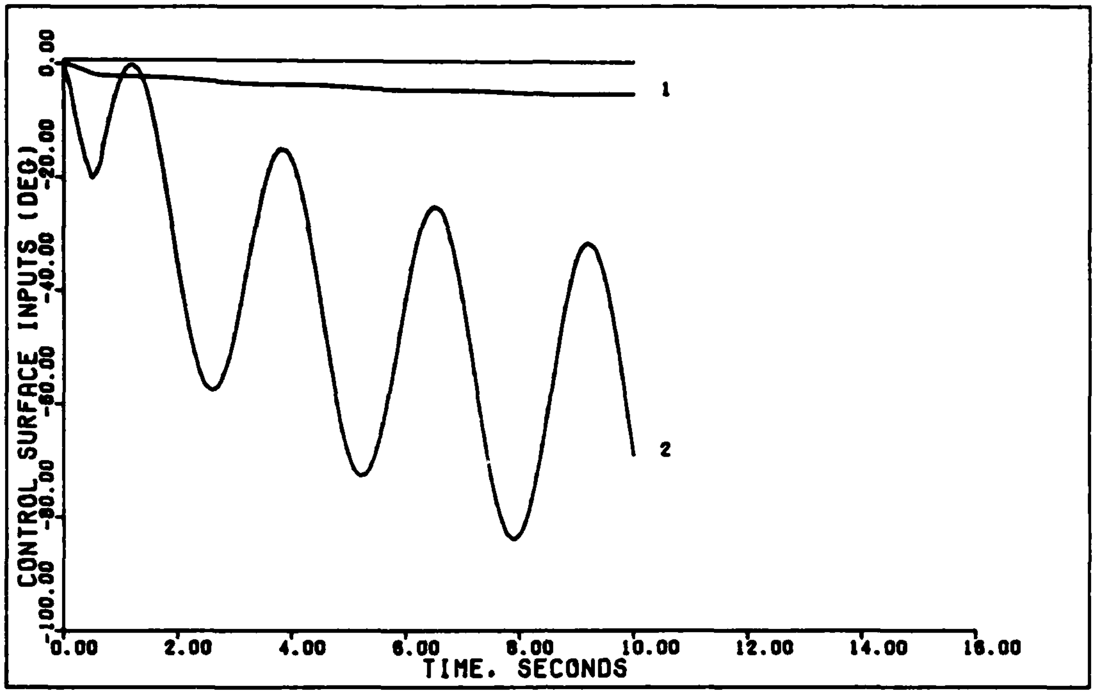

1.75 DEGREE PITCH POINTING (D. ALPHA=2. 0.6 MACH)

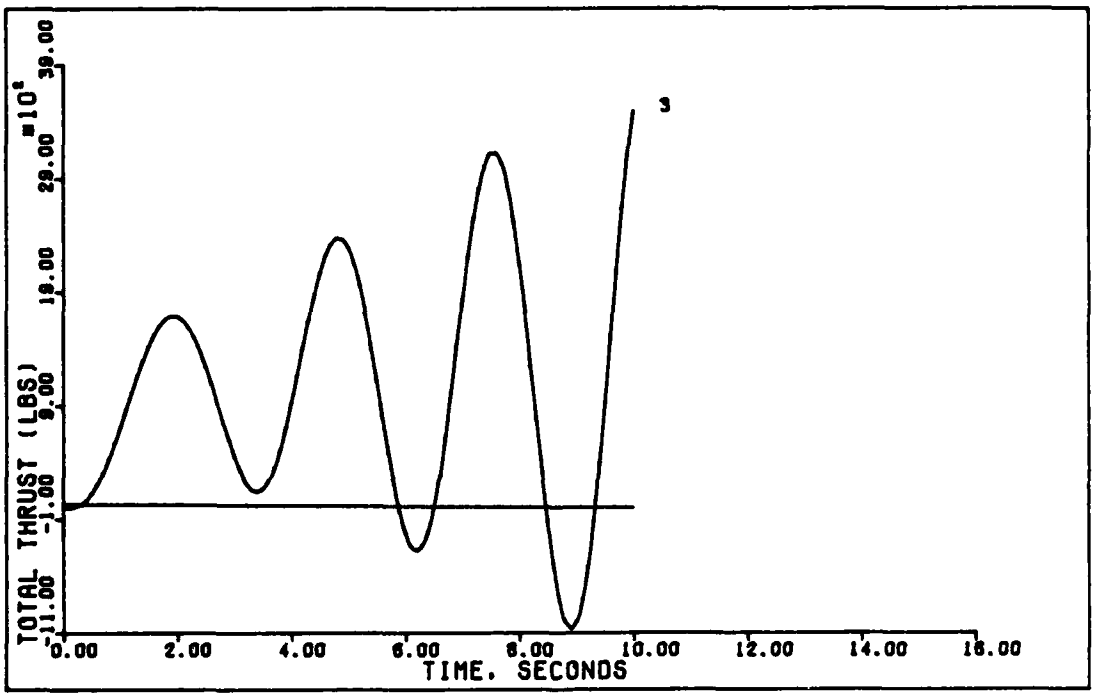

1.75 DEGREE PITCH POINTING (D. ALPHA=2. 0.6 MACH)

Figure 63. 1.75 Degree Pitch Pointing With Delay, Control Ratio Of Two (0.6 Mach, 0 Ft.)

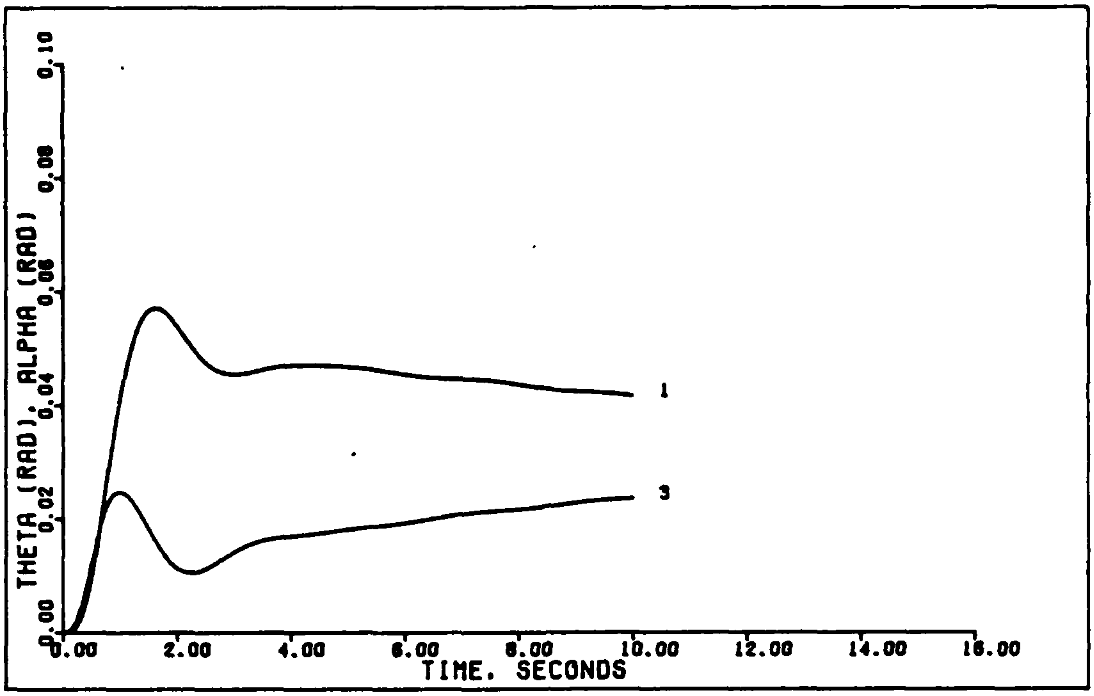

1.75 DEGREE PITCH POINTING (D. ALPHA=3. 0.6 MACH)

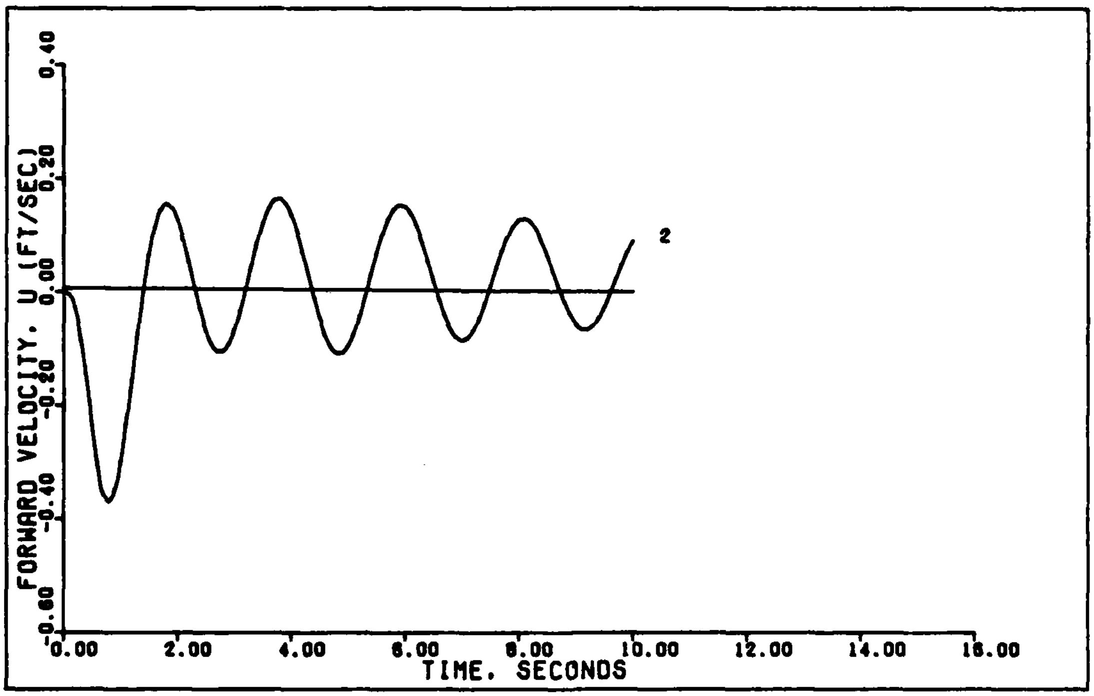

1.75 DEGREE PITCH POINTING (D. ALPHA=3. 0.6 MACH)

Figure 64. 1.75 Degree Pitch Pointing With Delay, Control Ratio Of Three (0.6 Mach, 0 Ft.)

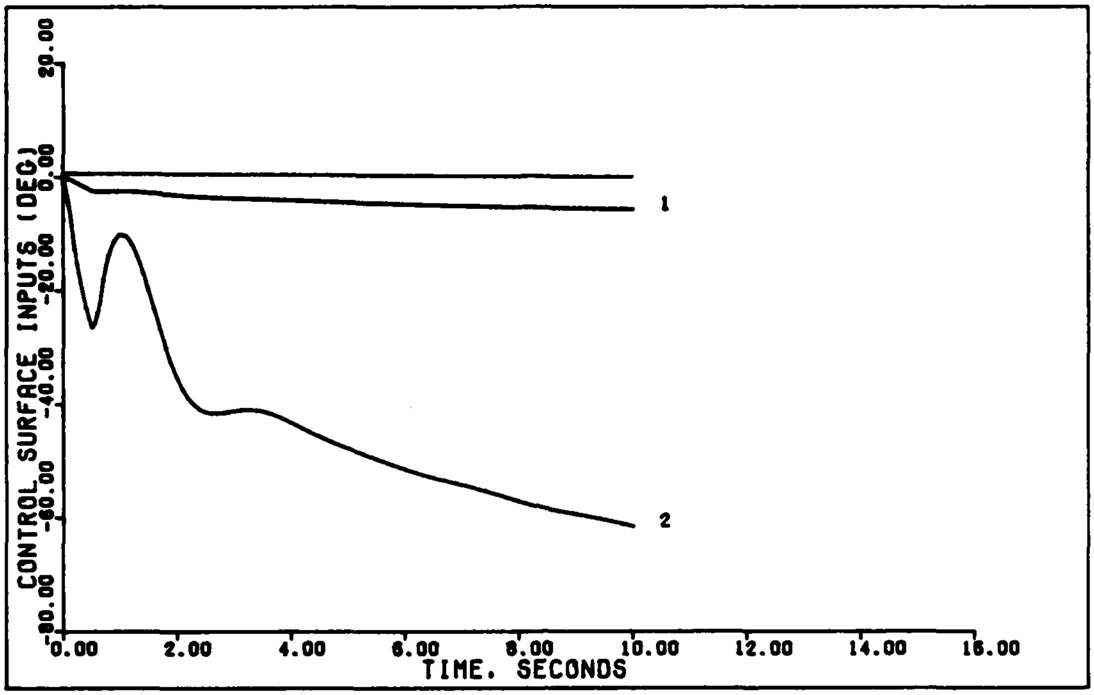

1.75 DEGREE PITCH POINTING (D. ALPHA=3. 0.6 MACH)

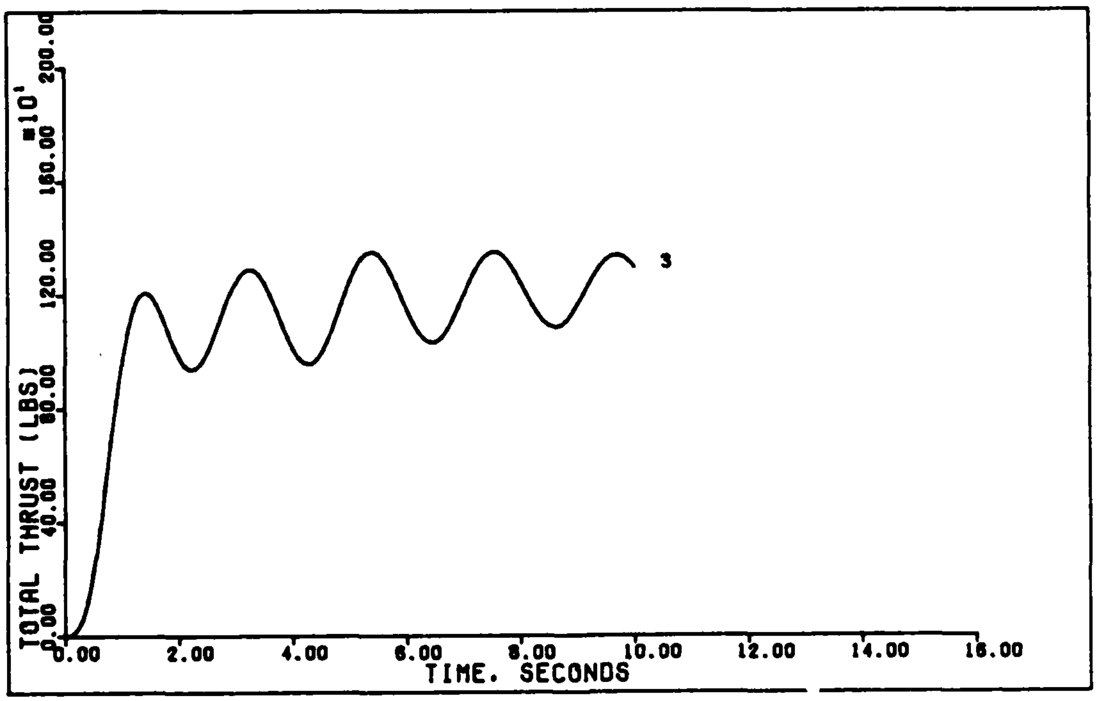

1.75 DEGREE PITCH POINTING (D. ALPHA=3. 0.6 MACH)

Figure 65. 1.75 Degree Pitch Pointing With Delay, Control Ratio Of Three (0.6 Mach, 0 Ft.)

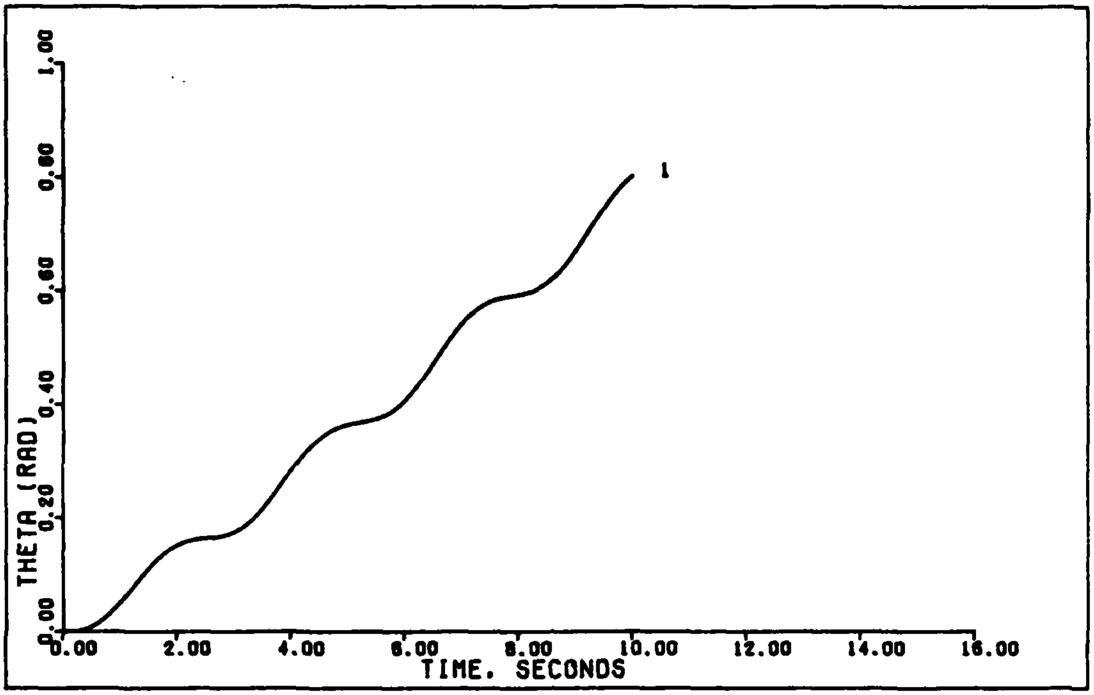

1.8 G DIRECT LIFT (D. ALPHA=2. 0.6 MACH)

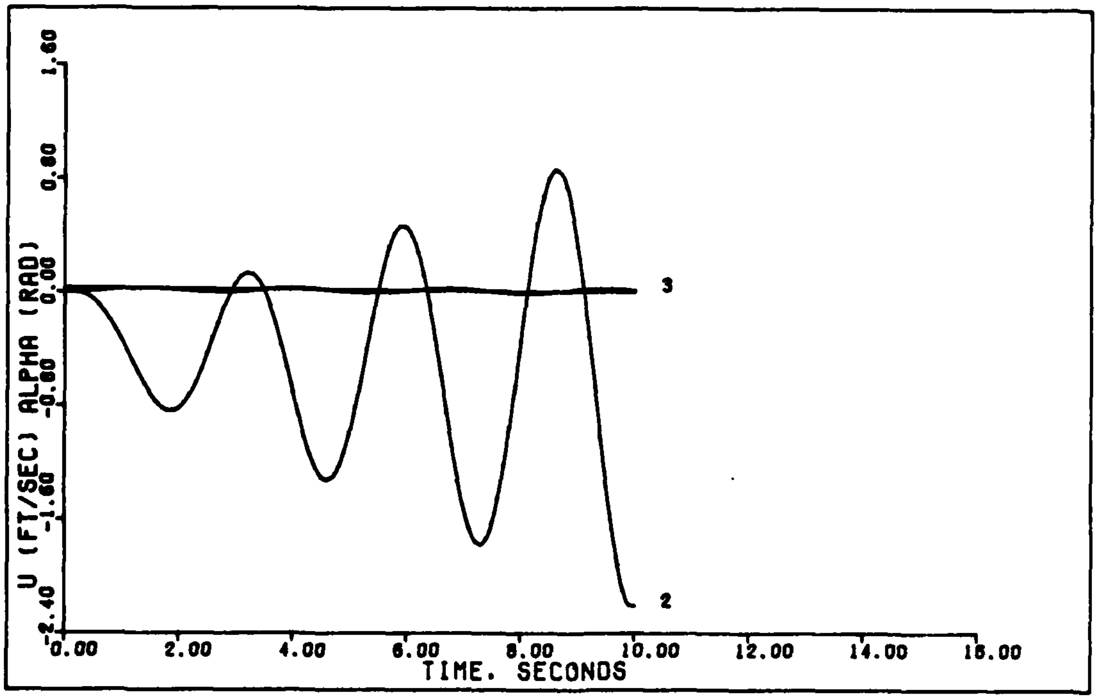

1.8 G DIRECT LIFT (D. ALPHA=2. 0.6 MACH)

Figure 66. 1.8 G Direct Lift With Delay, Control Ratio Of Two (0.6 Mach, 0 Ft.)

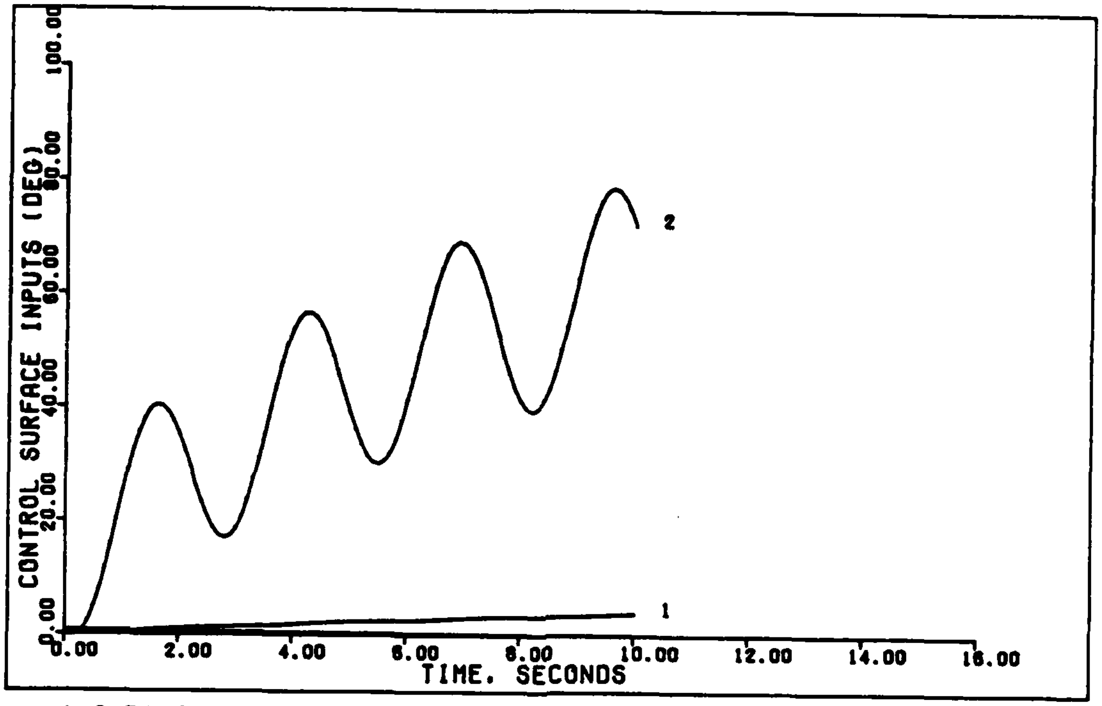

1.8 DIRECT LIFT (D. ALPHA=2. 0.6 MACH)

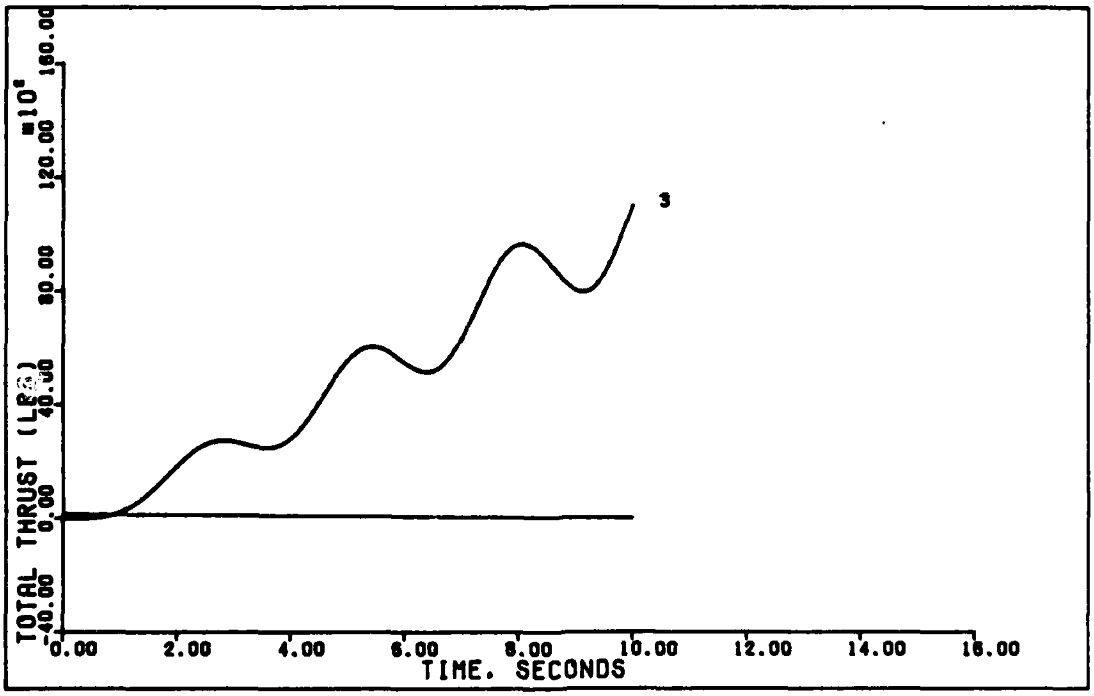

1.8 G DIRECT LIFT (D. ALPHA=2. 0.6 MACH)

Figure 67. 1.8 G Direct Lift With Delay, Control Ratio Of Two (0.6 Mach, 0 Ft.)

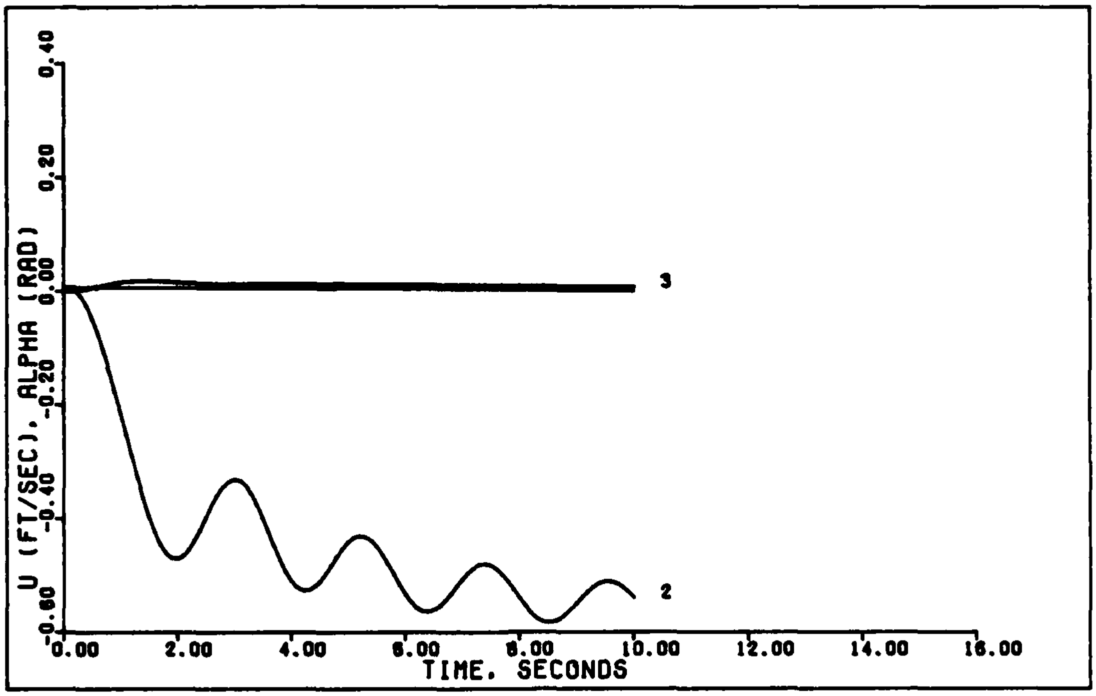

1.8 G DIRECT LIFT (D. ALPHA=3, 0.6 MACH)

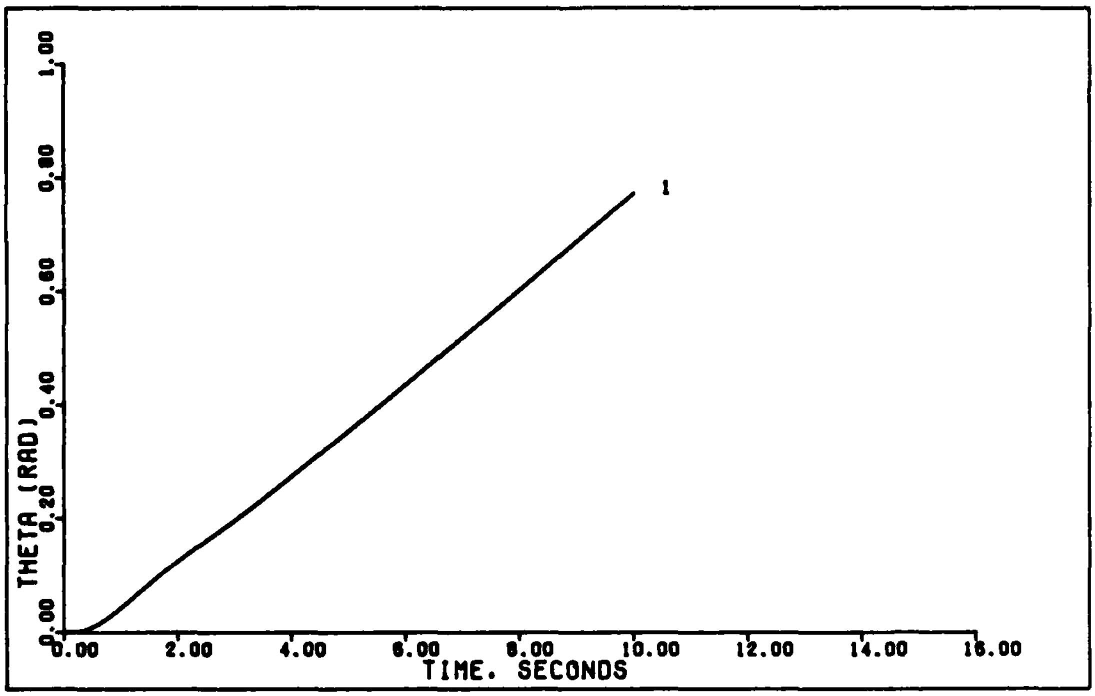

1.8 G DIRECT LIFT (D. ALPHA=3, 0.6 MACH)

Figure 68. 1.8 G Direct Lift With Delay, Control Ratio Of Three (0.6 Mach, 0 Ft.)

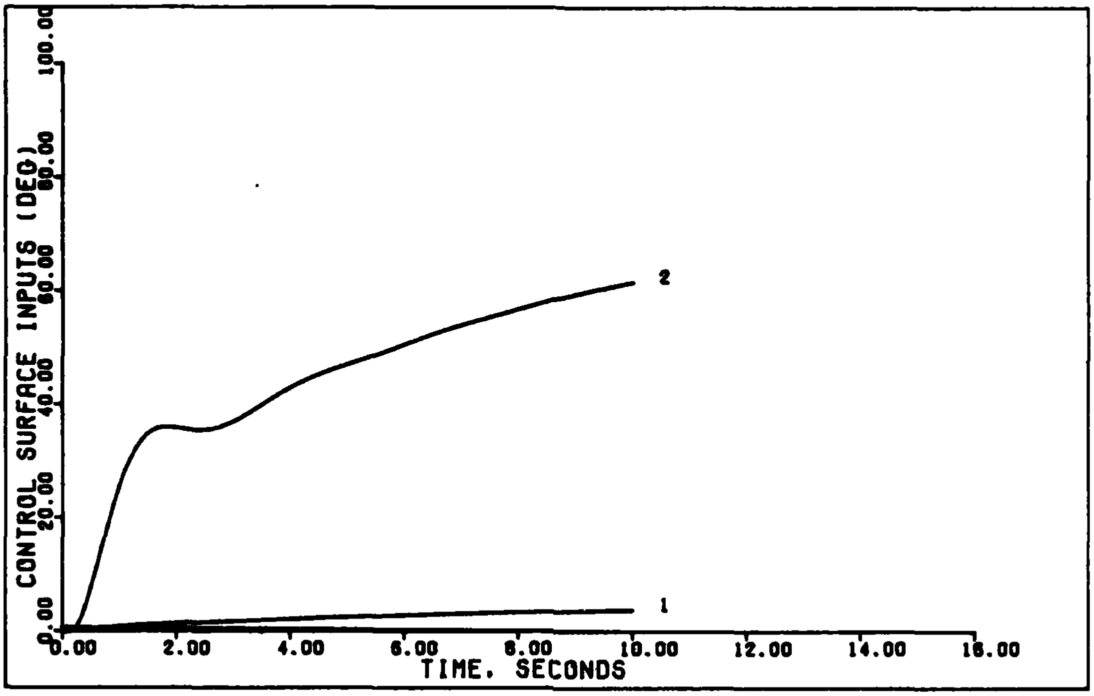

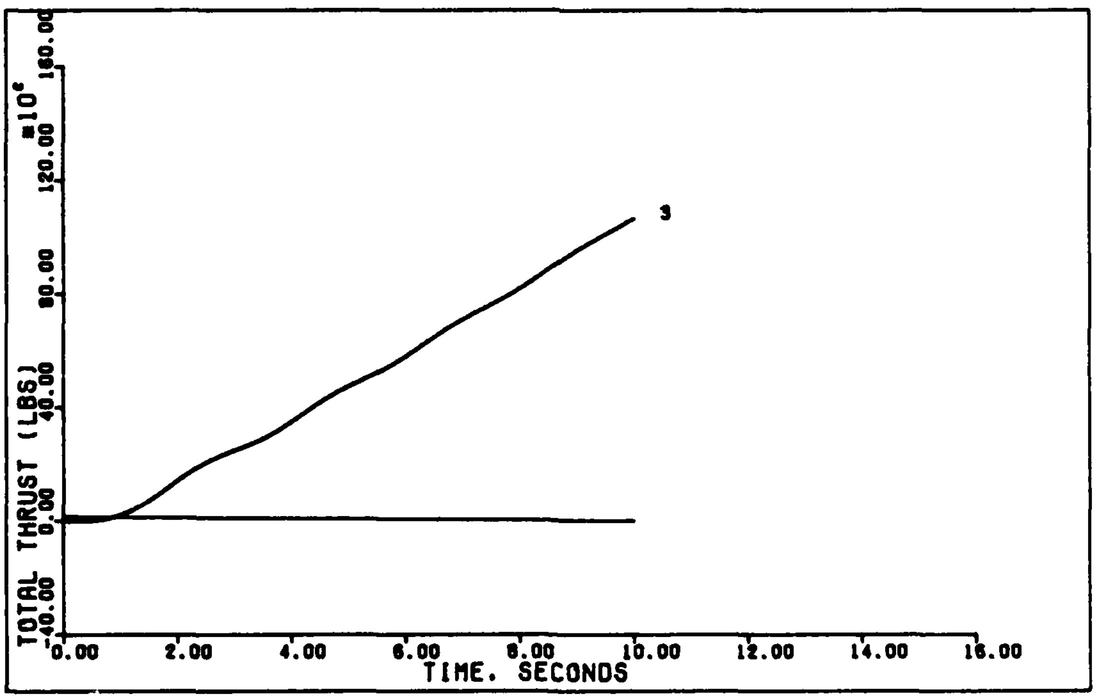

Figure 69. 1.8 G Direct Lift With Delay, Control Ratio Of Three (0.6 Mach, 0 Ft.)

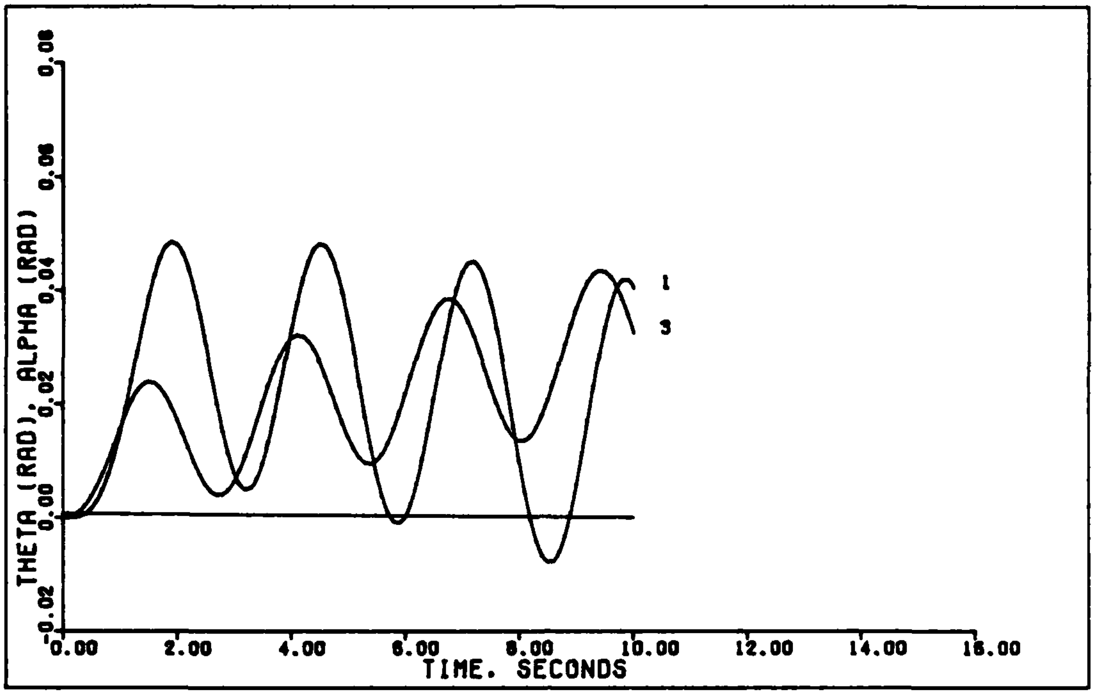

0.8 G VERTICAL TRANSLATION (D. ALPHA=2, 0.6 MACH)

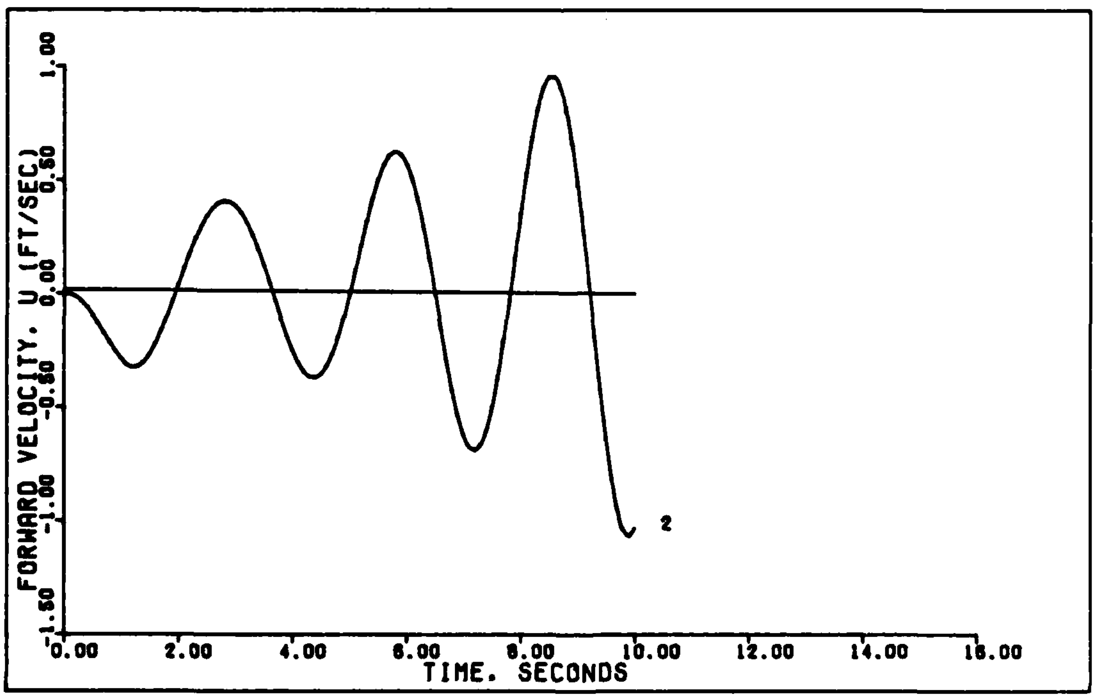

0.8 G VERTICAL TRANSLATION (D. ALPHA=2, 0.6 MACH)

Figure 70. 0.8 G Vertical Translation With Delay, Control Ratio Of Two (0.6 Mach, 0 Ft.)

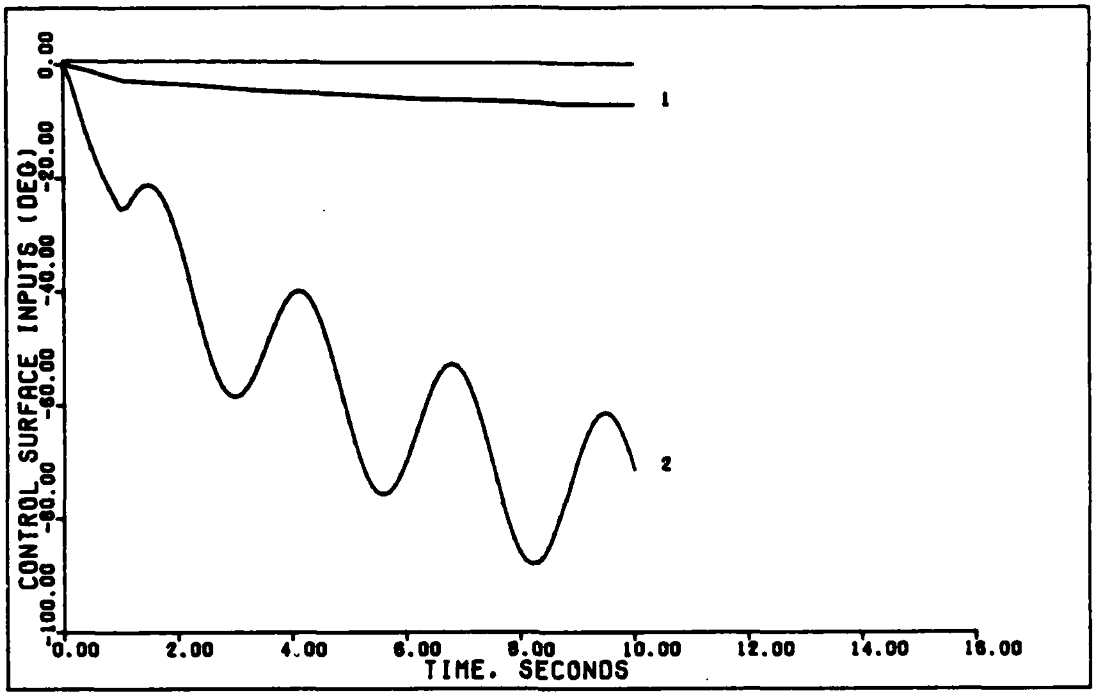

0.8 G VERTICAL TRANSLATION (D. ALPHA=2, 0.6 MACH)

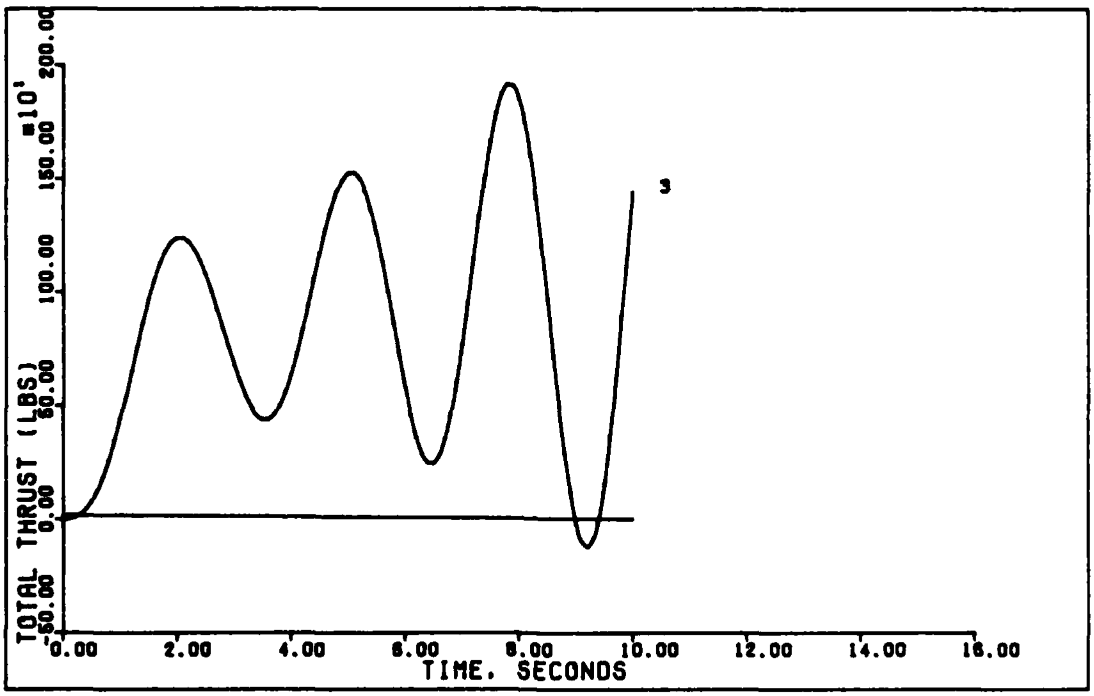

0.8 G VERTICAL TRANSLATION (D. ALPHA=2, 0.6 MACH)

Figure 71. 0.8 G Vertical Translation With Delay, Control Ratio Of Two (0.6 Mach, 0 Ft.)

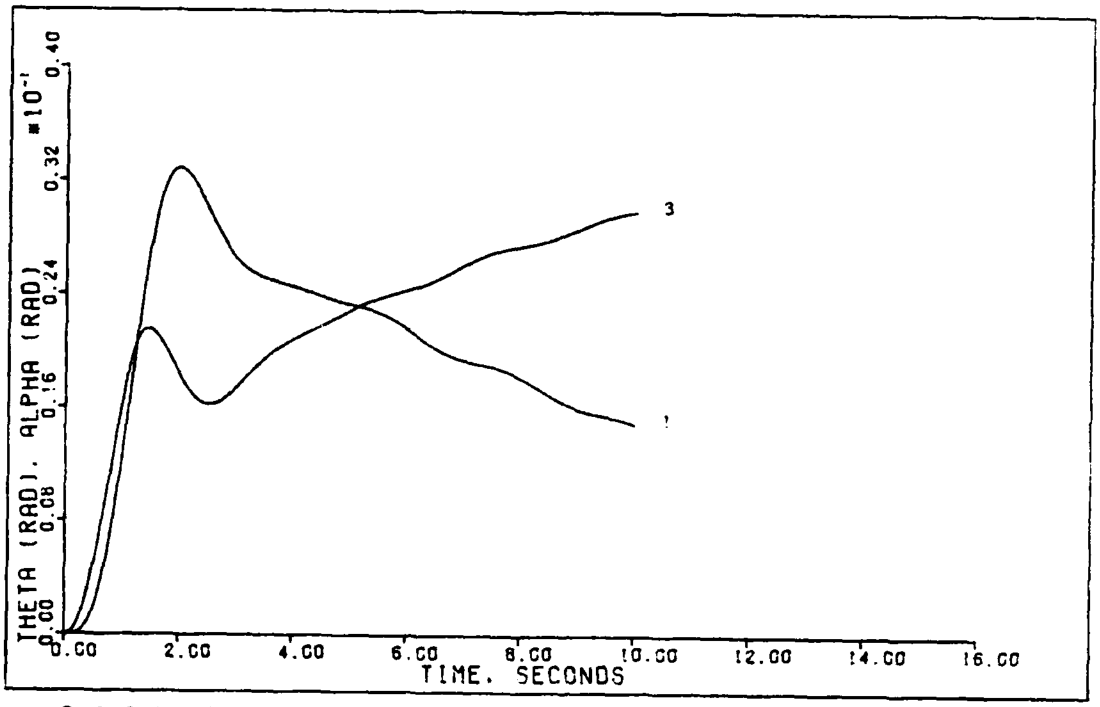

0.8 G VERTICAL TRANSLATION (D. ALPHA=3. 0.6 MACH)

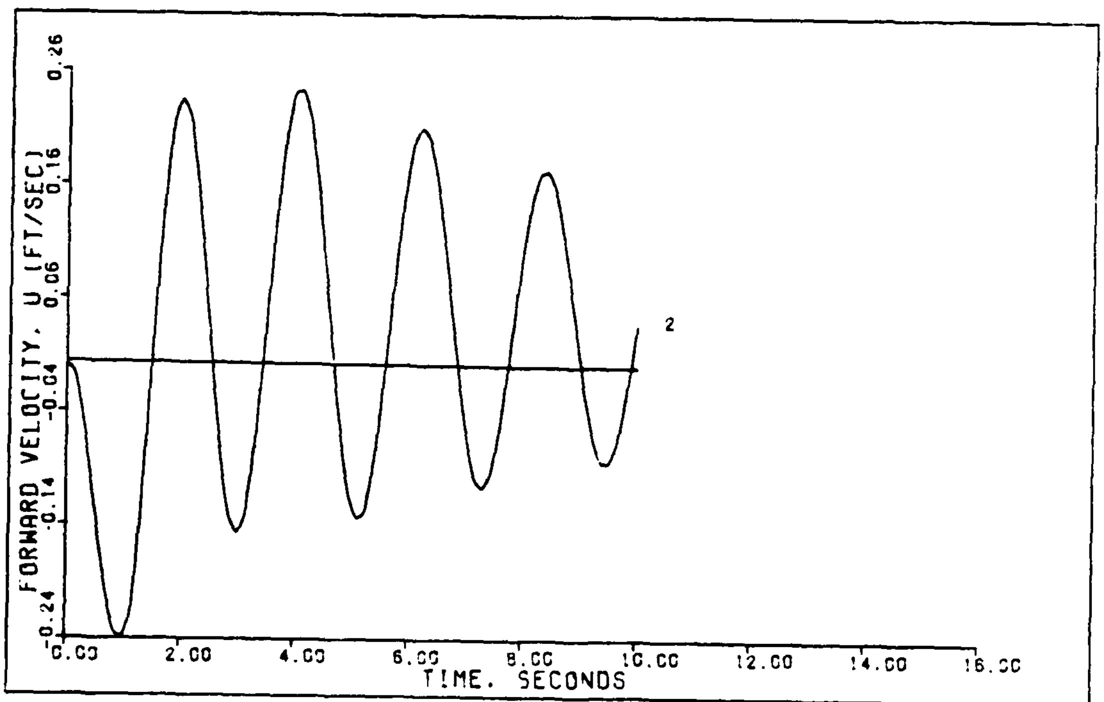

0.8 G VERTICAL TRANSLATION (D. ALPHA=3. 0.6 MACH)

Figure 72. 0.8 G Vertical Translation With Delay, Control Ratio Of Three (0.6 Mach, 0 Ft.)

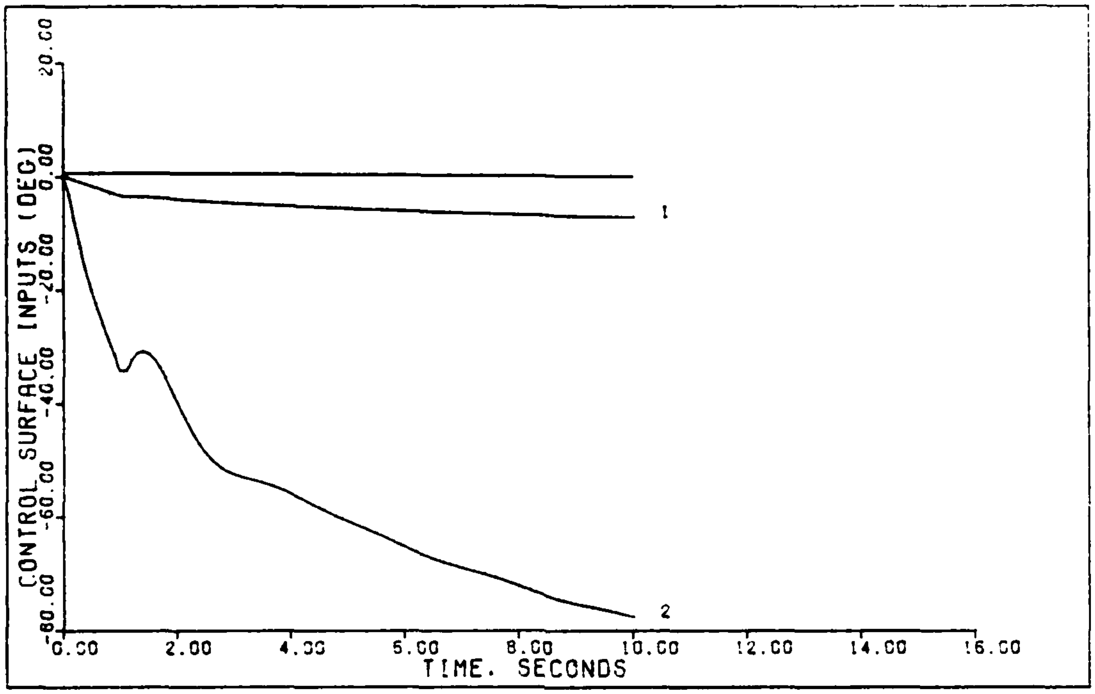

0.8 G VERTICAL TRANSLATION (D. ALPHA=3. 0.6 MACH)

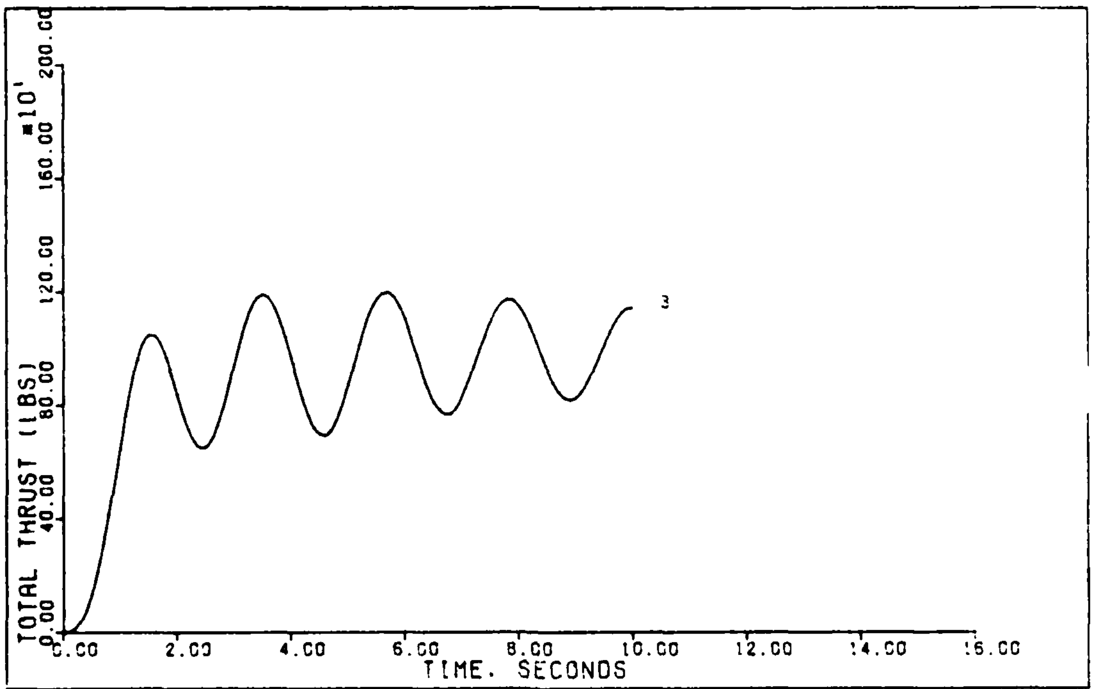

0.8 G VERTICAL TRANSLATION (D. ALPHA=3. 0.6 MACH)

Figure 73. 0.8 G Vertical Translation With Delay, Control Ratio Of Three (0.6 Mach, 0 Ft.)

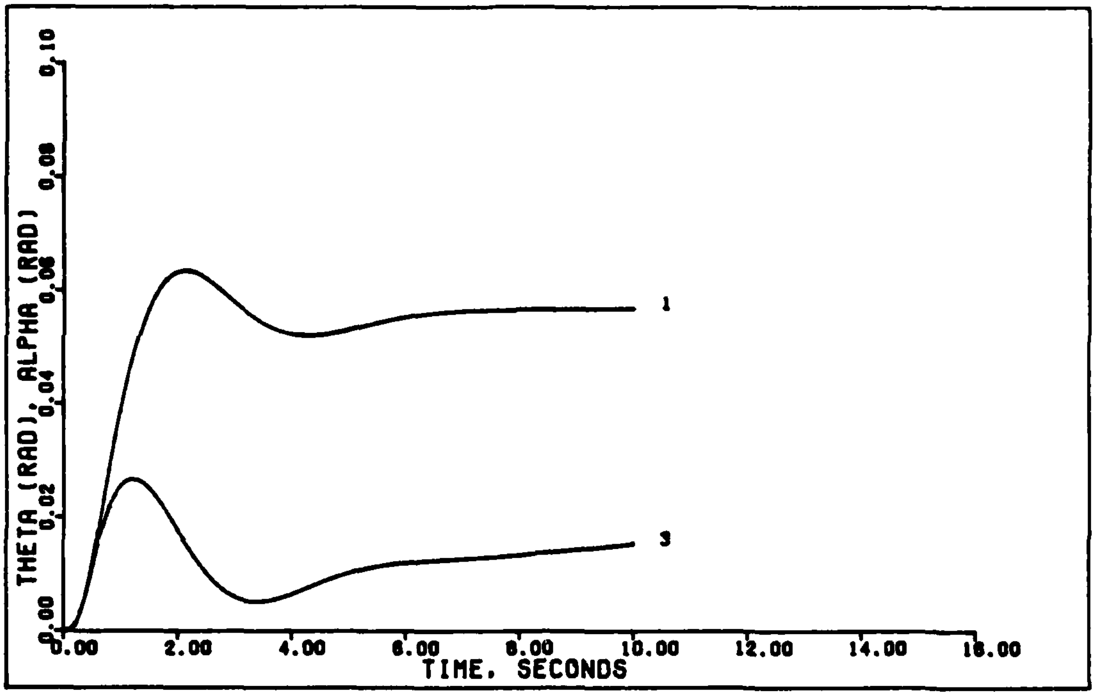

3 DEGREE PITCH POINTING (D. ALPHA=4. 0.9 MACH)

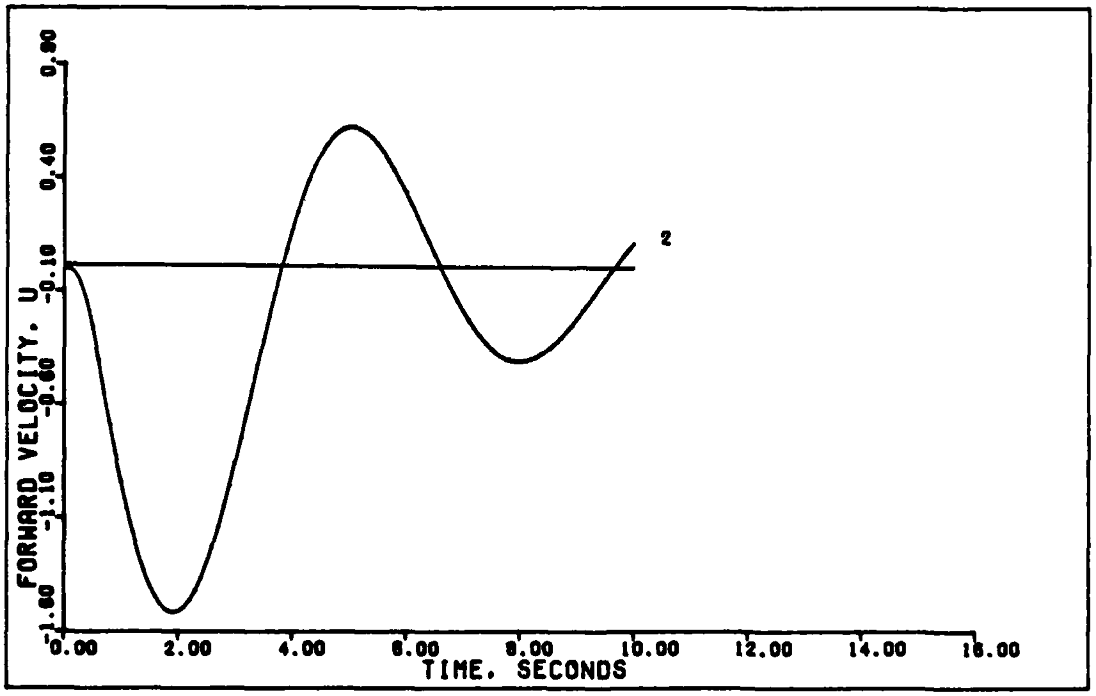

3 DEGREE PITCH POINTING (D. ALPHA=4. 0.9 MACH)

Figure 74. 3 Degree Pitch Pointing With Delay, Control Ratio Of Four (0.9 Mach, 30000 Ft.)

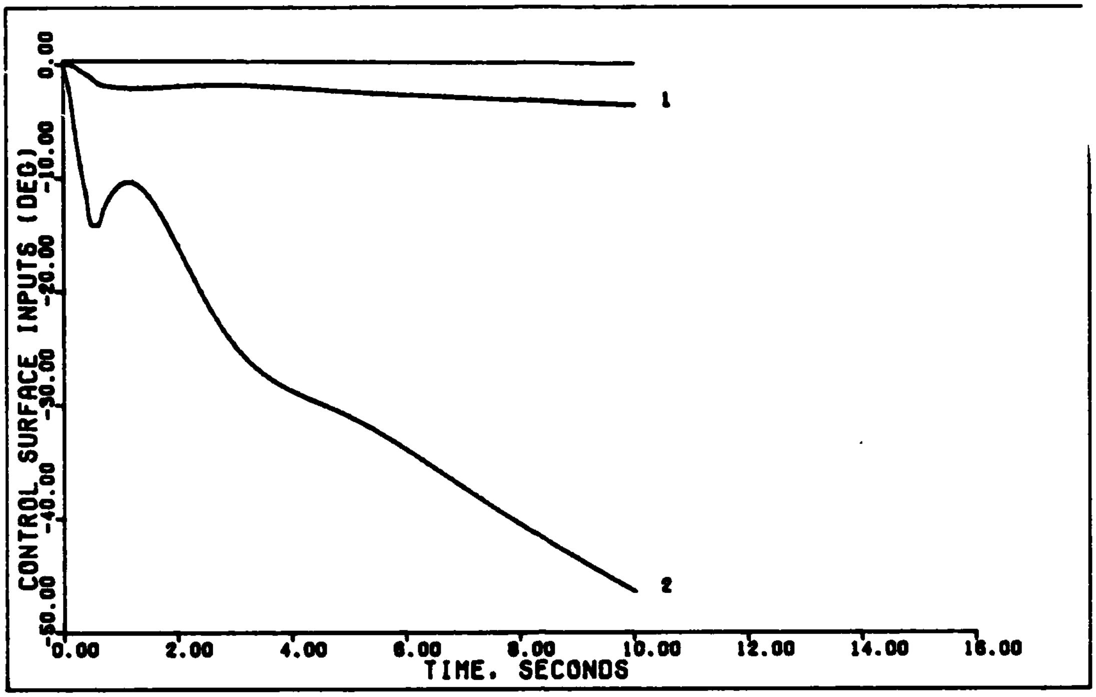

3 DEGREE PITCH POINTING (D. ALPHA=4, 0.9 MACH)

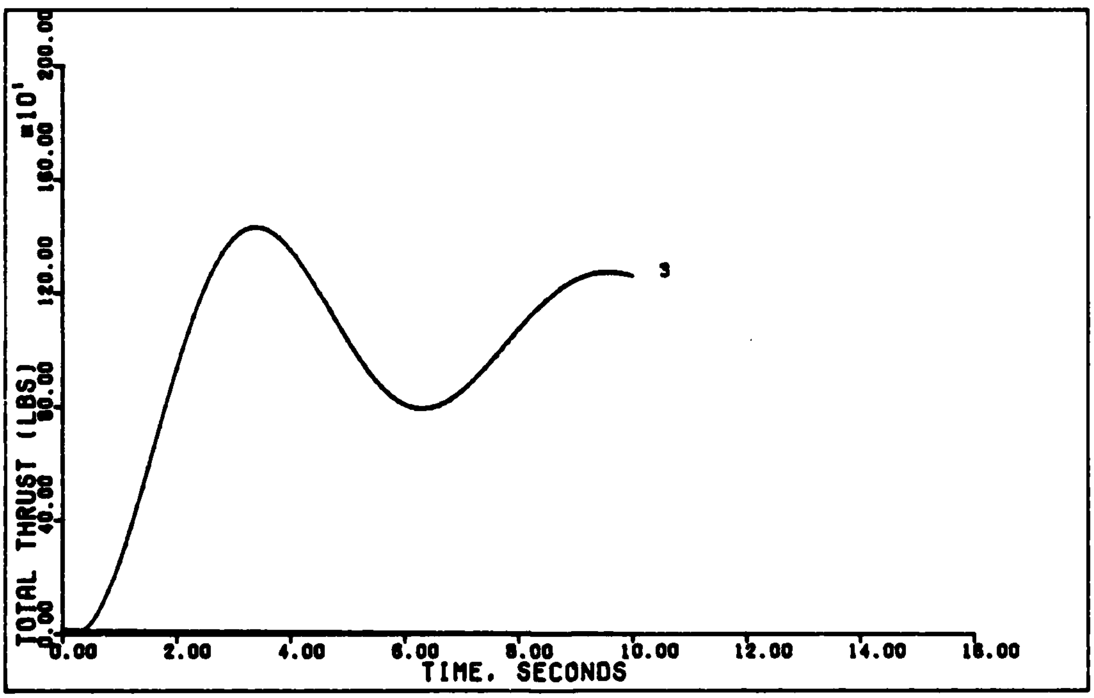

3 DEGREE PITCH POINTING (D. ALPHA=4, 0.9 MACH)

Figure 75. 3 Degree Pitch Pointing With Delay, Control Ratio Of Four (0.9 Mach, 30000 Ft.)

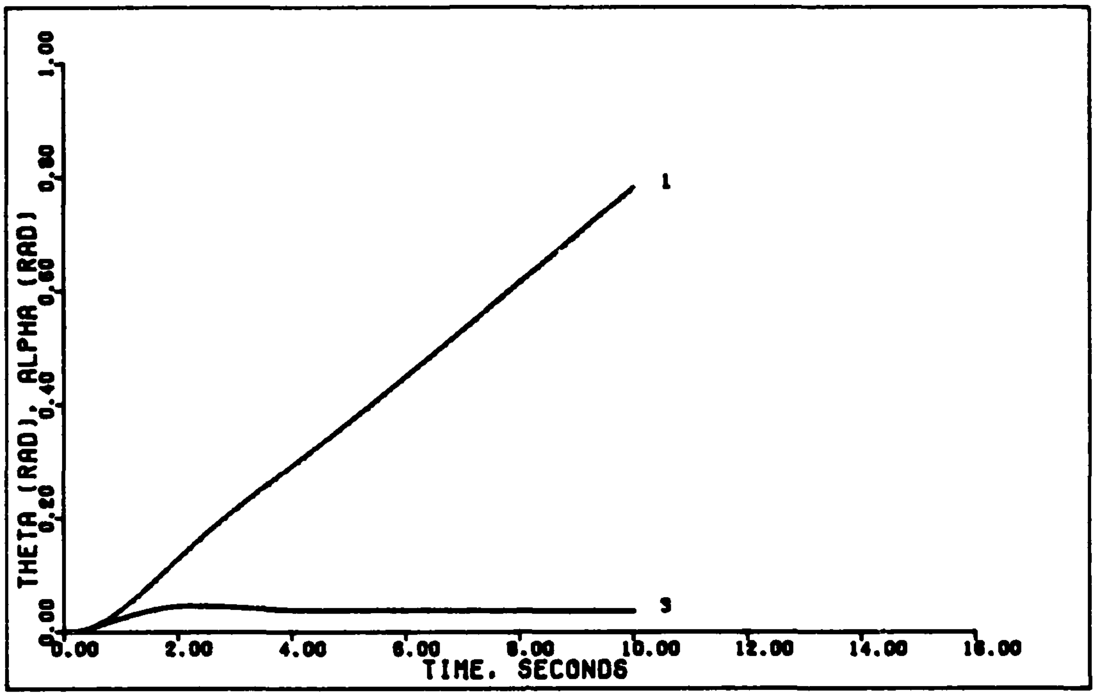

2.4 G DIRECT LIFT (D. ALPHA=4. 0.9 MACH)

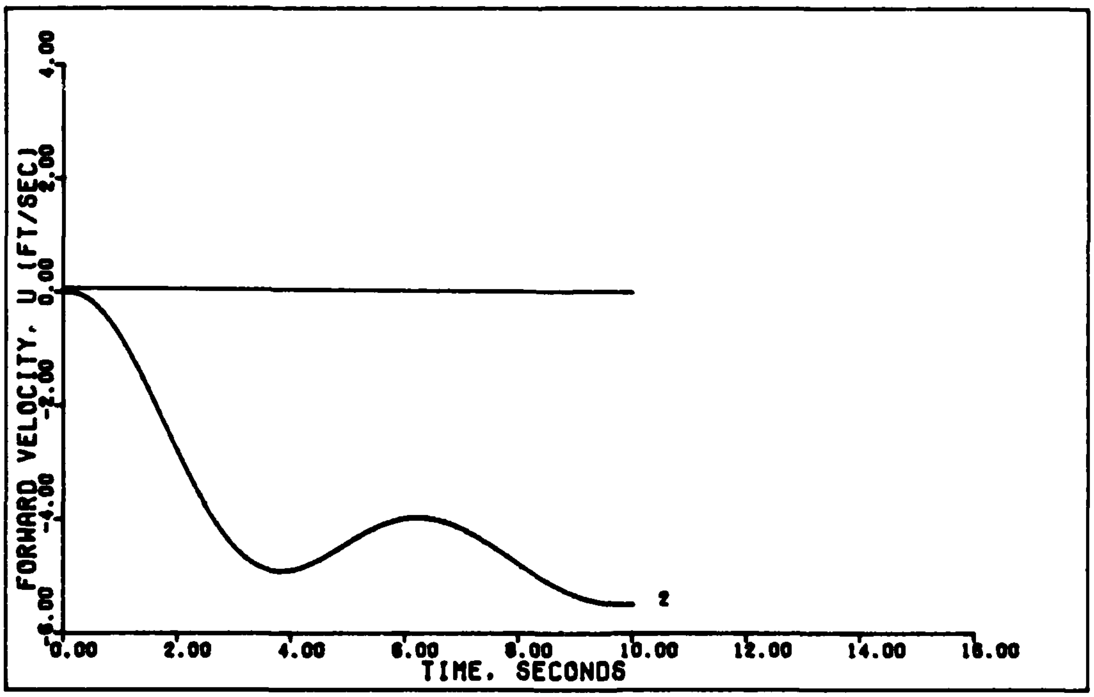

2.4 G DIRECT LIFT (D. ALPHA=4. 0.9 MACH)

Figure 76. 2.4 G Direct Lift With Delay, Control Ratio Of Four (0.9 Mach, 30000 Ft.)

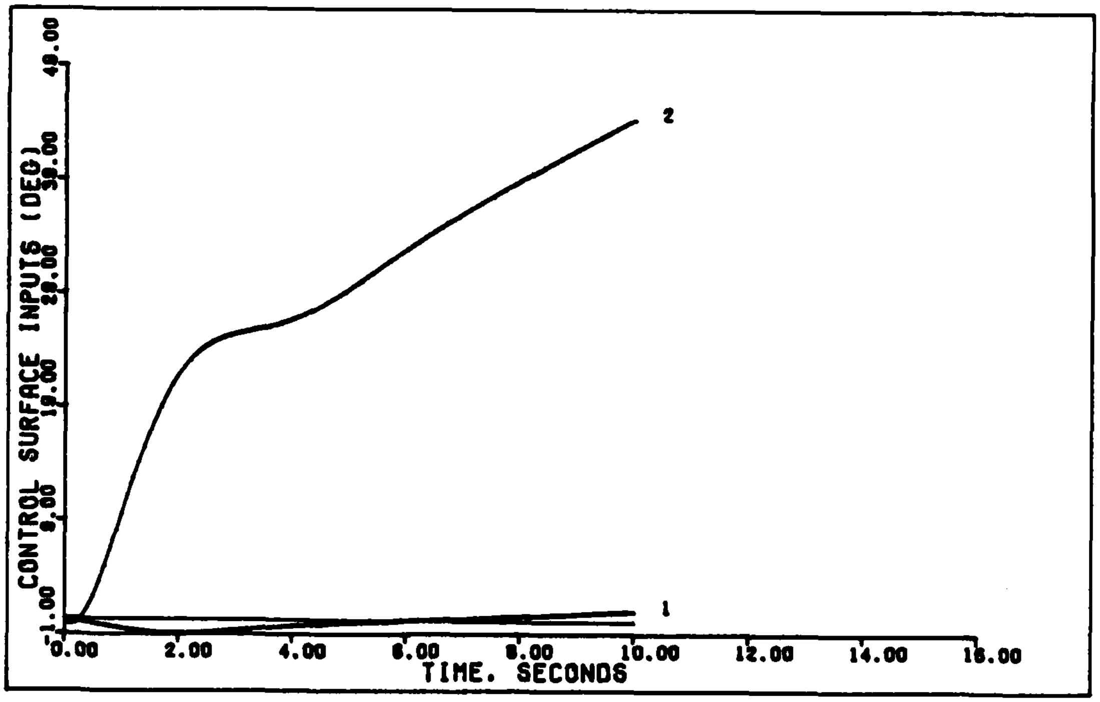

2.4 G DIRECT LIFT (D. ALPHA=4. 0.9 MACH)

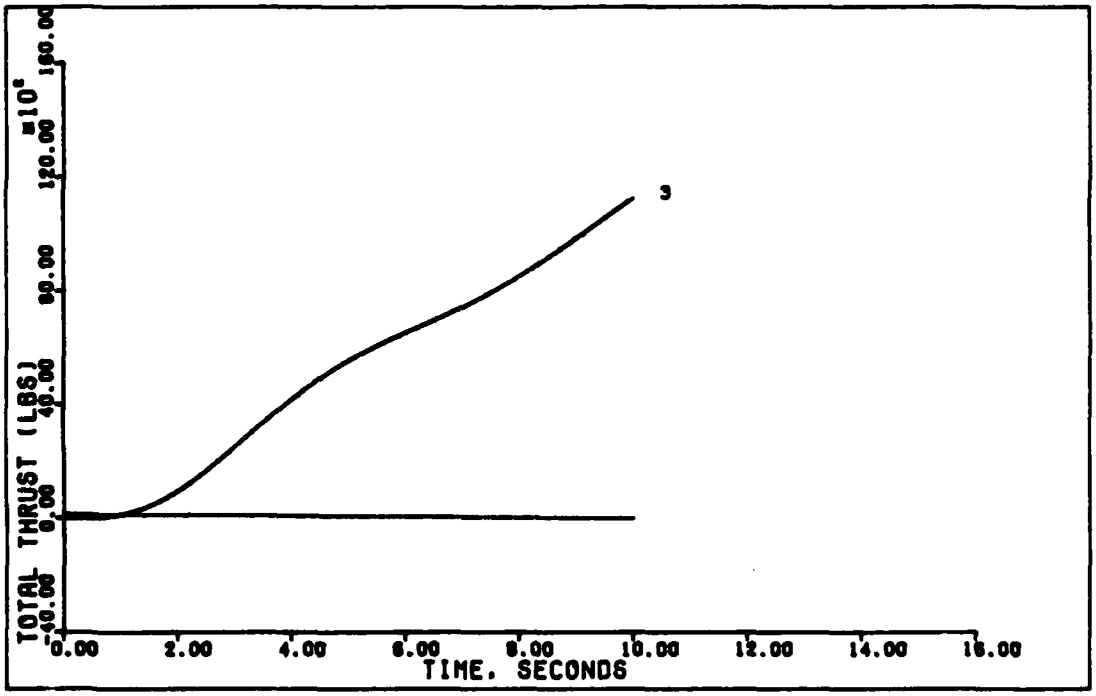

2.4 G DIRECT LIFT (D. ALPHA=4. 0.9 MACH)

Figure 77. 2.4 G Direct Lift With Delay, Control Ratio Of Four (0.9 Mach, 30000 Ft.)

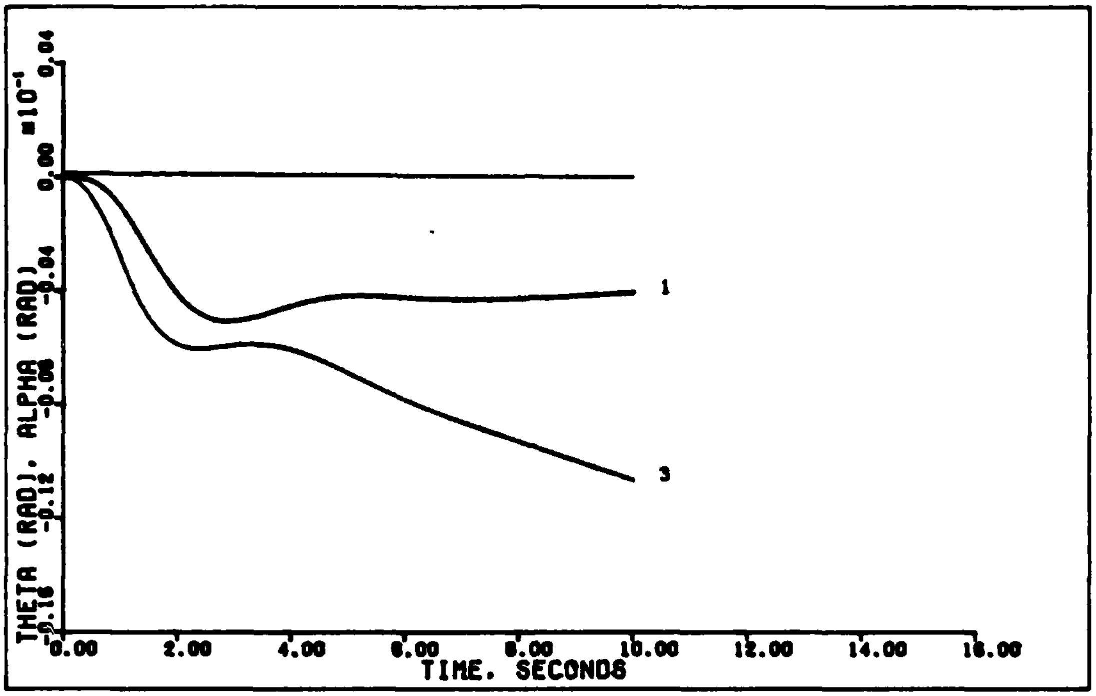

1 G VERTICAL TRANSLATION (D. ALPHA=4. 0.9 MACH)

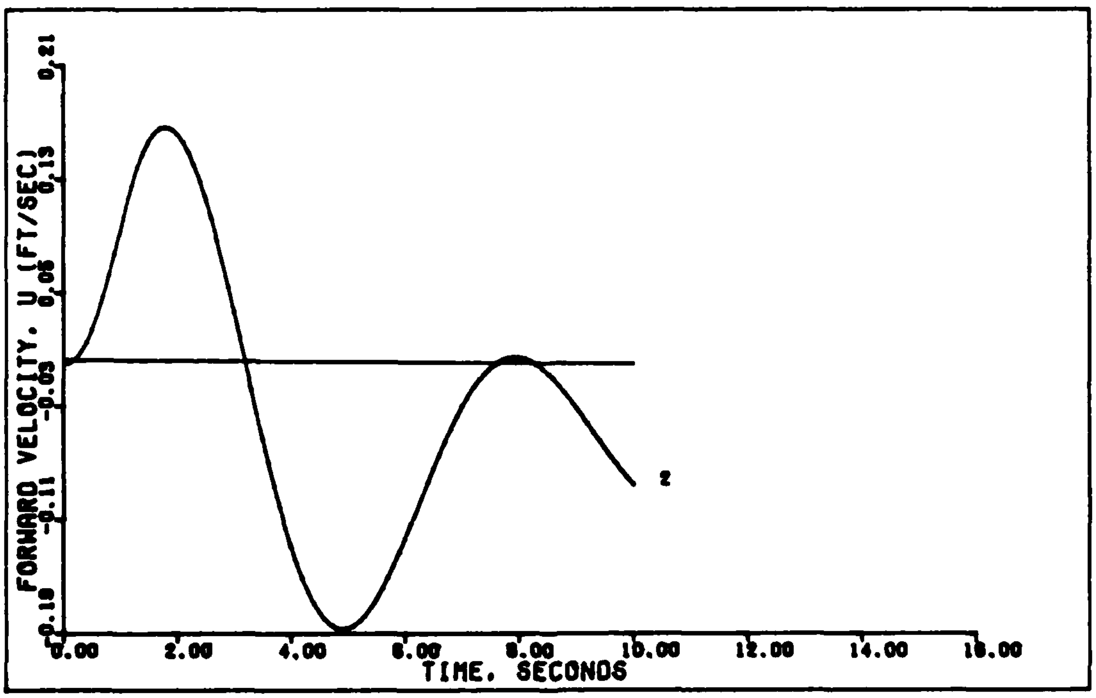

1 G VERTICAL TRANSLATION (D. ALPHA=4. 0.9 MACH)

Figure 78. 1 G Vertical Translation With Delay, Control Ratio Of Four (0.9 Mach, 30000 Ft.)

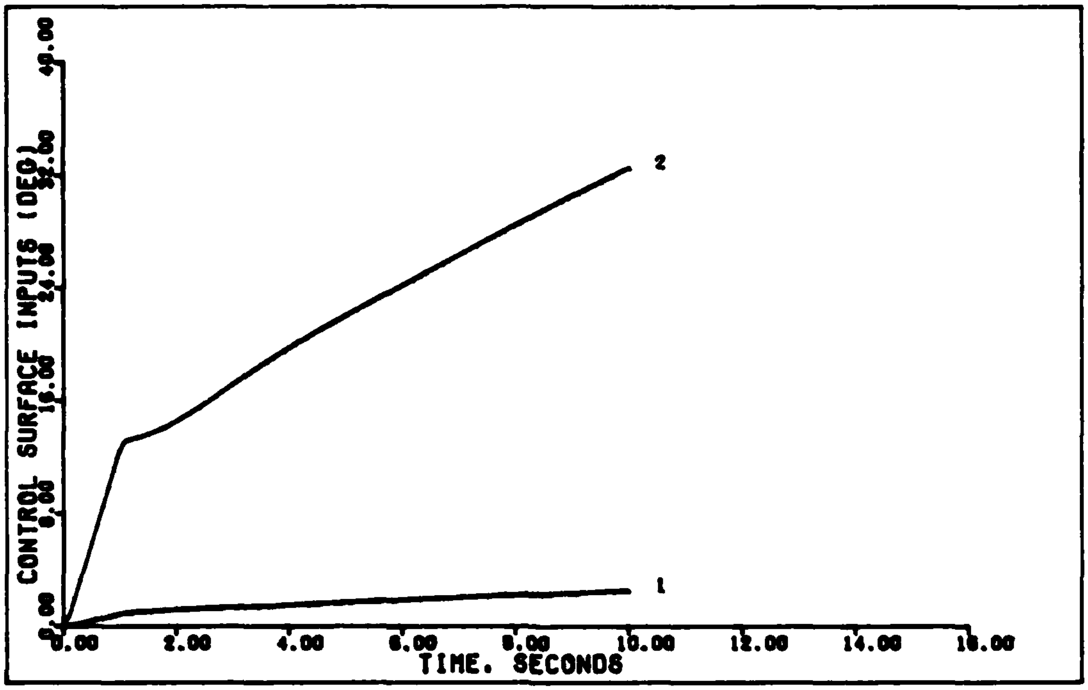

1 G VERTICAL TRANSLATION (D. ALPHA=4. 0.9 MACH)

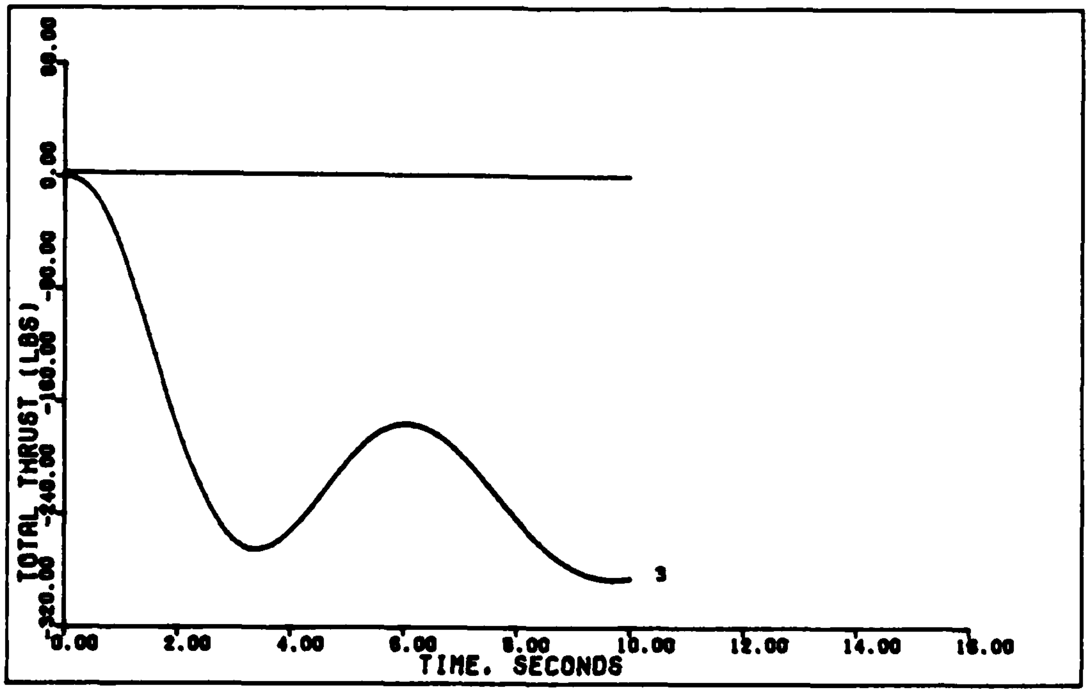

1 G VERTICAL TRANSLATION (D. ALPHA=4. 0.9 MACH)

Figure 79. 1 G Vertical Translation With Delay, Control Ratio Of Four (0.9 Mach, 30000 Ft.)

these results.

Starting with the pitch pointing maneuver at the 0.15 mach flight condition (Figures 53 through 55), the effects of the delay are most obvious in the angle of attach response. Both theta and alpha remain essentially unchanged in their response during the first 1.5 seconds when compared with the corresponding responses for no delay (Figures 12 through 14). After the initial 1.5 seconds the alpha response falls off considerably. The forward velocity, control surface deflections, and total thrust do not change much with the addition of the delay.

For the direct lift maneuver at 0.15 mach the introduction of the delay causes almost no change in the output responses (Figures 56 through 58) as compared to the same responses with no delay (Figures 15 through 17). For the control surfaces the effect of the delay is minimal, as is the effect of the delay upon the total thrust. Interestingly, this maneuver exhibits both the best responses with and without the delay.

Incorporation of the delay into the vertical translation maneuver at 0.15 mach (Figures 59 through 61) does degrade the alpha response significantly, although the theta response is essentially unchanged when compared to the responses without the delay (Figures 18 through 20). The forward velocity, control surface deflections, and total thrust responses have not changed much with the added delay.

Figures 62 through 63 show the results of adding the delay to the pitch pointing maneuver for the 0.6 mach, sea level flight condition. The added instability from the delay has caused the theta and alpha response to become oscillatory, and the forward velocity response has become unstable. The control surface deflections show the oscillatory nature and the total thrust demonstrates instability. Obviously these results are unacceptable compared to those without any delay (Figures 21 through 23).

However, if the ratio of proportional to integral controller matrices is increased to three from the original value of two, then most of the effect of the delay can be removed. Figures 64 through 65 show the responses for the pitch pointing maneuver at 0.6 mach, but with this ratio set to three. Compared with the undelayed responses the theta and alpha plots are not changed much, nor is the forward velocity response. The control surface deflections haven't changed much either, but the total thrust response has changed. The combination of the delay and increasing the proportional to integral control ratio has yielded a much more acceptable thrust response. It's important to point out that increasing the control ratio without the delay does not yield satisfactory results for all of the maneuvers at this flight condition.

The destabilizing effect of the delay is also apparent in the responses for the direct lift maneuver at 0.6 mach (Figures 66 through 67). The theta response has become oscillatory, with the forward velocity once again showing instability. The jet flaps also demonstrate an oscillatory response, with the total thrust apparently unstable. These results would have to be considered unsatisfactory when compared with the undelayed responses (Figures 24 through 26).

Increasing the ratio of proportional to integral control once again compensates for practically all of the deleterious effects of the delay. Figures 68 through 69 show the responses for the direct lift maneuver at 0.6 mach with the control ratio increased to three from the original value of two. The theta, alpha, and forward velocity responses are nearly identical to the undelayed responses, and the control surface deflections are very similar. The thrust response is actually improved, showing less oscillatory nature.

The vertical translation maneuver at 0.6 mach also follows right along with the previous results. Figures 70 through 71 show the responses with the control ratio unchanged but with the addition of the delay. The theta, alpha, and forward velocity curves show unstable oscillations as do the control surface deflections and the total thrust plots. These results are also unsatisfactory when compared to the original responses (Figures 27 through 29).

Unfortunately, increasing the control ratio to three from its initial value of two does not have quite the same impact as with the prior maneuvers (Figures 72 and 73). The theta and alpha responses have improved, but not to the point where they could be called similar to the undelayed responses. They are not very dissimilar either, but the effects of delay are not as completely compensated for as before. The forward velocity hasn't changed much, nor have the control surface deflections. But once again the thrust response has actually improved.

Figures 74 through 79 show the responses for the longitudinal maneuvers at the 0.9 mach, 30,000 ft. flight condition with attempted compensation thru increasing the ratio of proportional to integral control. These results can be compared to the undelayed responses for this flight condition (Figures 30 through 39). The pitch pointing maneuver is compensted very well, with an actual improvement in the forward velocity and thrust responses. The direct lift maneuver is also well compensated, but without any obvious improvement in the thrust or forward velocity responses. The vertical translation also is well compensated without any marked difference in any of the responses. Unfortunately, this last maneuver is one of the worst responding ones, even undelayed.

Conclusions. Due to time constraints in preparing the results of the effects of and compensating for time delay, all of the longitudinal maneuvers were tested instead of the lateral maneuvers at the 0.15 mach flight condition. This was done so that tentative conclusions could be drawn regarding the effect of delay on a universal controller.

Obviously, introducing a one sampling period time delay into the output of the PI controller introduces oscillations and instabilities into the time responses. The effect of the delay seems to increase with increasing speed and altitude, although this is a tenuous conclusion at best. For this aircraft, compensating for this time delay is effectively achieved through increasing the ratio of proportional to integral control in the PI controller matrices. Time limitations precluded rigorous searching for other methods of compensating for this delay. One of the most interesting results of compensating for the delay is an improvement of the velocity and/or thrust responses for some of the maneuvers. Overall, this method of compensation seems very promising.

Universal Controller Incorporating Delay

Extending these results to compensating a universal type controller, the logical conclusion would be that increasing the ratio of proportional to integral control should work, with the actual increase probably only found experimentally. To test this hypothesis, the universal controller discussed at the beginning of this chapter is tested by introducing the time delay. Figures 80 through 85 show the time responses for the universal controller using the longitudinal maneuvers at the 0.6 mach flight condition. Limited experimentation showed that a proportional to integral control ratio of four was close to the best value, with increasing ratios degrading the angle of attack response and decreasing ratios not compensating the delay enough. This is the same ratio used for the 0.9 mach flight condition, further reinforcing the choice of the design parameters from the 0.9 mach flight condition for the universal controller. Table XI summarizes the results.

Results. Figures 80 through 81 show the time responses of the universal controller to the 1.75 degree pitch pointing command. Comparing these to the results for the undelayed responses (Figures 44 through 46) shows no major changes in the time responses. The theta response has more overshoot, while the angle of attack shows greater error at the end of ten seconds. The transient response of alpha is almost unchanged. The forward

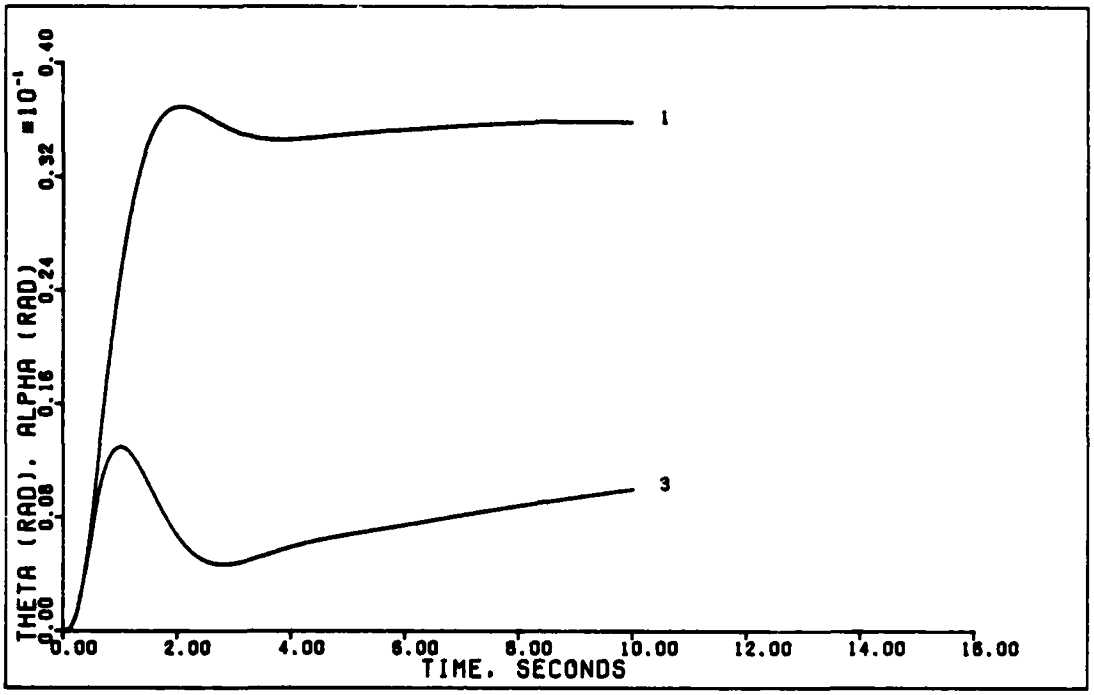

3 DEGREE PITCH POINTING (U. D. ALPHA=4. 0.6 M)

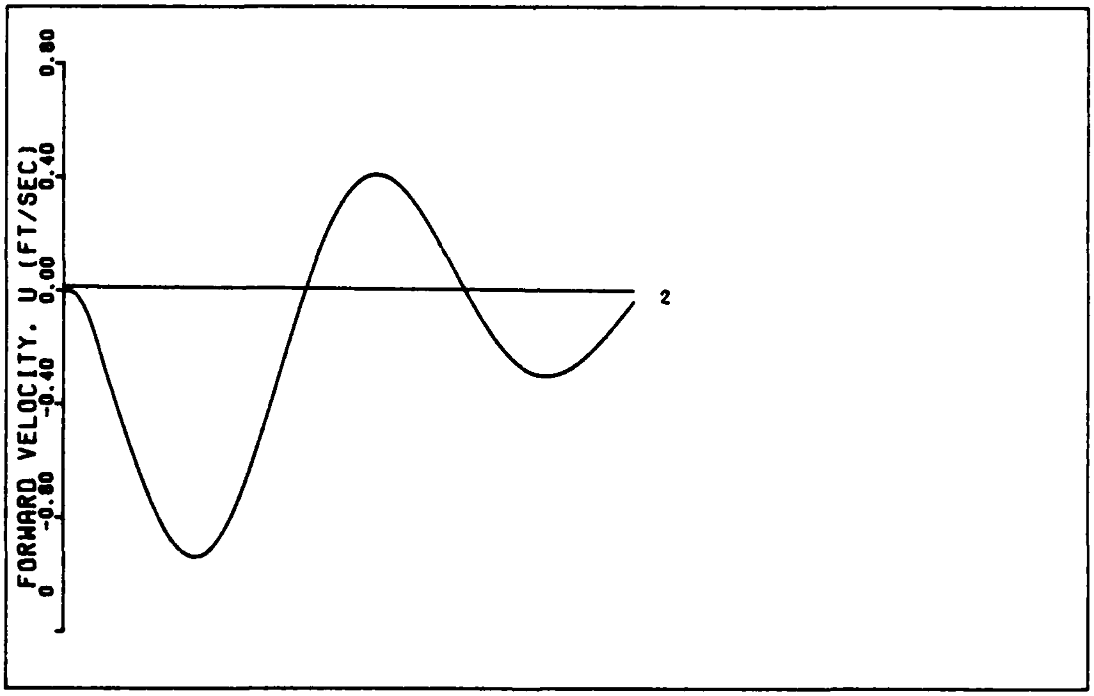

3 DEGREE PITCH POINTING (U. D. ALPHA=4. 0.6 M)

Figure 80. 1.75 Degree Pitch Pointing With Delay, Universal Controller (0.6 Mach, 0 ft.)

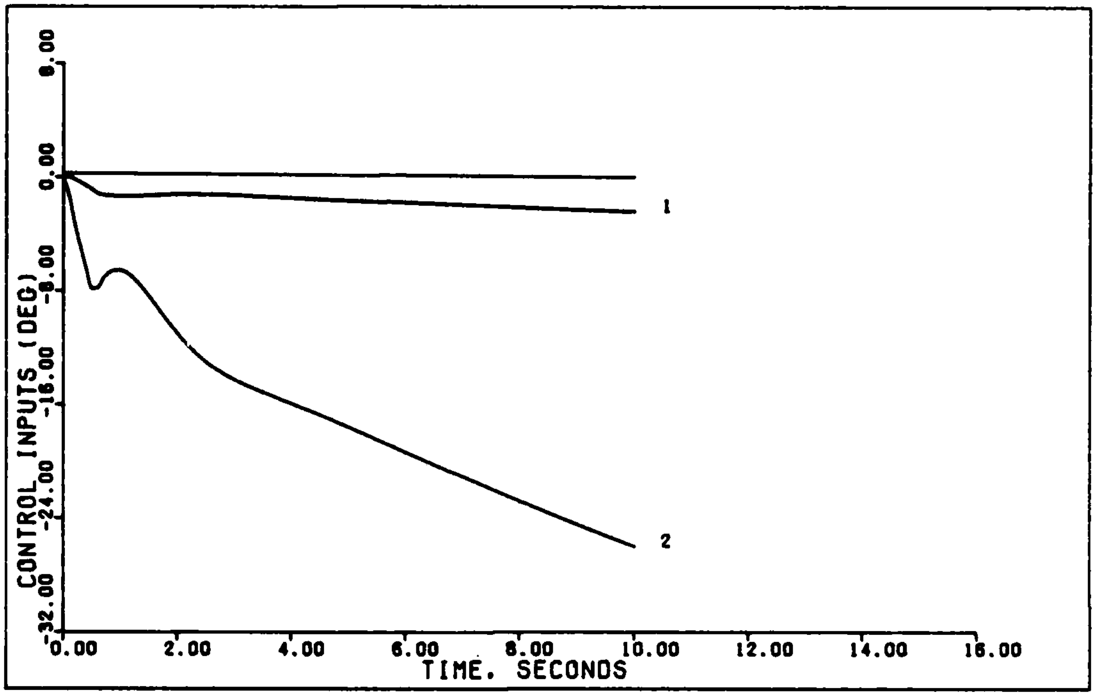

3 DEGREE PITCH POINTING (U. D. ALPHA=4, 0.6 M)

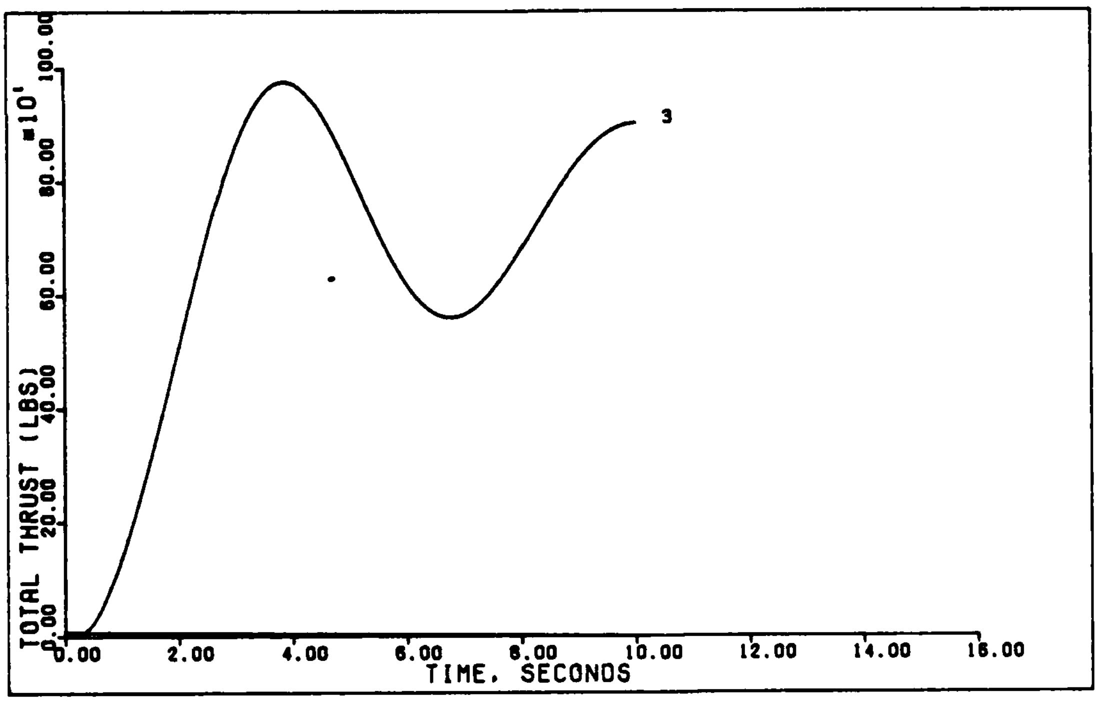

3 DEGREE PITCH POINTING (U. D. ALPHA=4, 0.6 MACH)

Figure 81. 1.75 Degree Pitch Pointing With Delay, Universal Controller (0.6 Mach, 0 ft.)

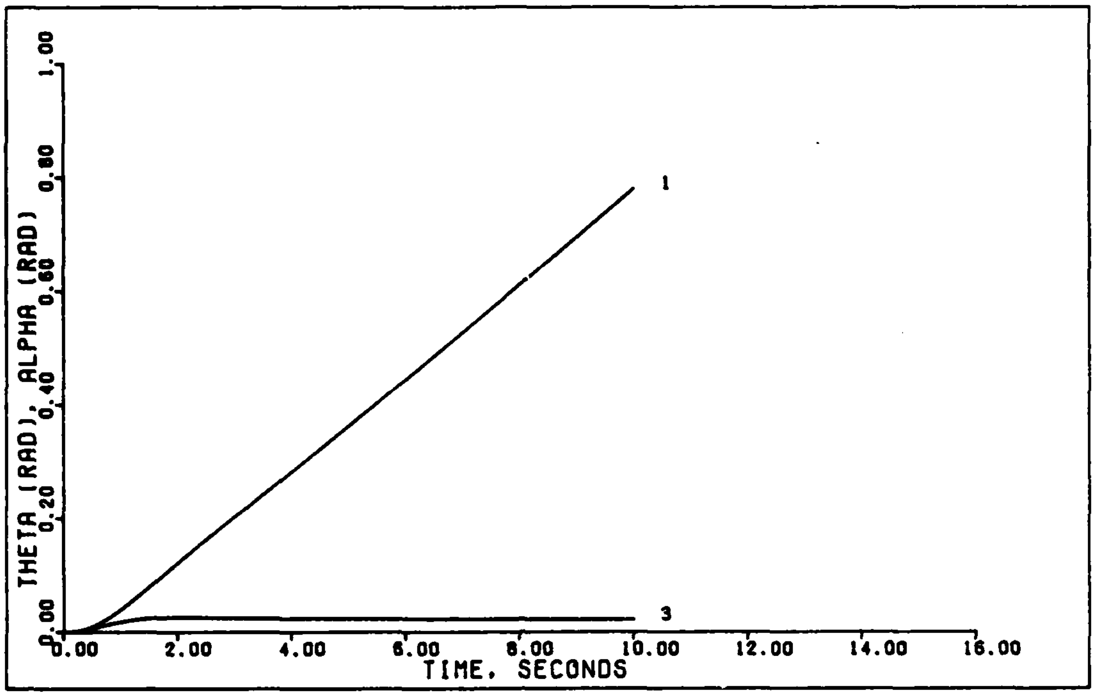

2.4 G DIRECT LIFT (U. D. ALPHA=4. 0.6 M)

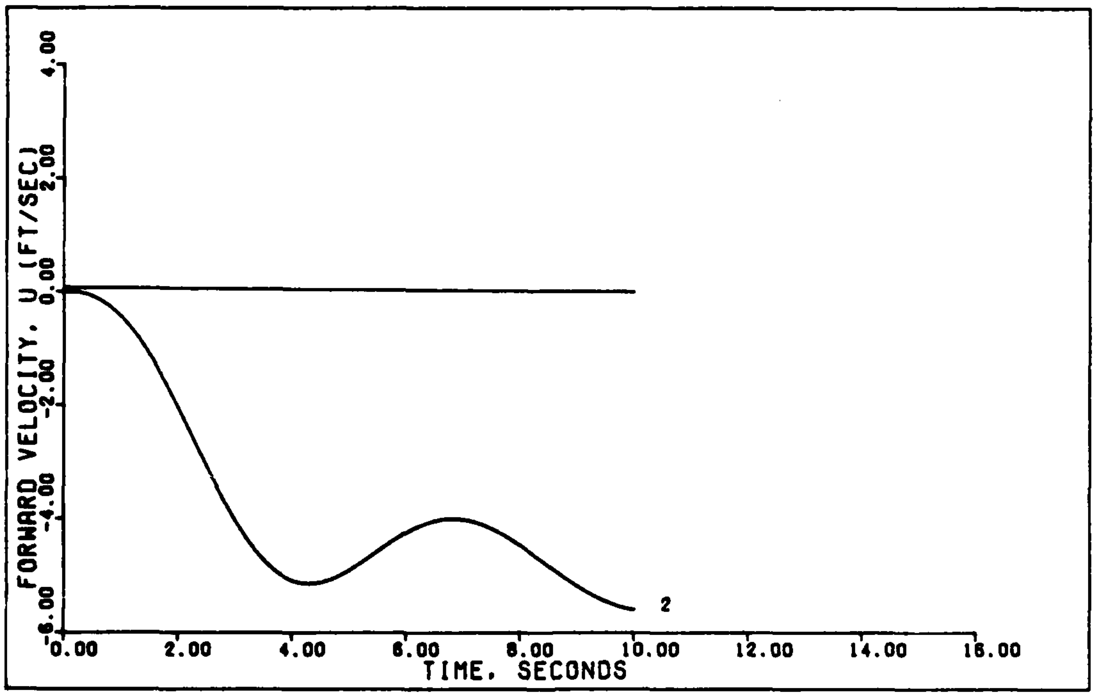

2.4 G DIRECT LIFT (U. D. ALPHA=4. 0.6 M)

Figure 82. 1.8 G Direct Lift With Delay, Universal Controller (0.6 Mach, 0 ft.)

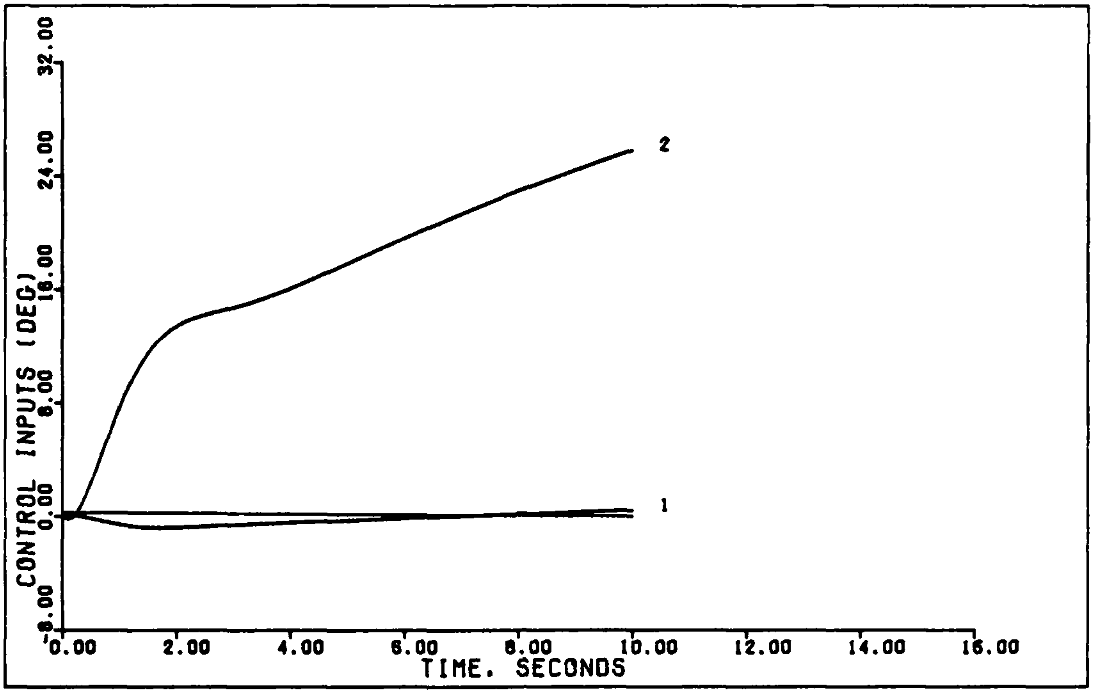

2.4 G DIRECT LIFT (U. D. ALPHA=4. 0.6 M)

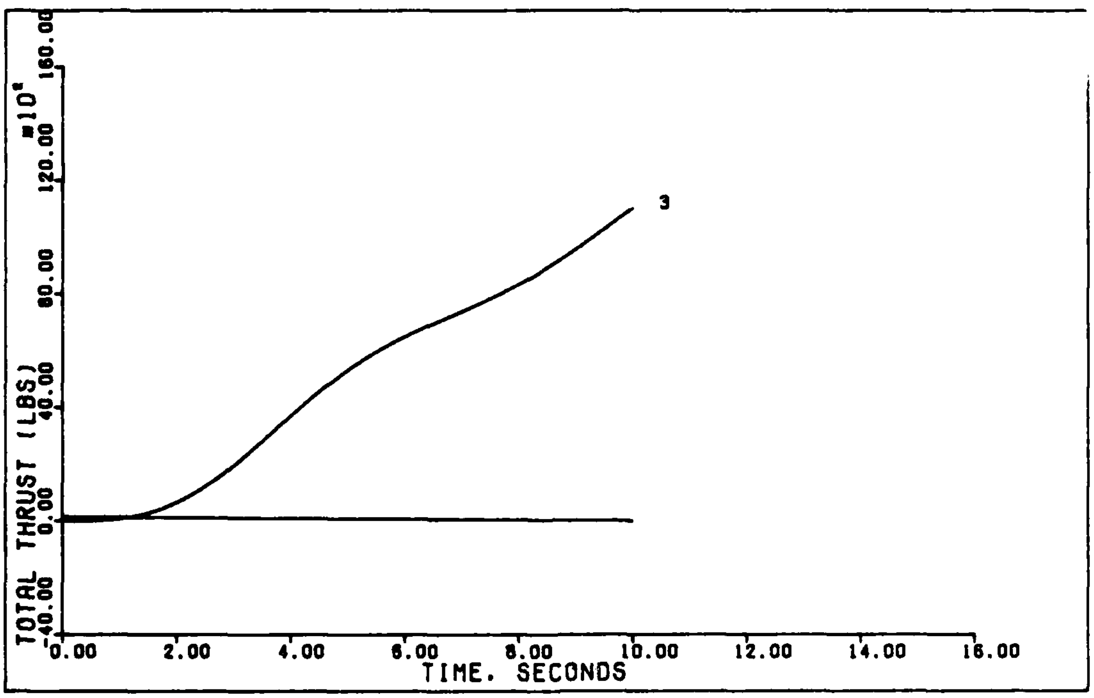

2.4 G DIRECT LIFT (U. D. ALPHA=4. 0.6 M)

Figure 83. 1.8 G Direct Lift With Delay, Universal Controller (0.6 Mach, 0 ft.)

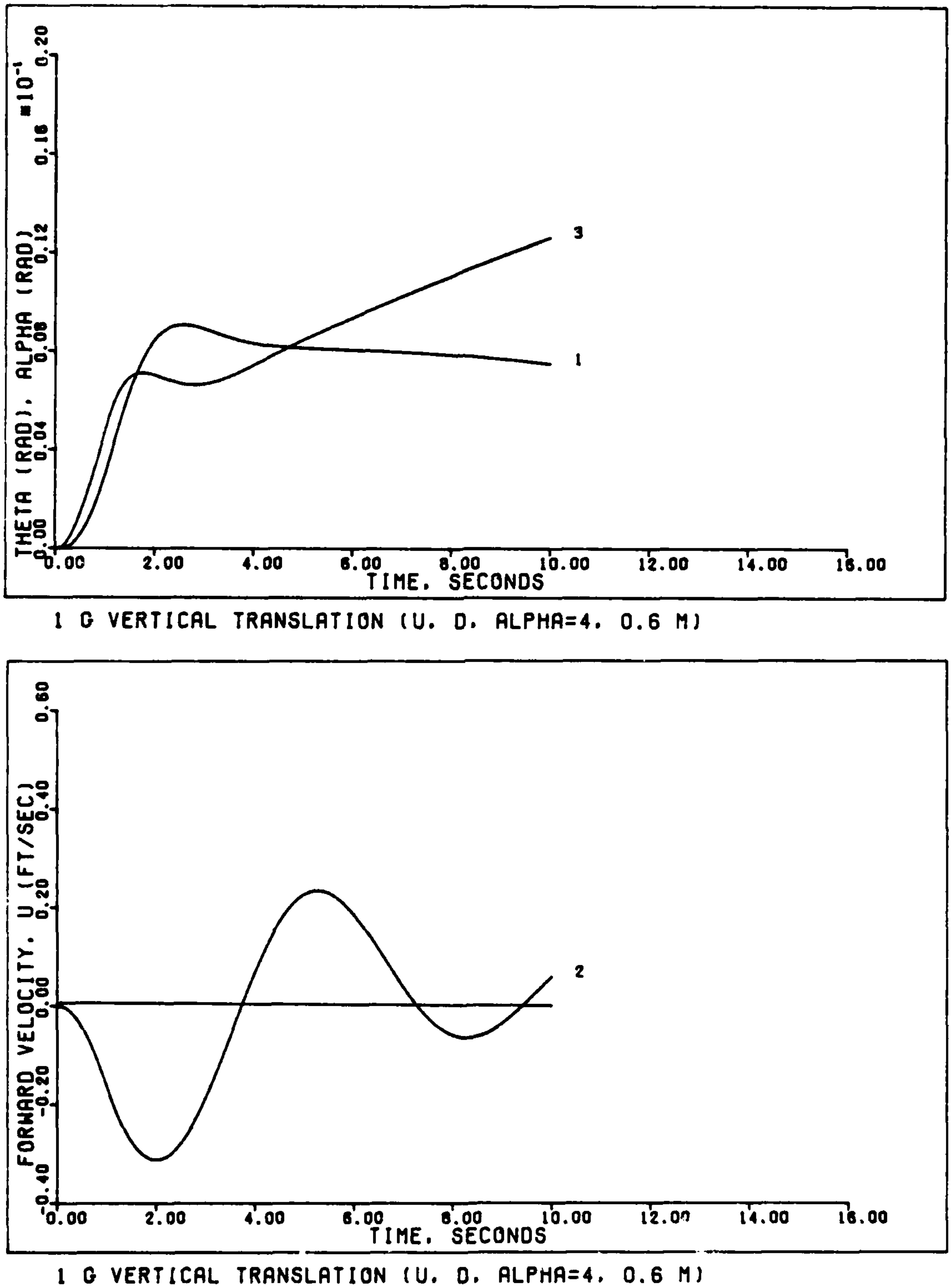

Figure 84. 0.8 G Vertical Translation With Delay, Universal Controller (0.6 Mach, 0 ft.)

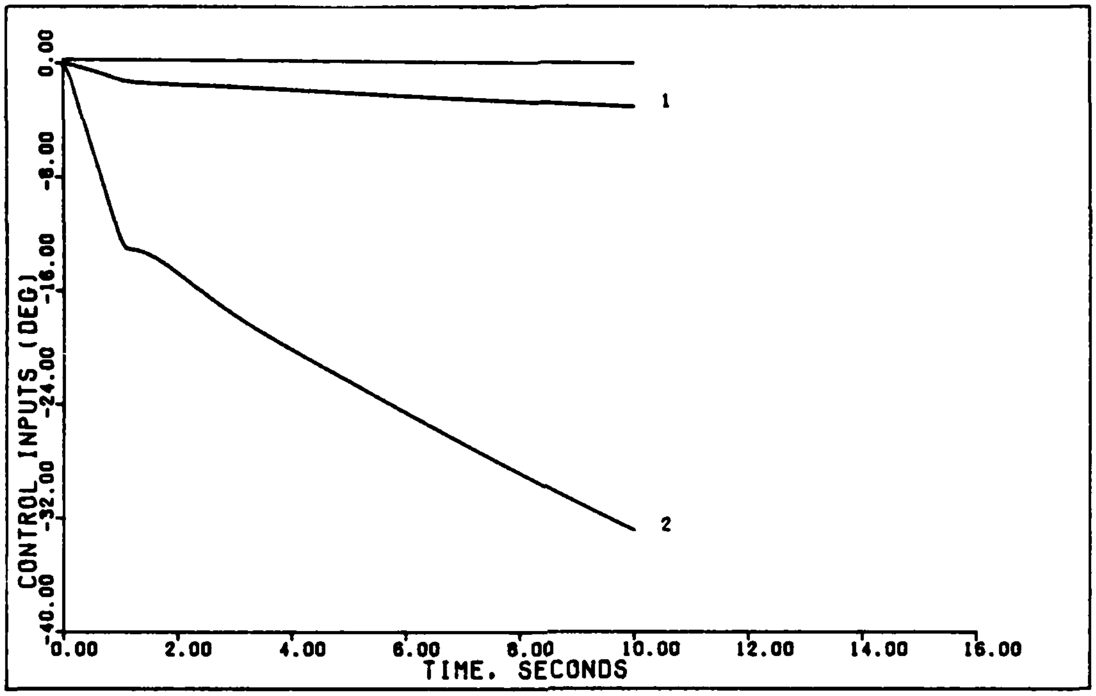

1 G VERTICAL TRANSLATION (U, D, ALPHA=4, 0.6 M)

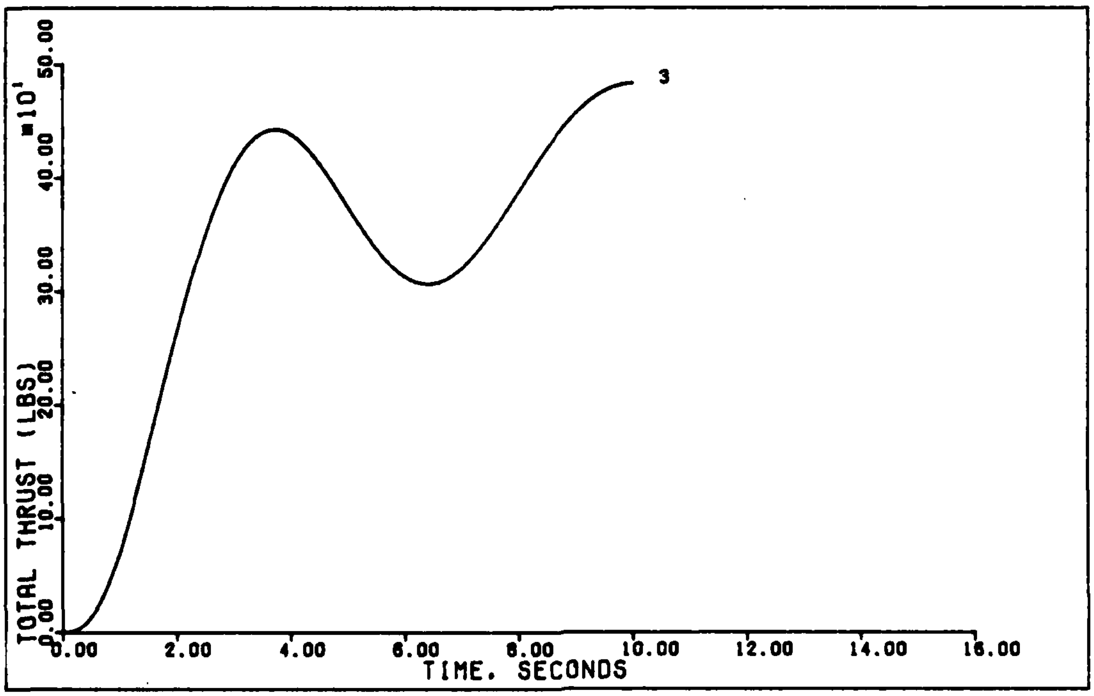

1 G VERTICAL TRANSLATION (U, D, ALPHA=4, 0.6 M)

Figure 85. 0.8 G Vertical Translation With Delay, Universal Controller (0.6 Mach, 0 ft.)

velocity shows increased damping but with about the same magnitude of deviation from zero. The control surface deflection for the horizontal canards hasn't changed much, while the jet flaps are not deflected as much. Total thrust requirements are reduced slightly.

From Figures 82 through 83 comparisons can be made with the undelayed responses (Figures 47 through 49) for the 1.8 g direct lift command. Once again, the responses have changed little with the introduction of the delay and subsequent compensation for the delay. The theta and alpha responses are practically identical, with only minor changes in the forward velocity response. As with the pitch pointing command, the canard deflection has not changed much, and the jet flaps are deflected less. The total thrust responses are very similar.

The final maneuver, the 0.8 g vertical translation (Figures 84 and 85), yields the most dissimilar results. The alpha response changes quickly after the first second, and after ten seconds is much less than for the undelayed response. The theta response shows more overshoot, but otherwise is very similar. Although the magnitude of the forward velocity response is about the same, the damping is much greater for the compensated delayed plot. Just as with the other maneuvers the canard deflection is basically unchanged while the jet flaps are deflected less. The thrust requirements are only slightly reduced.

<u>Conclusions</u>. Once again the overriding conclusion is that if the maneuver performs well without the delay, then the delay can be effectively compensated for by increasing the ratio of

proportional to integral control, whereas a maneuver's performance is not going to improve with the inclusion of the delay. As with other results from this thesis, the angle of attack response seems to be the limiting factor in trying to improve aircraft response. This is most evident in the pitch pointing maneuver where increasing the control ratio decreases the alpha response.

Minimizing Controller Matrices Elements

This section describes the efforts to reduce the number of elements needed in the controller matrices by finding common elements to be set equal to zero. If the same elements in either controller matix can be set to zero for all maneuvers at a given flight condition, then for that flight condition fewer memory locations need to be accessed, increasing computational speed. This is especially true in consideration of the fact that a memory access is one of the slowest microprocessor instructions. The greatest benefit would occur if the same elements could be eliminated for all flight conditions (or perhaps all common flight conditions). Unfortunately, the later case was not true for this thesis effort. The best results obtained were a reduction of two elements from the controller matrices for the longitudinal maneuvers at the 0.15 mach flight condition, and a reduction of one element for the lateral maneuvers at the same flight condition. This means that a combined controller for the 0.15 mach flight condition would need three fewer elements. For the other flight conditions no elements were found that could be set to zero for all of the maneuvers. In fact, for the 0.9 mach flight condition, there were no elements that could be set to zero for even two of the maneuvers (which was possible at 0.6 mach). Consequently, the following discussion covers only the controllers for the 0.15 mach flight condition.

Lateral Controller. For the lateral controller, the following matrix is used for the proportional and integral controller matices (which are the same). The zero element represents an element that could be removed from the algorithm used within the PI processor.

$$\underline{K}_{I} = \underline{K}_{0} = \begin{bmatrix} -.3823E-02 & .2993E+02 & 0 \\ .5047E-01 & .1904E+01 & -.1296E+02 \\ .2589E+00 & -.5821E+01 & .3962E+02 \end{bmatrix} \qquad (98)$$

Figures 86 through 87 show the responses of the aircraft to the 1.5 g horizontal translation command using the controller matrix from equation (98). Comparing these to the original responses to this command using the full controller matrices (Figures 5 through 6), yields some interesting observations. First, the side velocity response is almost exactly identical with the original and the yaw rate response has changed very little. However, the roll angle response has improved considerably. The control surface deflections show very similar characteristics also. This means that the maneuver actually improved by eliminating the element in the controller matrices.

From Figures 88 through 89 similar observations are made comparing the results of the reduced controller matrices responses to the 1 g flat turn to the original unmodified responses (Figures 7 through 8). The side velocity and yaw rate responses have changed very little while the roll angle

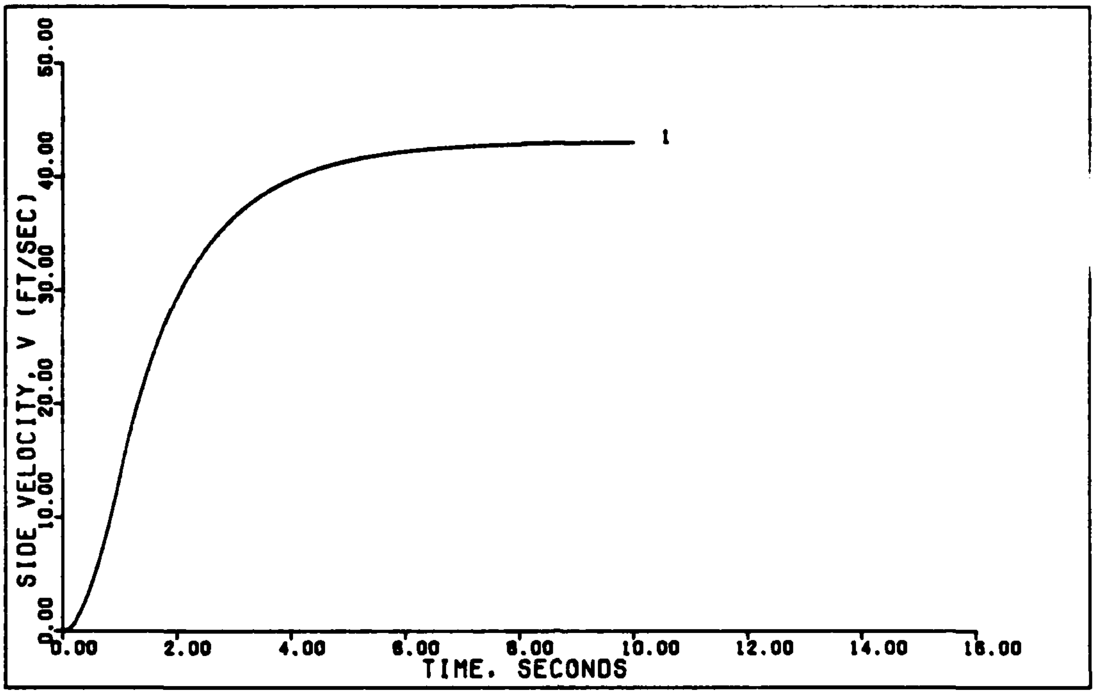

1.5 G HORIZONTAL TRANSLATION (Z. 0.15 MACH)

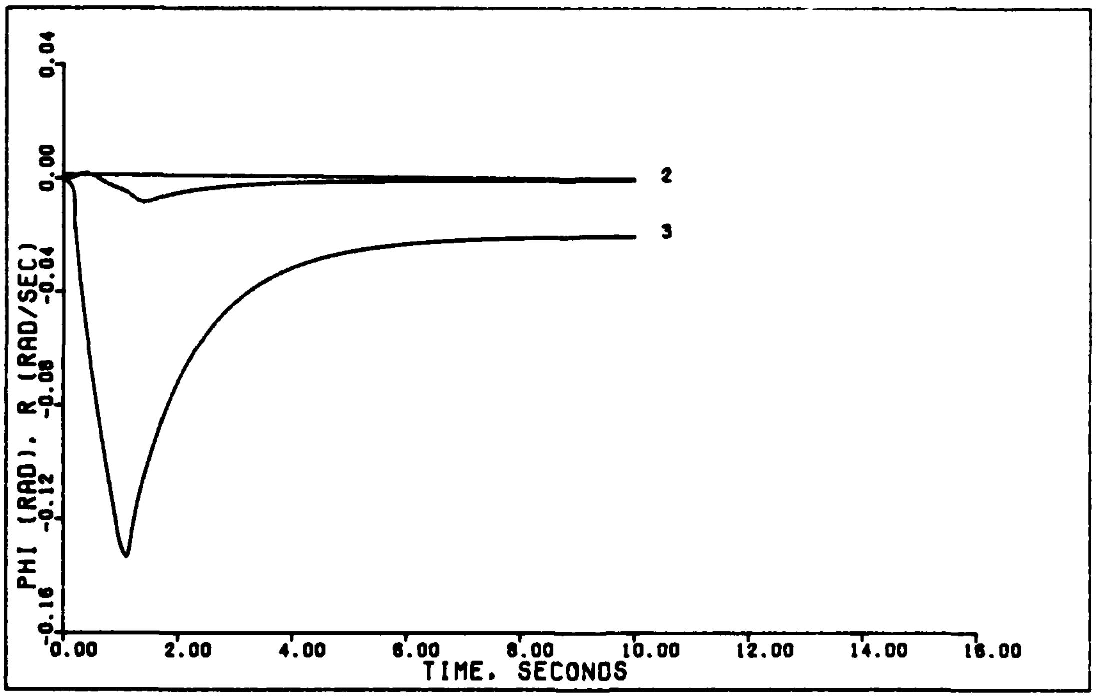

1.5 G HORIZONTAL TRANSLATION (0.15 MACH)

Figure 86. 1.5 G Horizontal Translation With Reduced Controller Matrices (0.15 Mach, 0 ft.)

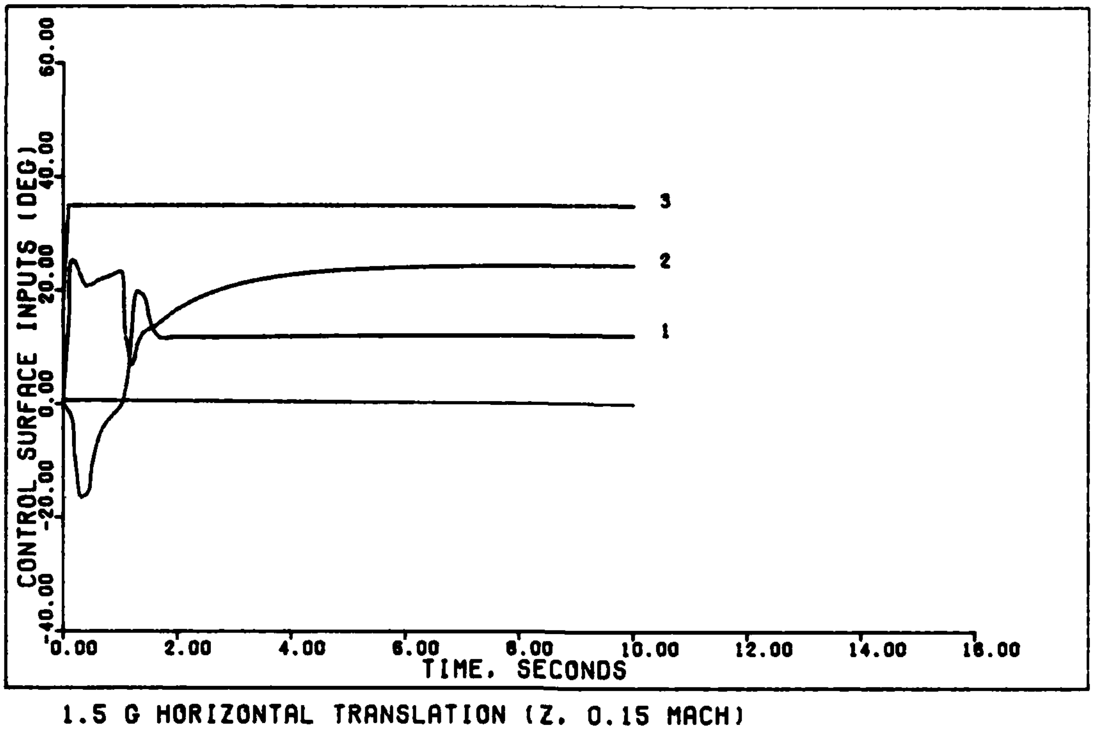

Figure 87. 1.5 G Horizontal Translation With Reduced Controller Matrices (0.15 Mach, 0 ft.)

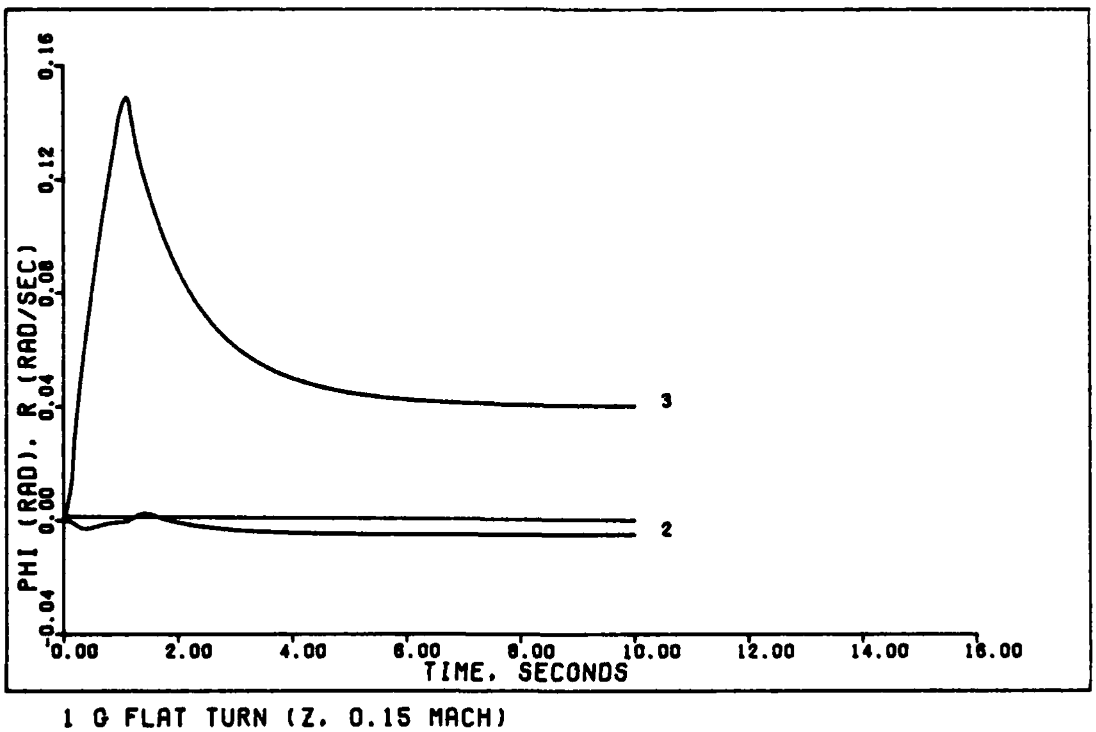

Figure 88. 1 G Flat Turn With Reduced Controller Matrices (0.15 Mach, 0 ft.)

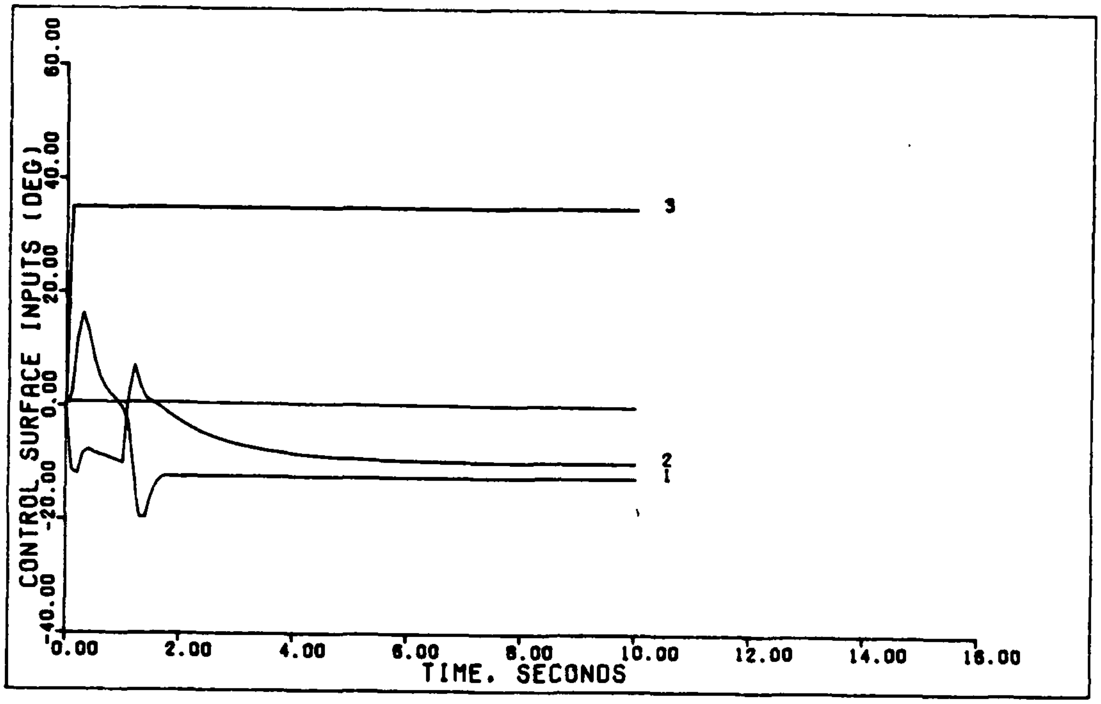

1 G FLAT TURN (Z, 0.15 MACH)

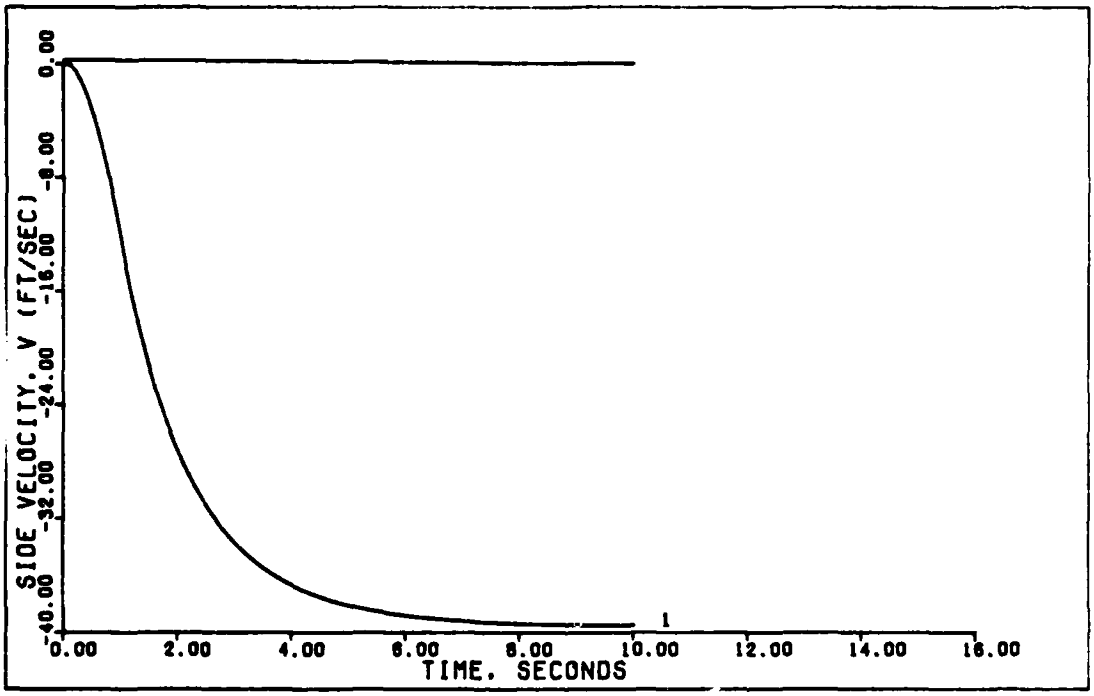

1 G FLAT TURN (Z, 0.15 MACH)

Figure 89. 1 G Flat Turn With Reduced Controller Matrices (0.15 Mach, 0 ft.)

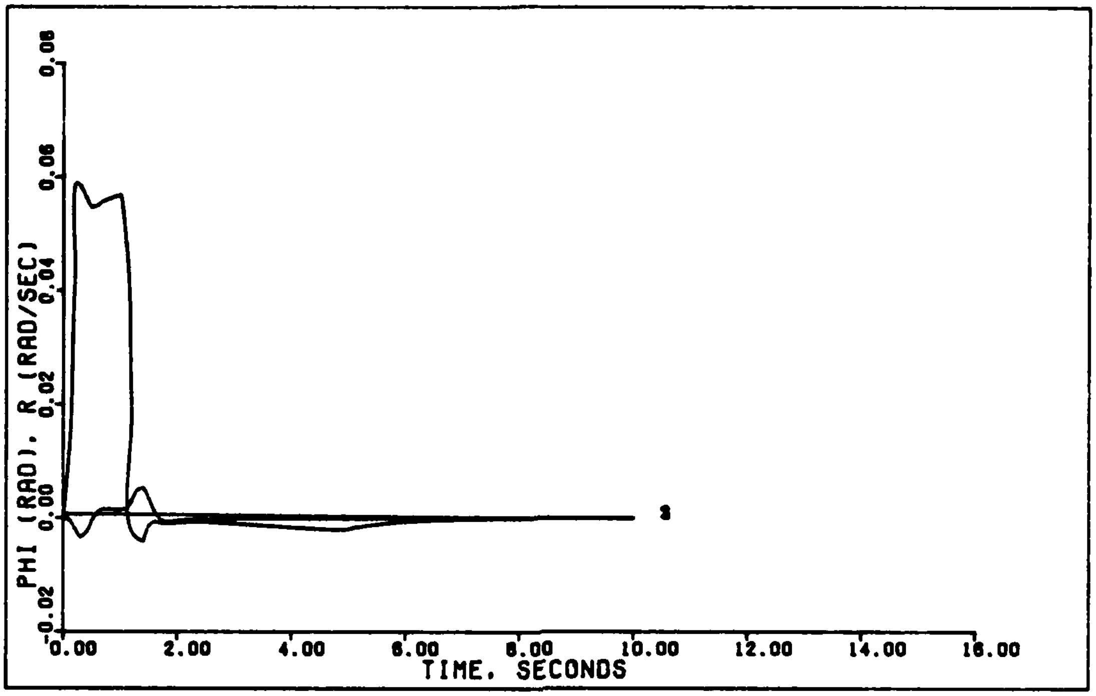

3 DEGREE YAW POINTING (Z, 0.15 MACH)

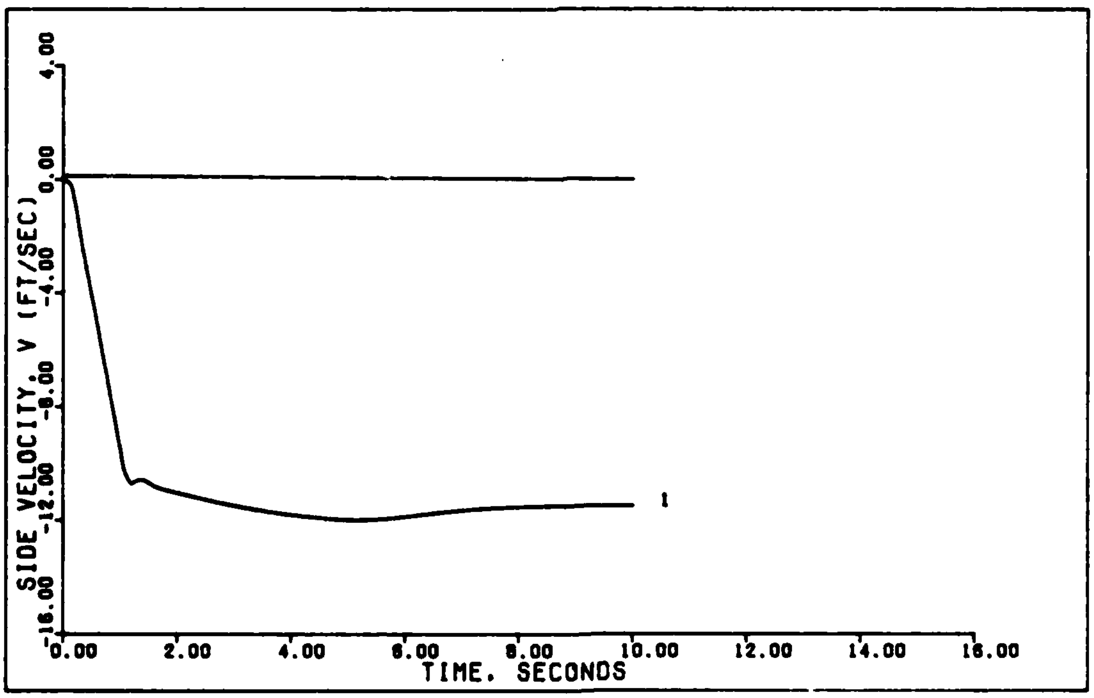

3 DEGREE YAW POINTING (Z, 0.15 MACH)

Figure 90. 3 Degree Yaw Pointing With Reduced Controller Matrices (0.15 Mach, 0 ft.)

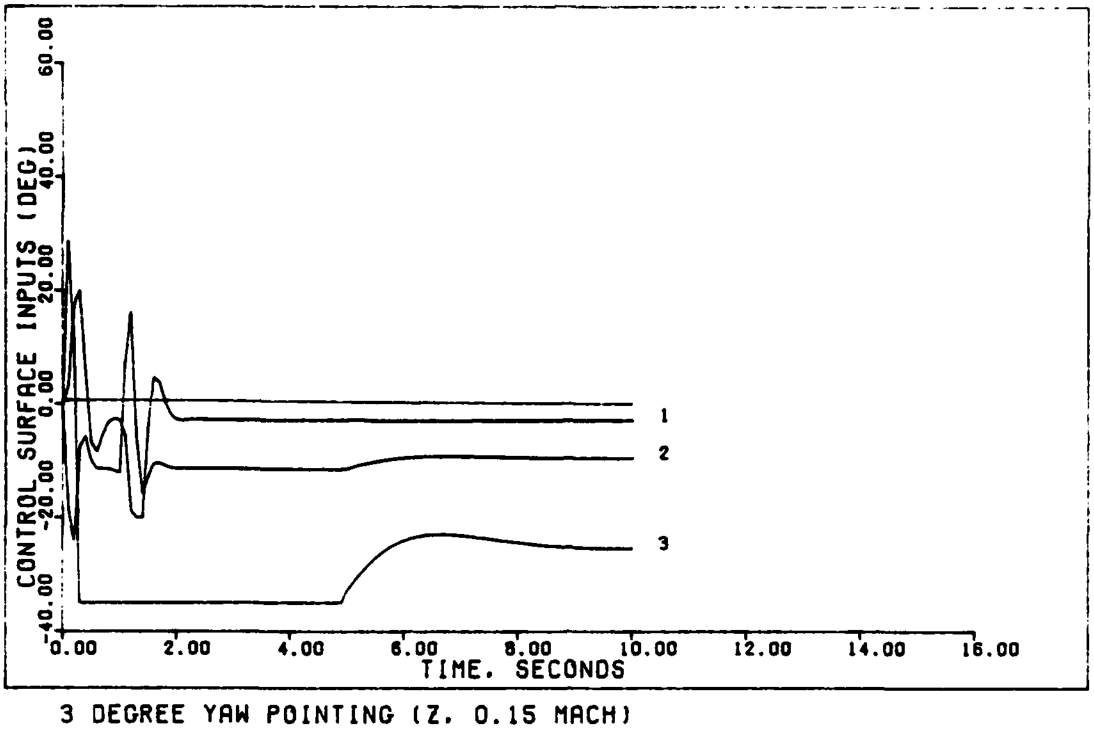

Figure 91. 3 Degree Yaw Pointing With Reduced Controller Matrices (0.15 Mach, 0 ft.)

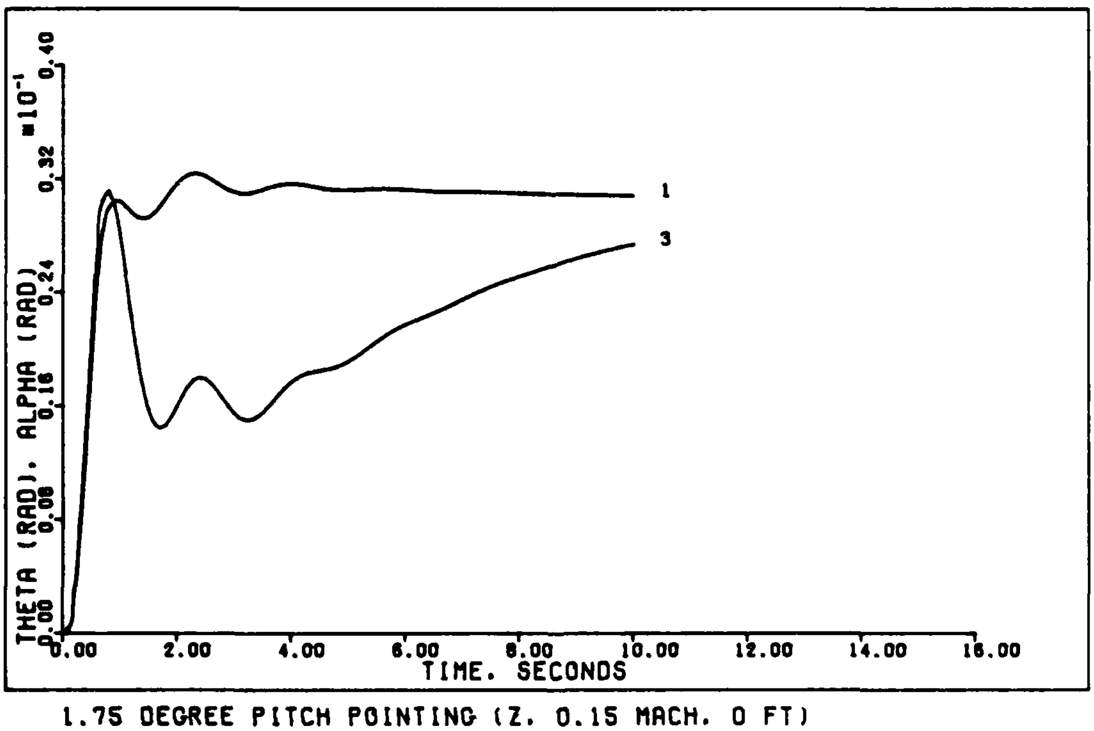

Figure 92. 1.75 Degree Pitch Pointing With Reduced Controller Matrices (0.15 Mach, 0 ft.)

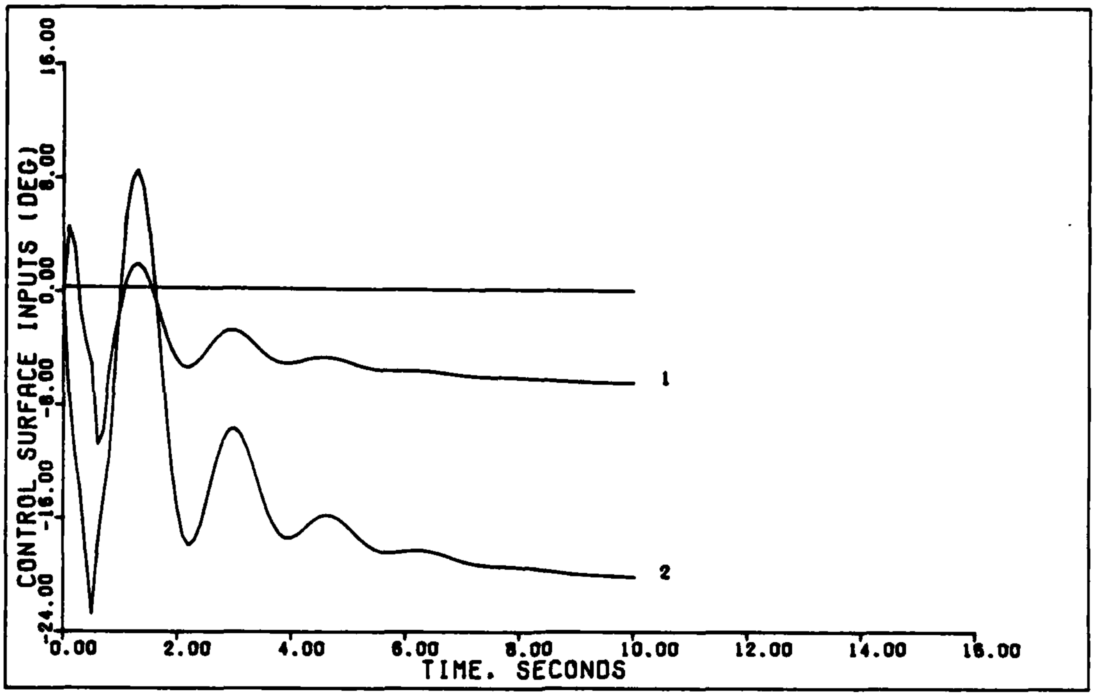

1.75 DEGREE PITCH POINTING (Z, 0.15 MACH)

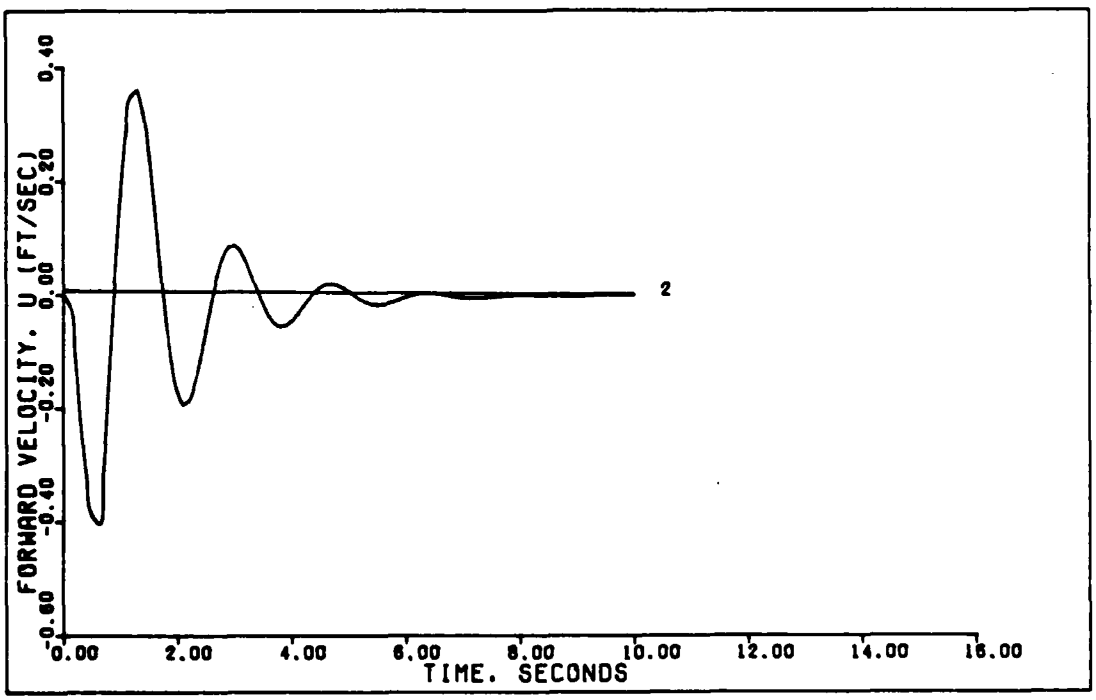

1.75 DEGREE PITCH POINTING (Z, 0.15 MACH)

Figure 93. 1.75 Degree Pitch Pointing With Reduced Controller Matrices (0.15 Mach, 0 f~)

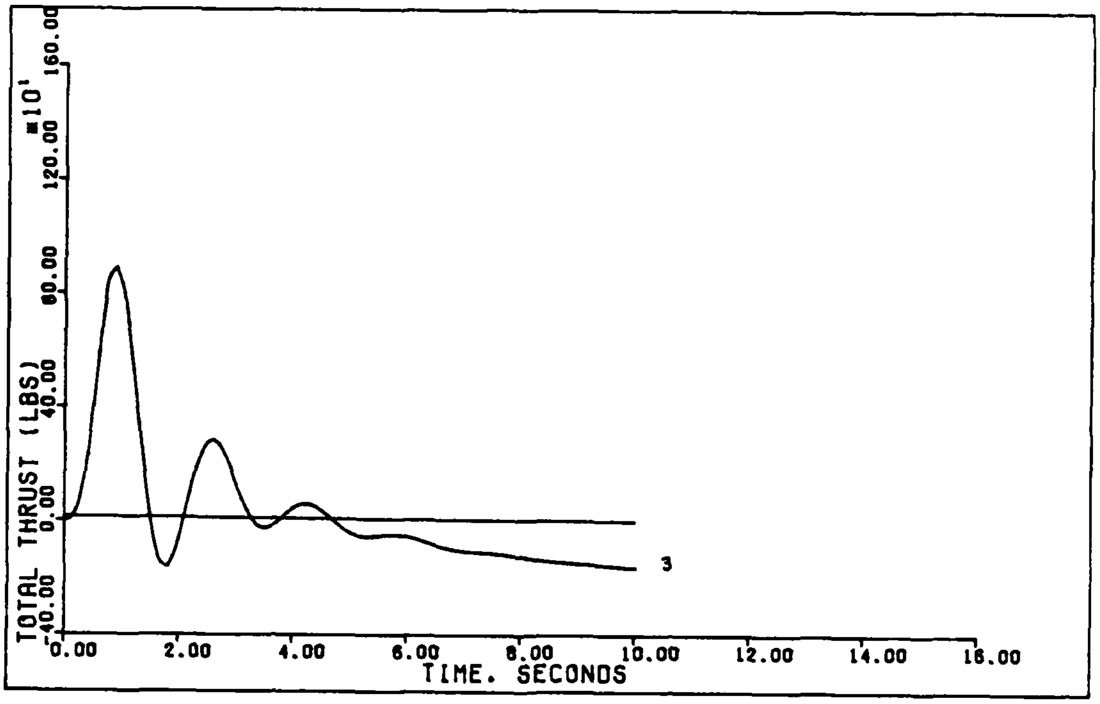

1.75 DEGREE PITCH POINTING (Z, 0.15 MACH)

Figure 94. 1.75 Degree Pitch Pointing With Reduced Controller Matrices (0.15 Mach, 0 ft.)

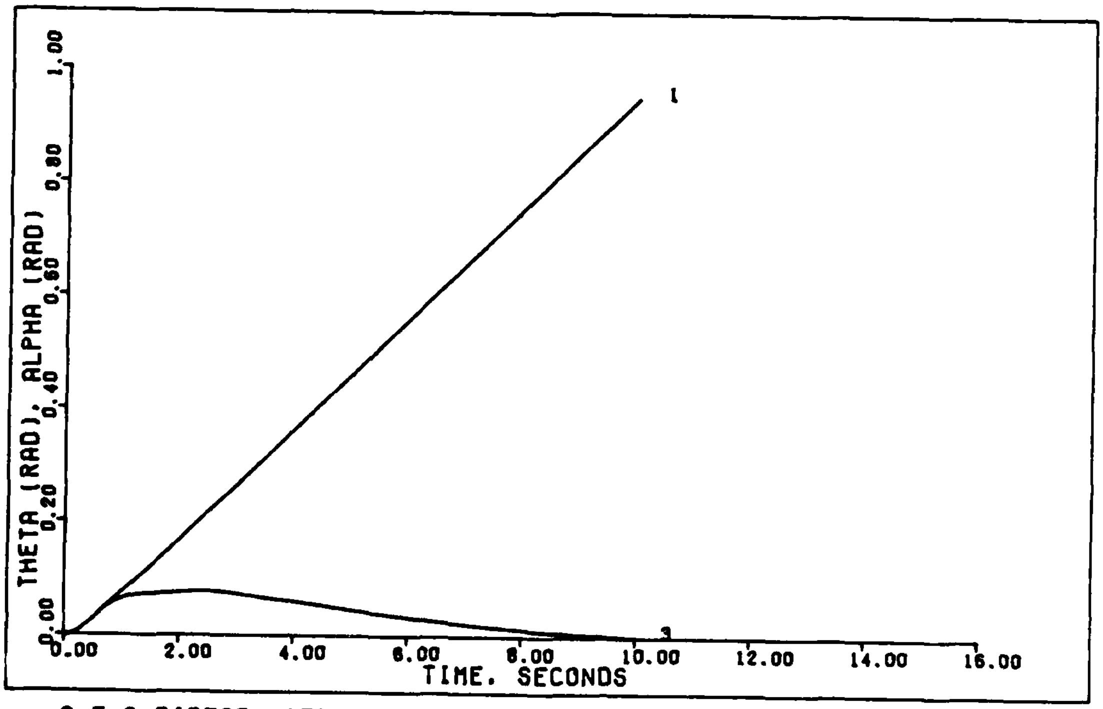

0.5 G DIRECT LIFT (Z, 0.15 MACH)

Figure 95. 0.5 G Direct Lift With Reduced Controller Matrices (0.15 Mach, 0 ft.)

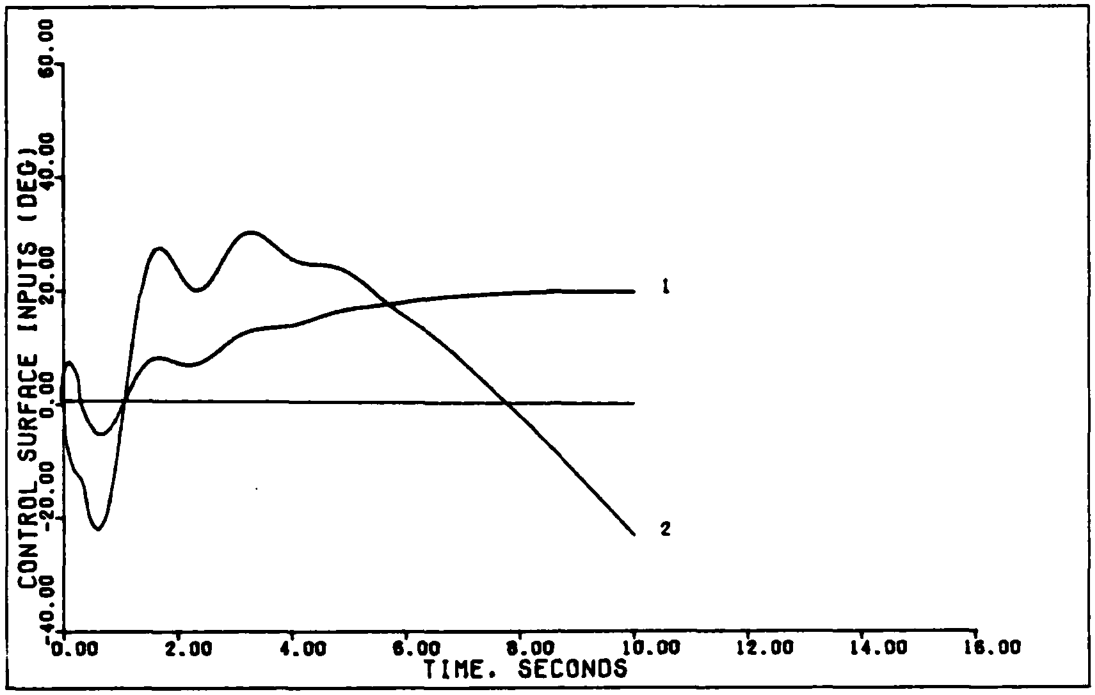

0.5 G DIRECT LIFT (Z, 0.15 MACH)

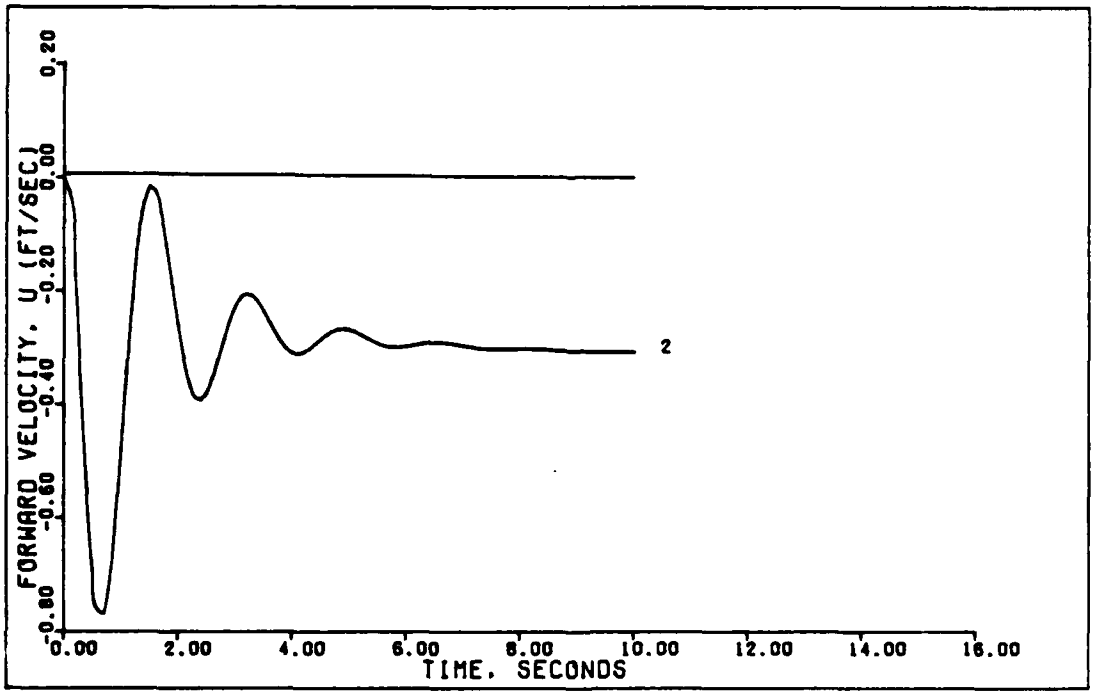

0.5 G DIRECT LIFT (Z, 0.15 MACH)

Figure 96. 0.5 G Direct Lift With Reduced Controller Matrices (0.15 Mach, 0 ft.)

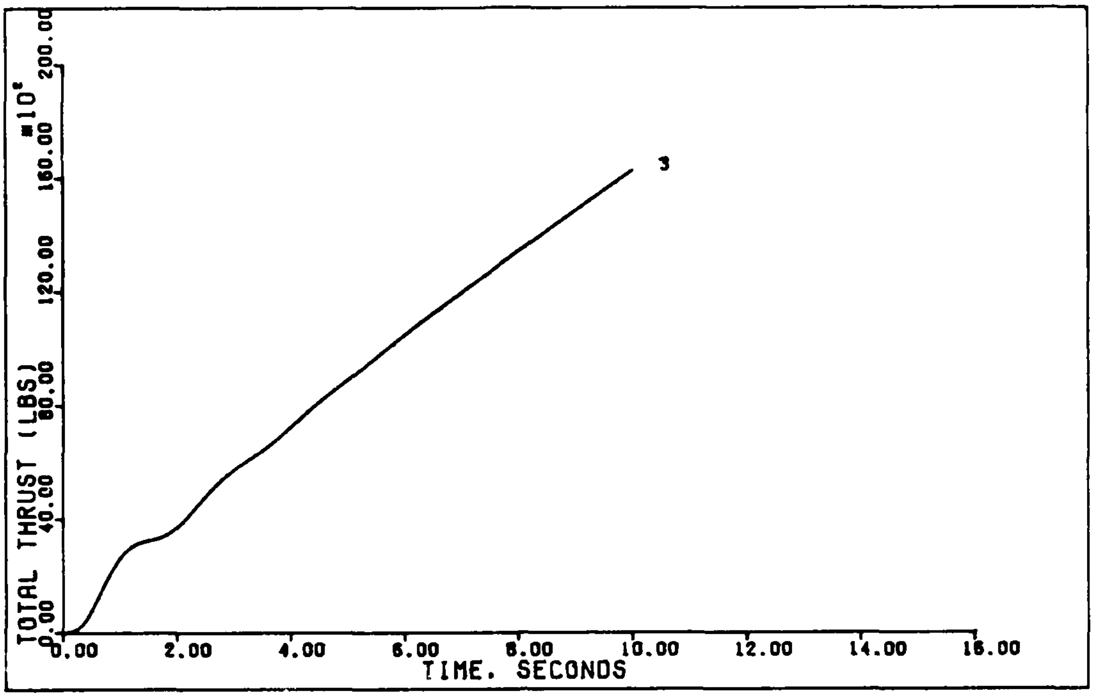

0.5 G DIRECT LIFT (Z, 0.15 MACH)

Figure 97. 0.5 G Direct Lift With Reduced Controller Matrices (0.15 Mach, 0 ft.)

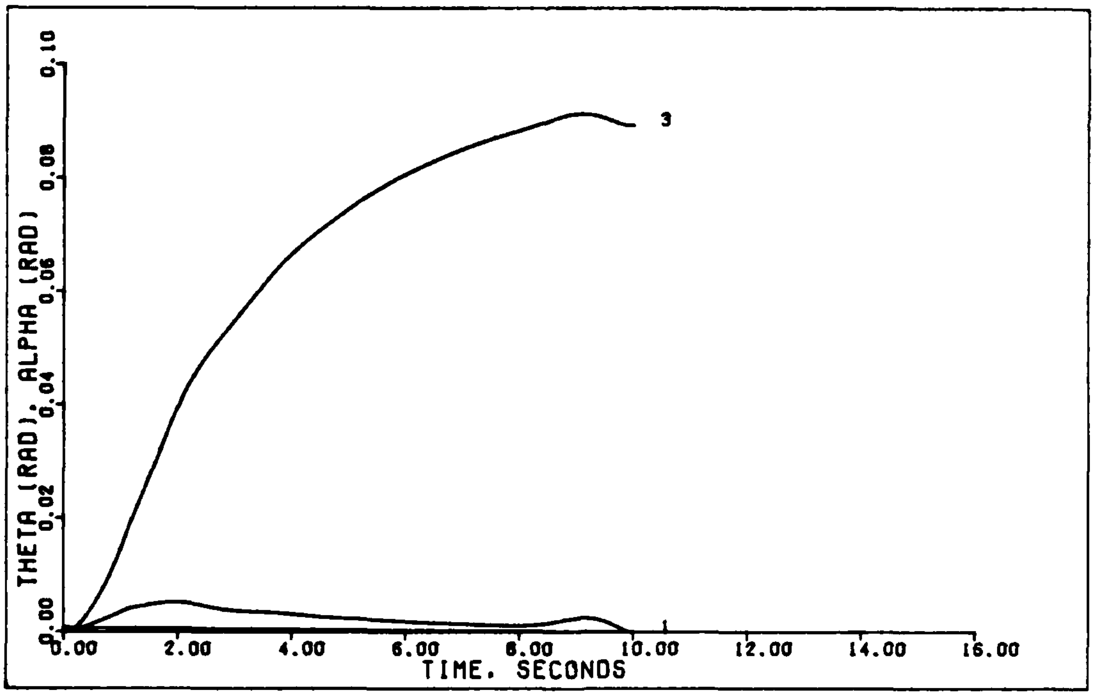

0.5 G VERTICAL TRANSLATION (Z, 0.15 MACH)

Figure 98. 0.5 G Vertical Translation With Reduced Controller Matrices (0.15 Mach, 0 ft.)

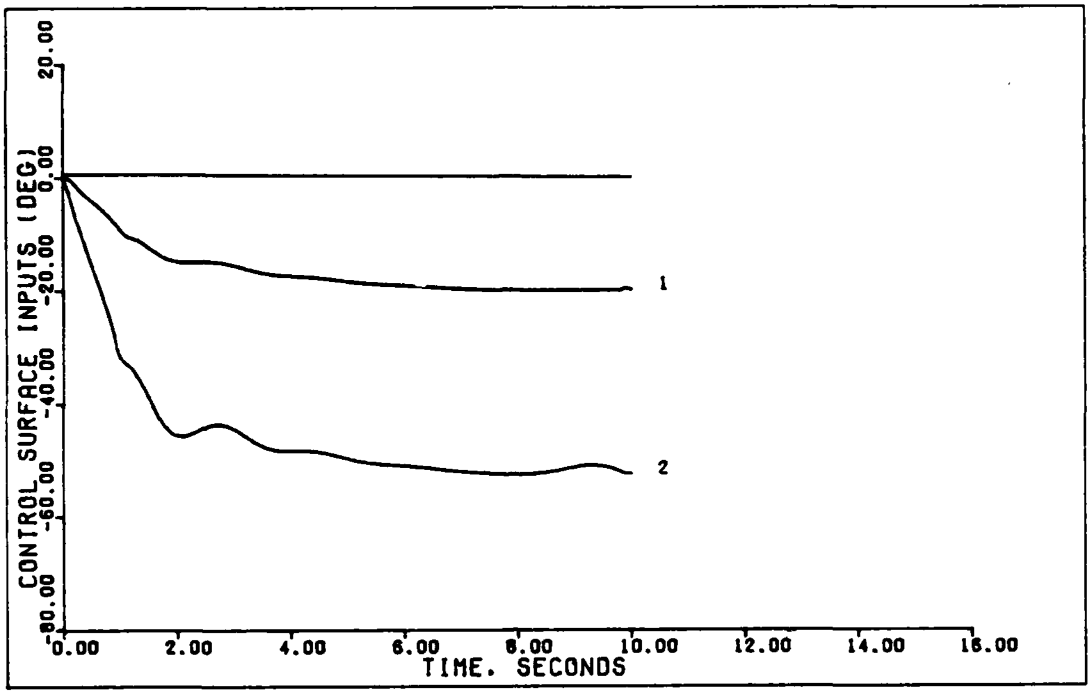

0.5 G VERTICAL TRANSLATION (Z, 0.15 MACH)

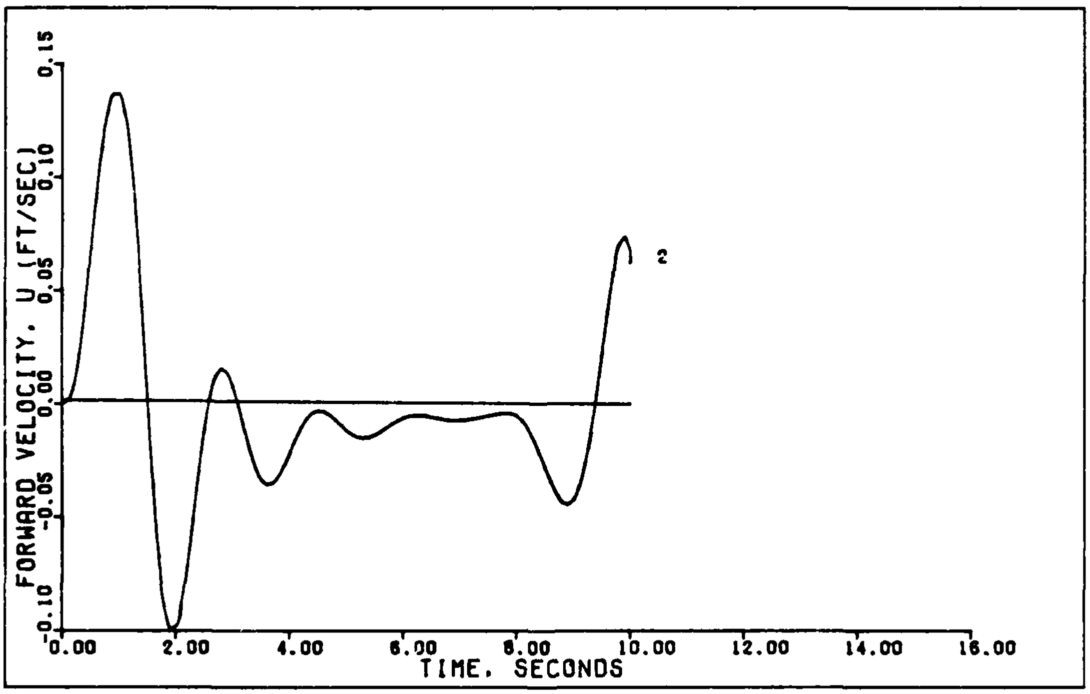

0.5 G VERTICAL TRANSLATION (Z, 0.15 MACH)

Figure 99. 0.5 G Vertical Translation With Reduced Controller Matrices (0.15 Mach, 0 ft.)

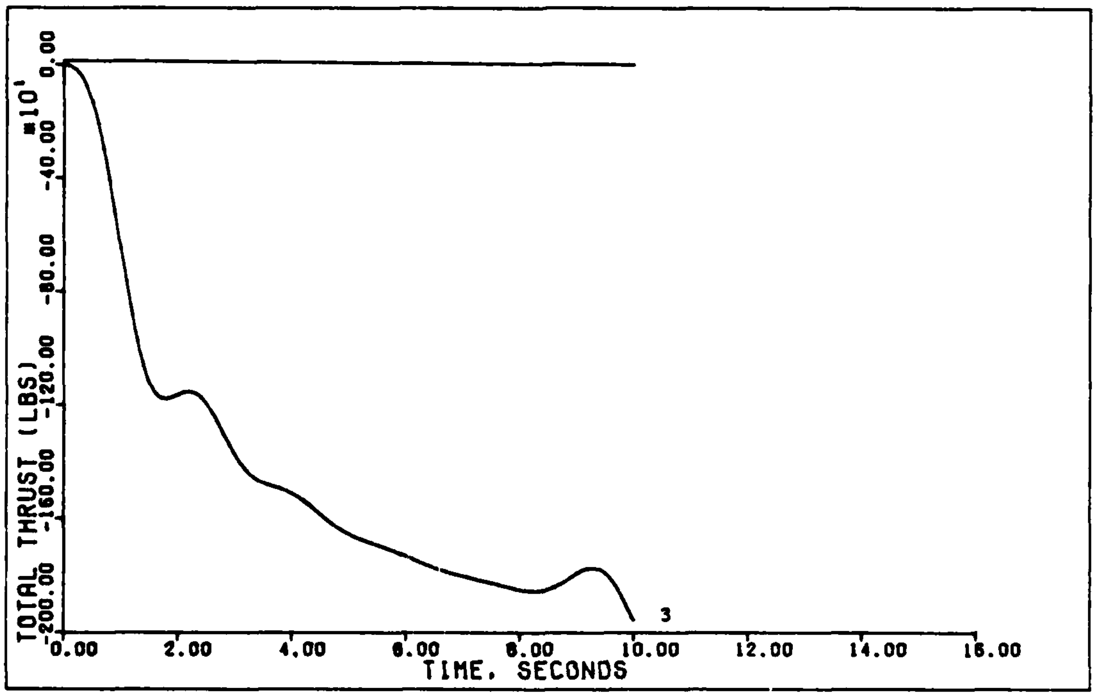

0.5 G VERTICAL TRANSLATION (Z, 0.15 MACH)

Figure 100. 0.5 G Vertical Translation With Reduced Controller Matrices (0.15 Mach, 0 ft.)

response has been improved quite dramatically. Once again the control surface deflections have not changed except for their transient response. This maneuver has also been improved merely by introducing a zero element in the controller matrices.

For the final maneuver, the 3 degree yaw pointing, Figures 90 through 91 show that very little changes have occured in any of the responses when compared with the original unmodified curves (Figures 9 through 11). In fact, the roll angle response has degraded just slightly.

Since the element set to zero would contribute to the aileron deflection depending on the error in yaw rate, then the aileron deflection would be based more upon roll angle error. This should reduce the roll angle error since roll angle is mainly governed by aileron deflection. The above results certainly seem a logical extension of this analysis. Unfortunately, this author found no apriori method of predicting which elements of the controller matrices could be set to zero based upon this type of analysis.

Longitudinal Controller. The following shows which elements of the controller matrices have been set to zero. Zero elements can be removed from the algorithm that is used within the PI controller to calculate the control inputs to the actuators.

$$\underline{K}_o = \begin{bmatrix} .1686E+02 & 0 & 0 \\ -.1852E+02 & -.5640E+00 & -.5098E+01 \\ .4280E+03 & .8979E+02 & -.1000E+03 \end{bmatrix} \tag{99}$$

$$\underline{K}_I = \underline{K}_o/2$$

Figures 92 through 94 show the responses of the reduced element controller to the 1.75 degree pitch pointing command. Comparing these results with the original responses with no modifications (Figures 12 through 14), a couple of observations are possible. The most striking is that although the responses of theta, alpha, forward velocity, and control surface deflections are almost identical with the original plots, the total thrust is not. In fact, with the introduction of the two zero elements, the maximum required thrust has been reduced by about a factor of four. Why this would be with no apparent changes in any of the other responses seems to have no obvious logical explanation.

Figures 95 through 97 show the responses for the reduced element controller to the 0.5 g direct lift command. Comparing these to the responses for the original unmodified controller (Figures 15 through 17), some observations can be made. Once again the theta and alpha response are essentially unchanged, but now the forward velocity shows a surprising change. Whereas with the original responses the velocity response seemed unstable after about six seconds, now the velocity response shows no such instability. There seems to be no obvious logical reason for this. The control surface deflections seem to have changed very little, but close inspection of the curves from Figure 96 shows that they also differ from the original curves after about six seconds. The most obvious difference is the thrust response, which has a marked lack of the oscillatory and possible unstable response of the original response. This maneuver has definitely been improved in the steady-state response by introducing the two zeros.

Figures 98 through 100 show that the instabilities present in the original responses to the 0.5 g vertical translation command (Figures 18 through 20) have not disappeared with the two zero elements in the controller matrices. The theta, alpha, and forward velocity responses haven't changed very much, although the velocity response shows slightly smaller peak values. The control surface deflections show little change, but the thrust response has changed significantly. Unfortunately, this maneuver shows no signs of improved response with the two zero elements, although there appears to be no degradation of the responses.

The two zero elements reduce the contributions to the horizontal canard deflection to just the pitch angle error. Following the train of thought from the lateral case, it would be expected that if anything would be improved it would be the theta response, and yet this did not happen. However, the one zero that corresponds to velocity error contributions to canard deflections is an obvious candidate for elimination. But the other zero, the angle of attack error effect on canard deflection is not such an obvious choice. Also, other seemingly obvious choices for zero elements did not work out.

Conclusions. Even though there seems to be no apriori way to pick the zero elements in the controller matrices, the possible choices will always be finite and can be tested using intelligent software. The expected benefits from doing this include possibly improved responses and the reductions of memory accesses needed in the controller algorithm. These factors would definitely recommend this technique for "polishing" the design.

CHAPTER VI

RESULTS, CONCLUSIONS, AND RECOMMENDATIONS

Introduction

This thesis incorporates Professor Porter's multivariable design method into the design of flight controllers for three flight conditions for the FPCC aircraft. The first flight condition represents a possible STOL-like operation, while the other two are more representative of normal operation and were also studied by Jon Bauschlicher in a previous thesis (Ref 2). One of the purposes of this thesis was to design longitudinal controllers for these two flight conditions using a different longitudinal model than Bauschlicher so as to make comparisons.

For the first flight condition, 0.15 mach at sea level, a complete controller is designed by decoupling the aircraft model into a longitudinal and a lateral model. The other two flight conditions, 0.6 mach at sea level, and 0.9 mach at 30,000 ft., are decoupled into a lateral and longitudinal model, but only the longitudinal design is accomplished because Bauschlicher had already designed controllers for the lateral model. An attempt to find a "universal" controller capable of performing all the maneuvers for all of the flight conditions failed, but the controller for the 0.9 mach flight condition is found to yield marginal results at the 0.6 mach flight condition.

A digital implementation of the PI controller would introduce a delay in the output of the controller, and the effects of this delay are studied for all of the maneuvers at all of the flight conditions. Finally, an attempt to find common elements of the controller matrices that can be eliminated is partially successful.

Additionally, the design tool MULTI, a program based upon Professor Porter's design method and capable of simulating aircraft response to commanded maneuvers, is upgraded with two more options added.

Results

Figures 5 through 11 show the time responses for the outputs and the flight control surface deflections for the 0.15 mach flight condition lateral controller. The figures of merit and the commanded inputs for each maneuver are listed in Table VII. One controller was used for all of the maneuvers yielding results that were not much different than if an optimum controller had been used for each maneuver. Of the three maneuvers, the yaw pointing showed the best results, with the horizontal translation fairly acceptable. The flat turn responses would have to be considered unacceptable.

Figures 12 through 20 show the time responses for the outputs and surface deflections for the three longitudinal maneuvers at 0.15 mach, sea level. Table VIII shows the figures of merit and commanded inputs for the maneuvers. Once again one controller was found for all three maneuvers, and once again the results are mixed. The pitch pointing maneuver is classified fair, with the direct lift considered very good. But the vertical translation would have to be termed poor.

Figures 21 through 39 show the same curves for the other two flight conditions, 0.6 mach at sea level, and 0.9 mach at 30,000 feet. Table VIII also lists the figures of merit and commanded inputs for these longitudinal maneuvers. At 0.6 mach, the direct lift maneuver shows the best results, which would have to considered very good. But the pitch pointing maneuver would be called poor, at best, and the vertical translation is certainly unacceptable. At 0.9 mach the results are about the same, with the direct lift showing very good results but the vertical translation and pitch pointing showing unacceptable results.

The general conclusion regarding the comparison with Bauschlicher's results is that the longitudinal model used in this thesis did not perform nearly as well as the one Bauschlicher used.

An attempt to find a universal controller failed, and the attempt to find a longitudinal controller that would work for two of the three flight conditions yielded marginal results. Figures 44 through 52 show the responses for the 0.6 mach flight condition using the 0.9 mach controller. The direct lift showed very good results, but the other two would have to be considered very poor. Table IX summarizes the results.

All of the longitudinal maneuvers for all three flight conditions were repeated with a one sampling period time delay added to the output of the PI controller. Figures 53 through 61 show these results for the 0.15 mach flight condition. As can be seen from all of the maneuvers, the addition of the delay introduces instability into the responses.

Figures 62 through 73 show the effects of delay on the longitudinal maneuvers for the 0.6 mach flight condition both with and without compensation. The compensation is an increase in the ratio of proportional to integral control within the PI controller. The uncompensated curves show quite dramatically the unstabilizing effect of the delay. From the compensated plots the conclusion is that the delay can be effectively cancelled out.

From Figures 74 through 79 the conclusion is that the delay can also be compensated for in the longitudinal maneuvers at the 0.9 mach flight condition. Table X summarizes these results for all of the longitudinal maneuvers at the three flight conditions.

Extending this testing to the semi-universal controller yields the results shown in Figures 80 through 85. Once again the conclusion is that the increase of the proportional to integral control ratio effectively compensates for the addition of the delay. Table XI summarizes these results.

The final testing performed is an attempt to reduce the number of gains needed in the controller matrices. Unfortunately, there were no common gains found that could be eliminated from all of the controller matrices for all three flight conditions. In fact, there were no gains that could be eliminated from the matrices for all three maneuvers at either the 0.6 or 0.9 mach flight condition. There were gains that could be removed from both the longitudinal and lateral controllers for the 0.15 mach flight condition. Figures 86 through 100 show that these reduced gain controllers show no degradation in response and even sometimes improve the response.

Conclusions

Summarizing the above results, the conclusions drawn are these:

1. Removing the maneuver flaps from the longitudinal model definitely degrades the responses to the commanded maneuvers.

2. Adding a delay to the output of the PI controller adds instability to the responses.

3. The effects of the delay can be effectively compensated for by increasing the ratio of proportional to integral control.

4. Setting certain elements of the controller matrices to zero can yield improved responses.

In addition to these conclusions, there are two important results worth summarizing:

1. A universal controller that yielded acceptable results compared to the individual controller responses was not found.

2. The aircraft responses were typically limited by the angle of attack response.

Recommendations

This section describes the recommendations this author has for future efforts involving both the design method and the design tool MULTI.

Design Method. The following is a list of the suggested areas for future work on the Porter method of controller design:

1. Investigate the transformation from the analog to the discete PI controller more closely. The current equations for the discete controller implement the integration via a first order rectangular integration approximation. Perhaps reworking these equations to yield more accurate integration approximations would be valuable.

2. More information about the relationship between the transmission zeros and the types of expected results is needed. Although Professor Porter's theory implies that the regular design should not have any limitations in the responses due to the transmission zeros, this author found that in general an irregular design yielded better results. If irregular designs are (and so far they do seem to be) going to be more prevelant in flight control design, then insight into how transmission zeros affect responses would certainly be helpful. An example of the type of questions that could be answered is: How do transmission zeros in the right half plane or at the origin affect controller design and expected responses?

3. Since irregular designs have been the most prevelant to date, most of the design work has centered around the use of angles instead of rates as outputs. This author feels more designs incorporating rates (and therefore typically regular designs) should be attempted. Reasons for this suggestion include the two considerations that current pilot controls command rates, and that regular designs have no inherent limitation upon the output responses due to the slow modes (as do irregular designs). Another factor is that for an initial aircraft attitude that is not straight and level, the use of angles is unappropriate.

<u>Design Tool, MULTI</u>. The following is a list of suggestions for improvements to the design tool MULTI:

1. In conjuction with the suggestion for improving the integration approximation in the design method, implement an improved integration routine within the simulation in MULTI.

Appendix B lists the program code for one such improvement.

2. Consideration should be given to implementing the exact discrete differential equations instead of using the current analog integration approximations, accomplished with the system library ODE (ordinary differential equation solver). This would not be a formidable task because the system marices are all time invariant (constant coefficients). Students receive the background necessary for this type of implementation in courses such as EE 7.12 and EE 6.44. If the simulation were written in this fashion and then segmented as a separate overlay it would be useful as a general purpose discrete simulation of analog systems.

3. The calculation of actuator (or control input) rates should be added to Option #28 in MULTI, along with a toggle switch that the user can use to specify either modified spline or linear curve fitting on the CALCOMP plots. These two features used together would allow the user to decide when to use linear curve fitting based on curve slopes. The program code to implement these two features is included in Appendix C.

4. MULTI needs to be completely rewritten in a language that has both dynamic memory allocation and more structure than FORTRAN. The dynamic memory allocation should allow for larger numbers of states, in addition to being more efficient in general. Using a language that causes program code to have more structure should help prevent what has happened to the current version of MULTI, which is a proliferation of GO TO statements. Because of this unstructured nature of FORTRAN, MULTI has evolved

into a program that is very hard to understand and maintain.

5. The addition of sensors and actuators to MULTI (Options #4 and #5) has caused severe problems. Some of these problems were corrected by this author, but a couple still remain. A quick summary of the known remaining problems are (all are within the simulation):

a. Formation of the $\underline{y}$ measurement vector YM is no longer correct and should be eliminated.

b. The use of YM to form the error vector E is also no longer correct and the YM should be replaced with Q, which is the output vector incorporating sensors (if present). This is currently causing erroneous data for a regular design that includes sensors.

c. The call to subroutine YOUT results in the actual values of the outputs to be plotted instead of the sensed values if there are sensors. However, this is not clear to either the programmer or the user. Addtionally, this means that there is no current way to plot the sensed values of the outputs. Something should be done, even if it is just improved documentation of the program code.

6. MULTI should be changed to allow the user to specify both the number and placement of the columns in the $\underline{M}$ matrix. This would permit the designer to chose which state derivatives should be measured (or estimated). Additionally, the provision for an $\underline{M}$ matrix should be added to the options for a regular design.

BIBLIOGRAPHY

1. Porter, B. Design of High-Performance Tracking Systems. USAME/DC/120/81. Air Force Flight Dynamics Laboratory, Wright-Patterson AFB OH, November 1981.

2. Bauschlicher, J. M. Design of a Complete Multivariable Digital Flight Control System. Master Thesis, Air Force Institute of Technology, Wright-Patterson AFB OH, December 1982.

3. Smyth, J. Digital Flight Control System Design Using Singular Perturbation Methods. Master Thesis, Air Force Institute of Technology, Wright-Patterson AFB OH, December 1981.

4. Heimbold, R. L., et al. Flight Propulsion Control Coupling (FPCC) and Dynamic Interaction Investigation, Volume I. AFFDL-TR-75-153, Air Force Flight Dynamics Laboratory, Wright-Patterson AFB OH, September 1975.

5. Houtz, J. E. FPCC Linear Analysis Digital Computer Program. AFFDL/FGL-TM-82-FGL, Air Force Flight Dynamics Laboratory, Wright-Patterson AFB OH, November 1977.

6. D'Azzo, J., Professor of Electrical Engineering. Lecture materials distributed in EE 7.08, Advanced Multivariable Control. School of Engineering, Air Force Institute of Technology. Wright-Patterson AFB OH, 1983.

7. Porter, D. Design and Analysis of a Multivariable, Digital Controller for the A-7D Digital II Aircraft and the Development of an Interactive Computer Design Program. Master Thesis, Air Force Institute of Technology, Wright-Patterson AFB OH, December 1981.

8. Porter, B. "Design of Error-Actuated Controllers for Unknown Multivariable Plants", Electronics Letters, Vol. 17, No. 3, (5 February 1981).

9. Ridgely, B., Banda, S., and D'Azzo, J. "Decoupling of High Gain Multivariable Tracking Systems" AIAA 21st Aerospace Sciences Conference, Reno, Nevada, January 1983, AIAA Paper No. 83-0280.

AD-A138 093 MULTIVARIABLE DIGITAL FLIGHT CONTROL DESIGN FOR THE FPCC (FLIGHT PROPULSI..(U) AIR FORCE INST OF TECH WRIGHT-PATTERSON AFB OH SCHOOL OF ENGI.. J A SIMMERS 3/3

UNCLASSIFIED DEC 83 AFIT/GE/EE/83D-61 F/G 1/3 NL

END

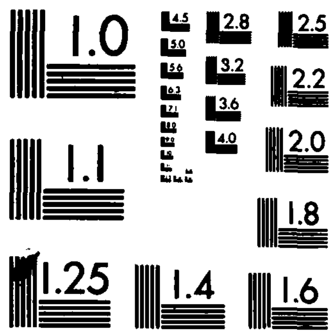

MICROCOPY RESOLUTION TEST CHART
NATIONAL BUREAU OF STANDARDS-1963-A

10. Heimbold, R. L., et al. Flight Propulsion Control Coupling (FPCC) and Dynamic Interaction Investigation, Volume II. AFFDL-TR-75-153, Air Force Flight Dynamics Laboratory, Wright-Patterson AFB OH, September 1975.

11. Porter, B. and D'Azzo, J. "Transmission Zeros of Linear Multivariable Continuous-Time Systems", Electronics Letters, Vol. 13, No. 24, (24 November 1977).

12. Porter, B. "High-Gain Error-Actuated Controllers for Linear Multivarible Plants With Explicit Actuator Dynamics", report given at IFAC Symposium on Computer Aided Design of Multivariable Technological Systems, West Lafayette, Indiana, September 1982, pp. 61-66.

APPENDIX A

JUSTIFICATION FOR ELIMINATION OF JET FLAPS FROM LATERAL MODEL

Introduction

This appendix derives the relationship between the jet flaps and the derivatives of the lateral states p and r, showing that the jet flaps can be removed from the lateral model used in this thesis. This relationship is expressed by two terms in the $\underline{B}$ matrix from the system equation

$$\dot{\underline{x}} = \underline{A}\underline{x} + \underline{B}\underline{u}$$

with x being the state vector. The two terms are in the first and second row, sixth column of the original 12 state system $\underline{B}$ matrix given in equation (48) from Chapter III. From equation (48) these two numbers are given as:

.00939

-.000238

This appendix demonstrates that these numbers should both be zero, removing the jet flaps from the lateral partition of the $\underline{B}$ matrix.

Derivation (Ref 4)

Starting with the rotation versus moment equations

$$\dot{p} = L_B/Ixx + (\text{non linear terms}) \tag{A-1}$$

$$\dot{r} = N_B/Izz + (\text{non linear terms}) \tag{A-2}$$

and substituting

$$L_B = L_S\cos\alpha - N_S\sin\alpha + Fy_B\Delta z + Fz_B\Delta y - Y_{eng1}z_{eng1} - Y_{eng2}z_{eng2} + Z_{eng1}y_{eng1} + Z_{eng2}y_{eng2} \tag{A-3}$$

$$N_B = L_S\sin\alpha + N_S\cos\alpha + Fx_B\Delta y + Fy_B\Delta x - X_{eng1}y_{eng1} - X_{eng2}y_{eng2} + Y_{eng1}x_{eng1} + Y_{eng2}x_{eng2} \tag{A-4}$$

where L_S and N_S represent the aerodynamic moments in stability axes. Pulling out the only terms that are dependent upon jet flap setting:

$$Fy_\beta \Delta z = 0$$

$$Fz_\beta \Delta y = 0$$

$$Fx_\beta \Delta y = 0$$

$$Fy_\beta \Delta x = 0$$

since Δx, Δy, and Δz, the components of the center of gravity offset from the moment reference point are all set to zero in the FPCC simulation program. Continuing with the terms that are dependent upon jet flap setting, the direct propulsion force terms are:

$$X_{eng1} = \eta_F F_1 \cos\delta_j \cos\Psi_{eng1} - CDI_1 \tfrac{1}{2}\rho V_T^2 S$$
$$X_{eng2} = \eta_F F_2 \cos\delta_j \cos\Psi_{eng2} - CDI_2 \tfrac{1}{2}\rho V_T^2 S$$
$$Y_{eng1} = \eta_F F_1 \cos\delta_j \sin\Psi_{eng1}$$
$$Y_{eng2} = -\eta_F F_2 \cos\delta_j \sin\Psi_{eng2}$$
$$Z_{eng1} = -\eta_F F_1 \sin\delta_j$$
$$Z_{eng2} = -\eta_F F_2 \sin\delta_j$$

Assuming the following equalities (which are true in the FPCC simulation program)

$$F_1 = F_2$$
$$\Psi_{eng1} = \Psi_{eng2}$$
$$CDI_1 = CDI_2$$
$$X_{eng1} = X_{eng2}$$
$$y_{eng1} = y_{eng2}$$

$$z_{eng1} = z_{eng2}$$

with

x_{eng1} = x distance from center of gravity to engine one

x_{eng2} = x distance from center of gravity to engine two

y_{eng1} = y distance from center of gravity to engine one

y_{eng2} = y distance from center of gravity to engine two

z_{eng1} = z distance from center of gravity to engine one

z_{eng2} = z distance from center of gravity to engine two

Ψ_{eng1} = yaw offset of engine one with respect to aircraft

Ψ_{eng2} = yaw offset of engine two with respect to aircraft

η_F = thrust adjustment factor (0.98)

V_T = scaler total velocity (square root of the sum of the squares of the body axis velocities)

ρ = air density

S = planform area

Substituting these terms back into equations (A-3) and (A-4) results in neither L_5 nor N_5 having any dependency on the jet flaps. This means that the jet flap deflection (considering the above stated symmetry and engines of equal thrust) has no effect on yaw or roll rates, a logical conclusion.

Since equations (A-3) and (A-4) substituted into (A-1) and (A-2) show that the derivatives of p and r have no dependency on the jet flap deflection, then these corresponding entries in the system $\underline{B}$ matrix are set to zero for the purposes of this thesis. Since the $\underline{B}$ matrix from equation (48) shows these numbers incorrectly as being non zero, then there is an error in the FPCC simulation program. Unfortunately, this means that any other data produced by the program is also suspect and so, consequently, are the results of this thesis.

APPENDIX B

IMPLEMENTING A FIRST FORWARD DIFFERENCE APPROXIMATION TO THE 1/S ROUTINE WITHIN THE PI CONTROLLER IN MULTI

Introduction

The simulation program MULTI currently uses the first backward difference approximation for the integration routine within the proportional plus integral (PI) controller. However, due to certain results in this thesis (see Figures 16, 19, and 20) there seemed to be a problem with the integration within the PI controller. The referenced plots demonstrate a feature that appears to be the result of windup, implying that the integration needed improvement. One simple way of improving a digital integration is to use the first forward difference approximation, which was tried with the routine within the PI controller with good results.

Implementation

The current integration within the PI controller in MULTI is done with the first backward difference approximation as expressed in the line of FORTRAN code as:

```
Z(I)=Z(I)+SAMPT*E(I)                                    (B-1)
```

which is the representation of:

$$Z[(k+1)T]=Z(kT)+Te[(k-1)T] \tag{B-2}$$

Since the line of code (B-1) appears after the calculation of the control input which is based upon Z(kT) in

$$\underline{u}(kT)=\{\underline{K}_0\underline{e}(kT)+K_I\underline{Z}(kT)\}/T \tag{B-3}$$

the error used in equation (B-2) is actually the previous error and thus the $e[(k-1)T]$ shown in equation (B-2). There is some question as to whether equation (B-2) is actually equivalent to Professor Porter's expression (Ref xx):

$$Z[(k+1)T]=Z(kT)+T[v(kT)-y(kT)] \tag{B-4}$$

Close examination of expression (B-4) shows that it is equivalent to expression (B-2) if the next iteration of kT starts at the sample and hold device of Figure 1. However, this would seem to conflict with expression (B-3) where the error used to generate the control input is in the same iteration as the Z. One way to resolve this problem would be to say that the kT iterations start with the sample and hold device and then to define:

$$Z[(k+1)T]=Z(kT)+Te(kT)$$

which is a first forward difference approximation.

What was tested first though, was an average of the first forward and first backward differences, which is still a rectangular approximation, thus keeping the "spirit" of Professor Porter's work. This averaged first difference can be expressed as:

$$Z[(k+1)T]=Z(kT)+T\{e(kT)+e[(k-1)T]\}/2 \tag{B-5}$$

The FORTRAN code implementation of expression (B-5) appeared in MULTI as:

```
Z(I)=Z(I)+SAMPT*(E(I)+PREVE(I))/2.0                    (B-6)
```

Note that in expressions (B-1) and (B-6) the running variable I is used to position within the vectors involved, not as a kT iteration counter, and that PREVE is the previous error.

With the code (B-6) substituted into the PI controller routine the plots for the longitudinal maneuvers at the 0.15 mach flight condition were regenerated. The only noticable changes were in the plots for the forward velocity with the direct lift command, and in the forward velocity and total thrust curves with the vertical translation command. Comparing the new curves (Figures B-1, B-2, and B-3) with the originals (Figures 16, 19, and 20), the effect of using the new integration approximation is to eliminate the instabilities near the end of the simulation.

After testing the averaged first difference approximation, a first forward difference approximation was implemented by changing (B-6) to

```
Z(I)=Z(I)+SAMPT*E(I)                                        (B-7)
```

This line of code was also moved before the calculation of the control input so that it does implement the first forward difference approximation. Limited testing indicates that this change also removes the instabilities due to using the first backward difference approximation.

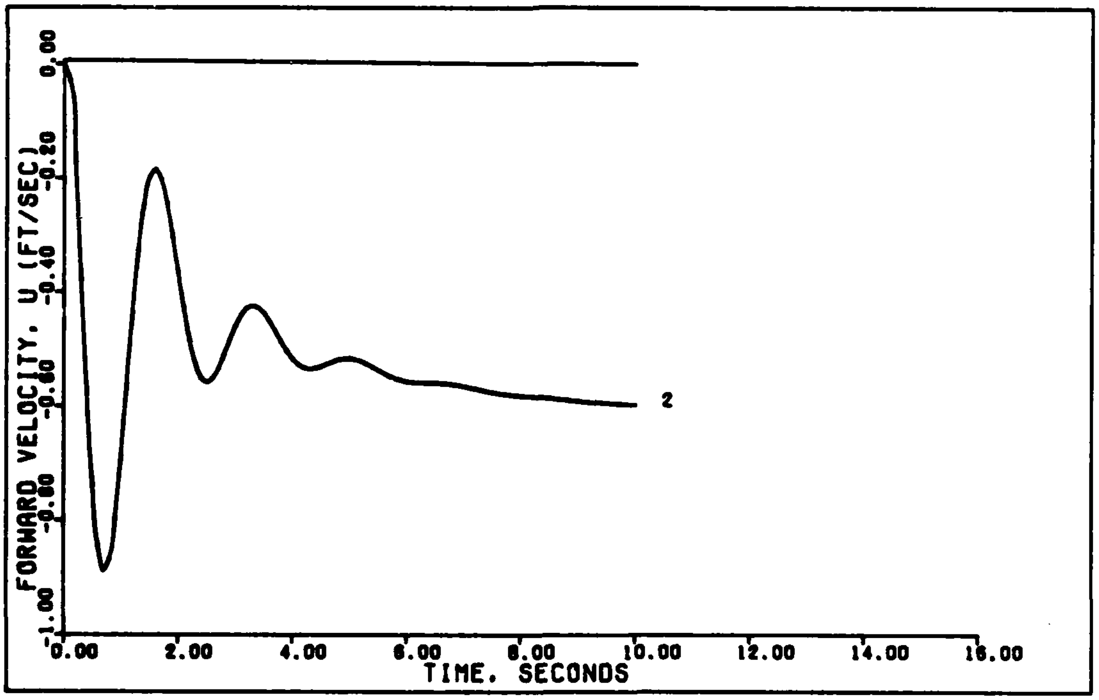

FIGURE B-1

Figure B-1. Forward Velocity Response to 0.5 G Direct Lift Command (0.15 Mach, 0 ft.)

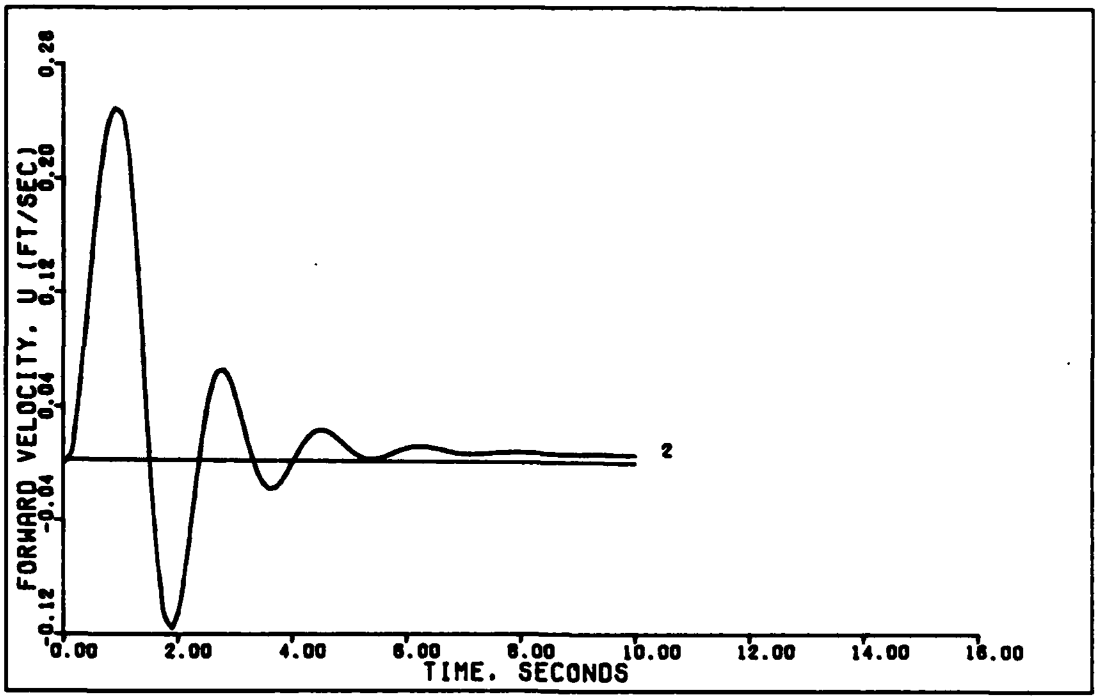

FIGURE B-2

Figure B-2. Forward Velocity Response to 0.5 G Vertical Translation Command (0.15 Mach, 0 ft.)

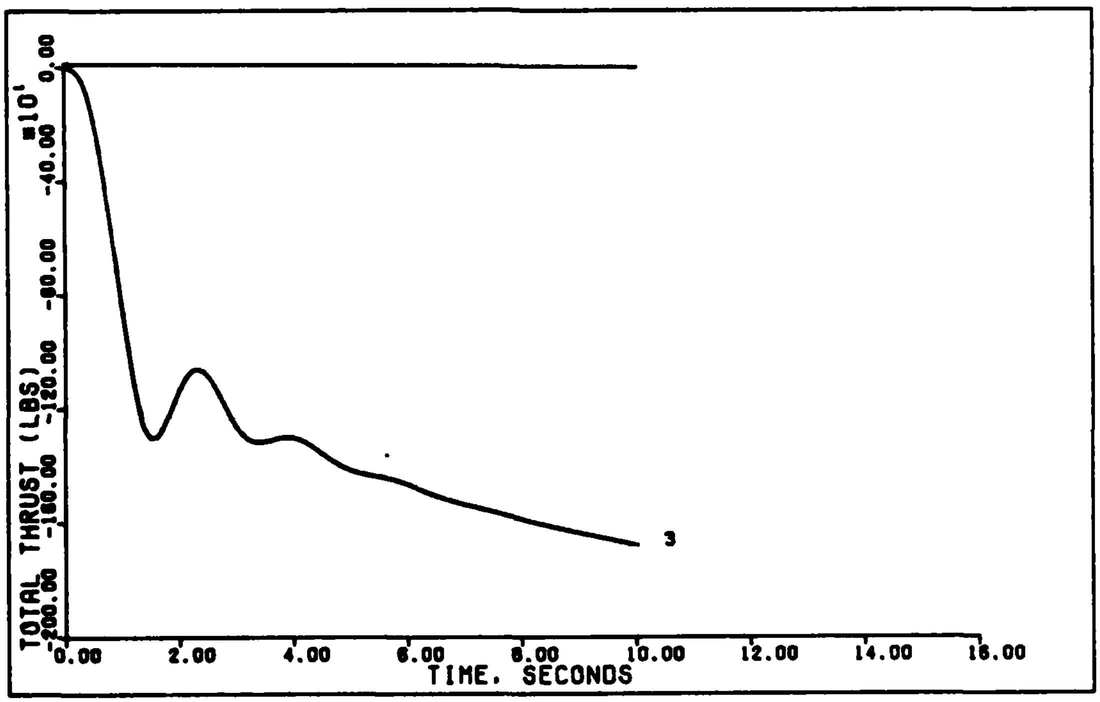

FIGURE B-3

Figure B-3. Total Thrust Response To 0.5 G Vertical Translation Command (0.15 Mach, 0 ft.)

APPENDIX C

ADDITIONS TO DESIGN PROGRAM MULTI

Introduction

This appendix briefly describes the two additions made to the design program MULTI by this author. The first addition allows the use of the local file names for the system, design, and simulation data files as command line arguments. Within MULTI, these command line arguments are then used in an Option #199 which performs the same functions as Options #9, #19, and #29. The second addition is Option #28, which calculates and displays several figures of merit from the latest simulation. At the end of this appendix is a short section on the addition of program code that would calculate and display maximum actuator rates. The final section is a description of another option that would allow the user to toggle the curve fitting for the CALCOMP plots from modified spline to linear and back.

Command Line Arguments and Option #199

The concept behind this addition is to allow the user to specify the local file names of the three files containing the system, design, and simulation parameters as command line arguments to be used with Option #199. For example, if the user had these three files named MEMO, MEM10, and MEM20, then the command (in response to Cyber's Command query)

COMMAND> MULTI(,,MEMO,MEM10,MEM20)

will start up MULTI execution in the normal manner, but will allow the user to type (in response to the Option query)

OPTION, PLEASE > #199

invoking Option #199. The user must type in all three local file names to use Option #199. If not, then a FORTRAN file read error upon attempting Option #199 will cause the user to be "bombed out" of MULTI and back into the Cyber command mode. Of course, the three local files must contain the data in the format necessary to satisfy MULTI's requirements. This currently means that the files must be in the format specified in the MULTI Users Manual for Options #9, #19, and #29 This manual can be obtained from the Electrical Engineering Department, Air Force Institute of Technology, Wright Patterson Air Force Base, Ohio, 45433.

Invoking Option #199 actually causes modified versions of Options #9, #19, and #29 to be sequentially executed. This means that the user can use Option #199 whenever the other three would be used. The following shows what the user will see after specifying Option #199:

OPTION, PLEASE > #199

DATA COPY COMPLETE FOR OPTIONS
#2, #3, #4

DATA COPY COMPLETE FOR OPTIONS
#11, #12, #13, #14, #16, #18

DATA COPY COMPLETE FOR OPTIONS
#21, #22, #23, #24, #25, #27

OPTION, PLEASE > #

At this point the user may continue as if Options #9, #19, and #29 had just been completed.

Local file names as command line arguments is not currently supported in CDC versions of FORTRAN 4. If MULTI were recompiled in FORTRAN 4, changing the program declaration line in the main program to read:

```
PROGRAM EXEC (PLOT,TAPE9=PLOT)
```

would be sufficient (not considering other syntax problems) to disable the command line argument and Option #199 feature. The code for implementing Option #199 would remain, so that changing the program declaration back to:

```
PROGRAM EXEC (PLOT,TAPE9=PLOT,TAPE10,TAPE35,TAPE40)
```

would then reactivate command line arguments and Option #199 capability.

Option #28, Figures of Merit

The second addition made to MULTI by this author is the calculation and display of several figures of merit using Option #28. Specifically, this option calculates the peak value, time to peak value, minimum value, time to minimum value, final value, and settling time. All of the calculations are performed upon the packed data used for the plots. Additionally, Option #28 checks to see if the simulation has been run prior to its execution, and if not, then informs the user and returns to the option query. Assuming the simulation has been performed, then using Option #28 would produce:

```
OPTION, PLEASE > #28

THIS OPTION CALCULATES THE FIGURES OF MERIT
CONTINGENT UPON COMPLETION OF SIMULATION

HOW MANY SEQUENTIAL OUTPUTS (STARTING WITH Y1)
DO YOU WISH FIGURES OF MERIT FOR? >1
Y1              PEAK=42.98407352055
Y1     TIME TO PEAK=9.999999999995
Y1           MINIMUM=0.
Y1 TIME TO MINIMUM=0.

DO YOU WISH TO CONTINUE WITH SETTLING TIME
CALCULATIONS? (1 FOR YES/0 FOR NO)>1
```

```
FINAL VALUE OF Y1=42.98407352055

DO YOU WISH TO USE DEFAULT VALUE OF WITHIN 2%
OF THIS VALUE FOR CALCULATION OF SETTLING TIME?
(1 FOR YES/0 FOR NO)>1

SETTLING TIME FOR Y1=6.499999999999
```

The user in this example only specified one output, but up to as many as there actually are can be specified, with the values given above being repeated for each output. Additionally, the user does not have to continue with settling time calculations, in which case the user is returned to the Option mode. If the user answers "0" to the question about using the default values for the settling time calculations, then this example would continue:

```
DO YOU WISH TO USE DEFAULT VALUE OF WITHIN 2%
OF THIS VALUE FOR CALCULATION OF SETTLING TIME?
(1 FOR YES/0 FOR NO)>0

ENTER UPPER BOUND FOR SETTLING VALUE
>40

ENTER LOWER BOUND FOR SETTLING VALUE
>39

SETTLING TIME FOR Y1=4.399999999999
```

If the response does not settle down within either the user specified band, or within the $\pm 2\%$ of final value range, then the message

```
SIMULATION DID NOT REACH A SETTLING TIME
```

is displayed, and the user is returned to Option query.

Almost all of the added code for Option #28 is contained in the last overlay in MULTI, OVERLAY(21,0).

Suggested Addition To Option #28

This section describes program code that would calculate and display the maximum positive and negative actuator rates.

First, two common blocks have to be added to OVERLAY(21,0):

```
COMMON /B  6 / DMATRIX,ACT,SEN
COMMON /B 13A/ UP(101,11)
```

Next, right before the common block declaration area add:

```
CHARACTER DMATRIX,ACT,SEN
```

At the end of the DIMENSION statements add:

```
DIMENSION RATEMAX(10),RATEMIN(10)
```

At the end of the DATA statements add:

```
DATA RATEMAX,RATEMIN/20*0.0/
```

Add the following to the indicated DO loop:

```
DO 1400 I=1,P
    DO 1400 J=1,LCOUNT

    IF(J.NE.1) THEN
        RATE=(UP(J,I+1)-UP(J-1,I+1))/(UP(J,1)-UP(J-1,1))
        IF(RATE.GT.RATEMAX(I)) RATEMAX(I)=RATE
        IF(RATE.LT.RATEMIN(I)) RATEMIN(I)=RATE
    ENDIF
1400 CONTINUE
```

RATEMAX and RATEMIN are used to store the maximum positive and maximum negative values of the rates, respectively. RATE is used to calculate each rate, with UP(J,I+1) storing the current value of the actuator deflection and UP(J-1,I+1) storing the previous value of actuator deflection. UP(J,1) and UP(J-1,1) store the time of the current and the time of the previous actuator deflections respectively. To display the results, the following code is added to the end of the overlay:

```
DO 1600 I=1,P
     IF(RATEMIN(I).LT.0) THEN
          IF(ACT.EQ.'Y') THEN
PRINT*,'MAXIMUM NEGATIVE ACTUATOR RATE #',I,'=',RATEMIN(I)
          ELSE
PRINT*,'MAXIMUM NEGATIVE CONTROL INPUT RATE #',I,'=',
       RATEMIN(I)
          ENDIF
     ENDIF
     IF(ACT.EQ.'Y') THEN
PRINT*,'MAXIMUM POSITIVE ACTUATOR RATE #',I,'=',RATEMAX(I)
     ELSE
PRINT*,'MAXIMUM POSITIVE CONTROL INPUT RATE #',I,'='
       RATEMAX(I)
     ENDIF
     PRINT*, ' '
1600 CONTINUE
```

This code correctly informs the user that the rates are for control inputs when there are no actuators.

This code has been tested on a copy of MULTI and seems to work correctly.

Suggested Addition, Option #38

This section lists the code that would implement Option #38, an option to toggle between modified spline and linear curve fitting for the CALCOMP plots. For more information on how this code works, the user is referred to the CALCOMP USER'S GUIDE available from either the AFIT Engineering Building (Bldg 640) or from the ASD Computer Center, Building 676.

The first step is to add the following to the common block statements in the main section of the program:

```
COMMON /B 13A/ UP(101,11),LINEFIT
```

and also add the following to the DATA list in the same section:

```
DATA LINEFIT/-1/
```

Next, add the following to OVERLAY(10,0):

First, to the common block list:

```
COMMON /B 13A/ UP(101,11),LINEFIT
```

To the listing of options:

```
PRINT*, '    38.  TOGGLE CALCOMP PLOT CURVE FITTING'
```

To the sequential option code listings

```
C  OPTION #38
 2038 LINEFIT=LINEFIT*(-1)
      PRINT*,'CALCOMP PLOT CURVE FITTING IS'
      IF(LINEFIT.EQ.1) PRINT*,'LINEAR'
      IF(LINEFIT.EQ.-1) PRINT*,'MODIFIED SPLINE'
      NOPT=0
      GO TO 8010
```

Then add the following to OVERLAY(12,0):

To the common block list:

```
COMMON /B 13A/ UP(101,11),LINEFIT
```

In two places in the code section replace

```
CALL FLINE (XAXIS,YAXIS,-N,1,1,72)
```

with

```
CALL FLINE (XAXIS,YAXIS,N*LINEFIT,1,1,72)
```

This option has been added to a copy of MULTI and tested with no problems. Option #38 acts like a switch, and is designed to be used whenever the modified Option #28 (with rates, above) displays rates that the user thinks are too high for the modified spline fit. These two options were used in the author's thesis to prevent actuator deflection plots from assuming non-functional shapes.

APPENDIX D

SYSTEM MATRICES, CONTROLLER MATRICES, AND DESIGN PARAMETERS FOR 0.6 MACH, SEA LEVEL, AND FOR 0.9 MACH, 30,000 FEET

Introduction

This appendix lists the system matrices, the design matrices, and the design parameters for the two flight conditions not discussed in detail in the text of this thesis, 0.6 mach at sea level, and 0.9 mach at 30,000 feet. The complete system matrices in the form of equation (48) from Chapter III can be found in Jon Bauschlicher's thesis (Ref 2).

0.6 Mach, Sea Level Flight Condition

$$\underline{A} = \begin{bmatrix} 0 & 0 & 0 & 1 \\ -32.1 & -.0297 & .105 & -12.1 \\ -.577 & -.0568 & -2.82 & 674 \\ 0 & -.0011 & .0639 & -.463 \end{bmatrix}$$

$$\underline{B} = \begin{bmatrix} 0 & 0 & 0 \\ .518 & .000923 & .00218 \\ -1.43 & -.616 & -.000069 \\ .640 & -.043 & -.00000448 \end{bmatrix}$$

$$\underline{C} = \begin{bmatrix} 1 & 0 & 0 & 0 \\ 0 & 1 & 0 & 0 \\ 0 & 0 & .00149 & 0 \end{bmatrix}$$

$$\underline{M} = \begin{bmatrix} 1 \\ 0 \\ 0 \end{bmatrix}$$

$\alpha = 2,\ \epsilon = .1,\ T = 0.01$

$$\underline{\Sigma} = \begin{bmatrix} 1 & 0 & 0 \\ 0 & 1 & 0 \\ 0 & 0 & .1 \end{bmatrix}$$

$$\underline{K}_o = \begin{bmatrix} .270 & -.0000417 & -1.27 \\ -.620 & -.0102 & -18.9 \\ -64.0 & 91.8 & 309 \end{bmatrix}$$

$$\underline{K}_1 = \underline{K}_o/2$$

0.9 Mach, 30,000 ft. Flight Condition

$$\underline{A} = \begin{bmatrix} 0 & 0 & 0 & 1 \\ -32.1 & -.0822 & .0472 & -19.7 \\ -.705 & -.0558 & -1.68 & 898 \\ 0 & -.00317 & .0303 & -.253 \end{bmatrix}$$

$$\underline{B} = \begin{bmatrix} 0 & 0 & 0 \\ .359 & -.00071 & .00218 \\ -.634 & -.464 & -.00008 \\ .527 & -.0325 & -.000004 \end{bmatrix}$$

$$\underline{C} = \begin{bmatrix} 1 & 0 & 0 & 0 \\ 0 & 1 & 0 & 0 \\ 0 & 0 & .00112 & 0 \end{bmatrix}$$

$$\underline{M} = \begin{bmatrix} 1 \\ 0 \\ 0 \end{bmatrix}$$

$\alpha = 2$, $\epsilon = .1$, $T = 0.01$

$$\underline{\Sigma} = \begin{bmatrix} 1 & 0 & 0 \\ 0 & .1 & 0 \\ 0 & 0 & .01 \end{bmatrix}$$

$$\underline{K}_o = \begin{bmatrix} .350 & -.0000258 & -.219 \\ -.469 & -.00155 & -3.56 \\ -57.8 & 9.18 & 34.9 \end{bmatrix}$$

$\underline{K}_1 = \underline{K}_o/2$

VITA

Jeffrey A Simmers was born in Harrisburg, Pennsylvania on January 9, 1953. He spent most of his secondary school years in Schenectady, New York. After graduating from high school he attended Texas A&M University for two years, then enlisted into the Air Force. Attending the University of Illinois through the Airman Education and Commissioning Program (AECP), he graduated with a B.S. degree in electrical engineering in December of 1979. After attending OTS he was commissioned as an officer in April of 1980.

His first assignment as an officer was as an analyst at the Foreign Technology Division (FTD) at Wright-Patterson AFB, Ohio until 1982, when he started at the Air Force Institute of Technology. His next assignment is with a detatchment of the Air Force Operational Test and Evaluation Center at Eglin AFB, Florida.

UNCLASSIFIED
SECURITY CLASSIFICATION OF THIS PAGE

REPORT DOCUMENTATION PAGE

1a. REPORT SECURITY CLASSIFICATION UNCLASSIFIED

1b. RESTRICTIVE MARKINGS

2a. SECURITY CLASSIFICATION AUTHORITY

2b. DECLASSIFICATION/DOWNGRADING SCHEDULE

3. DISTRIBUTION/AVAILABILITY OF REPORT Approved for public release; distribution unlimited.

4. PERFORMING ORGANIZATION REPORT NUMBER(S) AFIT/GE/EE/83D-61

5. MONITORING ORGANIZATION REPORT NUMBER(S)

6a. NAME OF PERFORMING ORGANIZATION School of Engineering

6b. OFFICE SYMBOL (If applicable) AFIT/ENG

7a. NAME OF MONITORING ORGANIZATION

6c. ADDRESS (City, State and ZIP Code) Air Force Institute of Technology, Wright-Patterson AFB, Ohio 45433

7b. ADDRESS (City, State and ZIP Code)

8a. NAME OF FUNDING/SPONSORING ORGANIZATION

8b. OFFICE SYMBOL (If applicable)

9. PROCUREMENT INSTRUMENT IDENTIFICATION NUMBER

8c. ADDRESS (City, State and ZIP Code)

10. SOURCE OF FUNDING NOS.

PROGRAM ELEMENT NO.	PROJECT NO.	TASK NO.	WORK UNIT NO.

11. TITLE (Include Security Classification) See Box 19

12. PERSONAL AUTHOR(S) Jeffrey A Simmers, B.S., 1Lt, USAF

13a. TYPE OF REPORT MS Thesis

13b. TIME COVERED FROM ______ TO ______

14. DATE OF REPORT (Yr., Mo., Day) 1983 December

15. PAGE COUNT 211

16. SUPPLEMENTARY NOTATION

Approved for public release: IAW AFR 190-17.
LYNN E. WOLAVER 7 Feb 84
Dean for Research and Professional Development
Air Force Institute of Technology (AIC)
Wright-Patterson AFB OH 45433

17. COSATI CODES

FIELD	GROUP	SUB. GR.

18. SUBJECT TERMS (Continue on reverse if necessary and identify by block number) Flight Control, Digital Flight Control, Multivariable Control, Proportional Plus Integral Control

19. ABSTRACT (Continue on reverse if necessary and identify by block number)

Title: Multivariable Digital Flight Control Design for the FPCC Aircraft

Thesis Chairman: Dr. John J. D'Azzo
Deputy Department Head
Electrical Engineering Department
Air Force Institute of Technology

20. DISTRIBUTION/AVAILABILITY OF ABSTRACT UNCLASSIFIED/UNLIMITED ☒ SAME AS RPT. ☐ DTIC USERS ☐

21. ABSTRACT SECURITY CLASSIFICATION UNCLASSIFIED

22a. NAME OF RESPONSIBLE INDIVIDUAL Dr. John J. D'Azzo

22b. TELEPHONE NUMBER (Include Area Code) 513-255-3576

22c. OFFICE SYMBOL AFIT/ENG

DD FORM 1473, 83 APR EDITION OF 1 JAN 73 IS OBSOLETE.

UNCLASSIFIED
SECURITY CLASSIFICATION OF THIS PAGE

Multivariable design techniques developed by Professor Brian Porter of the University of Salford, England, are used to develop digital control laws for the Flight Propulsion Control Coupling (FPCC) Aircraft. Control laws are developed for each of three flight conditions. A design tool, the computer program MULTI, is modified to calculate and display the figures of merit for each simulation.

The controllers developed utilize output feedback with proportional plus integral (PI) control. Due to the nature of the system model, certain derivatives of the states are measured and added to the feedback.

A robust controller is tested by performing specific maneuvers for multiple flight conditions, and these results are compared to those obtained with the controllers designed for each flight condition.

The individual controllers and the robust controller are tested with the addition of a delay that represents the processing delay within the proportional plus integral implementation. The results with delay are compared to those without delay.

All of the designs accomplished included first order models for the control surface actuators and assumed perfect knowledge of all aircraft states. The designs used reduced order state models with decoupled lateral and longitudinal models.

END

FILMED

3-84

DTIC